Copyright Warning & Restrictions

The copyright law of the United States (Title 17, United States Code) governs the making of photocopies or other reproductions of copyrighted material.

Under certain conditions specified in the law, libraries and archives are authorized to furnish a photocopy or other reproduction. One of these specified conditions is that the photocopy or reproduction is not to be "used for any purpose other than private study, scholarship, or research." If a, user makes a request for, or later uses, a photocopy or reproduction for purposes in excess of "fair use" that user may be liable for copyright infringement,

This institution reserves the right to refuse to accept a copying order if, in its judgment, fulfillment of the order would involve violation of copyright law.

Please Note: The author retains the copyright while the New Jersey Institute of Technology reserves the right to distribute this thesis or dissertation

Printing note: If you do not wish to print this page, then select "Pages from: first page # to: last page #" on the print dialog screen

ABSTRACT

COMPUTATIONAL AND EXPERIMENTAL INVESTIGATION OF ELEMENTAL SULFUR AND POLYSULFIDE

by
Jyoti Sharma

Petroleum processing results in the generation of significant quantities of elemental sulfur (S_8), leading to a surplus of sulfur worldwide. Despite its abundance and low cost, the use of sulfur in value-added organic compound synthesis is limited due to its unpredictable and misunderstood reactivity. This dissertation aims to address this issue by tackling it from two angles. Firstly, by utilizing Density Functional Theory (DFT) calculations, the reactivity of sulfur in the presence of nucleophiles is studied. This facilitates the identification of organic polysulfide intermediates that can be generated under different conditions, as well as the corresponding reactivity for each type of nucleophile. This computational study begins with a benchmarking of numerous DFT functionals against experimental data and high-accuracy ab initio computations to determine the best functional(s) for studying elemental sulfur and polysulfides in organic reactions. Using the best DFT method, the mechanism of monosulfide formation from cyanide and phosphines is explained. At the end of this computational study, the mechanism of 2-aminothiophene formation via the Gewald reaction is elucidated. Secondly, attempts are made to synthesize sulfur-based organic compounds using elemental sulfur or compounds with a sulfur source through the utilization of boron, imine, and aryne chemistry. In summary, this dissertation aims to expand the use of sulfur in organic chemistry by providing an understanding to predict its reactivity with nucleophiles, as well as demonstrating its potential for the low-cost synthesis of valuable sulfur-based organic compounds.

COMPUTATIONAL AND EXPERIMENTAL INVESTIGATION OF ELEMENTAL SULFUR AND POLYSULFIDE

by
Jyoti Sharma

A Dissertation
Submitted to the Faculty of
New Jersey Institute of Technology
in Partial Fulfillment of the Requirements for the Degree of
Doctor of Philosophy in Chemistry

Department of Chemistry and Environmental Science

August 2023

APPROVAL PAGE

COMPUTATIONAL AND EXPERIMENTAL INVESTIGATION OF ELEMENTAL SULFUR AND POLYSULFIDE

Jyoti Sharma

Dr.Pier Alexandre Champagne, Dissertation Advisor — Date
Assistant Professor of Chemistry and Environmental Science, NJIT

Dr. Kevin Belfield, Committee Member — Date
Dean of College of Science and Liberal Arts, Professor of Chemistry and Environmental Science, NJIT

Dr. Tamara Gund, Committee Member — Date
Professor of Chemistry and Environmental Science, NJIT

Dr. Yuanwei Zhang, Committee Member — Date
Assistant Professor of Chemistry and Environmental Science, NJIT

Dr. Vivek Kumar, Committee Member — Date
Associate Professor of Bio-Medical Engineering, NJIT

BIOGRAPHICAL SKETCH

Author: Jyoti Sharma

Degree: Doctor of Philosophy

Date: August 2023

Undergraduate and Graduate Education:

- Doctor of Philosophy in Chemistry,
  New Jersey Institute of Technology, Newark, NJ, 2023
- Master of Technology - Polymer Science and Engineering,
  Indian Institute of Technology (IIT), Delhi, India, 2013
- Master of Science - Organic Chemistry
  Institute of Science, Banaras Hindu University (BHU), Varanasi, India, 2010
- Bachelor of Sciences (HONS) - Chemistry
  Institute of Science, Banaras Hindu University (BHU), Varanasi, India, 2008

Major: Chemistry

Presentations and Publications:

Turner Newton, Keyan Li, Jyoti Sharma, Pier Alexandre Champagne, and Michael D Pluth "Direct Hydrogen Selenide (H 2 Se) Release from Activatable Selenocarbamates," *Chemical Science*, 2023.

Sharma, Jyoti and Champagne, Pier Alexandre, "Mechanisms of the Reaction of Elemental Sulfur and Polysulfides with Cyanide and Phosphines," *Chemistry-A European Journal*, vol. 29, pp e202203906, 2023.

Sharma, Jyoti and Champagne, Pier Alexandre, "Benchmark of Density Functional Theory Methods for the Study of Organic Polysulfides," *Journal of Computational Chemistry*, vol. 43, pp 2131-2138, 2022.

Buttard, Floris, Sharma, Jyoti and Champagne, Pier Alexandre, "Recent Advances in the Stereoselective Synthesis of Acyclic All-carbon Tetrasubstituted Alkenes," *Chemical Communications*, vol. 57, pp 4071-4088, 2021.

Jyoti Sharma, "Computational Investigations on the Mechanism of the Gewald Reaction," *Poster*, Physical Organic Chemistry Gordon Research Conference, NH, USA, 2023.

Jyoti Sharma, "Computational Investigations on the Mechanism of the Gewald Reaction," *Poster*, Middle Atlantic Regional Meeting, NY,USA, 2023.

Jyoti Sharma, "Computational Investigations on the Mechanism of the Gewald Reaction," *Oral talk*, ACS Spring, Crossroads of Chemistry, IN, USA, 2023.

Jyoti Sharma, "Computational Investigations on the Reactions of Elemental Sulfur with Nucleophiles," *Oral talk*, 29th International Symposium on the Organic Chemistry of Sulfur, Canada, 2022.

Jyoti Sharma, "Computational Investigations on the Mechanism of the Gewald Reaction," *Poster*, Heterocyclic Compounds Gordon Research Conference, RI, USA, 2022.

Jyoti Sharma, "Computational Investigations on the Reactions of Elemental Sulfur with Triphenylphosphine," *Poster*, Middle Atlantic Regional Meeting, NJ, USA, 2022.

Jyoti Sharma, "Computational Investigations on the Reactions of Elemental Sulfur with Nucleophiles," *Poster*, Organic Topical Group Fall Symposium, NJ, USA, 2021.

I dedicate this thesis to my loving husband, ***Debanjan Mahata*** *and my seven year old twin children* ***Shrestha*** *and* ***Darsh****. My husbands' unwavering support, encouragement, and belief in my abilities have been my constant source of strength throughout this academic journey. Without his patience, understanding, and sacrifices, I would not have been able to accomplish this significant milestone in my life.*

ACKNOWLEDGMENTS

I would like to begin by expressing my sincere appreciation to Dr. Pier Alexandre Champagne, my advisor, for his unwavering support and guidance over the past five years. I am deeply grateful to him for the opportunities he provided me and for inspiring me to become an independent researcher. Dr. Champagne's faith in me and his patience during times when I struggled with my research work was invaluable. He also gave me numerous opportunities to enhance my communication, writing, and presentation skills, and the knowledge I acquired from him will undoubtedly benefit me in my future research pursuits. Furthermore, he motivated me to engage in numerous exceptional conferences and scientific gatherings. I would also like to say thanks for giving me financial support. In summary Dr. Champagne remarkable passion and optimistic outlook on research served as the driving forces behind my graduate journey at the New Jersey Institute of Technology. Without his invaluable assistance, I would not have been able to successfully complete my doctoral studies.

I would also like to express my gratitude to each member of my Committee, namely Dr. Kevin Belfield, Dr. Yuanwei Zhang, Dr. Tamara Gund, and Dr.Vivek Kumar for their patience, professional guidance, and assistance.

Additionally, I am grateful to the American Chemical Society's Petroleum Research Fund for providing funding and support towards my research endeavors.

I would like to express my gratitude to the John Krane, and Genti Price for their invaluable administrative and logistic support.

I am grateful to Mengyuanrom Xiao, Andrea, and Sara for their valuable contributions in assisting with my experiments and recording and analyzing the mass and UV-visible spectroscopy data for some of my compounds.

I thank all my friends, namely, Dr. Tony Roy, Dr. Anil Kumar, Dr. Daniel Kasungi Isika, and Dr. Manavi Yadav from the bottom of my heart for being part of my journey and supportive peers during my doctoral studies.

I am grateful to my beloved parents and family members for demonstrating their boundless love and unwavering faith in me. I will always cherish the sacrifices my parents have made, and their support will forever hold a special place in my heart. I would like to express my heartfelt thanks to my mother-in-law for making the journey all the way from India and providing invaluable assistance during my PhD journey.

TABLE OF CONTENTS

TABLE OF CONTENTS
(Continued)

Chapter **Page**

TABLE OF CONTENTS
(Continued)

Chapter **Page**

TABLE OF CONTENTS
(Continued)

Chapter **Page**

TABLE OF CONTENTS
(Continued)

Chapter **Page**

LIST OF TABLES

LIST OF TABLES
(Continued)

Table **Page**

LIST OF FIGURES

LIST OF FIGURES
(Continued)

Figure **Page**

LIST OF FIGURES
(Continued)

Figure **Page**

LIST OF FIGURES
(Continued)

Figure **Page**

LIST OF FIGURES
(Continued)

Figure **Page**

LIST OF FIGURES
(Continued)

Figure **Page**

CHAPTER 1

INTRODUCTION

1.1 Sulfur

Sulfur (CAS No. 7704-34-9) is an element having the symbol S and atomic number 16, with electronic configuration $1s^2$, $2s^2$, $2p^6$, $3s^2$, $3p^4$. Sulfur has four known stable isotopes. The most stable isotope is ^{32}S, with 95.1 % abundance in nature, while other three isotopes ^{33}S, ^{34}S and ^{36}S are present in 0.74%, 4.2% and 0.016%, respectively. Sulfur's ability to form long chains using S-S bonds is attributed to its relatively large atomic radius and the stable covalent bonds it can form with other sulfur atoms. This characteristic of forming long chains is referred to as catenation. It should be noted that sulfur is among the few elements that exhibit this tendency. Due to the partial sp^3 hybridization resulting from the presence of two lone pairs, sulfur chains adopt three-dimensional structure. This non planar structure produces dihedral angle (γ) of $\approx 100^\circ$ (Figure 1.1).[1]

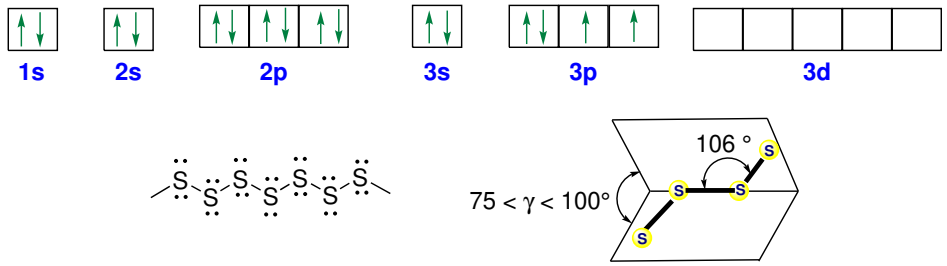

Figure 1.1 Ground state electronic configuration of a sulfur atom; two-dimensional representation of sulfur helix.

1.2 Sulfur Allotropes

Sulfur exists in the form of 30 solid allotropes, more than any other element[2] due to its **catenation** property (tendency of making bond with one another). Sulfur forms strong bonds with each other, with a bond energy of 265 kJ/mol, which

is only lower than that of hydrogen (435 kJ/mol) and carbon (330 kJ/mol).[3] In ambient conditions, elemental sulfur exists in a cyclic form. Up to this point, 15 crystalline ring structures ranging from S_6 to S_{20} are known. On the other hand, at very high temperatures, sulfur exists as long chain form. Out of all known allotropes, cyclic octatomic molecule S_8, is the most stable. It has a crown shaped structure with symmetry D_{4d}. Elemental sulfur (S_8) is bright yellow, crystalline solid at room temperature, while at low temperature it turns to snow white. Elemental sulfur (S_8) exist in three forms. The only stable form at standard temperature and pressure (STP) is α-S_8, which is also known as orthorhombic sulfur. At 369 K, α-S_8 transforms to monoclinic β-S_8, and stays stable up to its melting temperature (383 K). The monoclinic sulfur can be also obtained by slow cooling of molten sulfur, or by crystallization, from organic solvents. The third form of elemental sulfur is γ-S_8, which is a transient species.[4]

Depending on the specific allotrope of sulfur, the sulfur-sulfur bond length in elemental sulfur can vary. The S-S bond length of most stable form of sulfur (orthorhombic sulfur) is about 2.04 Å, The structure of most stable orthorhombic α-S_8, have been discussed in Subsection 1.2.1.

1.2.1 Orthorhombic α-S_8

The crystals of orthorhombic sulfur either occur naturally or can be grown in CS_2 solution.[5] The sulfur molecule was first studied by Bragg in 1914 as solid orthorhombic sulfur.[6] In 1935, the crystalline structure of orthorhombic α-S_8 was described by Warren and Burwell,[7] that was later improved by Abrahams in 1955.[8] Molecular structure parameters of the α-S_8 molecule is presented in Table 1.1.

Table 1.1 Molecular Structure Parameters of the α-S_8 Molecule at Temperature 298 K[9]

Parameter	Orthorhombic α-S_8
Bond Length (pm)	204.6
Bond Angle (°)	108.2
Torsion Angle (°)	98.5

In elemental sulfur, the S-S bond length is approximately 2.04 Å. In terms of bond order, for a single S-S bond with a bond order of 1, the bond length should be 2.08 Å, while for a bond order of 2, the length should be between 1.88 Å. Nevertheless, the actual reported value falls in between. This shows the double bond character in the S_8 molecule, which was previously suggested by Powell & Eyring (1943).[10]

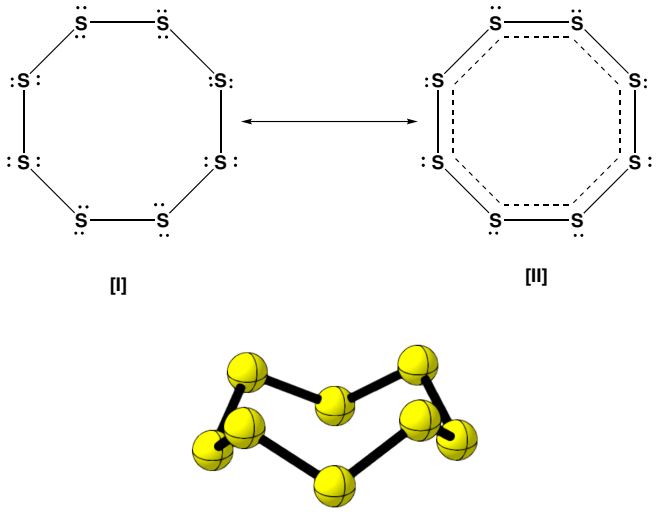

Figure 1.2 Resonance structure of elemental sulfur and Crown/Puckered conformation of elemental sulfur.

This is due to the utilization of 3d orbitals during bond formation, resulting in a certain degree of aromaticity (Figure 1.2). This makes the bond stronger and shorter compared to a single S-S bond. This fact can also be explained based on the dihedral angle. It was suggested by Abrahams in 1954 [11] that in free polysulfide, the average

dihedral angle is 78°, while in a ring, the dihedral angle is 98.5°. This makes the ring flatter and shows a tendency toward planarity with crown shape structure (Figure 1.2).

1.3 Oxidation States of Sulfur

The vacant and available 3d-orbital of sulfur for bonding leads to its multiple oxidation states, ranging from -2 to + 6 (Table 1.2). For achieving bivalency, sulfur gains two electrons (reduction) in the 3p orbital and become stable [Ne]$3s^2$,$3p^6$.

Table 1.2 Oxidation States of Sulfur

Oxidation State	Chemical Name	Formula
-2	Sulfides, Thiols, Sulfonium	S^{2-}
-1	Disulfides	S^{1-}
0	Elemental Sulfur	S^0
+2	Thiosulfite	${S_2O_3}^{2-}$
+3	Dithionite	${S_2O_4}^{2-}$
+4	Disulfite	${S_2O_5}^{2-}$
+4	Sulfite	${SO_3}^{2-}$
+5	Dithionate	${S_2O_6}^{2-}$
+6	Sulfate	${SO_4}^{2-}$

The bivalent sulfur compounds shows sp^3 hybridization. For hexavalency, sulfur looses 6 electrons by expanding d-orbitals and gains stable electronic configuration $1s^2$,$2s^2$,$2p^6$ with sp^3d^2 hybridization. The intermediate oxidation states of sulfur compounds are more stable biologically and chemically. The bivalent and hexavalent sulfur compounds play a major role in sedimentary, aquatic, and atmospheric transformation of sulfur. In anoxic marine environment, sulfur bacteria converts sulfate to sulfide (H_2S), During this cycle, several partially oxidized intermediate

Figure 1.3 Elemental sulfur piles from Claus process.

forms (elemental sulfur, polysulfides, sulfites, thiosulfates),[12–14] play an important role in the biogeochemical process.[15–17]

1.4 Sources of Elemental Sulfur

Sulfur is found naturally in many different forms, such as a pure element, compound, in minerals, and component of various types of fossil fuels. Sulfur can be found as underground deposits in some countries, which can be mined and extracted through Frasch process.[18] Sulfur can be also obtained from its two well known minerals *pyrite* (iron sulfide) and *galena* (lead sulfide) via the roasting process.[19]

Sulfur is produced as a byproduct of various industrial processes like petroleum processing. Petroleum includes crude oil, condensate, natural gas and solids like bitumen, oil sand, and tar. Around 0.03 % - 6 % of sulfur is present in crude oil and natural gas.[20] There are several techniques that can be used to remove sulfur from petroleum during the refining process. Some of the these techniques are *hydrotreating*, *Claus process*, *biofiltration*, and *adsorption*. Out of all these process, only Claus process [21] removes sulfur as elemental sulfur, while other removes sulfur in the form of sulfur compounds.

Every year large amounts of sulfur are produced and deposited as huge stockpiles and is estimated that seven million tons of excess sulfur is being generated annually (Figure 1.3).[22] This huge production of sulfur makes it the third most abundant element in fossil fuels after carbon and hydrogen. In-spite of having wide usage as an additive in asphalt for road pavement and production of sulfuric acid, it has been stored by refiners as massive piles in remote areas.

Although sulfur is non-toxic and environmentally friendly chemical, yet storing it on the ground for long periods could prove to be hazardous. Sulfur can change to sulfur dioxide or hydrogen sulfide, which can lead to a negative impact on humans and environment.[23] It is very important to make judicious use of sulfur and direct its usage in value added materials.

1.5 Applications of Sulfur

Sulfur has a wide range of applications globally, including agriculture, pharmaceuticals, batteries, human nutrition, vulcanization, and nanocomposites. A few of its major uses are discussed below.

1.5.1 Pharmaceuticals

Sulfur compounds have a variety of therapeutic applications in the pharmaceutical industry. Sulfur is one of the most abundant macrominerals found in breast milk and in the body. Natural products and drugs contain a range of sulfur-containing scaffolds that have been used as antivirals, antibacterials, antiallergics, antimalarials, and in the treatment of diseases such as schizophrenia, bipolar disorder, and depression.[24] FDA-approved drugs containing sulfur moieties[25] are shown in Figure 1.4. **Sulfonamide**-based drugs make up the largest portion of sulfur-containing drugs and are used in the treatment of blood pressure, diabetes, bacterial infections, and human immunodeficiency virus (HIV). The second most abundant

moiety is β-**lactam**, with various analogues, including the antibiotics penicillin, that have played a significant role in the treatment of syphilis and infections caused by staphylococci and streptococci bacteria.

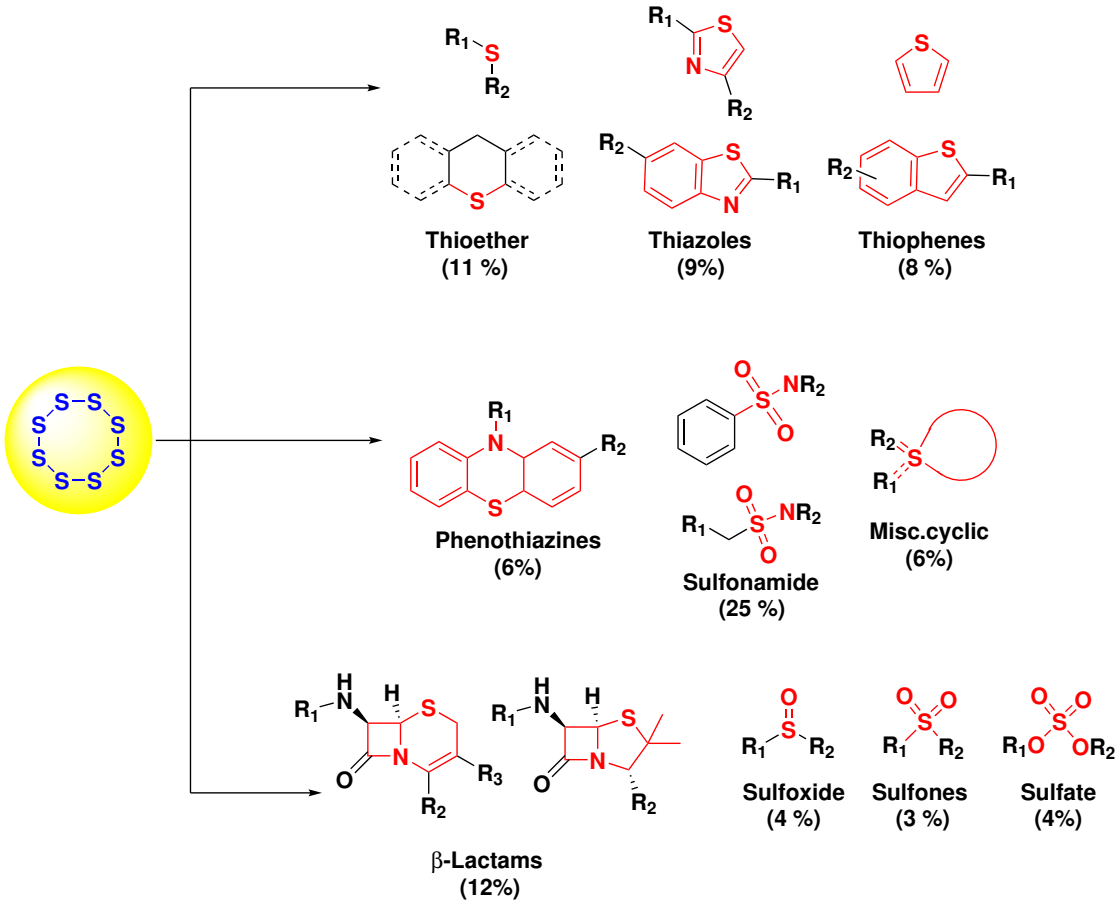

Figure 1.4 Structural diversity of sulfur-containing drugs.

β-Lactam are categorized based on their potency, spectrum, and ability to combat antibiotic resistance, and include penams, cephems, and monobactams. **Thioethers** are the third most common component of sulfur-containing drugs,[26] and well-known drugs such as cimetidine, ranitidine, nizatidine, and famotidine, are made up of thioether skeletons and are used in the treatment of gastroesophageal reflux disease (GERD). **Thiazole** containing drugs include pramipexole for Parkinson's disease, ritonavir for antiretroviral therapy, ticlopidine, clopidogrel, and prasugrel for antiplatelet therapy. Phenothiazines have a tricyclic core with

nitrogen and sulfur atoms and exhibit antipsychotic activity. **Sulfoxide** drugs are unique due to the presence of a chiral center with a lone pair of electrons on the sulfur center. Examples include sulfinpyrazone for the treatment of gout, omeprazole for Zollinger–Ellison syndrome, modafinil and armodafinil for sleep disorders, and fulvestrant for breast cancer. **Sulfon**, which make up 3% of total sulfur-containing drugs, include drugs for anxiolytic and muscle relaxant (chlormezanone) and migraines (eletriptan). **Sulfate** containing drugs are of special benefit due to their water solubility and are used as blood thinners, such as enoxaparin, dalteparin, and tinzaparin.

1.5.2 Agriculture

Sulfur is important for plant growth, legume formation, and the immune system. It is an essential element in living organisms and responsible for the biosynthesis of methionine, cysteine, vitamin, and coenzyme A. The roots of plants do not absorb elemental sulfur due to its insolubility in water, but heterotrophic, chemolithotrophic, and photoautotrophic microorganisms can oxidize it to sulfate ($SO_4{}^{2-}$) or thiosulfate ($S_2O_3{}^{2-}$), which can then be absorbed by the plant roots. Sulfate also enhances phosphorous uptake in plants, and elemental sulfur is an effective pesticide, rodenticide, and insecticide.[27] Magnesium sulfate ($MgSO_4$) was one of the earliest approved antifungal drugs.

1.5.3 Batteries

Sulfur is well known as a cathode in batteries, with anode partners made up of alkali metals like lithium (Li) and sodium (Na). The most well-known sulfur-based battery is the lithium-sulfur (Li-S) battery, which is high-power storage system. Sulfur in the Li-S battery is a promising cathode due to its high specific energy density, specific capacity, lower cost, lighter weight, and flexibility. Li-S batteries have practical

applications in portable devices, electric vehicles, and grid storage in the form of solar or wind renewable energies. Nevertheless, the major disadvantage of Li-S batteries is the "shuttle effect", where both the anode and cathode corrode by consuming the electrolyte, causing rapid capacity decay.[28] Various strategies have been taken in past few years to make Li-S batteries more efficient.[29] The sodium-sulfur (Na-S) battery is another class of battery with wide applications,[30] but its demand has decreased over time due to safety issues.

1.6 Role of Elemental Sulfur in Chemical Reactions

Sulfur is an odorless, non-hygroscopic, non-volatile, and low priced chemical that makes it lab friendly. Along with these properties sulfur has a wide spectrum of chemical application such as in sulfuration, green chemistry, catalysis, oxidizing and reducing agent.[31]

Sulfuration, involve C-S bond formation. C-S bonds play an essential role in the domains of pharmaceuticals and biology. Various sulfurating agents like thiol, thiocyanate, and Lawesson's reagent can be used to form a C-S bond. Nevertheless, due to their toxic nature, elemental sulfur has received considerable attention as sulfurating agent.[32–35] The sulfuration reaction can be done using one or two substrates with elemental sulfur. Some valuable heterocyclic compounds,[36] like thiophenes , thiiranes, thienoindoles , thienothiazoles , thiazoles , benzothiazoles, thiadiazoles and non heterocylic compounds [31] like thioamides, symmetrical sulfides and disulfides can be synthesized using elemental sulfur as a sulfurating agent (Figure 1.5).

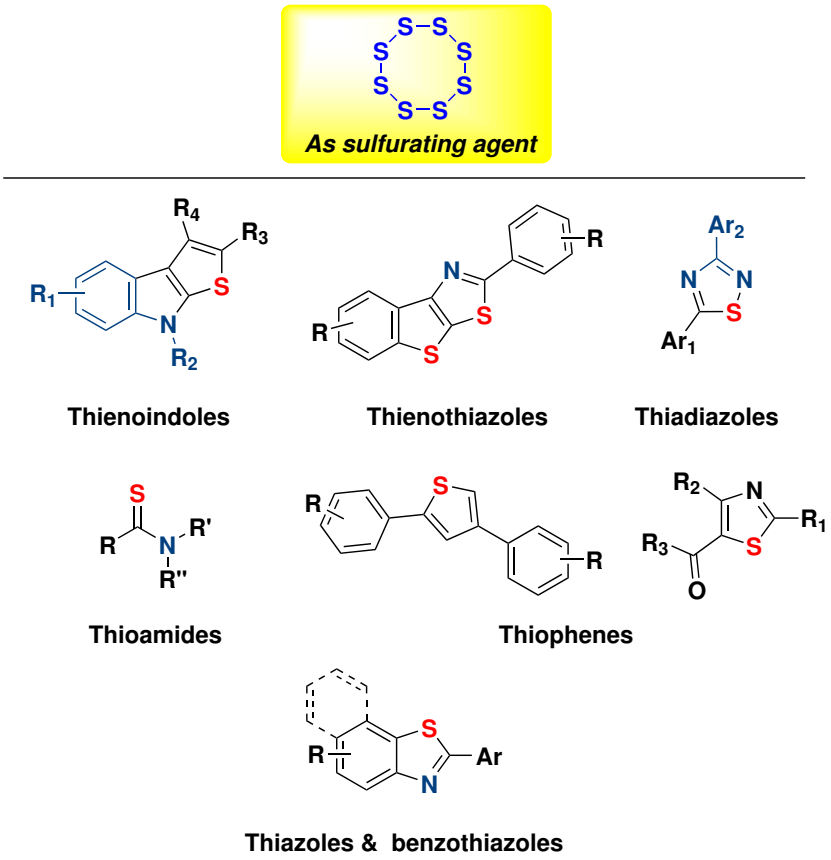

Figure 1.5 Sulfuration reaction of elemental sulfur.

Sulfur-based polymers are a class of **green polymers** (Figure 1.6) that provide a sustainable alternative and utilize industrial waste via inverse vulcanization, where sulfur incorporates into polymers such as dicylcopentadiene (DCPD), 5-Ethylidene-2-norbornene (ENB), and 1,3-diisopropenylbenzene (DIB).[37–39] In addition to their sustainability, sulfur-based polymers have several other advantages over traditional petroleum-based plastics. They are biodegradable and can be recycled, reducing their impact on the environment. They also have excellent thermal stability, making them useful in high-temperature applications. Polysulfides made from elemental sulfur and green monomers such as limonene, myrcene, farnesol farnesene, perillyl alcohol, cardanol benzoxazines, squalene, and eugenol allyl ether have applications in removing heavy metals like mercury (Hg) and lead (Pb) from water.[40]

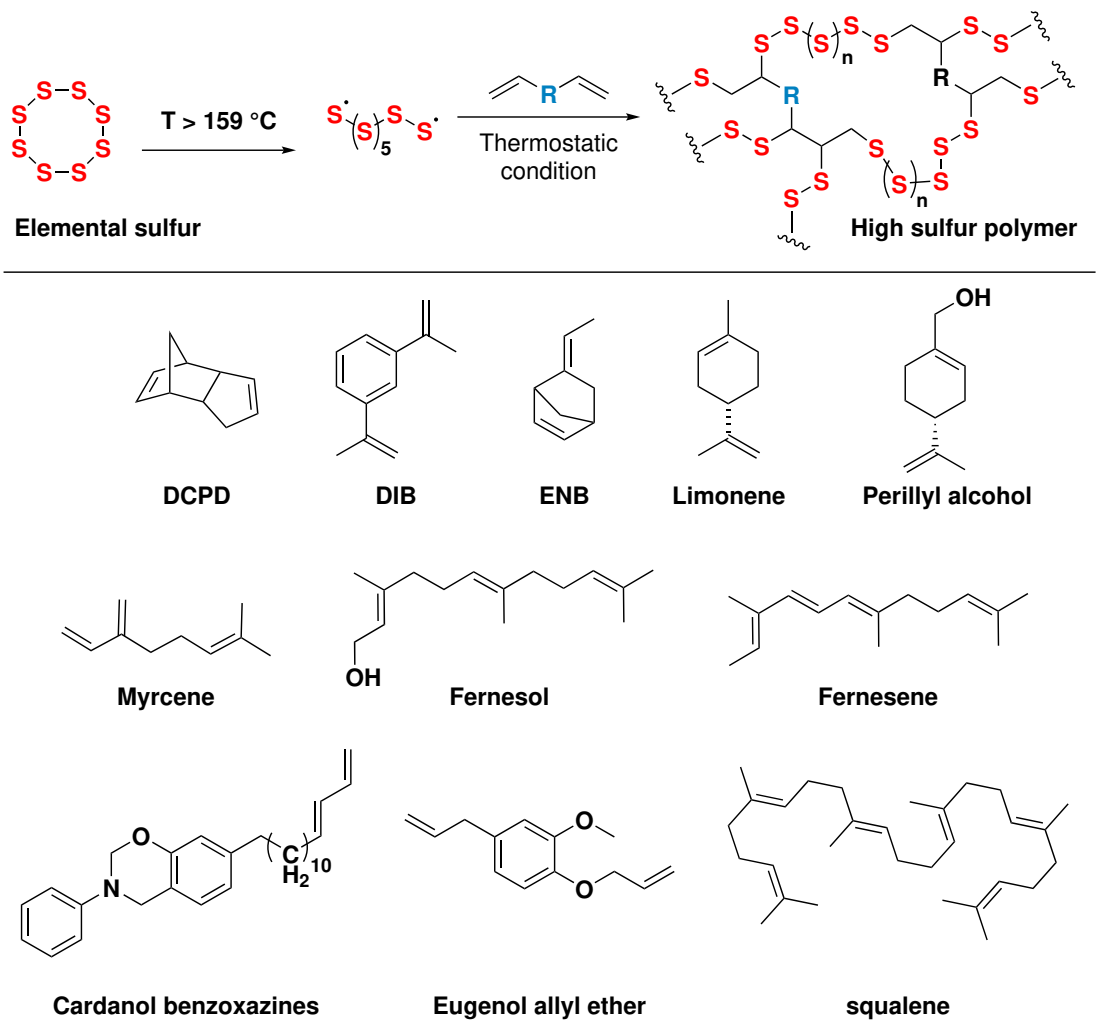

Figure 1.6 Polymerization reaction of elemental sulfur.

Sulfur can act as a **catalyst** in two ways in organic reactions (Figure 1.7). The first way involves pure elemental sulfur acting as the catalyst, such as in the preparation of dihydrooxazoles, quinolines, symmetrical urea, and, 2-oxazolidinones. The second way involves elemental sulfur and a metal working together as a catalyst, such as the iron-sulfur [Fe_8S_7] cluster, which is an active site in the redox transformation of atmospheric nitrogen to ammonia.[41] In organic synthesis, the Fe-S cluster transforms o-nitroaniline and 4-picolines into benzimidazole.[42] When combined with aliphatic alkyl amine, the Fe-S catalyst performs even better, allowing the synthesis of a wide variety of benzimidazoles.

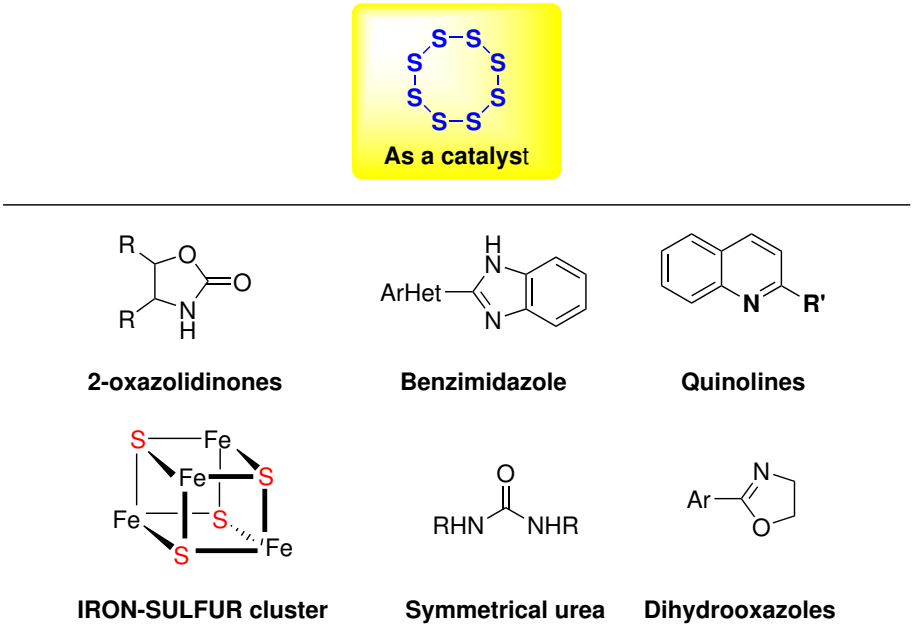

Figure 1.7 Role of elemental sulfur as a catalyst.

Last but not least, sulfur play major role as a **oxidant** or **reductant** in organic synthesis (Figure 1.8). Elemental sulfur acts as an oxidant in the preparation of compounds such as imidazo[1,5]pyridines, 2-substituted benzazoles, benzimidazole, benzothiazole, quinoxalines, di and triarylpyrazoles.[43–45] While in preparation of compounds such as, pyrroles, aniline, benzofurazan and benzotrifurazan[46] sulfur behave as a reducing agent.

Overall, the role of elemental sulfur in organic reactions depends on the specific reaction and the desired outcome. Its versatility and ability to participate in various types of reactions make it a useful reagent in organic chemistry.

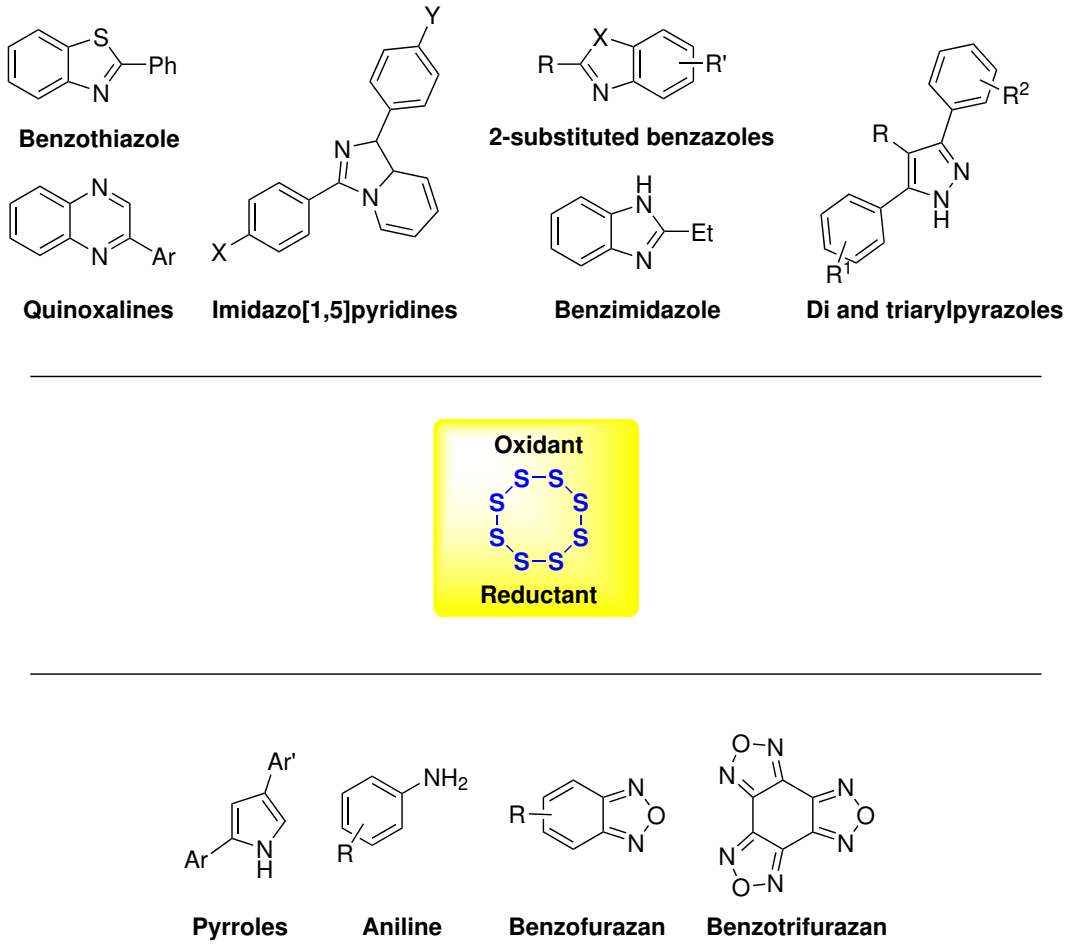

Figure 1.8 Role of elemental sulfur as a oxidant and reductant.

1.7 Understanding the Behavior of Sulfur with Various Nucleophiles

The most stable orthorhombic form of sulfur (S_8) participates in organic reactions. *This work focuses on chemical activation, in which elemental sulfur acts as an electrophile and can be activated or opened by different nucleophiles.* S_8 rings can open through the S_N2 reaction with nucleophiles and form polysulfides. Nevertheless, the presence of various nucleophiles under comparable conditions yields dissimilar sulfur products, and the connection between them remains indistinct. Below, we have discussed the fact that despite the unpredictable nature of sulfur, there are numerous organic transformations that utilize it, and these have been extensively studied.

1.7.1 Sulfur ring opening by strong nucleophile

Strong nucleophiles, including acetylide,[47] allylic,[48] phenyl,[49] vinyl,[50] inorganic carbon anions such as cyanide,[51] and triphenylphosphine[52] are well used to activate elemental sulfur (Figure 1.9).

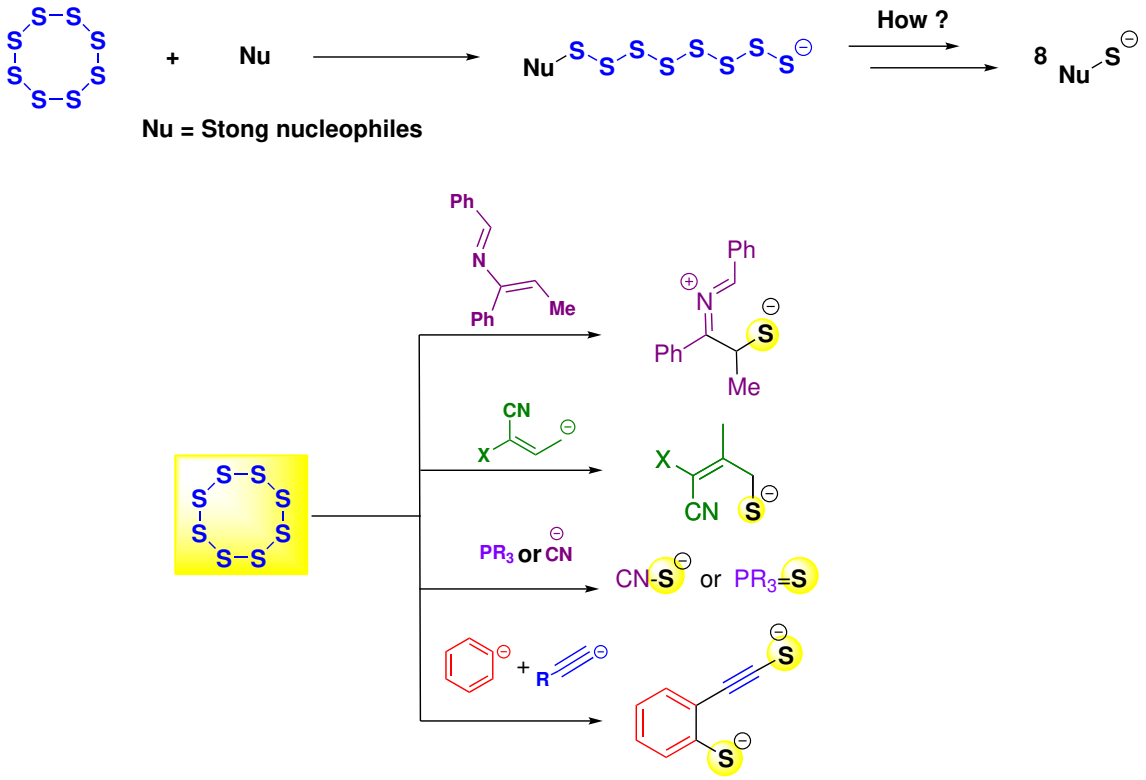

Figure 1.9 Monothio products from carbon nucleophiles with elemental sulfur.

While it is recognized that these nucleophiles can lead to the formation of monosulfide products from initial polysulfides, ***the precise reasons and mechanisms through which these reactions occur are not yet fully understood*** (Figure 1.9 -top part). The **Gewald reaction**, which is known for the synthesis of 2-aminothiophenes, proceeds via the reaction of elemental sulfur with a carbon nucleophile (Figure 1.9 - green nucleophile), the mechanism of which is still unknown.

1.7.2 Sulfur ring opening by oxygen nucleophile

Compared to nucleophiles containing carbon, oxygen-containing nucleophiles, including hydroxides, and alkoxides, exhibit distinct behavior (Figure 1.10).[50, 53–56]

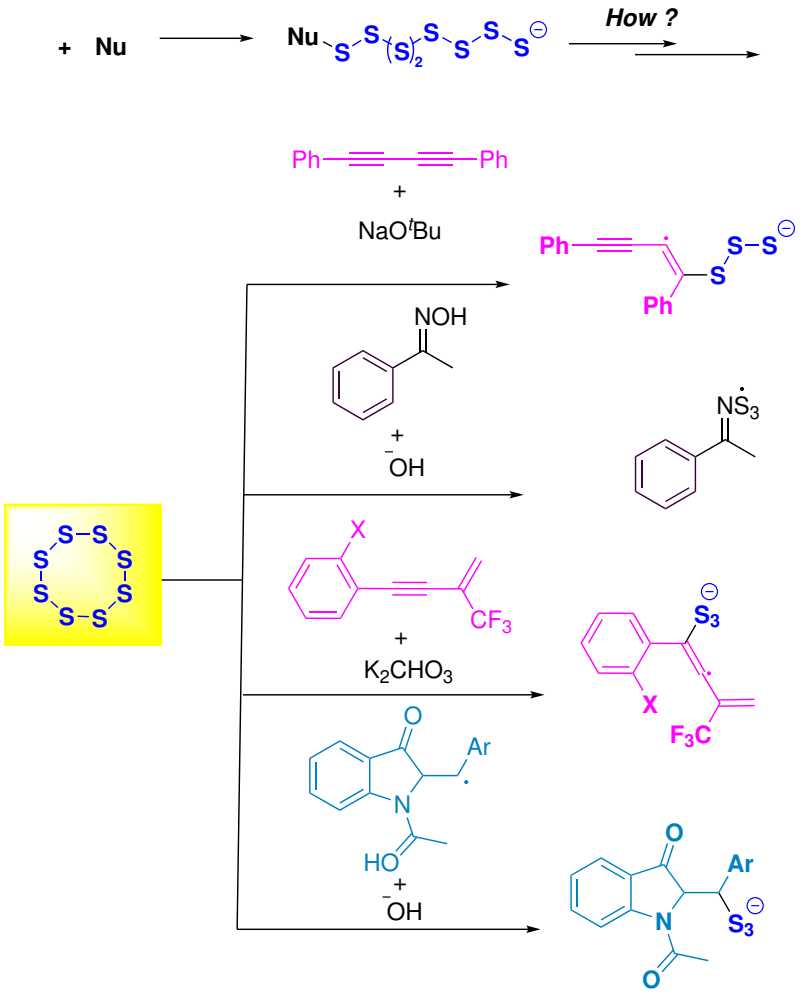

Figure 1.10 Trisulfur radical anion intermediate formation oxygen nucleophiles with elemental sulfur.

They generate trisulfur radical anions ($S_3^{\bullet -}$) in a solution from their corresponding polysulfides. ***Nevertheless, the precise reasons and mechanisms underlying the production of $S_3^{\bullet -}$ remain incompletely understood.*** The presence of $S_3^{\bullet -}$ in the solution has been verified using techniques such as electron paramagnetic resonance (EPR) spectroscopy and the use of radical scavengers like

(2,2,6,6-tetramethylpiperidin-1-yl)oxyl (TEMPO).[50, 54, 55, 57, 58] Trisulfur radical anions give rise to blue chromophores in ultramarine blues.

1.7.3 Sulfur ring opening by nitrogen nucleophile

Elemental sulfur exhibits reactivity towards primary and secondary amines at standard room temperature, while higher temperatures are required for its reaction with tertiary amines. The reaction of S_8 with liquid ammonia is well-known.[59]

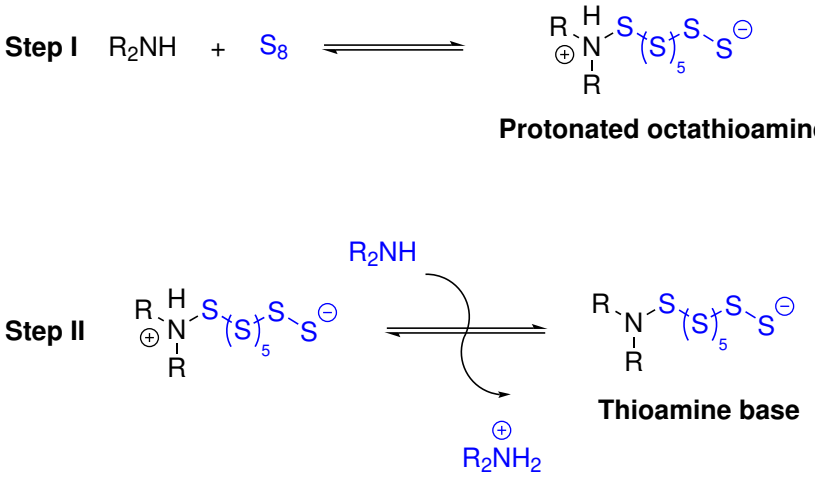

Figure 1.11 Reaction of secondary amine with elemental sulfur.

The nitrogen atom is more electronegative than carbon and phosphorous, which makes it unlikely to donate electrons to sulfur. The hydrogen atom on the amine is the driving force behind this reaction, producing a thioamine base as the final product. The reaction occurs in two steps, the first being a slow step that generates protonated octathioamine, which acts as a strong acid. The second step is fast and produces the thioamine base (polysulfide) in the presence of a second molecule of amine (Figure 1.11). A previous study showed the presence of different sulfur ionic species originating from various amine sources. For example, when elemental sulfur was dissolved in a primary amine, $[S_3]^-$ was found abundantly, along with some other polysulfides.[60] On the other hand, in the presence of a secondary amine, fewer ionic species were observed compared to a primary amine, and the presence

of polyoctasulfide $[S_8]^{n-}$ was reported.[61] The reaction of a tertiary amine with elemental sulfur has been thoroughly explored, and it has been hypothesized that $[S_8]^{n-}$ is the dominant species that takes part in the reaction (Figure 1.12).[62–65] Nevertheless, ***the precise mechanism behind the exceptional stability and non-degradability of polysulfides remains currently unknown.***

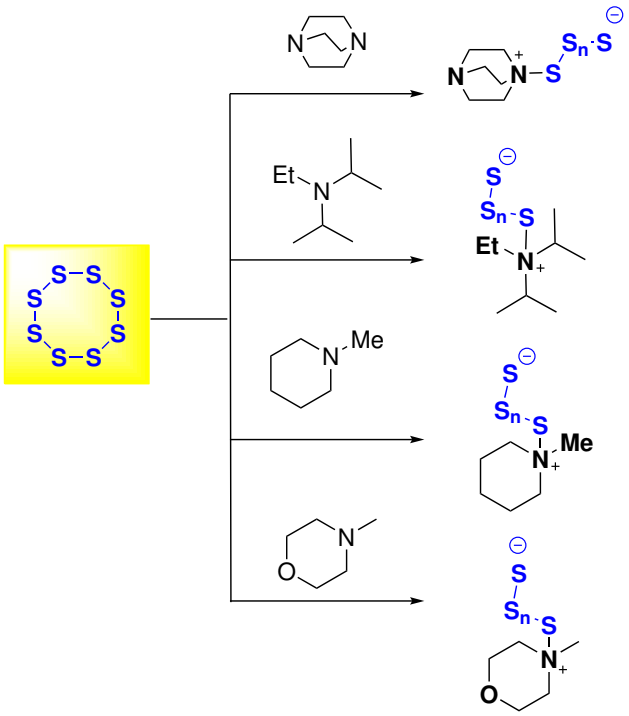

Figure 1.12 Polysulfide formation from nitrogen nucleophiles with elemental sulfur.

1.7.4 Sulfur ring opening by sulfur nucleophile

The significance of the sulfur opening by a sulfur nucleophile in physiological function is attributed to the generation of the signaling molecule H_2S in the presence of biological thiols, such as reduced glutathione (GSH) or cysteine (Cys) (Figure 1.13).[66] In 1966, Vineyard extensively discussed the mechanism of elemental sulfur opening by thiol in an alkali solution. This reaction gives rise to the formation of persulfide, trisulfide, and tetrasulfide, along with the production of H_2S.[67] Among these species, the predominant one is persulfide, which plays a crucial role in H_2S

generation. ***Nevertheless, the precise mechanism underlying the formation of H_2S remains inadequately investigated.***

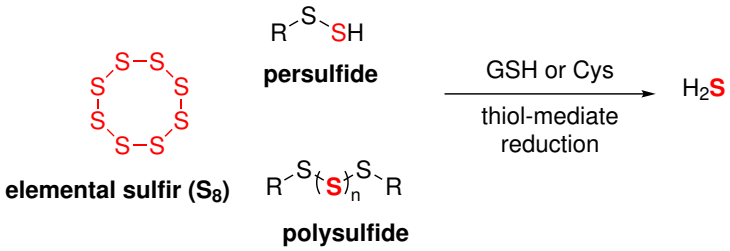

Figure 1.13 Biological Thiols: Catalyzing Hydrogen Sulfide (H_2S) Liberation via Reactivity with Sulfur-Containing Small Molecule Species (S^0).

Developing a thorough understanding of how sulfur reacts with nucleophiles is necessary for more researchers to take advantage of sulfur's significant potential. Nevertheless, the polysulfide generated from elemental sulfur is a highly reactive and transient species, making it difficult to study experimentally due to its unstable nature. Consequently, the well-known reaction of elemental sulfur in organic synthesis remains unknown. Computational chemistry could play a significant role in revealing the unknown mechanisms involved and would be helpful in understanding and potentially designing new sulfur reactions.

1.8 Focal Theme of the Dissertation

This chapter describes the brief history, role, chemical reactions, and applications of elemental sulfur. The objective of this dissertation is divided into two parts. Our first goal is to understand the behavior of sulfur with different nucleophiles and to solve the unknown reaction mechanism of some well-known reactions where sulfur is a key component, using density functional theory (DFT). The second goal of this dissertation is to synthesize sulfur-based organic compounds. Next, a brief description of each chapter is given.

- In the Chapter 2 of the dissertation, a benchmark of various DFT methods is done to identify the best method for the subsequent studies.
- In the third Chapter, using the best DFT method identified in Chapter 2, the behavior of phosphine and cyanide nucleophiles with elemental sulfur is investigated.
- In the fourth Chapter, the mechanism of the Gewald reaction for the synthesis of 2-aminothiophene is studied, as this reaction is widely used in medicine and pharmaceuticals. In Gewald reaction elemental sulfur is a key ingredient. Nevertheless, the reaction mechanism is still unknown.
- Hydrogen sulfide (H_2S) plays a significant role in the human body. Cysteine and glutathione persulfides (CysSSH and GSSH) are major sources of H_2S in cells. These persulfides release H_2S in the presence of thiol, In the fifth Chapter, mechanism of H_2S release from persulfide and its derivatives, is explored computationally.
- In Chapter 6, the dissertation includes an experimental section, where the synthesis of thiols using a boron source is explored and the synthesis of 2-substituted benzothiazoles using an aryne and imine precursor is investigated.
- The concluding section of a dissertation serves as the summary of the research and future work.

CHAPTER 2

BENCHMARK OF DENSITY FUNCTIONAL THEORY METHODS FOR THE STUDY OF ORGANIC POLYSULFIDES

This chapter was published as "Benchmark of Density Functional Theory Methods for the Study of Organic Polysulfides". (Sharma, J.; Champagne, P. A., Benchmark of density functional theory methods for the study of organic polysulfides. Journal of Computational Chemistry 2022, 43 (32), 2131-2138)

2.1 Introduction

In its elemental form, sulfur is an abundant material with widespread applications in organic, pharmaceutical, and materials chemistry. One of the major uses of sulfur is in manufacturing Li-S batteries, which are promising candidates for next-generation batteries that use sulfur as cathode material.[68–70] Indeed, sulfur is a low-cost and nontoxic powder with high energy storage density. Another significant use of sulfur is in the form of polysulfides, which have wide applications in polymer industries.[71] Along with these applications, sulfur plays an essential role in organic synthesis, as it can participate as a source of sulfur atoms, oxidant, reductant, catalyst, and several other roles.[31, 32] Nevertheless, the catenation property of sulfur leads to seemingly unpredictable behavior, which has been an obstacle to its widespread usage despite its availability at a cheap price. In spite of its complicated behavior, many organic transformations are known using elemental sulfur; but, their proposed reaction mechanisms often lack in detail due to our current poor understanding of polysulfide reactivity.[31, 32] Generally, sulfur's participation in organic reactions is facilitated by the attack of nucleophiles which results in the opening of its most common allotrope cyclooctasulfur (S_8),[72] producing polysulfides that further generate various products.

There is a strong interest in understanding the behavior of sulfur and polysulfides with nucleophiles. Due to the complexity of the equilibria involving polysulfides,[73] experimental determination of those mechanisms is difficult, which is why computational methods might allow for breakthroughs in this field. Density functional theory (DFT) has become a popular method for studying reaction mechanisms because of its right balance between accuracy and computational cost.[74] Nevertheless, since the performance of density functionals (DFs) is not uniform across all organic systems, there is no universally accepted DF. As far as polysulfides are concerned, only a limited number of prior benchmark studies devoted to assessing the accuracy of different approximations of the DFT exchange-correlation functional on such systems are reported. In 2009, Denk investigated geometries and the strength of the S-S bond in S_8 and disulfanes, using high precision thermochemical calculations (G_3, CBS-Q) and Boese-Martin (BMK) hybrid DFT.[75] Similarly, in 2017, Truhlar and coworkers benchmarked 39 DFT functionals for various isomers of lithium polysulfides (Li_nS_n,$2 \leq n \leq 8$) formed in the charging and discharging processes of lithium-sulfur batteries.[76] They concluded that meta-GGA (generalized gradient approximation) and doubly hybrid GGA methods perform better for binding and relative energies. Nevertheless, both works showed that the popular B3LYP functional is not ideal. In 2020, Hu and coworkers published CCSD(T) binding and deprotonation energies for inorganic polysulfides (HS_nH, $[HS_n]^-$, ${S_n}^{2-}$) and found that ωB97X-D was the most accurate functional.[77]

By design, these studies could not identify a DFT method that would be well suited to study elemental sulfur, organic polysulfides, and their transition structures when reacting with nucleophiles. Nevertheless, studying the mechanisms of organic reactions involving polysulfides would clarify the role that these intermediates play in organic synthesis and biochemical processes. We now report a benchmark of 12 popular DFT functionals against DLPNO-CCSD(T) (domain-based local pair-natural

orbital coupled-cluster) energies obtained on the MP2 (Møller–Plesset) optimized geometries of polysulfide structures related to nucleophilic reactions. In addition, structural and energy parameters extracted from minima and transition structures (TS) were analyzed to identify ideal DFT methods for the study of polysulfide mechanisms.

2.2 Methodology and Computational Details

We chose the reaction of cyanide with sulfur as the model system (Figure 2.1) since it is representative of the reaction of other strong nucleophiles (such as carbanions) with sulfur.[31, 32, 51] The first step in this transformation is the nucleophilic opening of the cyclooctasulfur (S_8), forming the anionic $[S_8CN]^-$ polysulfide (reaction A), which is believed to be rate-determining. An important feature of polysulfide reactivity with nucleophiles is that various products are formed depending on the nucleophile, as for example phosphorus and carbon-based nucleophiles give monosulfides as the final product,[51, 52] while hydroxide gives trisulfur radical anion as product.[78] As in all cases the initial opening of S_8 is rate-determining, it results that the product determining steps are also kinetically-invisible and thus unknown. This is why in this study we compared our results to high-accuracy ab initio values instead of experimental results, and proposed some unexplored but plausible pathways. The two pathways we modeled for the formation of thiocyanate (NCS^-), the known product of sulfur's reaction with cyanide, are the intermolecular cleavage by another cyanide (reaction B) and the intramolecular cleavage leading to cycloheptasulfur (S_7, reaction C). To consider the potential intermolecular attack on another sulfur atom of the polysulfide intermediate, we also modeled the formation of two $[S_4CN]^-$ polysulfides from $[S_8CN]^-$ with cyanide (reaction D). We also considered the intermolecular attack leading to the hexasulfur dianion ${S_6}^{2-}$ and $S_2(CN)_2$ (reaction E), as this dianion is a known precursor to the trisulfur radical anion ${S_3}^{-\cdot}$, a common product from

the reaction of sulfur with nucleophiles.[79] The subsequent homolytic cleavage of S_6^{2-} (reaction F) was also considered, although its open-shell singlet character led to complications (see below). Finally, to check the relative stability of the S_8 and S_6 allotropes, reaction energies of their interconversion were also considered (reaction G).

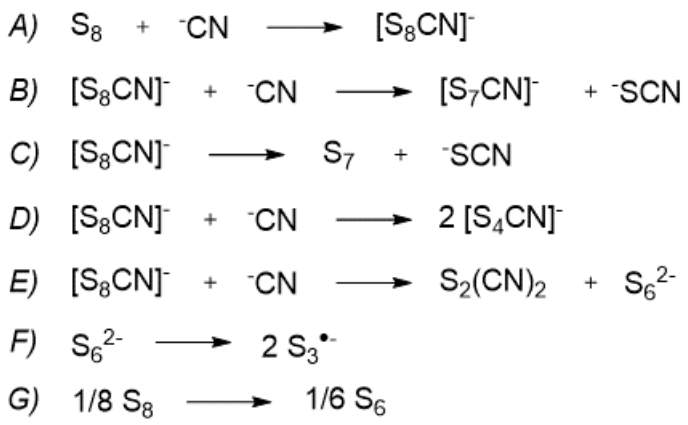

Figure 2.1 Studied transformations involved in the reaction of elemental sulfur and polysulfides with cyanide.

2.2.1 Geometry optimization

Geometry optimizations and frequency calculations of the considered ground state (GS) (Figure 2.2) and transition state structures (TS, if possible) (Figure 2.3) were performed with Gaussian 16 using the Møller-Plesset second-order perturbation theory (MP2) method with a tight-d-augmented triple-zeta basis set, necessary for obtaining good results on sulfur-containing molecules.[80, 81] Solvation effects were considered using the SMD implicit solvation model[82] for acetonitrile (ϵ = 35.69). Large solvation effects are anticipated since anions, dianions, and radicals are considered; thus, solvated structures were expected to correlate better with experimental results, which employed polar solvents.

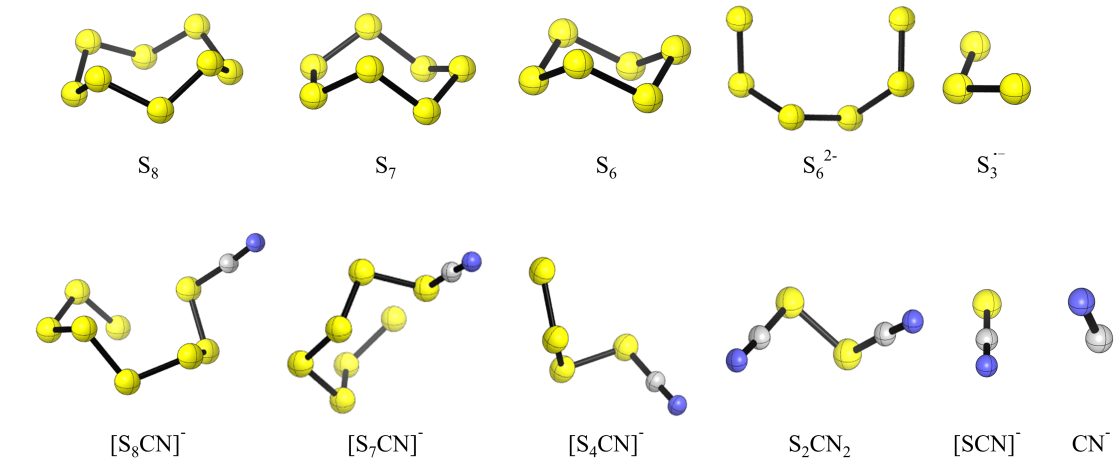

Figure 2.2 Ground state (GS) structures considered for this work, optimized at the MP2/aug-cc-pV(T+d)Z/SMD(MeCN) level of theory.

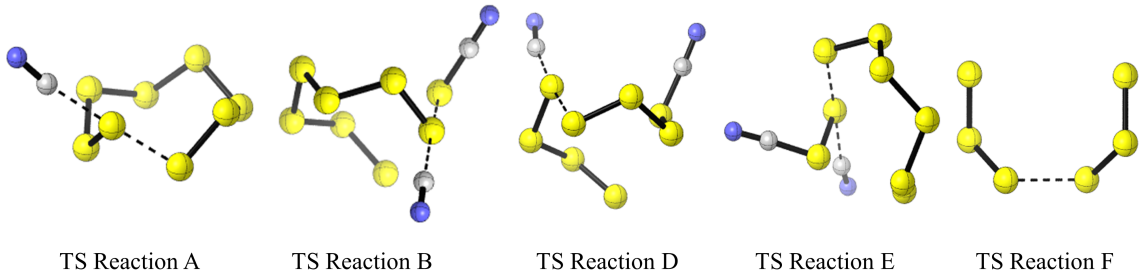

Figure 2.3 Transition structures (TS) considered for this work, optimized at the MP2/aug-cc-pV(T+d)Z/SMD(MeCN) level of theory.

2.2.2 Single-point energy calculation

Single-point energy (SPE) refinements on the MP2-optimized structures were obtained at the DLPNO-CCSD(T)[83–85] level of theory with the aug-cc-pV(Q+d)Z basis set (Tables S13–S16). Due to its prohibitive computational cost, the "gold standard" CCSD(T) method was not used as reference. Nevertheless, DLPNO-CCSD(T) is able to retain approximately 99.9 % of the canonical CCSD(T) correlation energy, with a computational cost comparable to DFT.[86] Calculations were performed both for the gas phase or using the SMD solvation model for acetonitrile. When reported, the final free energies were obtained by adding the free energy corrections obtained at the MP2 level to the electronic energies obtained with DLPNO-CCSD(T). Those SPE calculations were performed using ORCA with the "Tight PNO" as well as

with "Normal PNO" settings. For the benchmarking calculations presented below, Tight PNO was taken as a reference due to its reported better accuracy over normal PNO,[86] although the difference between these results and those from normal PNO were small in our case (Tables S78 and S79).

2.2.3 Assessment of density functionals

We selected 12 popular functionals for benchmarking, including some of the best methods identified in Wang and Truhlar's study.[76] All DFT optimizations were performed with Gaussian 16, employing the aug-cc-pVDZ basis set and the SMD solvation model for acetonitrile. Taking MP2-optimized structures as a reference, all structures were reoptimized, and their frequencies computed using two local functionals (MN15-L[87] and M06-L[88]) and six functionals with non-local exchange (B3LYP,[89],[90] M06-2X,[91] MN15,[92] PBE0,[93] TPSSh,[94] and mPW1PW91 [95]). To test the influence of dispersion corrections in these systems, we also considered four functionals with explicit dispersion corrections (B3LYP-D3(BJ),[96] B97D3,[97] ωB97X-D,[98] and PBE0-D3(BJ)[99]). All energies and thermochemical corrections can be found in Tables S1–S12. In order to compare the ability of DFT methods for reproducing high accuracy geometries, we identified a set of key structural parameters that were extracted from the structures, including bond lengths, angles, and dihedrals (Tables S65–S77). Of note, the MP2 geometries exactly reproduce known x-ray crystallography experimental values for sulfur allotropes (which were also used as standard in previous computational studies of such structures),[100] indicating the accuracy of this method (Table 2.1). Taking the MP2 structural data as reference, the average relative percentage error was calculated for the DFT-optimized structures. The energy accuracy of DFT functionals for reproducing activation and reaction energies with or without free energy or solvation corrections was evaluated in four instances (Tables S17–S64). In all cases, the DFT

results were compared to the DLPNO-CCSD(T)/aug-cc-pV(Q+d)Z//MP2/aug-cc-pV(T+d)Z/SMD(MeCN) values, considered standard.

Table 2.1 Comparison of MP2-optimized Structural Data with Existing x-ray Crystallography Data (S_8 [3], S_7 [101] and S_6 [102])

Structures	S-S bond length (Å) (x-ray)	Dihedral angle (°) (x-ray)	S-S bond length (Å) (MP2)	Dihedral angle (°) (MP2)
S_8	2.05	98.5	2.05	99.2
S_7	2.18, 2.05	-75.2	2.19, 2.04	-75.6
S_6	2.05	74.5	2.05	74.2

In the first instance, the electronic energies obtained from DFT/aug-cc-pV(T+d)Z SPE refinements on the MP2-optimized structures were compared to DLPNO-CCSD(T) values. Second, the electronic and free energies obtained directly from geometry optimization and frequency calculation using DFT/aug-cc-pVDZ/SMD (acetonitrile) were compared to the high-accuracy values. In the third and fourth instances, the electronic and free energies obtained from DFT/aug-cc-pV(T+d)Z SPE refinements on DFT-optimized structures were compared to DLPNO-CCSD(T) values. Of note, the average percentage error for imaginary frequencies was only compared with MP2 results (see Supporting information), since it would be impractical to perform frequency calculations for our system using DLPNO-CCSD(T).

2.3 Results and Discussion

We first obtained the Gibbs free energies of activation and reaction for the seven considered reactions with the two ab initio methods DLPNO-CCSD(T) and MP2 (Table 2.2). Due to the highly exergonic nature of the formation of S_7 and $^{-}$[SCN]

(reaction C), we could not locate the presumably early TS. For the cleavage of S_6^{2-} to $S_3^{-\cdot}$, we could not obtain DLPNO-CCSD(T) corrections due to the limitations in the current implementation, so we include MP2 values. In all cases, we notice that the MP2 free energies are consistently underestimated versus the DLPNO-CCSD(T) values, confirming the need for single-point energy refinements. Of note, the computed enthalpy of activation for reaction A from DLPNO-CCSD(T) (9.1 kcal/mol) matches with the experimentally measured enthalpy of activation for the reaction of S_8 with cyanide,[51] which is consistent with the idea that the first opening of sulfur is the rate-determining step in this reaction.

Table 2.2 Activation and Reaction Free Energies (kcal/mol) for the Considered Reactions at the DLPNO-CCSD(T)/aug-cc-pV(Q+d)Z/SMD and MP2-/aug-cc-pV(T+d)Z/SMD Levels

Reaction	$\Delta G^{\ddagger}$ DLPNO-CCSD(T)	ΔG_{rxn} DLPNO-CCSD(T)	$\Delta G^{\ddagger}$ MP2	ΔG_{rxn} MP2
A	19.1 (9.1)[a]	13.0	14.8 (4.9)[a]	7.7
B	14.7	-19.5	11.6	-22.6
C	–	-25.5	–	-24.5
D	23.0	-2.5	18.5	-4.2
E	23.0	15.8	17.3	12.4
F	–	–	21.7	-0.3
G	–	0.5	–	0.6

[a]Enthalpy of activation($\Delta H^{\ddagger}$).

2.3.1 Performance of density functionals for geometry optimization

While the DFT geometries overall match well with the MP2 structures, none of the considered DFT methods accurately reproduced the MP2 geometry for the TS leading

to S_3 radical anion from S_6^{2-}, instead optimizing to long S-S bond distances and weak imaginary frequencies.

Table 2.3 Average Error (%) on the Set of Structural Parameters for DF-optimized Ground State (GS) and Transition State (TS) Structures Versus MP2

Functional	GS structures	TS structures
MN15-L	1.4	2.0
M06-L	1.6	6.2
B3LYP	2.2	3.6
M06-2X	1.4	1.8
MN15	0.8	3.2
PBE0	1.1	2.4
TPSSh	1.9	2.3
mPW1PW91	1.2	2.4
B3LYP-D3(BJ)	2.3	3.6
B97D3	2.9	3.5
ωB97X-D	1.3	2.5
PBE0-D3(BJ)	1.0	2.6

Whether that issue arises from an inaccurate MP2 structure or a systematic error in DFT for open-shell singlet homolytic cleavages will need to be investigated. To avoid tainting the rest of the data, we did not consider that TS in our analysis, although the data can still be found in the Supporting information. As shown in Table 2.3, both local functionals showed good agreement for GS structures, while M06-L displayed the largest error for TS structures (6.2 %) of all considered methods. For functionals with nonlocal exchange applied to GS structures, MN15 performs best with 0.8 % of error. PBE0, mPW1PW91, and M06-2X also performed well with less than 1.5 % error, while TPSSh and B3LYP showed slightly larger errors. For

TS structures, the M06-2X functional is superior to others, although most methods provide reasonable results. For functionals with explicit dispersion, ωB97X-D and PBE0-D3(BJ) perform the best for both GS and TS. Notably, addition of a dispersion correction does not always improve the results. While many of the bestperforming methods contain such a correction (M06-2X, ωB97X-D, PBE0-D3(BJ)), this is not a requirement for accurate results (see PBE0, MN15-L) and some dispersion-corrected functionals do not seem to benefit from the correction (B3LYP-D3(BJ), B97D3).

2.3.2 Energy results from DFT SPE on MP2 optimized structures

To assess the accuracy of DFT methods on a single set of structures, we compared the DFT single-point electronic energies on the MP2 geometries to the DLPNO-CCSD(T) results, also obtained on the MP2 geometries (Figure 2.4 and Tables S80–S129). Our results from the local functionals show that, with a solvation model, MN15-L and M06-L perform similarly for activation energy, while for reaction energies MN15-L performed better. For the gas phase, M06-L performed better for activation energies, with an average error of 0.6 kcal/mol, while MN15-L performed better for reaction energies. In the category of functionals with non-local exchange, M06-2X is superior with an error of only 1.0 (gas) and 1.5 (SMD) kcal/mol for reaction energies. All non-local functionals perform well for activation energies with or without solvation corrections with less than 1.5 kcal/mol of error, except B3LYP, which also shows the largest error in reaction energies. For dispersion-corrected functionals, all four of them performed well for both reaction and activation energies with or without solvation, with B3LYP-D3(BJ) performing the best. It was noted that M06-2X, MN15, and B3LYP-D3(BJ) performed best among all 12 DFT functionals.

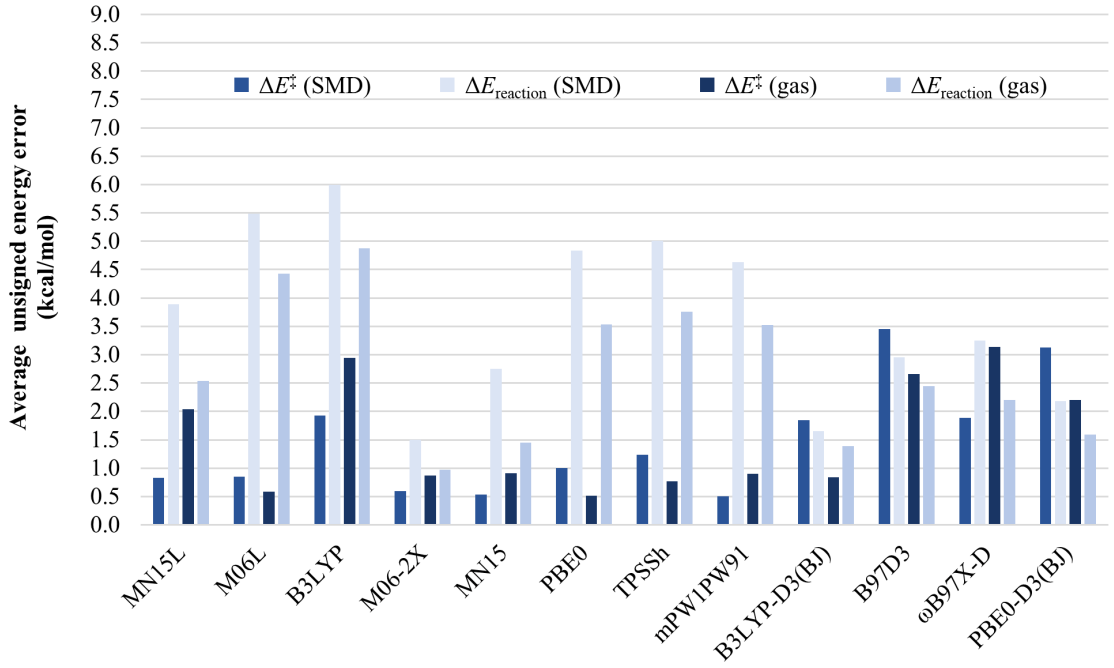

Figure 2.4 Average DFT/aug-cc-pV(T+d)Z single point reaction and activation electronic energy errors (kcal/mol) on MP2-optimized structures, when compared to DLPNO-CCSD(T)/aug-cc-pV(Q+d)Z.

Overall, most methods seem adequate for the treatment of activation energies, with B97D3 providing the largest error. Nevertheless, dispersion-corrected functionals seem essential for the accurate treatment of reaction energies. Looking at the individual reactions, we noted that the high average reaction energy errors for functionals that do not include dispersion are due to an inaccurate treatment of reaction D, as the energy of the $[S_4CN]^-$ polysulfide is overestimated (Tables S130–S133). The effect of solvation is also moderate. Although the activation and reaction energies are significantly different with or without the solvation model, there is a limited difference between the errors computed.

2.3.3 Performance of density functionals for energy results from DFT optimized structures

We then compared the DLPNO-CCSD(T) results to those obtained directly from DFT optimization and frequency calculation. As those calculations are performed

with a double-ζ basis set, we expected larger errors. Indeed, most methods provided average errors in excess of 3.0 kcal/mol (Figure 2.5 and Tables S80–S129). Of the tested local functionals, MN15-L performed better for both reaction and activation free energies with errors of 6.6 and 1.5 kcal/mol, respectively. In contrast, M06-L performed worst with an average error of 8.5 and 4.1 kcal/mol.

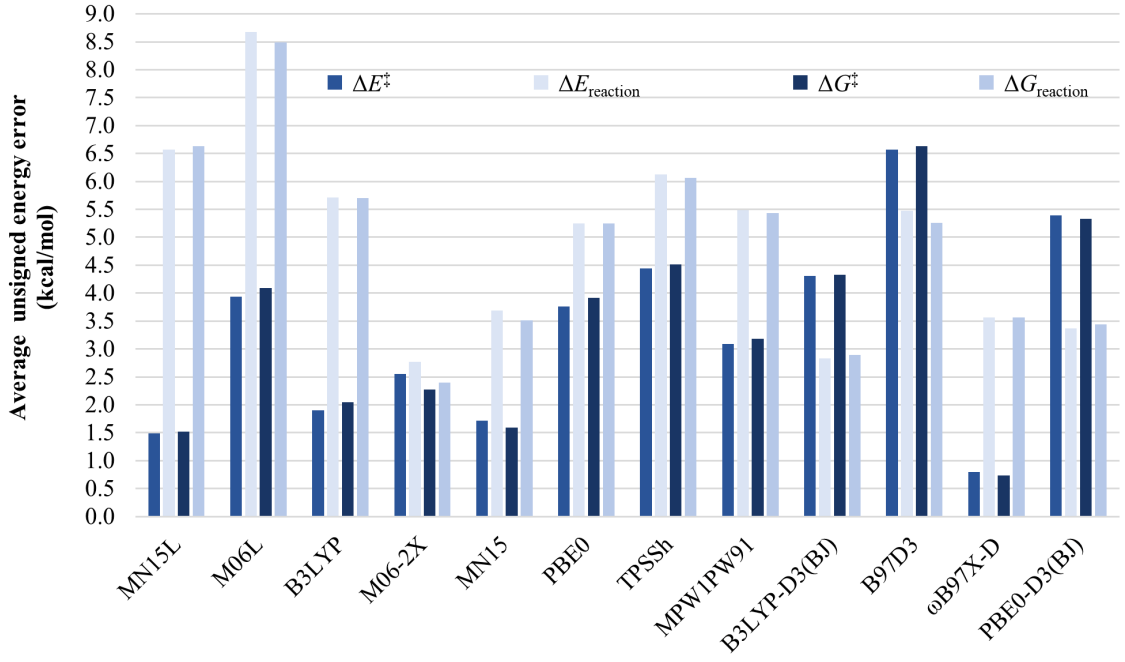

Figure 2.5 Average DFT/aug-cc-pVDZ reaction and activation energy errors (kcal/mol), when compared to DLPNO-CCSD(T)/aug-cc-pV(Q+d)Z/SMD(MeCN).

In the functionals with non-local exchange, the trends for reaction and activation free energies were not identical. The M06-2X functional performed best for reaction free energies with an average error of 2.3 kcal/mol among all 12 DFT functionals. For activation free energies, the MN15 functional is superior with an error of 1.6 kcal/mol. In the four functionals with explicit dispersion, B3LYP-D3(BJ) performed better than other functionals with an error of 2.9 kcal/mol for reaction free energies. For activation free energies, ωB97X-D performed best among all functionals, with an error of 0.7 kcal/mol. In order to determine if the free energy corrections had an impact on the errors, we also compared the electronic energies with DLPNO-CCSD(T) and found

that they follow the same trends as shown for free energies. These results, compared to those obtained with SPE refinements with a larger basis set (see below), serve as a reminder that although geometry optimizations and frequency calculations are usually performed with a double-ζ basis set in organic mechanistic studies, electronic energy refinements with a triple-ζ basis set are required for accurate results.

2.3.4 Energy results from DFT SPE on DFT optimized structures

The most relevant workflow for a computational study of organic mechanisms would involve refining the electronic energies with a triple-ζ basis set after optimization with a smaller basis set. We thus compared the results of DFT SPE on DFT-optimized structures to the DLPNO-CCSD(T) values both for the gas phase as well as with solvation. The results for electronic energies are shown in Figure 2.6 and the results with the free energy corrections are shown in Figure 2.7 (see Tables S80–S129). Overall, we found the results similar to the DFT SPE on MP2-optimized structures (Figure 2.4). This is not entirely surprising, considering all DFT methods reproduce the MP2 geometries relatively accurately. As expected, the average errors obtained with the larger aug-cc-pV(T+d)Z basis set are significantly smaller than those computed with the smaller aug-cc-pVDZ. As such, both local and non-local functionals provide good results for activation energies but large errors for reaction energies, again mostly due to an inaccurate prediction of the S_4CN anion formation as endergonic. M06-2X and MN15 both outperform the other methods from that category.

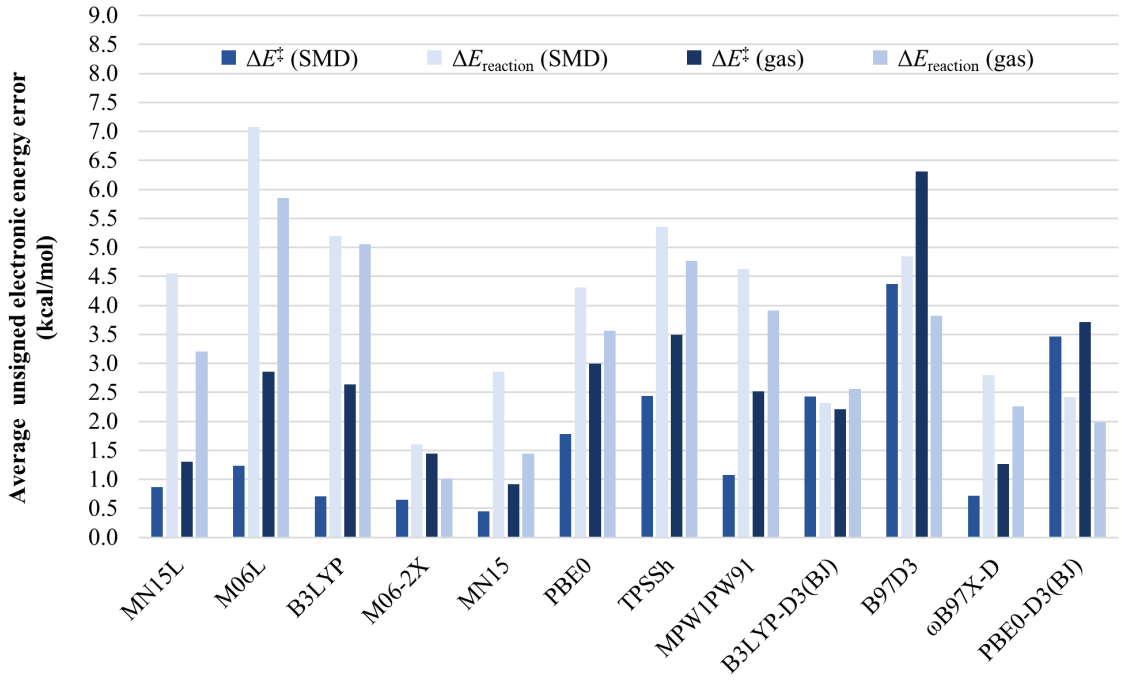

Figure 2.6 Average DFT/aug-cc-pV(T+d)Z single point reaction and activation electronic energy errors (kcal/mol) on DFT-optimized structures, when compared to DLPNO-CCSD(T)/aug-cc-pV(Q+d)Z.

When free energy corrections are included (Figure 2.7), both methods have comparable profiles, but for electronic energies (Figure 2.6) M06-2X displayed lower errors (only 1.0 and 1.6 kcal/mol for gas phase and SMD, respectively) than MN15 (1.5 and 2.7 kcal/mol for gas phase and SMD, respectively) for reaction energies. Functionals with explicit dispersion followed the same trend as found for the SPE on MP2 structures. Consistently, they performed among the best of the tested methods, providing improved results for activation energies and significantly lower errors for reaction energies. It was also noticed that the reaction energy errors are in general lower for the gas phase as compared to the solvation model, while activation energy errors followed the opposite trend. In addition, the difference in error for electronic energies versus free energies is minimal, and the application of free energy corrections to the SPEs does not impact the results significantly. For an accurate and consistent treatment of both reaction and activation (free) energies, B3LYP-D3(BJ), ωB97X-D,

M06-2X, and MN15 provide the best results out of the 12 DFT functionals tested. The significant average error of the uncorrected B3LYP functional for reactions energies is in line with the previous benchmarks that had identified issues with this method, but for activation energies, it shows a excellent performance.

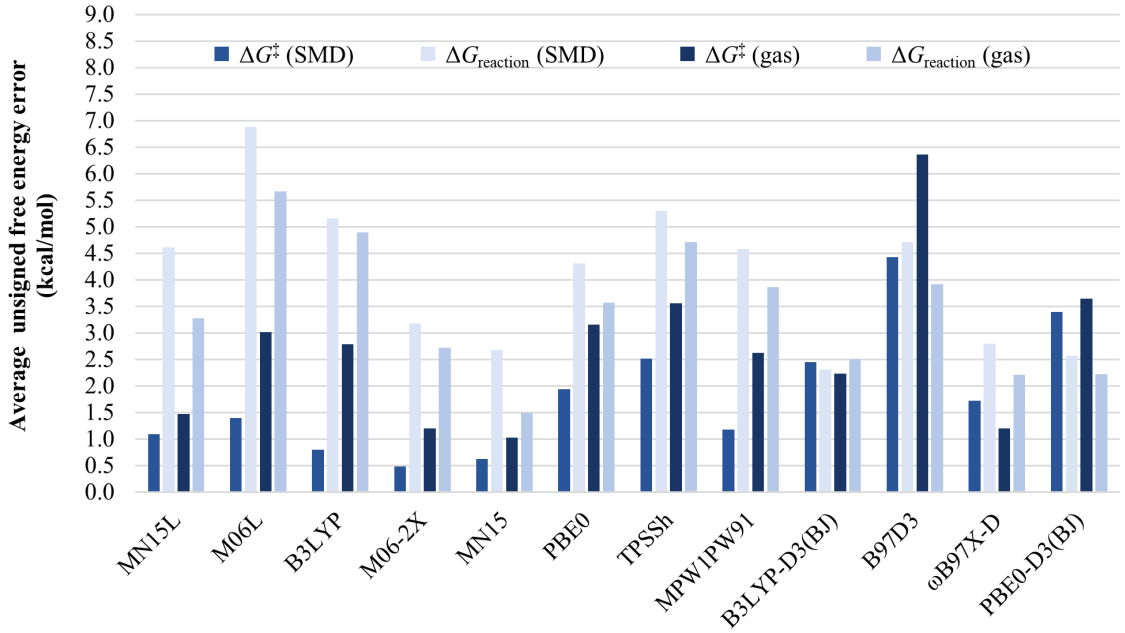

Figure 2.7 Average DFT/aug-cc-pV(T+d)Z single point reaction and activation free energy errors (kcal/mol) on DFT-optimized structures, when compared to DLPNO-CCSD(T)/aug-cc-pV(Q+d)Z

2.4 Conclusion

In this work, we studied various reaction pathways of elemental sulfur and polysulfides with cyanide and benchmarked 12 common DFT functionals versus MP2 geometries and DLPNO-CCSD(T) energies. It was found that most functionals provided ground state geometries in agreement with MP2, except B97D3 for which the errors were slightly larger. For TSs, MN15-L and M06-2X provided the best geometries, although all methods provided good results overall. In terms of singlepoint energies, we found that all considered functionals were able to reproduce DLPNO-CCSD(T) data on the MP2-optimized and DFT optimized structures with activation energy errors of at most 4.4 (SMD) and 6.4 (gas phase) kcal/mol (for B97D3). Furthermore, M06-2X,

MN15, and ωB97X-D performed best with less than 1.7 (SMD) and 1.2 (gas phase) kcal/mol activation (free) energy average errors, while most functionals showed less than 3.0 kcal/molof error. For reaction energy from single-point energies, the M06-2X and B3LYP-D3(BJ) functionals performed best with 1.6 and 2.3 kcal/mol of error, followed by the MN15 and ωB97X-D methods. Dispersion-corrected functionals show a more consistent error between reaction and activation energies, due to their more accurate energetic treatment of some polysulfides, while functionals without dispersion corrections show a larger error difference between reaction and activation (free) energies. Inclusion of the free energy corrections did not impact the results significantly. Globally, our results indicate that DFT can be appropriate for studying the reactions of sulfur and polysulfides, especially considering that it is impractical to optimize geometries with MP2 and the triple-zeta basis set due to their high computational cost. Instead, for mechanistic investigations the structures can be optimized using DFT and a double-zeta basis set, as long as SPE refinements are performed with larger basis sets subsequently. The use of dispersion corrections is recommended to avoid large errors for some polysulfide ground state structures. Based on our results, M06-2X, B3LYP-D3(BJ), ωB97X-D, and MN15 appear as good candidates for such purposes. Our benchmarking work reported in this paper will allow researchers to start tackling the mechanistic study of sulfur and polysulfide mechanisms with confidence, which is currently underway in our group.

CHAPTER 3

MECHANISMS OF THE REACTION OF ELEMENTAL SULFUR AND POLYSULFIDES WITH CYANIDE AND PHOSPHINES

This chapter was published as "Mechanisms of the Reaction of Elemental Sulfur and Polysulfides with Cyanide and Phosphines". (Sharma, J.; Champagne, P. A., Mechanisms of the Reaction of Elemental Sulfur and Polysulfides with Cyanide and Phosphines. Chemistry–A European Journal 2023, e202203906.)

3.1 Introduction

Elemental sulfur is a major byproduct of petroleum processing for which scientists are searching for new and improved applications. Among those, sulfur and the related polysulfides have found a major role in organic synthesis (mostly as a source of sulfur atoms),[31, 32] materials science [36] (e.g., in polymers obtained through inverse vulcanization),[39, 103] and other areas such a lithium-sulfur batteries,[104, 105] simultaneously, polysulfides have recently been identified as important intermediates in biochemistry, related to the mammalian signaling agent H_2S.[106–109] As such, understanding the chemical properties of sulfur and polysulfides can provide critical insights in various fields of chemistry. Due to its rather unique catenation behavior, elemental sulfur has multiple allotropes, with the most stable being cyclooctasulfur (S_8).[72] Sulfur is mostly known for its reactivity as an electrophile, but the types of products obtained vary based on the nature of the nucleophile. Strong nucleophiles like phosphines,[52, 110] sulfite,[111] or cyanide [51, 112] provide monosulfide products exclusively. Similarly, carbon based nucleophiles usually provide products with the incorporation of a single sulfur atom, for example in the Gewald [113–115] or Willgerodt–Kindler[116] reactions.[117–122] Nitrogen-based nucleophiles are often proposed to open S_8 as part of complex mechanisms,[31, 32]

oxygen bases generate sulfur radical anions or thiosulfate,[123] while hydrogen sulfide and thiols react with sulfur to form complex mixtures of polysulfides.[67, 124–126] In most cases, the opening of S_8 by the nucleophile is believed to be rate-determining; therefore, the product-determining steps are kinetically invisible and thus still poorly characterized. Indeed, experimental investigations of polysulfide mechanisms are complicated by their thermodynamic instability[73, 127–129] and recent evidence shows that they interconvert faster than they are trapped by chemical probes.[130–132] As such, computational investigations seem uniquely-positioned to provide key mechanistic information to understand the seemingly unpredictable reactivity of sulfur and polysulfides under various conditions. The precise determination of the mechanism of these reactions would allow for greater predictability in the design of reactions involving sulfur and polysulfides and facilitate the study of biochemical polysulfides.[109, 133]

To tackle this problem, we decided to focus on the simple but representative reactions of sulfur with cyanide and phosphines, which generate the monosulfide products $^{-}$SCN (thiocyanate) or $R_3P{=}S$ (phosphine sulfides) quantitatively. The reaction of sulfur with phosphines was first reported in 1837[110] and the formation of the phosphine sulfide was shown to be almost instantaneous.[134] From 1955, Bartlett and coworkers reported kinetic studies on the reaction of elemental sulfur with triarylphosphines[52] and cyanide,[51, 112] where they provided strong evidence that the rate-determining step for the formation of the observed products is the bimolecular opening of the S_8 ring by the nucleophile. They proposed the mechanism shown in path A of Figure 3.1, which was first formulated by Foss.[111] In this proposal, the thiocyanate or phosphine sulfide is displaced by nucleophilic attacks on the adjacent sulfur of the progressively shrinking polysulfides, starting with the octasulfide **1**. Another proposal for the decomposition of the polysulfides came from Schmidt who argued, based on claims of resonance between sulfur atoms in polysulfide

chains, that the negatively-charged terminal sulfur was in fact the most electrophilic position and could be abstracted by the nucleophile (Figure 3.1- path B).[42] Due to limited experimental support for either mechanism, over the following decades both the Foss-Bartlett[135–138] and Schmidt[139] mechanisms were presented as correct in books and reviews of the topic. Since these reactions have fast rates and clean product profiles, they have found applications for the titration[112] or detection of elemental sulfur[140, 141] in complex biochemical settings. We now report a comprehensive computational study of these reaction pathways, which provides the first evidence that the Foss-Bartlett mechanism, albeit plausible, is an incomplete picture of the reactivity of polysulfides with cyanide or phosphines.

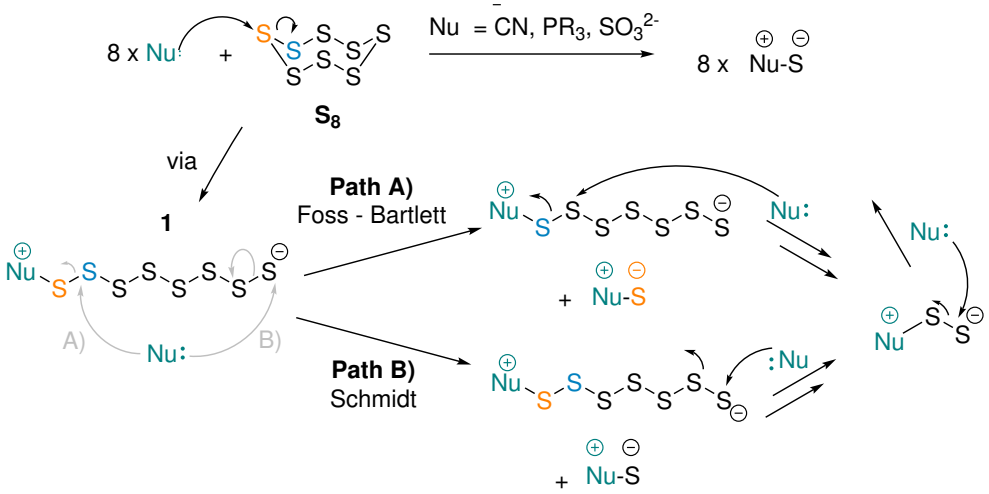

Figure 3.1 Proposed mechanisms of monosulfide formation via A) Foss-Bartlett and B) Schmidt pathways.

3.2 Computational Methodology

All Density Functional Theory (DFT) calculations were performed using Gaussian 16. The ωB97X-D functional[98] was selected as we have shown in our earlier work that it is one of the most accurate methods for studying the reaction of polysulfides with nucleophiles.[142] For geometry optimizations and frequency calculations, the aug-cc-pVDZ basis set was used. For polysulfides structures that are highly

conformationally flexible, the helix conformer was chosen as it was shown to be the lowest energy structure for similar polysulfides.[77] Single-point energy refinements were then obtained with various methods and the triple-zeta tight-d-augmented basis set aug-cc-pV(T + d)Z, necessary to obtain accurate energies for sulfur compounds.[81] All considered functionals (ωB97X-D, M06-2X, B3LYP-D3(BJ), MN15) agree on the conclusions of the study. At all stages, solvation effects were considered using the SMD solvation model for acetonitrile,[143] a representative polar solvent used in those transformations. The results presented in the main text are those obtained at the ωB97X-D/aug-cc-pV(T + d)Z/SMD(MeCN)//ωB97X-D/aug-cc-pVDZ/SMD(MeCN) level of theory. Full computational details are available in the Supporting Information. For the study of reaction pathways with phosphines, we selected trimethylphosphine (PMe_3) as a model to reduce computational costs.

3.3 Results and Discussion

3.3.1 The Foss-Bartlett and Schmidt mechanisms

We began our study by investigating the bimolecular opening of sulfur by the nucleophiles, for which all experimental evidence indicates is the first and rate-determining step in these reactions. The opening of cyclooctasulfur (S_8), elemental sulfur's most common allotrope,[72] is endergonic with both nucleophile types, an indication of the stable nature of S_8. The octasulfide **1** lies 11.9 kcal/mol higher in free energy for cyanide and 2.6 kcal/mol for PMe_3 (Figure 3.2). These reactions occur through S_N2-like transition structures, with linear arrangement of the nucleophile, substituted sulfur, and leaving sulfide. With cyanide, the free energy of activation is 21.9 kcal/mol ($\Delta H^{\ddagger}$ = 11.7 kcal/mol), while with PMe_3 it is lower at 17.3 kcal/mol ($\Delta H^{\ddagger}$ = 5.0 kcal/mol). The nucleophilic character of the phosphine has a significant impact on the barrier and reaction energy. With the bulkier and less electron-rich PPh_3, $\Delta G^{\ddagger}$ is 23.0 kcal/mol ($\Delta H^{\ddagger}$ = 8.1 kcal/mol) and the reaction is endergonic by 17.7 kcal/mol.

As shown below, polysulfides **1** have many decomposition pathways with negligible barriers, so if this initial opening of S_8 is rate-determining then the barriers located here are reasonable for reactions happening at room temperature.

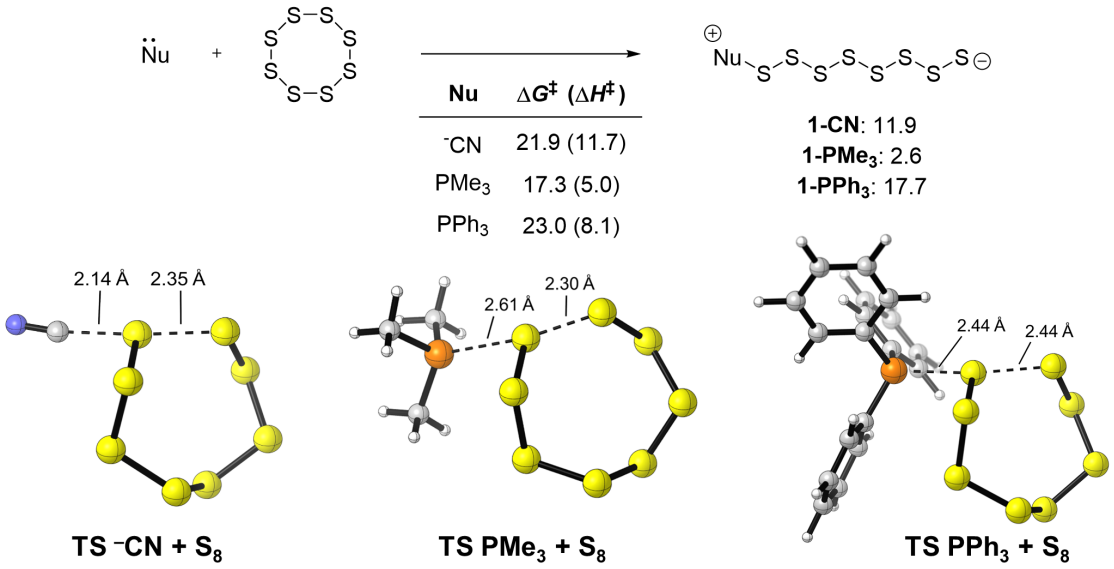

Figure 3.2 Formation of octasulfides **1** from S_8 with nucleophiles. Free energies (enthalpies) in kcal/mol.

We then considered how the generated polysulfide **1** could undergo the Foss-Bartlett or Schmidt pathways for the generation of monosulfides. *A priori*, **1** can be attacked by another nucleophile on any sulfur of the chain forming, depending on which bond is cleaved, either two sulfur products containing each a nucleophile (monosubstituted (poly)sulfides, blue pathway, Figure (3.3) or a sulfur product with two nucleophiles attached and a dianionic (poly)sulfide (disubstituted polysulfides, orange pathway). For the monosubstituted pathways (Figure 3.4), attack at S^1 (closest to the nucleophile) represents a nucleophile exchange pathway that is isoneutral and happens with a 21.5 ($^-$CN) or 24.0 (PMe_3) free energy barrier. Attack at S^2 is the Foss-Bartlett proposal, forming the resonance-stabilized thiocyanate ($^-$SCN) or trimethylphosphine sulfide ($Me_3P{=}S$) as leaving groups with $^-$CN or

PMe_3, respectively, in addition to a heptasulfide that can be further decomposed (see below).

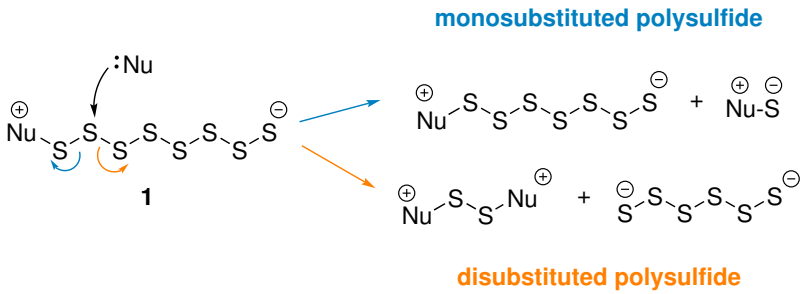

Figure 3.3 Example products from both possible bond cleavages upon nucleophilic attack on polysulfides **1**.

Indeed, in both systems, the attack at S^2 has the lowest free energy of activation, 13.4 ($^-$CN) and 13.0 (PMe_3) kcal/mol. This pathway is highly exergonic with reaction free energies of -22.3 ($^-$CN) and -29.9 (PMe_3) kcal/mol due to the stability of the monosulfide products. These activation barriers are heavily impacted by the entropic penalty for bimolecular reactions, since the activation enthalpy is only 4.5 ($^-$CN) and 2.5 (PMe_3) kcal/mol, demonstrating the excellent leaving group ability of both monosulfides ($^-$SCN and Me_3P=S). Attacks on S^3 to S^7 are consistently less exergonic by around 15 kcal/mol, since the polysulfide anions that are formed do not enjoy similar stabilization as thiocyanate or phosphine sulfide. In addition, the activation barriers increase as the nucleophile attacks closer to the terminal (anionic) sulfur of **1**. This effect is not due to thermodynamic considerations and is lesser for the neutral phosphine nucleophile than for cyanide. For example, while nucleophilic attacks at S^3 or S^7 generate the same products ($NuSS^-$ and ^-S_6Nu), attack at S^3 is 7.2 ($^-$CN) and 3.5 (PMe_3) kcal/mol less favorable than attack at S^2, while attack at S^7 is 20.1 kcal/mol less favorable for cyanide but only 13.6 kcal/ mol less favorable for PMe_3. Attack at S^8 corresponds to the Schmidt hypothesis for the generation of thiocyanate or trimethylphopsine sulfide, and as such has the same exergonicity as attack at S^2. Although this pathway represents a nucleophilic attack on a formally anionic

sulfur atom, the barriers of activation are surmountable, 29.4 ($^{-}$CN) and 23.4 (PMe_3) kcal/mol. Nonetheless, these barriers are 16.0 ($^{-}$CN) and 10.4 (PMe_3) kcal/mol higher than those for the Foss-Bartlett mechanism. Therefore, there is a strong preference in these systems for the formation of the monosulfide as a leaving group instead of through the abstraction of one sulfur atom by the nucleophile. As such, the Schmidt mechanism is unlikely to be relevant in these transformations.

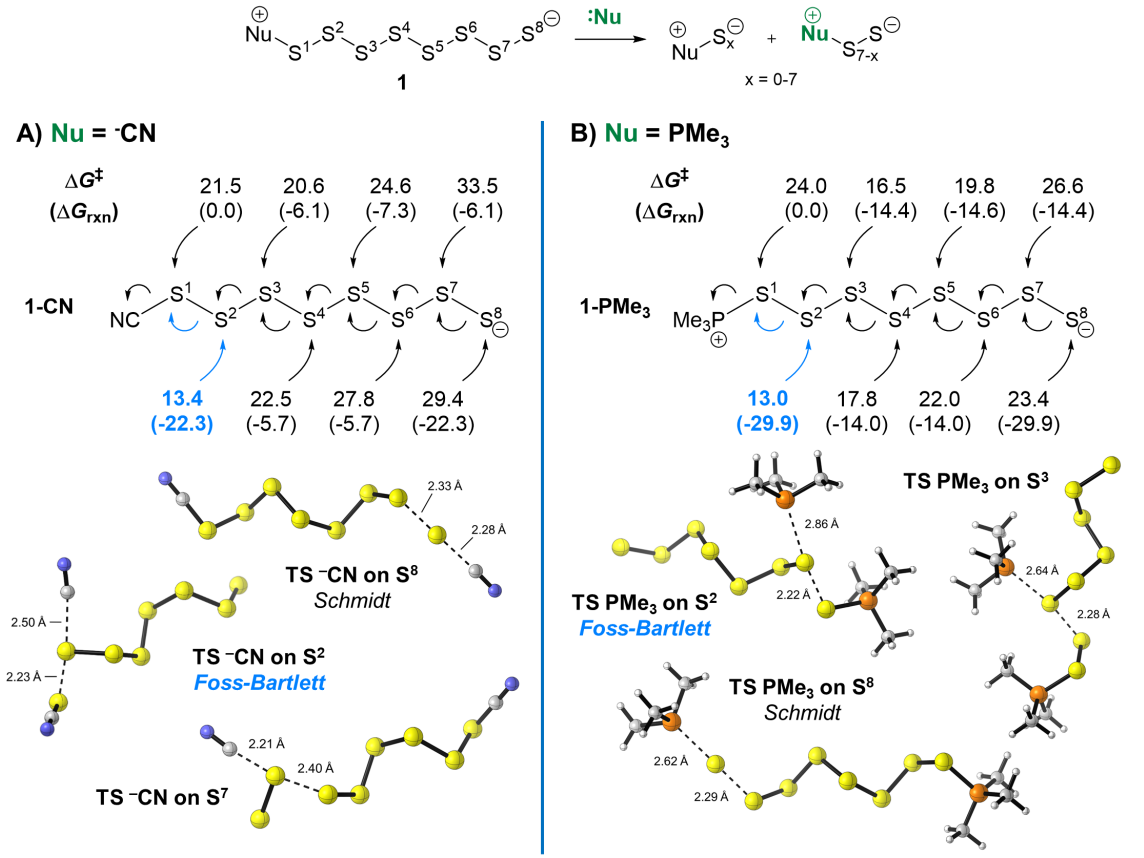

Figure 3.4 Possible pathways for attack of A) cyanide on cyanopolysulfide **1-CN** or B) PMe_3 on phosphoniumpolysulfide **1-PMe$_3$** to form monosubstituted polysulfides. Free energies of activation (free energies of reaction in parenthesis) are in kcal/mol and are relative to polysulfide **1** + Nu. See Supporting Information for visualizations of all transition structures and minima (Figures S1–S6).

Nucleophilic attacks that result in disubstituted polysulfides are kinetically and thermodynamically unfavorable compared to the monosubstituted pathways (Figure 3.5). Indeed, all such attacks are endergonic and thus reversible, except PMe_3 attack

on S^1 of **1-PMe$_3$** that has a 2.6 kcal/mol reaction free energy. The lowest activation barriers for these pathways are found for attack on S^1 for both nucleophiles, forming NCSCN or $[PMe_3SPMe_3]^{2+}$ with the heptasulfide dianion (S_7^{2-}). This reaction requires 15.0 ($^-$CN) and 16.8 (PMe_3) kcal/mol of activation free energy. That the disubstituted cleavage mode is unfavorable can be explained to the formation of polysulfide dianions as leaving groups, which is increasingly endergonic for shorter dianionic polysulfides and thus prohibitively difficult as the attack occurs on sulfur atoms closer to the terminal sulfur. The transition structures for the most favorable S^1 attack, in addition to other representative examples, are shown in Figure 3.4 with all other structures in the Supporting Information (Figures S7 and S8).

These geometries display a strong influence of thermodynamics as predicted by the Hammond postulate. As the length of the leaving dianionic polysulfide shortens, the TSs happen later along the reaction coordinate, with shorter Nu···S forming bonds and longer S···S breaking bonds. One dianionic polysulfide of particular interest is the hexasulfur dianion (S_6^{2-}), which is a product of attack on S^2 via the disubstituted pathways. This polysulfide has been proposed as a precursor for the trisulfur radical anion ($S_3^{-\bullet}$) that is often observed in reactions of elemental sulfur.[104] Our calculations predict that the homolytic cleavage of S_6^{2-} has a low free energy barrier of 15.2 kcal/mol and is exergonic by 5.4 kcal/mol in acetonitrile (Figure 3.5 C) , in line with previous computational results.

Overall, our results of Figure 3.4 and 3.5 are consistent with the experimental results, since the formation of thiocyanate or phosphine sulfide (through attack at S^2) is both kinetically and thermodynamically favored. We conclude that attack at S^2 in the monosubstituted cleavage mode is the main nucleophilic decomposition pathway of octasulfides **1**. Our results predict that dianionic polysulfides, which can be accessed through the disubstituted pathways, should not be formed. This explains why sulfur radical anions are not observed in the reaction of elemental sulfur

with cyanide and phosphines. In the case of cyanide, formation of the heptasulfur dianion (S_7^{2-}) requires a barrier that is only 1.6 kcal/mol higher than thiocyanate formation, nevertheless it is endergonic by 7.5 kcal/mol thus reversible. For PMe_3, formation of (S_7^{2-}) is slightly exergonic, but it requires a 3.8 kcal/mol larger barrier than phosphine sulfide formation, ensuring the latter pathway is kinetically preferred.

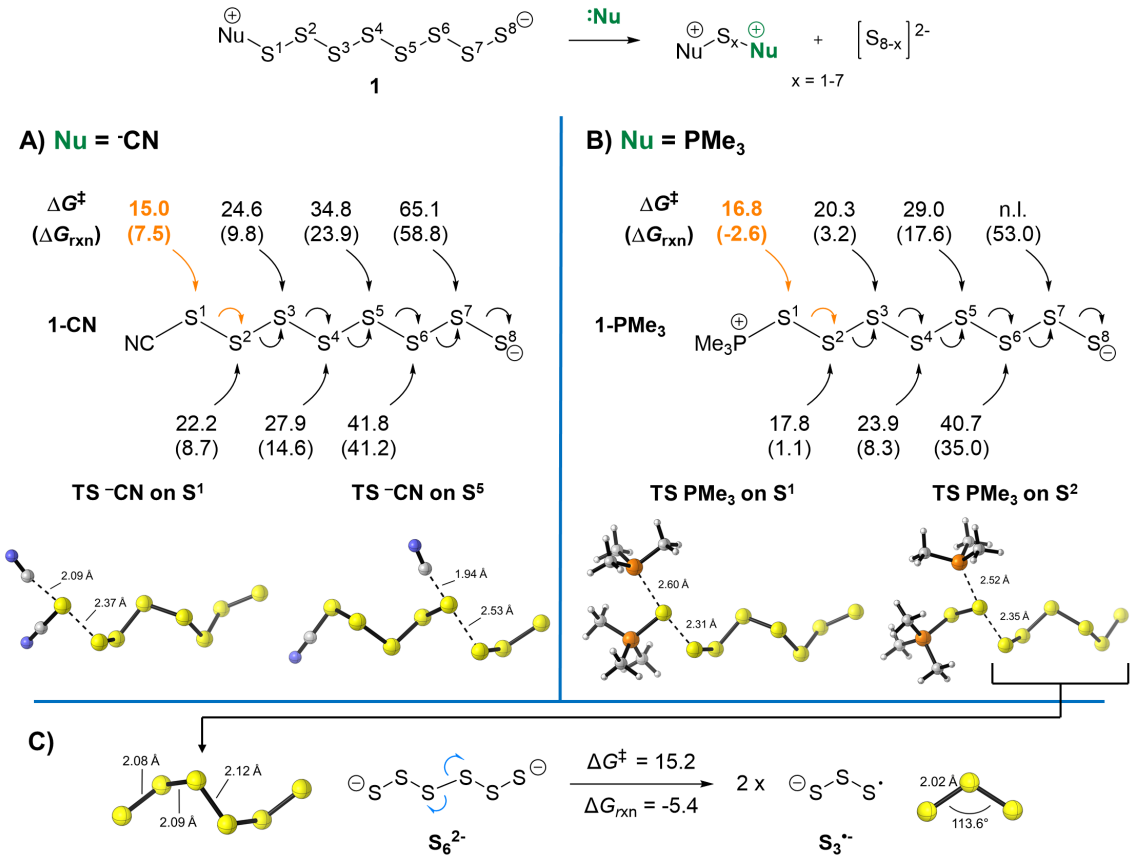

Figure 3.5 Possible attack pathways of A)cyanide on cyanopolysulfide **1-CN** or B)PMe_3 on phosphonium polysulfide **1-PMe$_3$** to form disubstituted polysulfide products. C)Homolytic cleavage of S_6^{2-} to form trisulfur radical anion. Free energies of activation (free energies of reaction in parenthesis) are in kcal/mol and are relative to polysulfide **1** + Nu. n.l.: not located. See Supporting Information for visualizations of all transition structures and minima (Figures S1–S8).

3.3.2 Intermolecular decomposition

The Subsection 3.3.1 results indicate that the Foss-Bartlett mechanism is the most likely nucleophilic decomposition pathway of cyano and phosphonium polysulfides.

In this proposal, the shrinking polysulfide is successively attacked at S^2 by the nucleophile until exclusive formation of the monosulfide is completed. With this in mind, we then investigated the Foss-Bartlett cleavage on shorter polysulfides expected from thiocyanate or trimethylphosphine sulfide generation from cyanopolysulfides or trimethylphosphonium polysulfides (Table 3.1).

Table 3.1 Activation and Reaction Energies (kcal/mol) for Intermolecular Degradation of Polysulfides with Cyanide or PMe_3 as Nucleophile

Polysulfide	n	$\Delta G^{\ddagger}$ NC^-	$\Delta G_{reaction}$ NC^-	$\Delta G^{\ddagger}$ PMe_3	$\Delta G_{reaction}$ PMe_3
$Nu^+S_8^-$	6	13.4	-22.3	13.0	-29.9
$Nu^+S_7^-$	5	14.1	-21.9	12.3	-29.9
$Nu^+S_6^-$	4	15.4	-22.2	13.2	-30.8
$Nu^+S_5^-$	3	16.8	-23.4	15.0	-31.1
$Nu^+S_4^-$	2	18.9	-21.9	16.0	-30.4
$Nu^+S_3^-$	1	22.4	-22.6	18.8	-31.3
$Nu^+S_2^-$	0	19.8	-37.6	16.2	-45.4

Our results indicate that as the sulfur chain gets shorter, the activation free energy for attack at S^2 increases, culminating at 22.4 kcal/mol for the generation of cyanopersulfide $NCSS^-$ and 18.8 kcal/mol for trimethylphosphonium persulfide $Me_3P^+SS^-$ from $Nu^+S_3^-$ (n = 1). This increase of the barrier is not related to the thermodynamics of the reaction, as the free energy of reaction remains somewhat constant around -22 kcal/mol for cyanide, and -30 kcal/mol for PMe_3. Interestingly, the final cleavage of Nu^+SS^- occurs with as lightly smaller activation barrier of 19.8

kcal/mol with $^{-}$CN and 16.2 kcal/mol with PMe_3, despite requiring nucleophilic attack on a formally anionic sulfur atom (see Figure 3.6). This can be explained by the highly exergonic nature of these reactions yielding two resonance-stabilized monosulfides (37.6 and 45.4 kcal/mol), lowering the activation barriers through the Bell-Marcus-Hammond-Evans-PolanyiThornton-Leffler effect. [144]

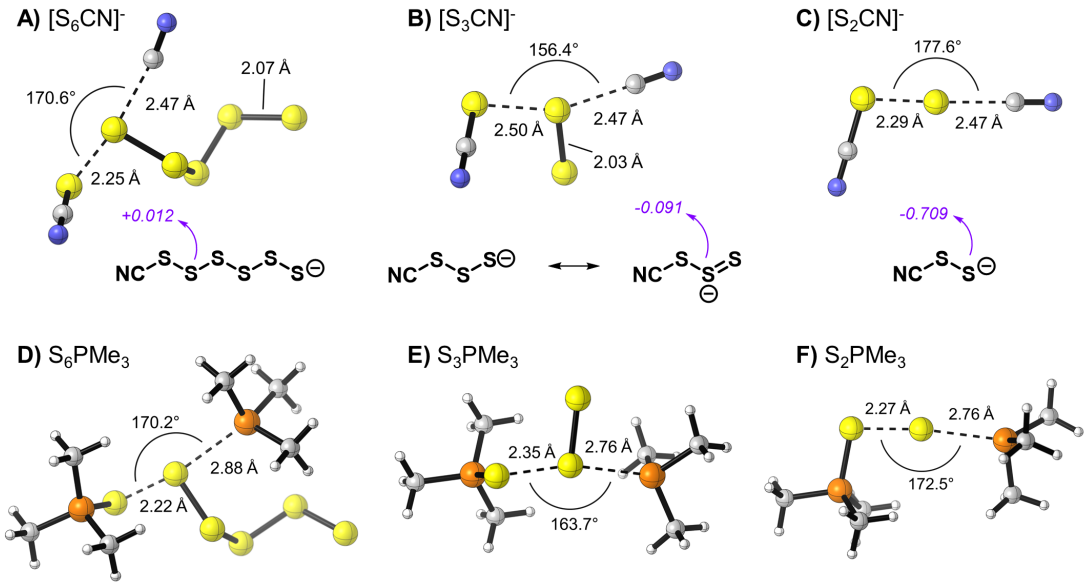

Figure 3.6 Representative TSs for the bimolecular Foss-Bartlett decomposition of polysulfides by nucleophiles. NBO charges indicated as purple value.

The increase of activation energy from n = 6 to n = 1 can be explained by the requirement of the electron-rich nucleophile to approach progressively closer to the anionic terminal sulfur of the chain for shorter polysulfides. This is supported by two main observations. First, this effect is less pronounced for the neutral phosphine nucleophile than for the anionic cyanide. For $^{-}$CN, the difference between the activation barriers for attack on $Nu^{+}S_8^{-}$ versus $Nu^{+}S_3^{-}$ is 9.0 kcal/mol, while it is only 5.8 kcal/mol for PMe_3. Second, the NBO charge on S^2 (where the nucleophile attacks) decreases monotonically from +0.026 in $[S_8CN]^{-}$ to 0.091 in $[S_3CN]^{-}$ (Table S4), consistent with less electrophilic S^2 positions for shorter polysulfides. Representative TSs for intermolecular degradation are shown in Figure 3.6, all others

can be found in the Supporting Information (Figures S9 and S10). For all TSs, the length of the bond forming between nucleophile and sulfur is similar to those found for the initial attack on **1-CN** or **1-PMe$_3$** (Figure 3.4), while the breaking S-S bond length varies from 2.22 to 2.50 Å. As with all previous examples, the nucleophile approaches the σ^*_{S-S} orbital with a typical S_N2 geometry, closer to 180° with longer polysulfides for which less electronic repulsion between nucleophile and terminal sulfur are present. NBO analysis of the cyanopolysulfides confirmed that in all cases, the σ^* orbital between S^1 and S^2 is indeed their LUMO, which has larger coefficients on S^2 (Table S3 and Figure S11). This is consistent with the Foss-Bartlett pathway that expects S^2 as the best position for nucleophilic attack. $Nu^+S_3^-$ has the least electrophilic S^2 position as the terminal anionic charge is delocalized significantly on S^2 (as seen from NBO charges, Figure 3.6 a–c). The electrostatic repulsion between the terminal anionic sulfur and the nucleophile also distorts the S_N2 geometry during attack, with a lesser effect seen for the neutral phosphine (Nu···S···S angle of 156° for CN^-, 164° for PMe_3, Figure 3.4 e). Both effects probably contribute to this polysulfide showing the largest activation barrier for nucleophilic attack. Other TSs of particular interest are that of $NCSS^-$ with CN^- and of $Me_3P^+SS^-$ with PMe_3 (Figure 3.6 c, f). Those structures represent the final decomposition of polysulfides to form two monosulfide products, or the first step in the putative reversible formation of S_8 from the monosulfides. Our results demonstrate clearly why the reverse reaction is not possible. From two thiocyanate anions, this TS would require 57.4 kcal/mol, while for two Me_3P=S,the TS would require 61.6 kcal/mol, two prohibitively high barriers.

Nevertheless, the Foss-Bartlett mechanism, as computed here, has two potential flaws. First, both for cyanide and PMe_3, nucleophilic attack on the trisulfide ($Nu^+S_3^-$) to form a monosulfide and persulfide (Nu^+SS^-) has a larger barrier than the initial opening of S_8 by the nucleophile (Figure 3.2). Indeed, for cyanide the

$\Delta\Delta G^{\ddagger}$ is + 0.5 kcal/mol (22.4 vs. 21.9), while for PMe_3 it is + 1.5 kcal/mol (18.8 vs. 17.3). This would suggest that the rate-determining step is not the opening of S_8 and that the reaction should not be first-order in nucleophile. In addition, **1-CN** lies 11.9 kcal/mol higher in free energy than S_8 and the Foss-Bartlett attack on this species requires an additional 13.4 kcal/mol. As such, relative to S_8, this second TS is higher in free energy than the initial S_8 opening TS (25.3 vs. 21.9 kcal/mol) and would be rate-determining, once again contradicting experimental evidence. Based on these discrepancies, we searched for other pathways that could explain the formation of the products.

3.3.3 Unimolecular decomposition of polysulfides

We hypothesized that polysulfides could decompose without the action of an external nucleophile, using their terminal sulfide anion as nucleophile and S^2 as the most electrophilic site in a Foss-Bartlett-like reaction. Such unimolecular decomposition would generate thiocyanate (^{-}SCN) or trimethylphosphine sulfide ($Me_3P{=}S$), in addition to a smaller sulfur allotrope that could be attacked by the nucleophile or other polysulfides (see below). Indeed, we located these cyclization TSs and found that for long polysulfides they are exergonic and almost barrierless (Table 3.2). Nevertheless, cyclization of $Nu^{+}S_5^{-}$ to S_4 becomes endergonic and displays large barriers for both systems (17.5 kcal/mol for ^{-}CN, 19.8 kcal/mol for PMe_3), larger than their Foss-Bartlett nucleophilic decompositions. Cyclization of $Nu^{+}S_4^{-}$ to S_3, surprisingly, is not as endergonic and displays activation barriers that are lower than nucleophilic decomposition. Some representative TS geometries are displayed in Figure 3.7.

Table 3.2 Activation and Reaction Free Energies (kcal/mol) for Unimolecular Decomposition of Polysulfides

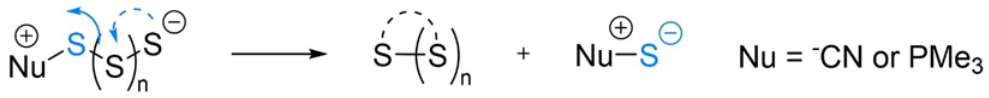

Polysulfide	n	$\Delta G^{\ddagger}$ ($^{-}$CN)	$\Delta G_{reaction}$ ($^{-}$CN)	$\Delta G^{\ddagger}$ (PMe_3)	$\Delta G_{reaction}$ (PMe_3)
$Nu^+S_8^-$	6	0.4	-25.7	3.7	-24.7
$Nu^+S_7^-$	5	1.9	-25.5	4.2	-24.8
$Nu^+S_6^-$	4	5.2	-15.1	6.5	-13.5
$Nu^+S_5^-$	3	17.5	8.2	19.8	8.9
		10.6[a]	-0.2[a]	16.0[a]	0.5[a]
$Nu^+S_4^-$	2	11.7	-0.1	12.8	0.0
		4.3[b]	-2.3[b]	n.l.[b]	-2.3[b]
$Nu^+S_3^-$	1	n.l.	14.5	n.l.	14.7

(a) Decomposition to the open (C_{2v}) form of S_4.

(b) Decomposition to the bent form of S_3. n.l. : not located.

Structures show a clear influence of the Hammond postulate, changing from early TSs for the exergonic cyclization of $Nu^+S_8^-$ (long forming S-S bond, short leaving S-SNu bond), to late TSs for the more endergonic cyclizations of $Nu^+S_5^-$ and $Nu^+S_4^-$. The putative cyclization of $Nu^+S_9^-$ to S_8 is highly exergonic (-33.8 and -33.0) and we were unable to locate its presumably early TS. We thus anticipate an essentially barrierless process, meaning polysulfides with 6 or more sulfur atoms and bearing excellent leaving groups are expected to decompose spontaneously and without significant barriers.

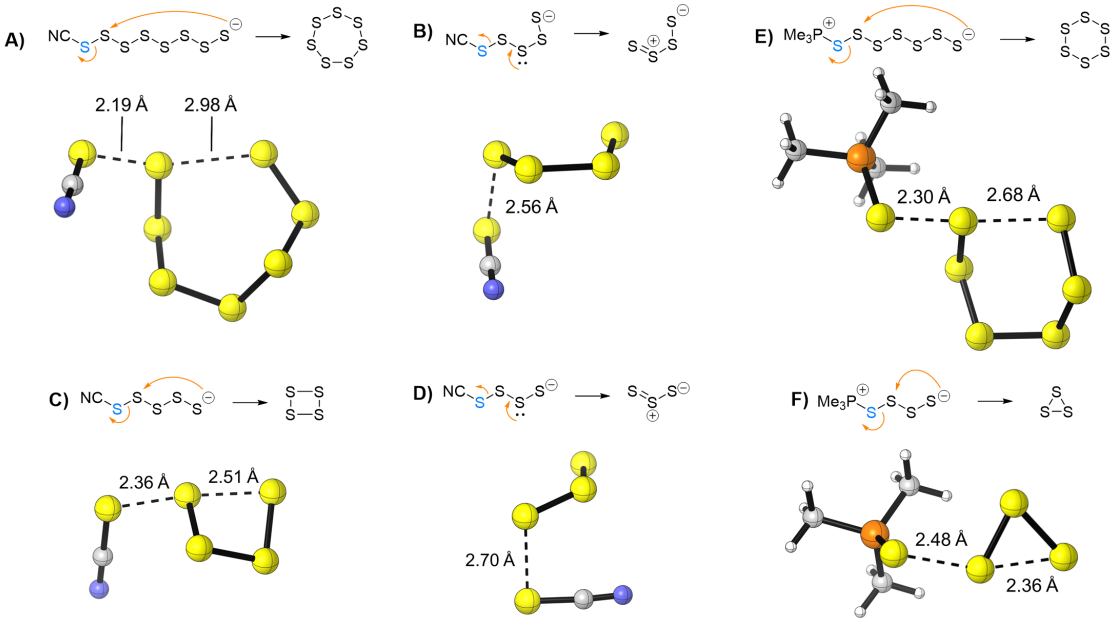

Figure 3.7 Representative TS structures for unimolecular decomposition. All reactions liberate a monosulfide product (not shown). Other structures can be found in Figures S13 and S15.

Unimolecular decompositions of $Nu^+S_5^-$ and $Nu^+S_4^-$ are also possible without cyclization. Previous computations showed that the cyclic forms of S_4 and S_3 are not the most stable, as the C_{2v} (S_4) and bent (S_3) geometries are the lowest in energy.[145–147] We thus searched for TSs that would lead from $Nu^+S_5^-$ and $Nu^+S_4^-$ directly to these sulfur allotropes. For the cyanide system, such TSs were located although they displayed some diradical character (see Figure S12 and related discussion). A similar cleavage was located for $PMe_3{}^+S_5^-$, but not for $PMe_3{}^+S_4^-$. In all cases, the direct formation of the open forms of S_4 or S_3 makes the reactions more exergonic than cyclization to the cyclic forms, especially for S_4, which also lowers the activation barriers. Non-cyclizative pathways could not be located for any polysulfide longer than $Nu^+S_5^-$. For the decomposition of $Nu^+S_3^-$ to S_2 that is inherently not a cyclization, we could not locate TSs, and our calculations indicate that this reaction is endergonic by 14.5 ($^-$CN) and 14.7 (PMe_3) kcal/mol. Even though unstable allotropes of sulfur are generated in the cyclization of short polysulfides, the excellent leaving

group ability of thiocyanate or phosphine sulfide ensures that the barriers are in the range of the Foss-Bartlett decompositions. Non-cyclizative pathways display lower activation barriers when located, but they are not necessary for unimolecular decompositions to compete favorably with Foss-Bartlett pathways up until $Nu^+S_3^-$. Sulfur allotropes from S_7 to S_3 react with the nucleophiles ^-CN and PMe_3 with lower activation barriers than S_8, confirming that such intermediates would be trapped quickly under the reaction conditions, forming new polysulfides (Tables S5 and S6). Overall, these results for unimolecular decompositions indicate that long polysulfides with excellent leaving groups are expected to cyclize rapidly to form monosulfide products without the involvement of external nucleophiles. Nevertheless, for shorter polysulfides the picture is muddier, since the formation of cyclic allotropes have larger activation free energies while decomposition to open forms cannot always be located or display radical character that might not be properly modeled with our computational methods. Unimolecular decomposition also does not provide a clear viable pathway for the decomposition of trisulfides, for which nucleophilic decomposition has the highest activation barrier.

3.3.4 Scrambling of polysulfides

We then wondered if short polysulfides could themselves act as nucleophiles (Figure 3.8), using other polysulfides (type I) or sulfur allotropes (type II) as electrophiles in bimolecular reactions. We term these pathways "scrambling", since polysulfides are both the reactants and products of such reactions. Similar reactions of polysulfides have been invoked for the generation of long chain polysulfides from S_8.[148–150] Due to the predicted rapid decomposition of octa, hepta, and hexasulfides through the unimolecular pathway (see above), we only considered polysulfides from $Nu^+S_5^-$ to $Nu^+S_2^-$ for scrambling pathways. We first computed the activation and reaction free

energies for the bimolecular decomposition of each species by another polysulfide of any length, using the Foss-Bartlett attack (type I).

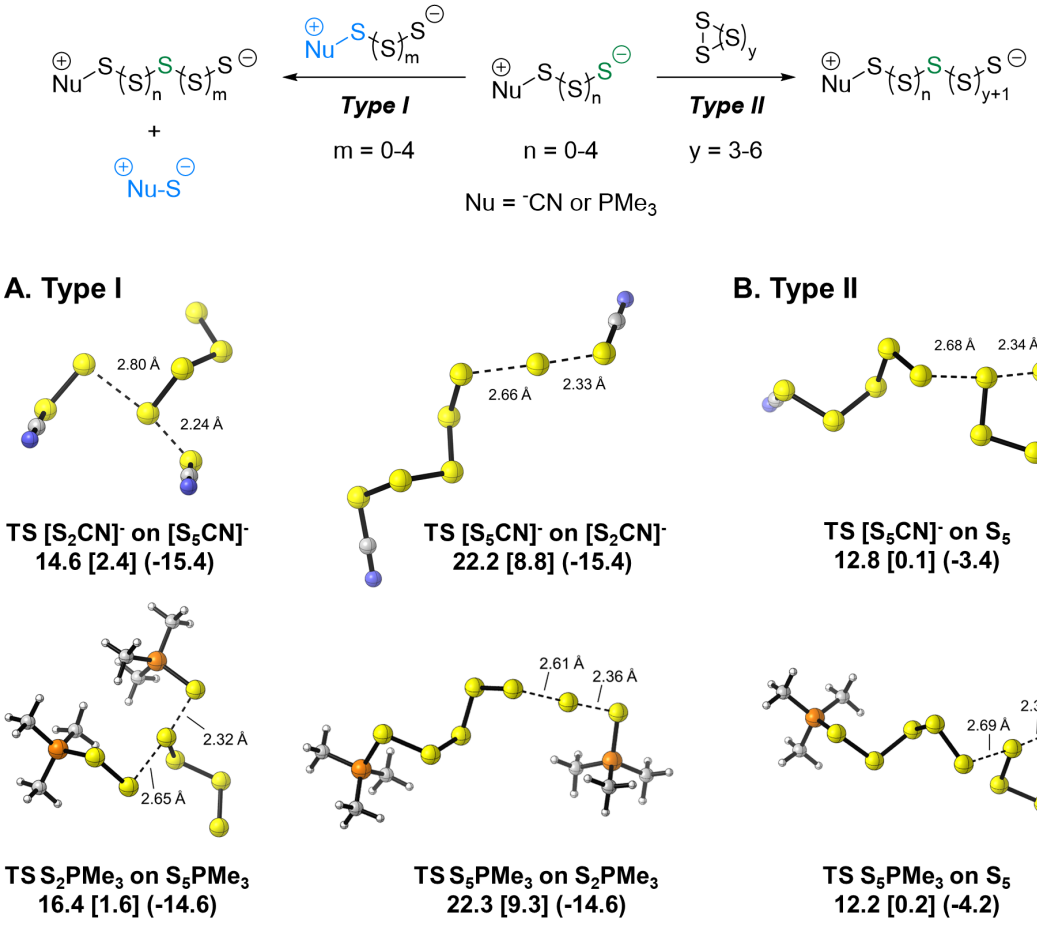

Figure 3.8 Key transition structures of A)type I and B)type II scrambling pathways. Activation free energies and enthalpies (in brackets), as well as reaction free energies (in parenthesis) are shown in kcal/mol. All other computed structures can be found in Figures S16–S19.

All values have been reported in the Supporting Information (Tables S7 and S8). For both nucleophiles, the lowest activation barrier corresponds to the attack of $Nu^+S_2^-$ on $Nu^+S_5^-$ (14.6 ($\Delta H^‡$ = 2.4 kcal/mol) for $^-$CN and 16.4 ($\Delta H^‡$ = 1.6 kcal/mol) for PMe3), while the largest activation barrier corresponds to the attack of $Nu^+S_5^-$ on $Nu^+S_2^-$ (22.2 ($\Delta H^‡$ = 8.8 kcal/mol) for $^-$CN and 22.3 ($\Delta H^‡$ = 9.3 kcal/mol) for PMe_3). Representative TS structures are shown in Figure 3.8, all others can be found in Figures S16 and S17. As was seen for nucleophilic decomposition

(Table 3.1), shorter polysulfides are weaker electrophiles due to the enhancement of the repulsive force between the terminal sulfide anion and the nucleophile. In contrast, the identity of the nucleophilic polysulfide has only a small effect on the barriers, with shorter polysulfides being marginally better nucleophiles. For instance, the barriers for attack of $Nu^+S_2^-$ on $Nu^+S_2^-$ are slightly lower (21.1 ($\Delta H^‡$ = 9.7 kcal/mol) for ^-CN and 21.5 ($\Delta H^‡$ = 8.8 kcal/mol) for PMe_3) than for $Nu^+S_5^-$ on $Nu^+S_2^-$. TS geometries and reaction free energies do not depend upon the chain length of the polysulfide and are similar for all the possible type I scramblings, with reaction free energies between 14 to 18 kcal/mol in all cases. This confirms that scrambling on shorter polysulfides might be kinetically difficult but would be thermodynamically favorable. Two polysulfides for which type I scrambling pathways could compete with other decomposition routes are $Nu^+S_5^-$ and $Nu^+S_3^-$. For NCS_5^-, scrambling using two identical molecules has an activation free energy of 17.3 kcal/mol, similar to unimolecular cyclization (17.5 kcal/mol) and nucleophilic decomposition by cyanide (16.8 kcal/mol), but higher than non-cyclizative decomposition (9.6 kcal/mol). For $Me_3P^+S_5^-$, bimolecular scrambling requires 16.2 kcal/mol, lower than unimolecular cyclization (19.8 kcal/mol) but similar to non-cyclizative decomposition (15.7 kcal/mol) and nucleophilic decomposition by PMe_3 (15.0 kcal/mol). Similarly, for NCS_3^- the bimolecular scrambling has a barrier of 19.6 kcal/mol, smaller than nucleophilic decomposition by cyanide (22.4 kcal/mol) which is the only other pathway for which we could locate a TS. For $Me_3P^+S_3^-$, bimolecular scrambling has a barrier of 16.1 kcal/mol, smaller than nucleophilic decomposition by PMe_3 (18.8 kcal/mol). Considering the low-energy pathways for unimolecular decomposition outlined above, which generate shorter sulfur allotropes, another possibility is that short polysulfides could act as nucleophiles in the opening of such allotropes (type II scrambling, see Figure 3.8 B for example structures). Our results (Tables S9 and S10) show that as the size of the sulfur allotropes decreases, the activation free energies

and enthalpies for their opening decrease for any given polysulfide nucleophile. For example, $Me_3P^+S_5^-$ attack on S_8 requires 22.1 kcal/mol ($\Delta H^‡$ = 8.0 kcal/mol) but only 11.8 kcal/mol ($\Delta H^‡$ = 0.9 kcal/mol) for attack on S^5. As such, for short sulfur allotropes the activation barrier is almost entirely due to the entropic cost for bimolecular reactions. We could not locate any TS for attack on S^4 or shorter allotropes but based on the above trend it is likely that, if they could be located, they would be enthalpically barrierless with 12–14 kcal/mol entropic barriers, similar to the S_5 openings shown in Figure 3.8B. Our results also indicate that type II scrambling pathways do not depend on the nature of the nucleophilic polysulfide, as the activation barriers are barely impacted by changing its length or swapping the cyanide terminus for a trimethylphosphonium. From the point of view of the sulfur allotropes, type II scrambling pathways have larger activation barriers than opening by PMe_3 (Table S10), meaning they are unlikely to compete in any situation for S_8 decomposition by phosphines. Sulfur allotrope openings by cyanopolysulfides (type II scrambling), on the other hand, have lower activation barriers than opening by ^-CN (Table S9), meaning they could compete if nucleophile concentration is low. Globally, scrambling reactions are less likely to occur with long polysulfides (more than 5 sulfur atoms) than with short polysulfides. While scrambling reactions that use long polysulfides as electrophiles have negligible enthalpy barriers, their bimolecular nature incurs an entropic cost that raises the free energy barrier by 10–14 kcal/mol. Considering it is also unlikely to find a significant concentration of such long polysulfides in solution since they decompose unimolecularly with negligible barriers, the rates of polysulfide scrambling reactions are expected to be low, so they are unlikely to play a significant role in the decomposition of long polysulfides. For short polysulfides, nevertheless, intramolecular decomposition and Foss-Bartlett attack by nucleophiles display larger activation barriers, meaning short polysulfides could accumulate in solution. In that case, both their type I and type II scramblings would become competitive with other

possible pathways, especially if nucleophile concentration is low. This is only true if a significant concentration of polysulfides can be found in solution which, considering their other means of decomposition, might not be realistic.

3.3.5 Sulfane sulfur thiosulfoxides

Another potential pathway involved sulfane sulfur thiosulfoxides, compounds with the general structure $R_2S{=}S$ that have been proposed for decades as intermediates in nucleophilic reactions of polysulfide reagents, sometimes with contested evidence.[151–153] Both FSSF and its thiosulfoxide isomer F_2SS have been isolated,[154] and seem to have a similar energy. Nevertheless, for other systems, there is limited evidence that branched sulfur chains are stable. In fact, Foss convincingly argued in 1950 that thiosulfoxides are high-energy structures that are unlikely to be relevant in reactions of polysulfides,[111] and various computational investigations of such species are in line with this hypothesis.[155–160] Our calculations also agree with this view, and we find that thiosulfoxide pathways are not competitive with simple attack of the nucleophiles on the unbranched chain of sulfur atoms (Figure 3.9). The first mystery with thiosulfoxides is the mechanism of their formation. Unimolecular TSs between alkyl disulfides (RSSR, where R=H,Me, allyl) and the corresponding thiosulfoxides ($R_2S{=}S$) have been located in previous studies but are not energetically accessible (between 50 - 80 kcal/mol).[155, 161] For the polysulfides considered in this study, we could not locate similar 1,2-rearrangement transition structures. For S_8, the only structure we could locate for its transformation to the thiosulfoxide isomer **2** required 68.5 kcal/mol. For the cyanooctasulfide **1-CN**, the only intramolecular TS we could locate uses an unusual [2,2]-shift to form the S^5-thiosulfoxide, with a reasonable 19.7 kcal/mol barrier (Figure S21). No similar TSs could be found that lead to other possible thiosulfoxide intermediates from **1-CN** or from other thiosulfoxides. We

also found intermolecular transition structures involving two polysulfides, which had activation barriers of 18.8–23.9 kcal/mol (Figure S21).

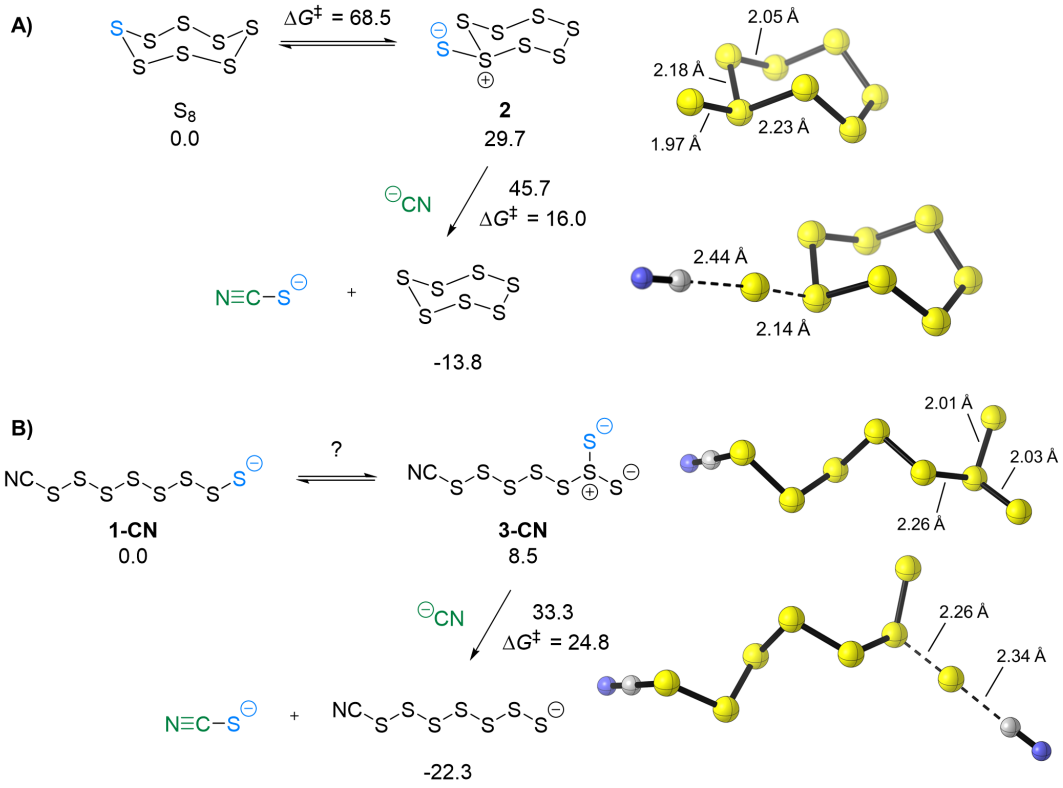

Figure 3.9 Lowest-energy thiosulfoxide pathways from a) S_8 and b) **1-CN.** Free energies in kcal/mol.

Critically, the thiosulfoxide pathways we studied here are much higher in energy than those described in the literature. Thiosulfoxide **2**, displaying the most stable chair conformation of cycloheptasulfur,[100, 162, 163] is 29.7 kcal/mol higher in free energy than the crown conformer of S_8 and is likely inaccessible at the temperatures where the reaction of sulfur with cyanide occurs. Cyanide attack on the pendant sulfur atom of **2** has a similar barrier (16.0 kcal/mol) to intermolecular decompositions of regular polysulfides. Assuming that there is an easier, yet unknown pathway for the formation of **2** that does not require the TS we located, the formation of thiocyanate from S_8 via the thiosulfoxide pathway would still require at least 45.7 kcal/mol. For the linear octasulfide **1-CN**, we computed all possible thiosulfoxide isomers (Figure

3.9, see Figures S21 and S25 for all structures) and obtained a similar conclusion. The lowest energy thiosulfoxide is at the penultimate sulfur atom S^6 **(3-CN**, + 8.5 kcal/mol), while the highest-energy isomer is on S^1 (+ 29.3 kcal/mol). Nevertheless, attack of cyanide on any thiosulfoxide's pendant sulfur atom requires between 13.7 (S^1) to 24.8 (S^6) kcal/mol, so the total free energy required from **1-CN** is at least 33.3 kcal/mol through **3-CN.** Overall, this lowest-energy thiosulfoxide pathway to generate thiocyanate still requires 19.9 kcal/mol more than the Foss-Bartlett attack at S^2 of **1-CN**, which only requires 13.4 kcal/mol. Similar results were obtained for thiosulfoxides on phosphonium polysulfides (Figure S25). We also confirmed that longer branching (i.e., a pendant disulfide) is higher in energy, and that thiosulfoxides on shorter or longer cyanopolysulfides are similarly disfavored (Figures S21–S22). In addition, attacks on internal sulfur atoms connected to the polysulfide's trivalent sulfur are as favorable as attack on the pendant sulfur atom (Figure S23), and as such the intermediacy of thiosulfoxides in the reaction would yield products which have not been observed experimentally.

Overall, sulfane sulfur thiosulfoxides are high-energy structures that are in equilibrium with their corresponding unbranched polysulfides or S_8. Cyanide attack on those structures is less favorable than on the unbranched polysulfides, as it does not benefit from the highly stable thiocyanate or phosphine sulfide as leaving groups. For the polysulfides we considered, thiosulfoxide isomers can be as close as 8.2 kcal/mol higher in energy than the unbranched structure, which is not as unstable as those reported for disulfides RSSR (13–34 kcal/mol for R=H, Me, Et, Pr, allyl, Cl, Br),[155, 160] nevertheless the mechanism by which they could be formed is still unclear. As Foss and others have suggested, it seems unlikely that such species are relevant in the decomposition of elemental sulfur and polysulfides.

3.3.6 Monosulfide exchange pathways

As a final task, we evaluated the sulfur exchange pathways of polysulfides and monosulfides. It is known that no sulfur exchanges occur between thiocyanate and cyanide or phosphines, nor between phosphine sulfides and thiocyanate.[51] Our computations reproduce this behavior (Figure 3.10). Sulfur exchange from thiocyanate with cyanide (A) requires 48.0 kcal/mol, while between phosphine sulfide and phosphine (B) requires 41.5 kcal/mol. The cross-reaction of phosphine sulfide with cyanide (C) has a 47.3 kcal/mol barrier and is endergonic by 8.3 kcal/mol. Although this transformation cannot occur due to its prohibitively high barrier, its endergonic nature confirms the better thiophilic character of phosphines versus cyanide.[164] Conversely, the leaving group ability of thiocyanate or phosphine sulfide is such that we predict that their exchange from attack at S^2 on octasulfides is accessible despite the low nucleophilicity of the monosulfides.

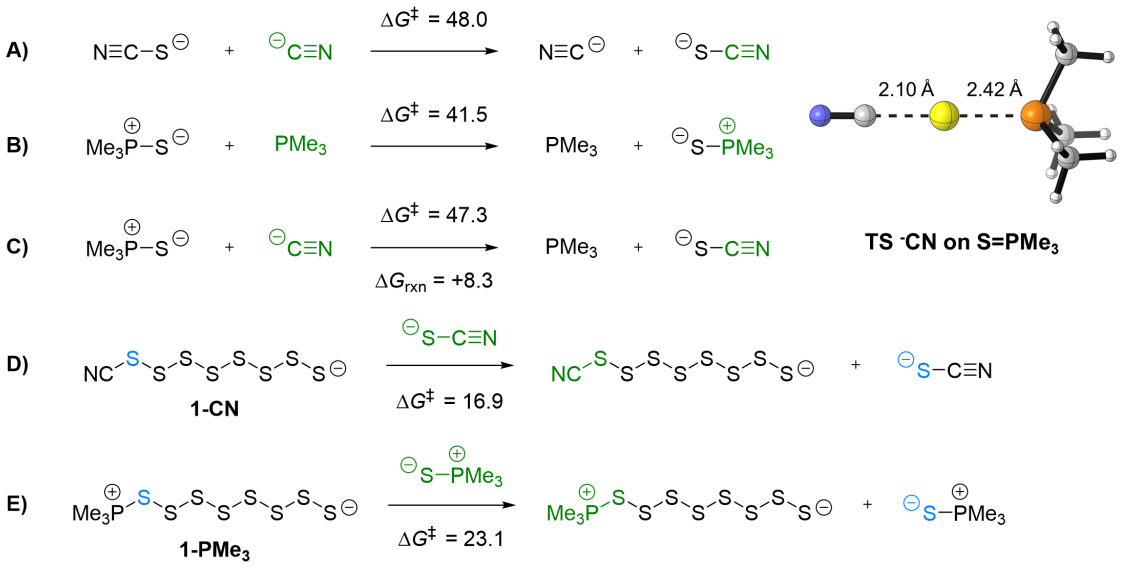

Figure 3.10 Monosulfide exchange pathways from monosulfides and octasulfides. Free energies in kcal/mol.

From **1-CN**, SCN exchange (D) has a 16.9 kcal/mol barrier, while S^+PMe_3 exchange from **1-PMe$_3$** (E) has a 23.1 kcal/mol barrier. Although these barriers are higher than other decomposition pathways described above, it hints at the potential

scrambling between polysulfides that would be generated in the presence of more than one nucleophile.

3.4 Full Reaction Pathways

Shown below in Figure 3.11 and 3.12 are the overall pathways for the decomposition of elemental sulfur by cyanide and phosphines. For both systems, the initial opening of sulfur is followed by three almost barrierless unimolecular cyclizations and re-opening of the sulfur allotropes by the nucleophile. For cyanide (Figure 3.11), S_5 could also enter in type II scrambling pathways (orange pathways) with polysulfides in solution. Nevertheless, the concentration of such polysulfides is likely small and thus opening by cyanide to form $[S_5CN]^-$ should prevail. From there, unimolecular decomposition (green pathway) is still faster than nucleophilic decomposition (blue pathway) until $[S_3CN]^-$. At this stage, it is unclear if unimolecular decomposition is still possible, as it is highly endergonic and no TS could be located for its transformation to S_2. Bimolecular decomposition has a 22.4 kcal/mol barrier, larger than the initial opening of S_8 by cyanide. Despite the type I scrambling pathway of $[S_3CN]^-$ having a lower 19.6 kcal/mol barrier, the rate of that reaction is expected to be small unless the concentration of $[S_3CN]^-$ increases sufficiently to compare with that of the cyanide nucleophile. If $[S_3CN]^-$ does accumulate, then type II scrambling pathways of S_5, S_4 and S_3 might become competitive as well. In conditions where the nucleophile is in large excess, which represents most conditions in which this reaction is used, nucleophilic decomposition of $[S_3CN]^-$ to $[S_2CN]^-$ and then to ^-SCN should display significantly larger rates than any scrambling reactions. As such, the reaction of elemental sulfur with cyanide most likely employs unimolecular decomposition for long polysulfides, and nucleophilic decomposition for tri- and persulfides.

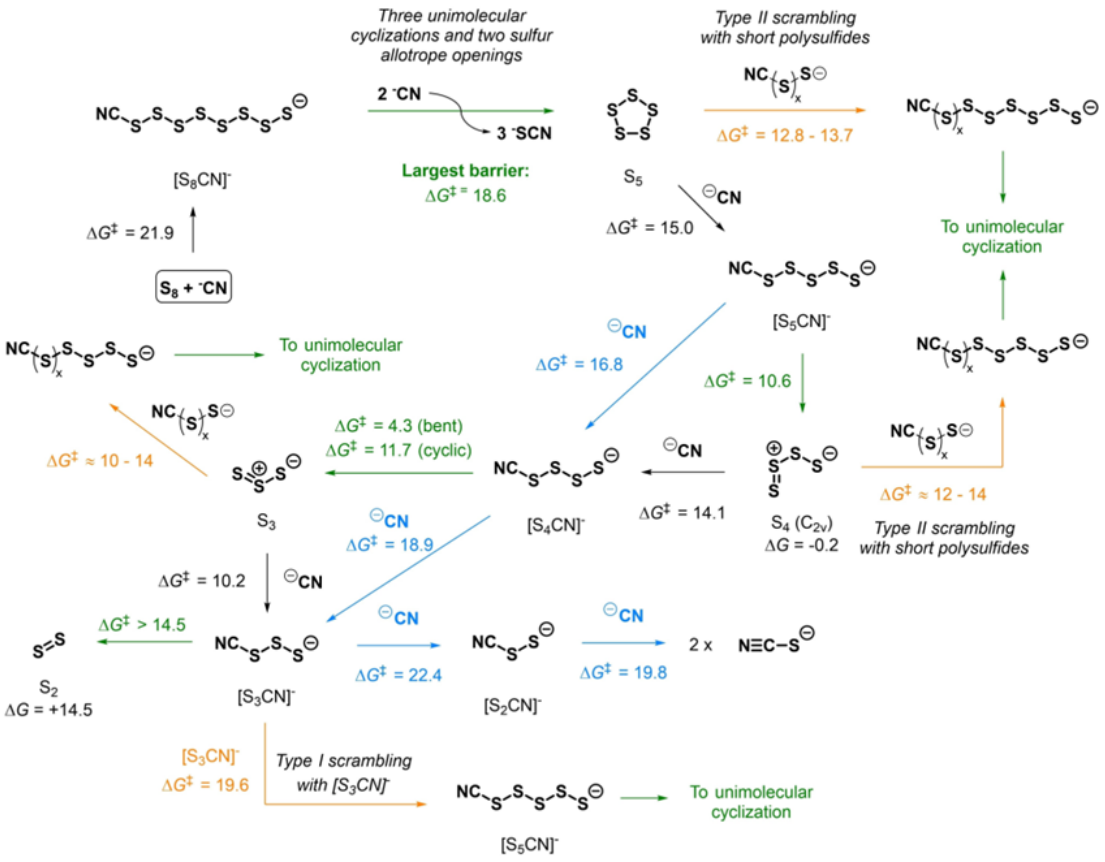

Figure 3.11 Plausible reaction pathway for thiocyanate formation from the reaction of elemental sulfur with cyanide. Green pathways: unimolecular decomposition; blue pathways: nucleophilic decomposition; orange pathways: scrambling reactions; black pathways: sulfur allotrope attack by cyanide. All pathways except sulfur allotrope attack by cyanide or polysulfides (type II scrambling) generate a thiocyanate ($^{-}$SCN) product (not shown). Activation and reaction free energies (in kcal/mol) are relative to the preceding intermediate.

For phosphine (Figure 3.12), after the first three unimolecular cyclizations, S_5 has a lower barrier for its opening by PMe_3 versus the type II scrambling pathways with polysulfides present in the solution. As such, the rate of the former would dominate over the latter, also due to the small expected concentration of polysulfides. From this point on, S_5PMe_3 has three potential pathways with almost identical barriers: type I scrambling with another (16.2 kcal/mol), unimolecular decomposition to $S_4(C_{2V})$(16.0 kcal/mol), or nucleophilic decomposition by PMe_3 (15.0 kcal/mol),

with the last two options being the most likely considering the small concentration of polysulfides.

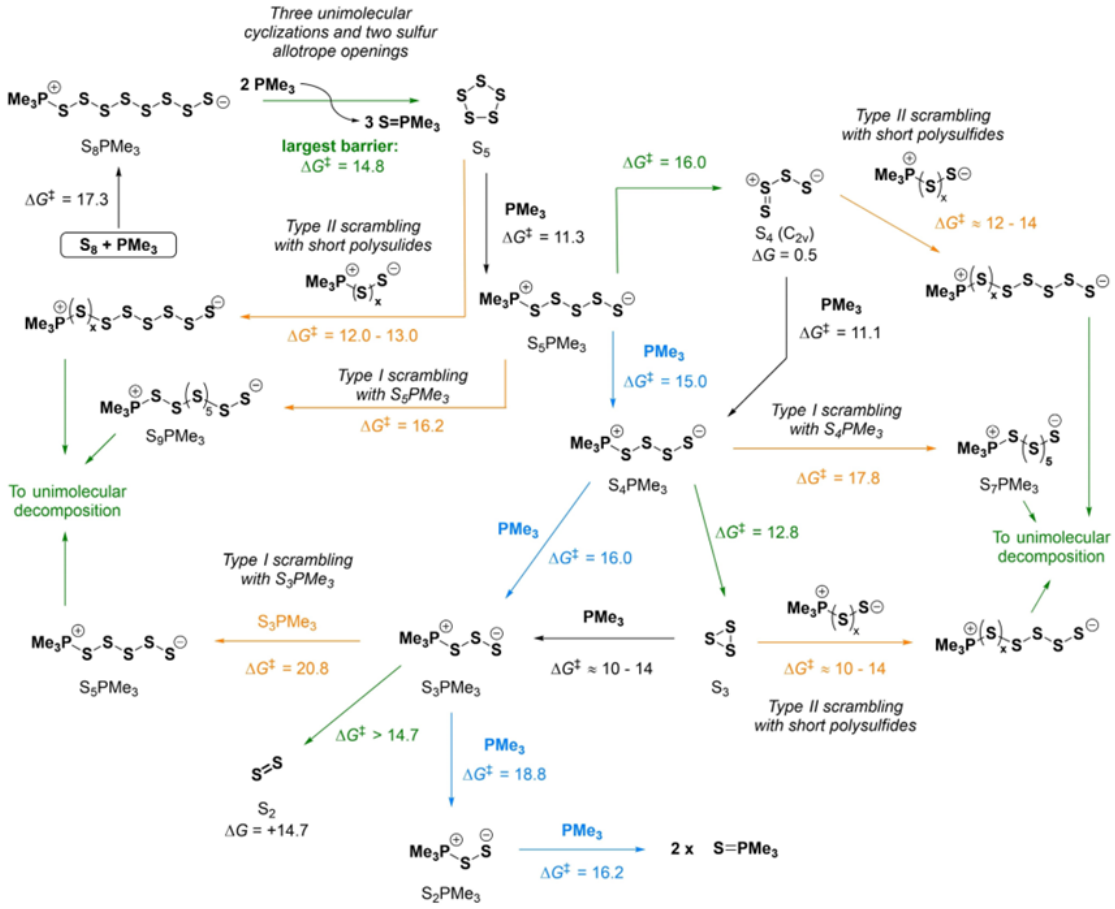

Figure 3.12 Plausible reaction pathway for phosphine sulfide formation from the reaction of elemental sulfur with PMe_3.Green pathways: unimolecular decomposition; blue pathways: nucleophilic decomposition; orange pathways: scrambling reactions; black pathways: sulfur allotrope attack by PMe_3. All pathways except sulfur allotrope attack by PMe_3 or polysulfides (type II scrambling) generate a phosphine sulfide ($S{=}PMe_3$) product (not shown). Activation and reaction free energies (in kcal/mol) are relative to the preceding intermediate.

S_4PMe_3 can then form S_3 with a maximum barrier of 12.8 kcal/mol, then form S_3PMe_3 upon nuclephilic attack, after which many possibilities arise. The formation of S_2 is strongly endergonic and reversible, and nucleophilic decomposition with PMe_3 has a larger barrier (18.8 kcal/mo) than the initial opening of S_8. Considering this pathway has a lower barrier than type I scrambling of S_3PMe_3, it is likely to

be kinetically favored, leading to the phosphonium persulfide S_2PMe_3, which can then complete the formation of $S{=}PMe_3$. As such, the decomposition of elemental sulfur by phosphines is expected to use unimolecular cyclizations until S_5PMe_3, then transition to a mixture of unimolecular and nucleophilic decompositions for shorter intermediates. Scrambling pathways are unlikely in that context.

3.5 Conclusions

We have performed a comprehensive DFT study of the reaction pathways of elemental sulfur and polysulfide decomposition by cyanide and PMe_3 nucleophiles, which revealed a large number of unexpected conclusions. Our initial investigations into the bimolecular nucleophilic decomposition of polysulfides highlighted that the Foss-Bartlett mechanism is more likely than the Schmidt mechanism, as the S^2 sulfur is the most electrophilic position on any cyano or phosphonium polysulfide. Nevertheless, the nucleophilic pathways hinted at reactions that would not be first order in nucleophile, so we located other plausible pathways. We showed that intramolecular cyclization is essentially barrierless for polysulfides with more than 5 sulfur atoms with excellent leaving groups, while for shorter polysulfides a mixture of unimolecular decomposition and nucleophilic decompositions can be expected. Multiple scrambling reactions between polysulfides and sulfur allotropes are also possible based on low activation barriers, nevertheless, the rates of these reactions would be negatively impacted by the small concentration of such intermediates in solution, given their other fast reactions. If scrambling reactions do occur, long polysulfides would be formed that can then decompose through unimolecular cyclization. The mechanisms of polysulfide decomposition are expected to depend heavily on the nature of the polysulfide substituent, and the pathways located here might not be operative without the good leaving group ability of thiocyanate or phosphine sulfide. In addition, we have shown that even in an arguably simple system,

the mechanisms of polysulfide decomposition are complex and vary depending on the length of the polysulfide. These findings can be used as a starting point to study polysulfide involvement in the mechanisms of organic reactions using elemental sulfur, or in biochemical pathways, both of which will be reported in due course.

CHAPTER 4

COMPUTATIONAL INVESTIGATIONS ON THE MECHANISM OF THE GEWALD REACTION

4.1 Introduction

Elemental sulfur is a highly favored source of sulfur atoms in organic synthesis owing to its abundant availability and cost-effectiveness. It has found extensive usage in the creation of sulfur-based heterocyclic compounds.[32] Out of all known heterocyclic compounds, 2-aminothiophene has shown interesting uses in the areas of medicinal,[165, 166] pharmaceutical,[167, 168] and dyes.[169, 170] Their are various method for synthesis of 2-aminothiophenes such as Curtius rearrangement,[171] Schmidt reaction,[172] Hoffman reaction,[173] Beckmann rearrangement,[174] cyclization of thioamides, and S-alkyl derivative[175–177]. Nevertheless, the Gewald reaction is the most efficient procedure for synthesizing a variety of substituted 2-aminothiophenes. The Gewald reaction was first introduced by Gewald et al in 1965, this reaction has proved to be highly productive.[178]

The Gewald reaction has undergone four distinct iterations in the past, each offering unique advantages (Figure 4.1).[48, 114, 172, 179, 180] These iterations include: **(i)** the condensation of α-mercaptoketones or aldehydes with α-activated acetonitrile, in presence of basic catalyst like triethylamine or piperidine with solvent such as ethanol, dimethylformamide, dioxane or water at 50 °C **(ii)** a one-pot multi-component reaction of α-activated carbonyl compounds with α-activated acetonitrile and elemental sulfur in presence of amine such as diethylamine, morpholine, and tertiary amine. Some of the key nitrile components include malonodinitrile, cyanoacetic ester, cyanoacetamide, and ω-cyanoacetophenone.[181]

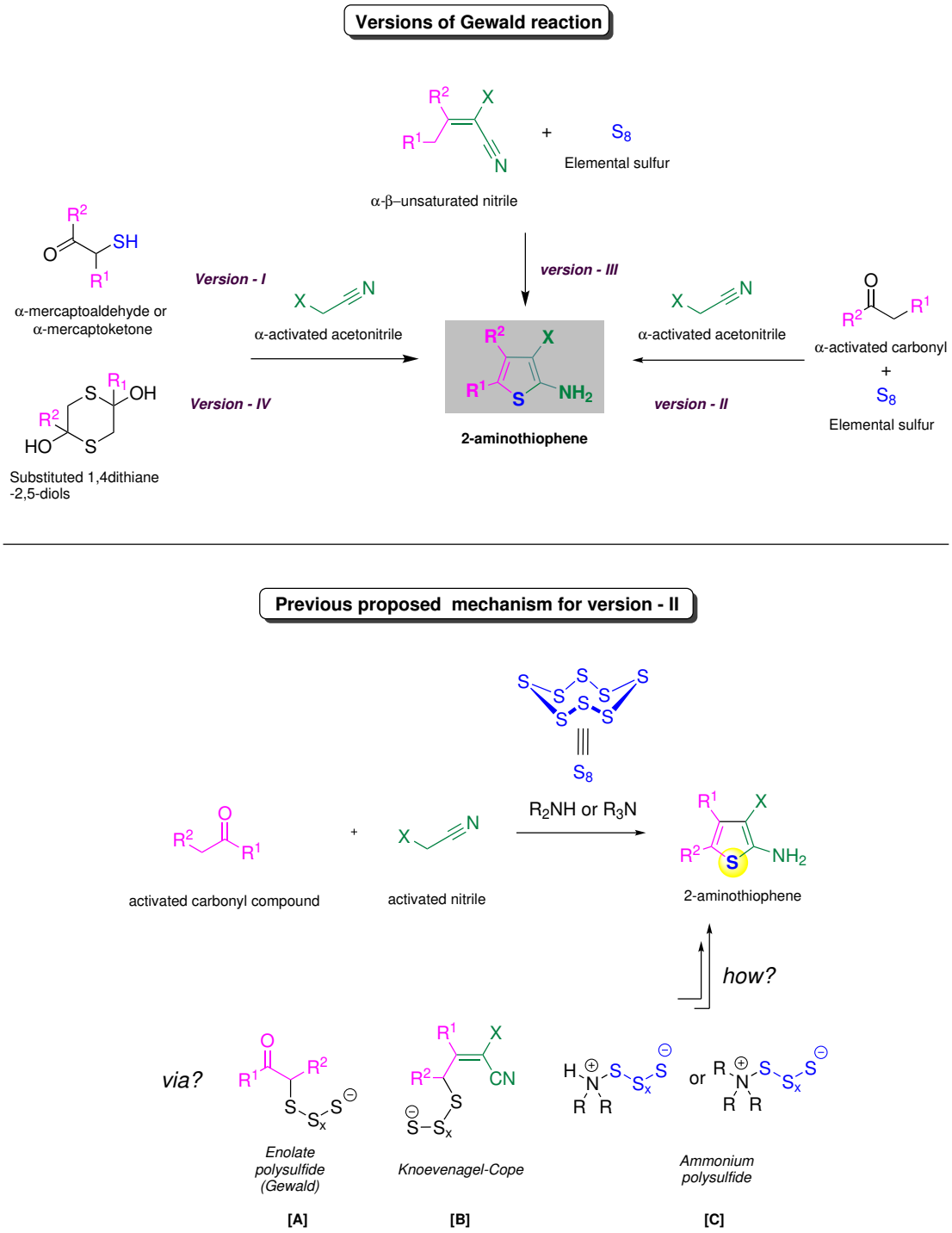

Figure 4.1 Versions and previous proposed mechanism (for version II) of Gewald reactions.

The preferred solvents are ethanol, dimethylformamide, dioxane, excess ketone such as methyl ethyl ketone or cyclohexanone **(iii)** Two-pot reaction that involve

reaction of α,β-unsaturated nitrile (Knoevenagel-Cope condensation product) with elemental sulfur and **(iv)** an improved version of (i) involving the cyclization of α-activated nitriles with dimer α-mercaptoketones or aldehydes. Secondary amine is a requisite base for this reaction, which is carried out at ambient temperature. The reaction can be performed using solvents such as cyclohexanone, methyl ethyl ketone, ethanol, and dimethylformamide.

The **second version** of the Gewald reaction, which is a one-pot multi-component procedure, stands out as the simplest and most efficient iteration. Nevertheless, its reaction mechanism remains a mystery. In the past, three pathways have been postulated for the reaction mechanism, as illustrated in Figure 4.1. According to Gewald, the enolate derived from the activated carbonyl compound initiates the opening of elemental sulfur, resulting in an enolate polysulfide prior to condensation (Figure 4.1 - product [A]).[178] Other scholars have suggested that the α, β unsaturated nitrile that is formed after the Knoevenagel-Cope condensation can be deprotonated by an amine base, leading to the opening of the sulfur ring.[114, 182–184] (Figure 4.1 - product [B]). In contrast, a contrasting hypothesis posits that the amine base initiates the opening of the sulfur ring, and the resulting ammonium polysulfide (Figure 4.1 - product [C]) is subsequently attacked by the carbanions of the α,β unsaturated nitrile.[185] As part of our group's ongoing investigation into the mechanisms of elemental sulfur and polysulfides,[142, 186] we have undertaken a study of the Gewald reaction using DFT calculations. *We now report a comprehensive study of the mechanisms, which finds that which pathway is responsible for initiating the opening of the elemental sulfur ring. Additionally, we elucidate the various mechanisms that account for the formation of 2-aminothiophene from the organic polysulfide that is initially generated.*

4.2 Computational Detail

All of our Density Functional Theory (DFT) calculations were conducted using Gaussian 16, and we used the **ωB97X-D/aug-cc-pVDZ** [98, 187] level of theory to fully optimize the geometries of all reactants, transition states, intermediates, and products. We selected the **ωB97X-D** functional due to its proven effectiveness in our previous investigations into the reaction of polysulfides with nucleophiles.[142] Throughout the calculations, we accounted for solvation effects using the SMD solvation model,[143] which is appropriate for polar solvents such as **ethanol**, a representative solvent commonly used in such transformations. To minimize the computational cost of our calculations, we selected simpler reactants, we used **butanone** and **malononitrile** as a source of α-methylene carbonyl and activated nitrile compounds, respectively,[181] while **N,N-diethylamine (DEA)** was used as the amine base source. The results reported in the main text are derived from calculations conducted at the **ωB97X-D/aug-cc-pVDZ/SMD(EtOH)** level of theory.

4.3 Results and Discussion

4.3.1 Role of amine base

To investigate which path is more energetically favored in Figure 4.1, it is important to determine which intermediate formation is more energetically favorable and can subsequently participate in the next step. To obtain answers to these questions, we must first examine the role of the base in the one-pot system. To investigate the potential role of the amine base (**DEA**), we devised three distinct pathways (as illustrated in Figure 4.2). For intermediate **A**, **A**', and **B**, the amine act as a base and removes the acidic hydrogen from activated carbonyl compound and activated nitrile, respectively, generating possible intermediates for enolate polysulfide **(A and A')** and Knoevenagel-Cope condensation **(B)** (Figure 4.1). For intermediate **C**, amine

functions as a nucleophile, opening the octa sulfur ring and yielding ammonium-polysulfide (intermediate for path C - Figure 4.1). Our computational results for the selected molecules, demonstrate that intermediate **B**, which produces the malononitrile anion (the first intermediate of the Knoevenagel-Cope condensation), is the most favorable route, with a reaction energy of only 1.6 kcal/mol, while the other two pathways exhibited high reaction energies of 25.9 [**A**], 23.7[**A'**], and 32.0 [**C**] kcal/mol, as shown in Figure 4.2. Nevertheless, the ammonium polysulfide (**C**) can stabilize itself by transferring its proton to a sulfide ion (i), releasing 10.1 kcal/mol of energy, or by donating it to the DEA base present in the solution (ii), which release 17.0 kcal/mol of energy (Figure 4.2).

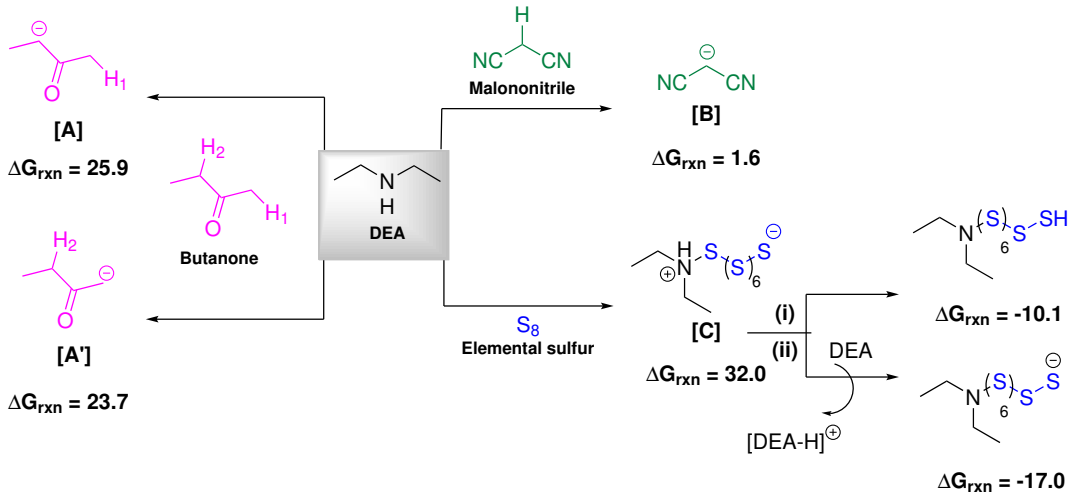

Figure 4.2 Reaction energy (kcal/mol) for deprotonation of reactants and sulfur opening by DEA (No transition structures could be located).

DFT calculations were also conducted with other amine bases, such as morpholine and triethylamine, in addition to DEA, for elemental sulfur openings. Nevertheless, in all cases, we observed high reaction energies (Figure 4.3), indicating that ammonium polysulfide won't be able to compete with malononitrile anion (**B**) formation. Furthermore, our calculations clarify that enolate polysulfide (**intermediate A** - Figure 4.1) and DEA-polysulfide (**intermediate C** - Figure 4.1) are not involved in the generation of 2-aminothiophene at room temperature.

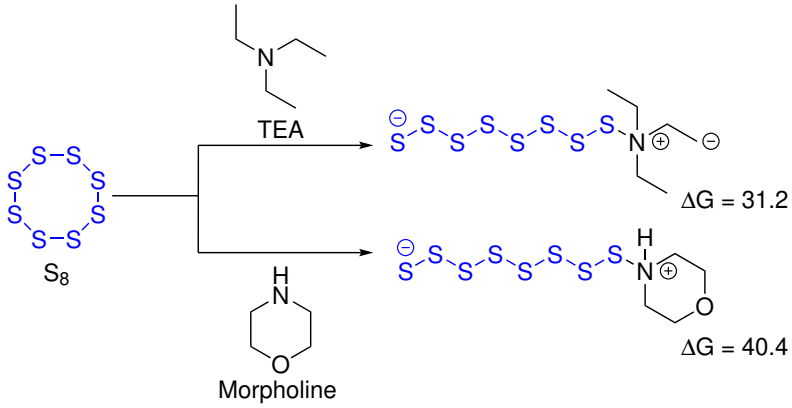

Figure 4.3 Elemental sulfur opening by TEA and morpholine. Reaction free energy in kcal/mol.

4.3.2 Sulphuration or Knoevenagel-Cope condensation

The DFT calculations clearly indicate that the initial formation of the malononitrile anion (Figure 4.2 - [**B**]) represents the first step in the one-pot Gewald reaction.

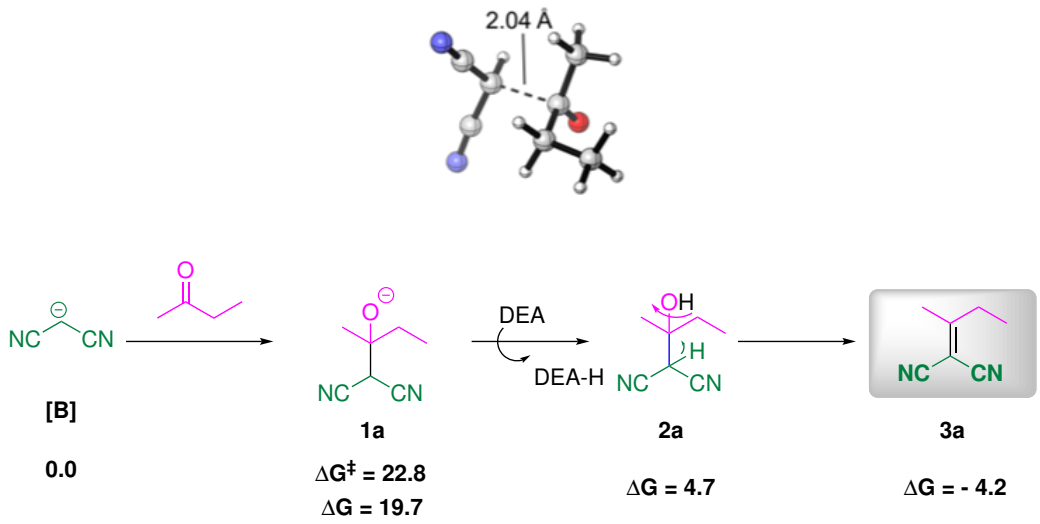

Figure 4.4 Formation of **3a** via Knoevenagel-cope condensation from malononitrile anion **(B)** and butanone.

Once formed, this intermediate enters into second step of the Knoevenagel-Cope condensation followed by the sulphuration step (i.e., opening of the octa sulfur ring). The calculation results for the second step of the Knoevenagel-Cope condensation

are presented in Figure 4.4. Our calculations demonstrate that the condensation pathways require an activation energy of 22.8 kcal/mol. Furthermore, the reaction is endothermic, necessitating 19.7 kcal/mol of reaction energy for the generation of **1a**, which can quickly form **2a** by proton transfer, releasing 15.0 kcal/mol of energy. Moreover, **2a** further stabilizes itself by undergoing dehydration, releasing an additional 8.9 kcal/mol of energy, ultimately yielding the final product of Knoevenagel-Cope condensation, namely, **3a**. This compound can then participate in the Gewald reaction.

4.3.3 Sulphuration

This step represents a key step in the overall process, as it entails the opening of the cyclooctasulfur ring **(S_8)** by a nucleophilic agent. The initial stage of the sulfuration pathway involves the deprotonation of the α,β-unsaturated malononitrile **(3a)** by **DEA**. As a result, an anionic species is generated, serving as a nucleophile capable of opening S_8 ultimately giving rise to the formation of the α,β-unsaturated malononitrile-polysulfide compound. DFT calculations were conducted for both potential malononitrile anions, namely **4a** and **5a** (Figure 4.5). The results of the calculations indicated (Figure 4.5) that the reaction energy for the formation of both anions is approximately equal (**4a** - 7.6 kcal/mol, **5a** - 6.9 kcal/mol from 3a). This finding led the question of which anion would be responsible for opening the S_8 in S_N2 fashion. To address this query, further calculations were performed to explore the ring opening by both anions, resulting in the formation of **4b** and **5b**, respectively. The DFT calculation outcomes revealed that the opening of elemental sulfur from 4a and 5a requires 21.5 and 22.4 kcal/mol of activation energy, respectively. Due to a lower barrier and reaction energy of 0.9 kcal/mol and 4.5 kcal/mol (in parenthesis) associated with 4a, the formation of 4b is favorable compared to 5b and remains as the dominant polysulfide in the solution.

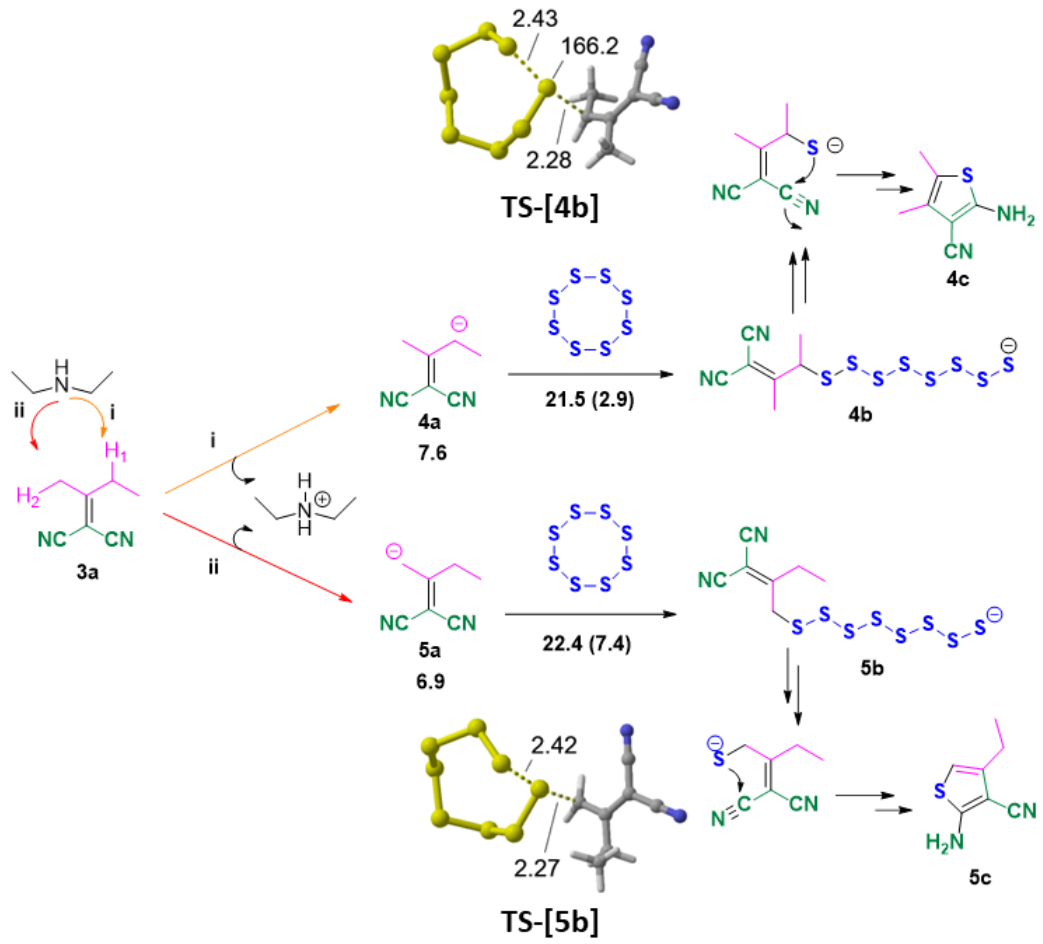

Figure 4.5 Elemental sulfur opening from respective anions of **3a**. Free energy in kcal/mol.

In this study, various carbon nucleophiles have been studied, along with **3a**, for opening the elemental sulfur that has been discussed in the appendix (Table 1).

4.3.4 α,β-unsaturated malononitrile-polysulfide (4b) to 2-aminothiophene

It is clear from the calculations that **4b** is likely the major polysulfide intermediate after S_8 opening. Nevertheless, the final product of the Gewald reaction is **2-aminothiophene**, which has only one sulfur atom in its skeleton. To get rid of the extra seven sulfur atoms, (further involve in product formation) **4b** must undergo some degradation. In previous literature, various mechanisms have been proposed for the generation of 2-aminothiophene. Vinogradoff (1986) suggested a mechanism

in which the first step involves the removal of the cycloheptasulfur ($\mathbf{S}_7$) molecule, followed by cyclization and proton transfer leading to the formation of the desired product.[188] Sabnis et al., in their review article on Gewald reaction, and other scientists proposed a concerted mechanism where cyclization and $\mathbf{S}_7$ removal occur simultaneously.[172, 189, 190] Nevertheless, in both of these mechanisms, **4a** does not play any further role, indicating that both mechanisms involve unimolecular intramolecular cyclization. Nevertheless, it is crucial to investigate whether **4a** or another smaller polysulfide will participate in polysulfide degradation via the bimolecular reaction pathway. Experimental evidence or kinetic studies regarding the degradation of polysulfides and the formation of mercaptides are still lacking.

To explore potential pathways for the degradation of polysulfides and the generation of 2-aminothiophene, we have designed several plausible paths, which are discussed below.

4.3.5 Unimolecular cyclization vrs bimolecular degradation

For the purpose of investigating the shrinkage route for polysulfide **4b**, DFT calculation has been conducted on **4b**, using a **bimolecular decomposition** (Figure 4.6) with an external nucleophile **(4a)**. The calculated results from the bimolecular reaction (**for monosubstituted polysulfide formation**) reveal that the nucleophile's attack on the middle sulfur shows the most favorable activation energy, with a value of $\Delta G^{\ddagger}$ 23.1 **($\mathbf{S}^4$)** and 24.3 **($\mathbf{S}^5$)** kcal/mol (Figure 4.6). This favorable energy barrier can be attributed to its distance from the bulky group at the $\mathbf{S}^1$ position, as well as the lesser repulsive force exerted by the sulfide anion. On the other hand, the activation energy required for an attack on $\mathbf{S}^2$, $\mathbf{S}^6$, and $\mathbf{S}^7$ exhibits significantly higher barriers 6.4, 7.7, and 7.8 kcal/mol, respectively, in comparison to $\mathbf{S}^4$ due to the shorter distance from $\mathbf{S}^1$ and the sulfide anion, which causes more steric hindrance and repulsion. The NBO analysis of NuS_8^- provides additional evidence,

confirming that the σ^* orbital between S^3 and S^4 is indeed their LUMO, with larger coefficients on S^4 (see appendix Table 4). From the calculation results, it is clear that trisulfide $^-$**[S_3Nu]** and tetrasulfide $^-$**[S_4Nu]** (**Nu = 4a**), along with their respective fragments, are the most favorable options.

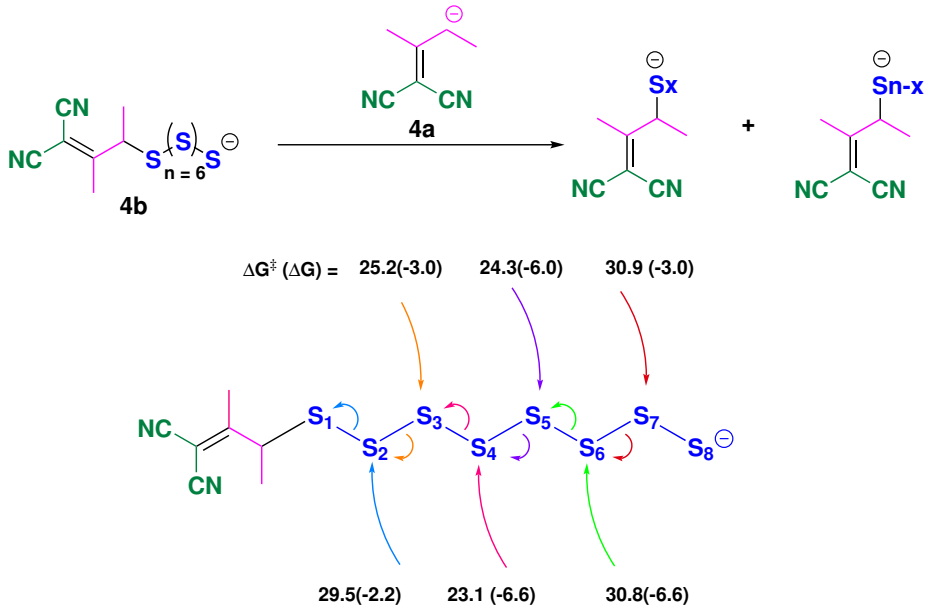

Figure 4.6 Possible pathways for attack of **4a** on **4b** to form monosubstituted polysulfides. Free energies of activation (free energies of reaction in parenthesis) are in kcal /mol. See appendix Information for visualizations of all transition structures and minima.

Figure 4.7 illustrates the transition structures representing the most favorable $\mathbf{S}^4$ and least favorable $\mathbf{S}^7$ attack. Detailed information and additional structures can be found in the appendix (Figure 6). These geometries represent a thermodynamic effect. The S...S bond length for the attack on $\mathbf{S}^4$ is 2.43 Å, while for $\mathbf{S}^7$, it has increased by 0.17 Å, aligning with the predictions of the Hammond postulate.

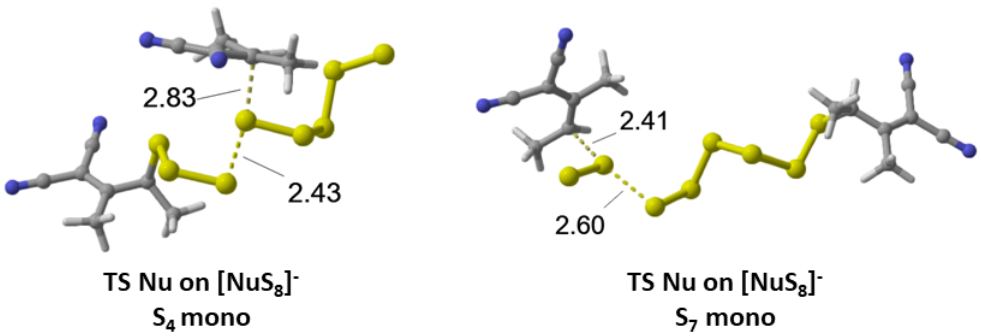

Figure 4.7 Associates TS structures for bimolecular reaction for attack on S^4 and S^7.

The complete degradation of polysulfide via bimolecular decomposition at $\mathbf{S}^2$ has been calculated due to formation of the monosulfide, which would lead to the thiophene quickly, is not favorable here compared to our previous study. Detailed calculation results and associated TS structures, have been shown in the appendix (Table 5 and Figure 7). For the other considered carbon nucleophile, the first step of bimolecular decomposition for poly-(octasulfide) has also been calculated and shown in the appendix (Table 2).

Notably, bimolecular decomposition in another fashion, which leads to the formation of a **disubstituted polysulfide** and a **dianionic polysulfide**, was also conducted and is shown in Figure 4.8. The transition state for attack on all the sulfur was successfully located except S^1. Based on the activation energy values, it can be inferred that as the nucleophile approaches the sulfide anion of polysuldide, both the activation barrier and reaction energy increase due to repulsion between attacking nucelophile and sulfide anion. A significant increase in reaction energy was observed between the attack on $\mathbf{S}^4$ and $\mathbf{S}^5$, resulting in 11.3 kcal/mol more reaction energy for $\mathbf{S}^5$. The calculation results reveal that the formation of $\mathbf{S}_3$, $\mathbf{S}_2$, and $\mathbf{S}_1$ dianions is not energetically favorable. Nevertheless, the negative values of reaction energy for attack on $\mathbf{S}^1$ and $\mathbf{S}^2$ show that these two attacks can be competitors for the poly-(octasulfide) session, leading to the formation of $\mathbf{S}_7$ and $\mathbf{S}_6$ **dianions**, along with their disubstituted partners **Nu-S-Nu** and **Nu-S-S-Nu**.

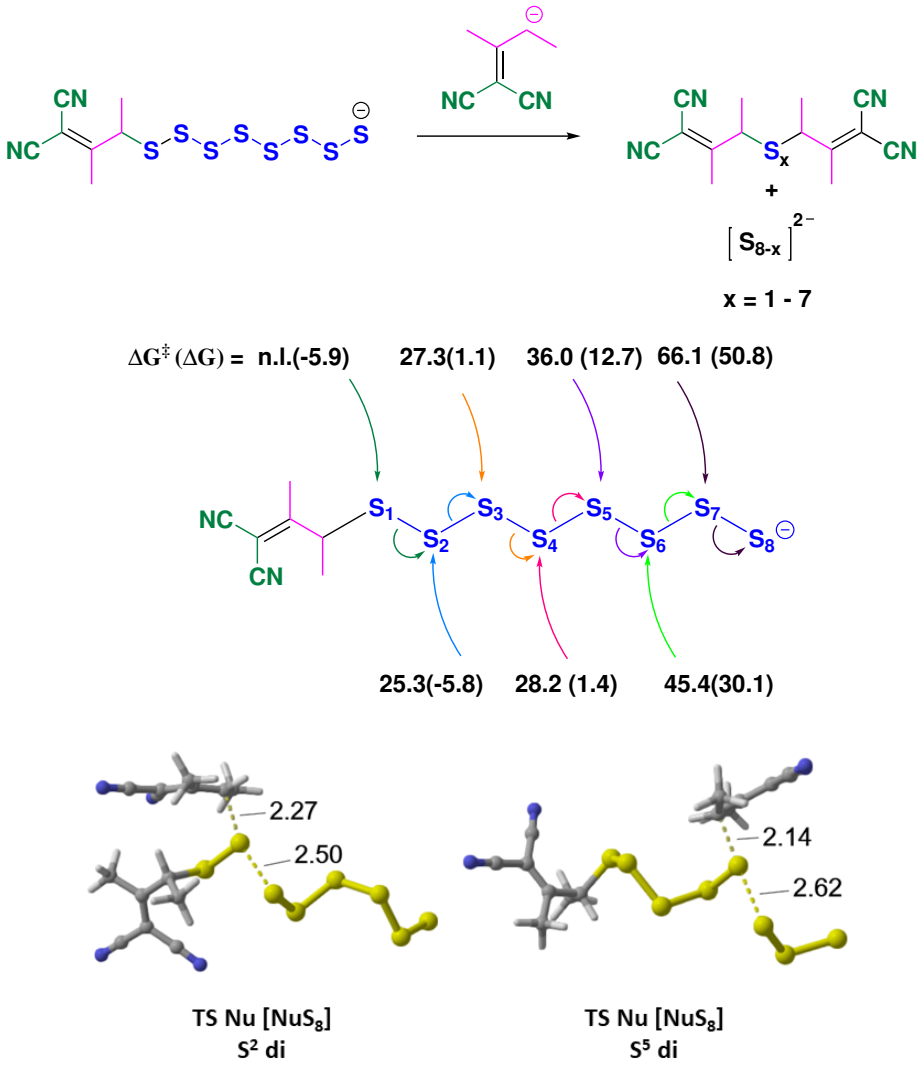

Figure 4.8 Possible pathway for attack of **4a** on **4b** to form disubstituted polysulfide products.

To confirm whether these products can participate in further reactions, additional calculations were performed, as shown in Table 4.1. The first step of the reaction is the protonation step by DEA. The calculation results show that as the chain length of the dianion decreases, the reaction energy for protonation decreases **(step - I)**, due to an increase in pKa value. In contrast, the value of the reaction energy increases for **step - II** as the chain length of the thiol anion decreases. Nevertheless, in all of these transformations, there is no driving force that favors the

formation of the final product. Therefore, there is a high chance that all the products will further change back into reactants and ultimately form poly-(octasulfide), which takes another path for its decomposition.

Table 4.1 Reaction Free Energies (kcal/mol) for Protonation-induced Intermolecular Degradation of Dianion

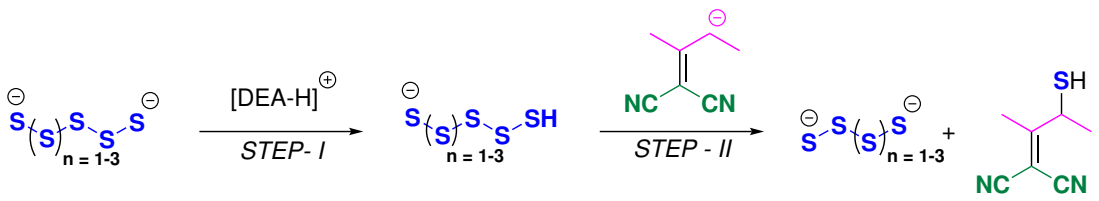

Dianion	n	$\Delta G_{reaction-stepI}$	$\Delta G_{reaction-stepII}$
S_7^{2-}	3	4.1	-3.9
S_6^{2-}	2	2.5	-1.0
S_5^{2-}	1	-0.2	3.8

The further possible route for the decomposition of poly-(octasulfide) is through **unimolecular intramolecular cyclization**, as shown in Figure 4.9. This route involves the ring-closing process, resulting in the generation of sulfides and their corresponding cyclic sulfur allotropes. The calculation results indicate that the most favorable transformation occurs through shrinking at $\mathbf{S}^3$, with an activation energy of $\Delta G^{\ddagger}$ = 11.9 kcal/mol. This leads to the formation of cyclic hexa sulfur (S_6), accompanied by the generation of disulfide $^{-}[S_2Nu]$. On the other hand, attacks on $\mathbf{S}^2$ ($\Delta G^{\ddagger}$ = 16.2 kcal/mol) and $\mathbf{S}_4$ ($\Delta G^{\ddagger}$ = 17.1 kcal/mol) lead to the formation of monosulfide $^{-}[SNu]$ and trisulfide $^{-}[S_3Nu]$, along with the formation of $\mathbf{S}_7$ and $\mathbf{S}_5$ rings. This outcome contrasts with the bimolecular path, where the attack on $\mathbf{S}^4$ was more favorable. The results suggest that unimolecular cyclization is primarily governed by the stability of cyclic sulfur allotropes and the interplay of steric and repulsive effects when **4b** shrinks.

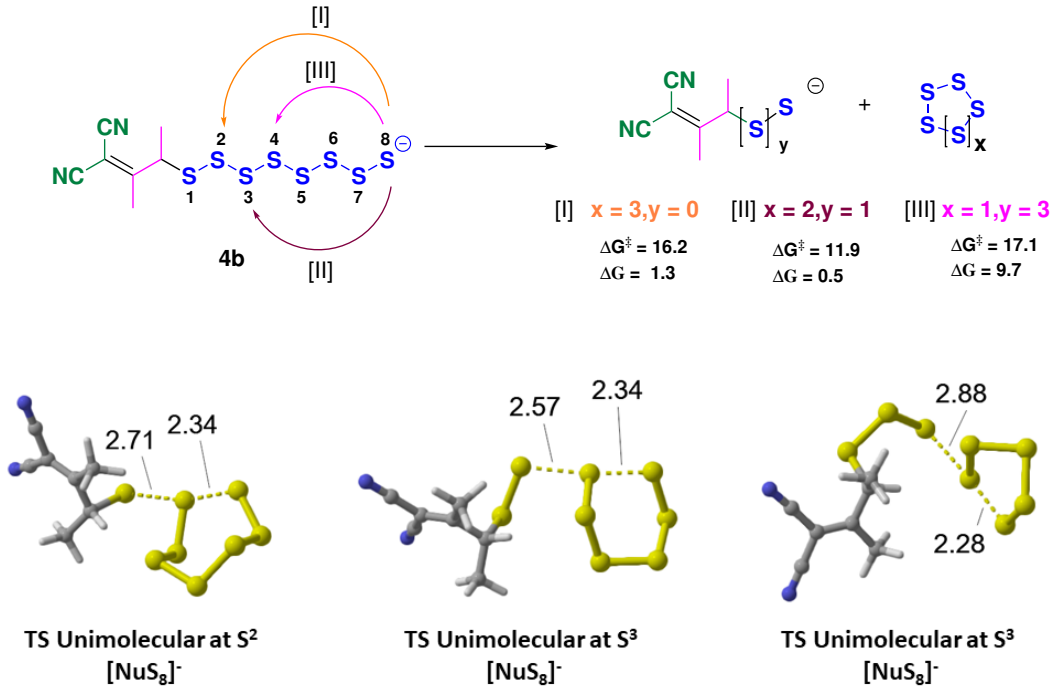

Figure 4.9 Possible attack of sulfide anion via unimolecular cyclization route (top) with free energy in kcal/mol. Associated TS structures (bottom).

Notably, cyclic $\mathbf{S}_6$ exhibits greater stability in comparison to cyclic $\mathbf{S}_5$ and cyclic $\mathbf{S}_7$.[72] This observation is further supported by the obtained reaction energies, which is lesser for attack on $\mathbf{S}^3$ (ΔG = 0.5 kcal/mol), while becoming more endothermic for attack on $\mathbf{S}^2$ and $\mathbf{S}^4$ (ΔG = 1.3 and 9.7 kcal/mol), respectively, as smaller and less stable cyclic sulfur allotropes start to form from **4b**. The transition state **(TS)** structures demonstrate the influence of the Hammond postulate, with a shorter leaving S...SNu bond observed in the TS on $\mathbf{S}^4$ compared to the TS on $\mathbf{S}^3$. Despite the less favorable nucleophilic attack on $\mathbf{S}^2$, we investigated the unimolecular cyclization on $\mathbf{S}^2$ for all successively smaller polysulfides, as shown in Subsection **4.3.6.** This is because the direct formation of monosulfide serves as a precursor for the generation of 2-aminothiophene. Interestingly, we observe that, when compared to $^{-}$**CN** and $\mathbf{PMe}_3$ nucleophiles, the formation of monosulfide (via attacks at $\mathbf{S}^2$ through the bimolecular and unimolecular cyclization routes) from **4b** does not exhibit the lowest activation energy in any of the pathways.[186] This variation arises because the sulfide

anion of monosulfide from $^{-}$**CN** and $\mathbf{PMe_3}$ benefits from resonance stabilization, which enhances its formation in comparison to other larger sulfide fragments. In contrast, the monosulfide derived from **4b** lacks resonance stabilization. Unimolecular cyclization for other considered carbon nucleophile, at $\mathbf{S}^2$ has been shown in appendix (Table 3).

When examining the calculation results obtained from bimolecular and unimolecular path, for the formation of monosubstituted sulfides with **4b** shrinkage, it becomes clear that kinetically, the later path is more favorable. This can be attributed to the significant difference of 11.2 kcal/mol in activation energy between their respective lowest values. Nevertheless, in unimolecular reaction pathway, product and reactants are in equilibrium due to the positive value of the reaction energy.

4.3.6 Unimolecular decomposition of polysulfides on $\mathbf{S}^2$ assisted by Ring Opening

Poly-(octasulfide), through unimolecular cyclization, generate two stable cyclic allotropes of sulfur, $\mathbf{S}_7$ and $\mathbf{S}_6$, through attacks on $\mathbf{S}^2$ and $\mathbf{S}^3$. Nevertheless, for polysulfides shorter than [NuS_8^-], such as [NuS_7^-] and [NuS_6^-] the cyclization on $\mathbf{S}^2$ is always the most favored compared to $\mathbf{S}^3$ due to the formation of a larger sulfur ring. As a result, the unimolecular cyclization on $\mathbf{S}^2$ for all successively smaller polysulfides was investigated. The calculation result shows that, the cyclization of shorter polysulfide such as [NuS_6^-] and [NuS_5^-], which exhibited a 6.3 kcal/mol higher barrier as indicated in Table 4.2 compare to longer polysulfide (NuS_7^- and NuS_8^-). It is important to note that as the chain length of the polysulfide shortens, the cyclization reaction becomes energetically increased, resulting in a more endothermic process. Nevertheless, in contrast to unimolecular cyclization, the opening of their corresponding allotropes by **4a(Nu)** showed an opposite trend.

Table 4.2 Activation and Reaction Free Energy (kcal/mol) for Unimolecular Decom-position of Polysulfides on S^2 and Sulfur Allotrope Opening by **4a**

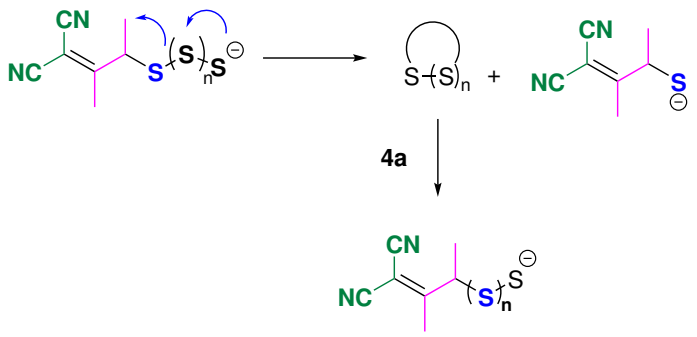

Polysulfide	n	$\Delta G^{\ddagger}$	$\Delta G_{reaction}$	Cyclic sulfur allotrope	$\Delta G^{\ddagger}$	$\Delta G_{reaction}$
NuS_8^-	5	16.2	1.3	S_7	16.8	-3.5
NuS_7^-	4	15.2	0.5	S_6	19.3	-3.5
NuS_6^-	3	21.5	12.2	S_5	12.0	-16.3
NuS_5^-	2	n.l.	35.1	S_4	7.0	-35.4

For example, the cyclization of NuS_6^- to S_5 and monosulfide exhibited an activation energy of 21.5 kcal/mol, while the opening of S_5 was exothermic (-16.3 kcal/mol reaction energy) with a lower activation barrier of 9.5 kcal/mol. This is due to the formation of a shorter and unstable strained sulfur ring. The representative TS structures for both the path has been shown in Figure 4.10. The calculation results also shows that if smaller allotropes are formed in solution, they will always be opened faster than initial S_8 opening. The TS structures associated with sulfur allotropes opening by 4a has been shown in appendix (Figure 8).

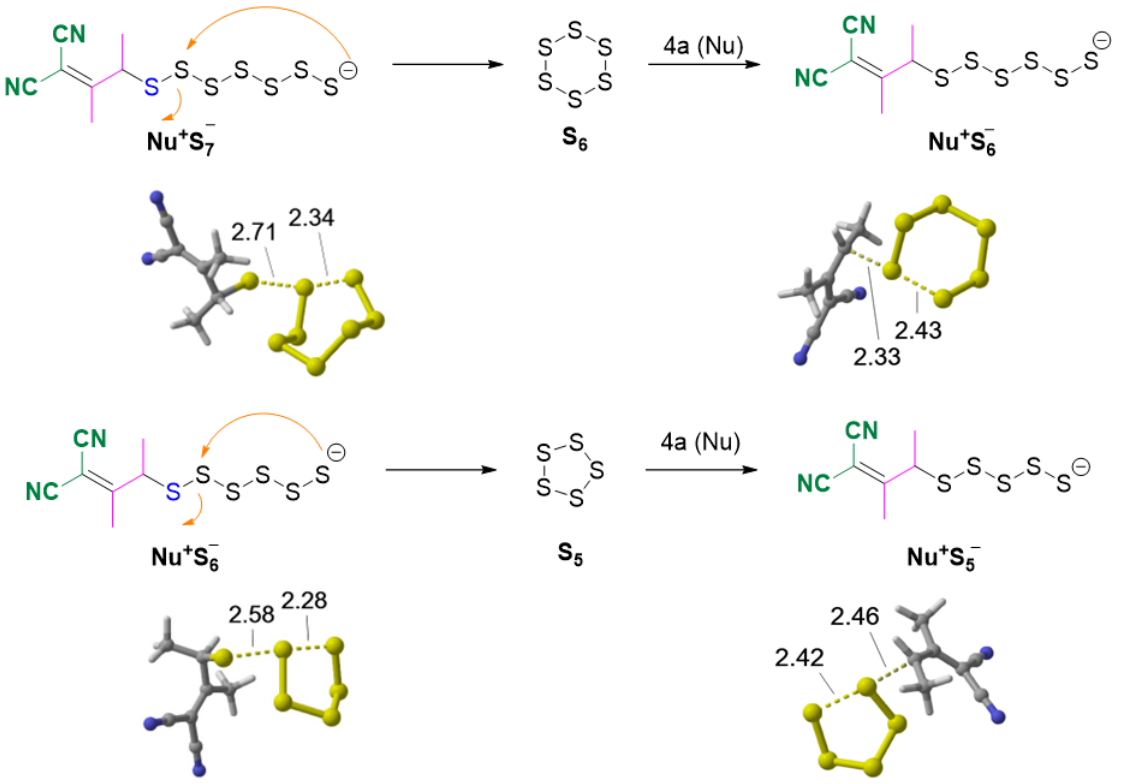

Figure 4.10 Representative TS structures for unimolecular decomposition and sulfur allotrope ring opening.

4.3.7 Scrambling of polysulfides

Subsequently, we considered the probability of short polysulfides acting as nucleophiles in bimolecular reactions, while the same polysulfide or a different chain length of polysulfide or sulfur allotropes would function as electrophiles. For the scrambling, in first part of investigation, we focused on $\mathbf{S}_8$ as the electrophilic allotrope partner due to its high concentration in solution. In second part of investigation, various chain length of polysulfide were scrambled together. Table 4.3 displays the reaction energy for ($\mathbf{S}_8$) opening when considering polysulfides as the nucleophilic source. From the observed trend, it has been observed that as the chain length of polysulfides decreases, the reaction energy for ($\mathbf{S}_8$) opening decreases as well, shows strong nucleophilic nature of smaller polysulfides in comparison to larger ones. Nevertheless, the reaction

energy for all the scrambling remains high when compared to the previous shown pathway.

Table 4.3 Reaction Free Energy (kcal/mol) Associated with Scrambling of Considered Polysulfide with S_8

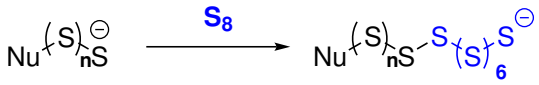

Polysulfide	$\Delta G_{reaction}$
NuS_5^-	13.2
NuS_4^-	11.5
NuS_3^-	9.3
NuS_2^-	7.0
NuS^-	6.0

In the second part, scrambling between polysulfides was explored, where $[NuS_2]^-$ was selected as nucleophile and scrambled on $[NuS_2]^-$ to $[NuS_6]^-$ at their most electrophilic sulfur atom (see appendix Table 4). The results showed almost equal reaction energy for all the polysulfides considered (Table 4.4). Along with this calculation, scrambling at various sulfur positions of polysulfide was also tested. For this calculation, $[NuS_6]^-$ was scrambled with $[NuS_6]^-$ at various positions (Figure 4.11). The calculation results revealed that attacking the sulfide anion or its adjacent position is the best site.

Table 4.4 Reaction Free Energy (kcal/mol) Associated with Scrambling of $[NuS_2]^-$ with Considered Polysulfide as Electrophile

Electrophile	$\Delta G_{reaction}$
NuS_6^- (at S^4)	-3.6
NuS_5^- (at S^3)	0.0
NuS_4^- (at S^2)	-2.0
NuS_3^- (at S^2)	- 1.5
NuS_2^- (at S^2)	-1.8

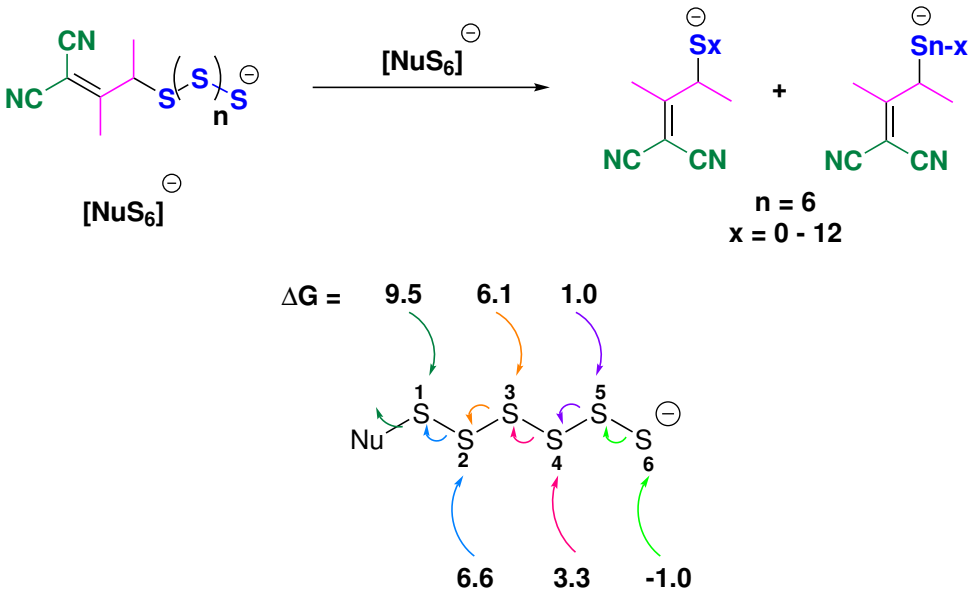

Figure 4.11 Reaction free energy (kcal/mol) associated with scrambling of $[NuS_6]^-$ with $[NuS_6]^-$as electrophile on various position.

Unfortunately, we were unable to identify the transition state associated with any of the considered scrambling reactions. Therefore, it is difficult to say whether, despite having negative reaction energy for few scramblings, the reaction would be favorable. Overall, none of the scramblings show particularly favorable reactions thermodynamically, further remonstrating that the various polysulfide lengths are under equilibrium.

4.3.8 Protonation-induced intermolecular degradation of polysulfides

Along with above possible route, we searched for additional plausible pathways. In contrast to the reaction of sulfur with cyanide and phosphines, the Gewald reaction involves an acid-base equilibrium and a protic solvent. Thus we wondered whether protonation of the polysulfide could provide a favorable pathway to the monosulfide. We speculated whether **4b** undergoes protonation by the **[DEA-H]**$^+$ in the solution (**step - 1**), subsequently triggering the cleavage of the SH bond in **4b'** via bimolecular degradation (**step - II**). This process is facilitated by **4a**, leading to the formation of thiol (**4b"**) along with their corresponding smaller polysulfides.

Table 4.5 Activation and Reaction Free Energies (kcal/mol) for Protonation-induced Intermolecular Degradation of Polysulfides

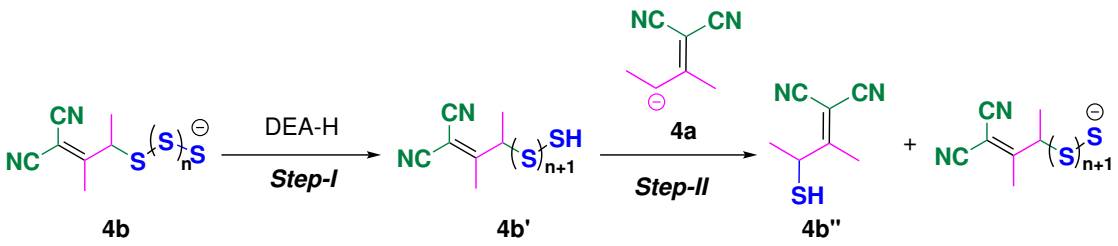

Polysulfide	n	$\Delta G_{reaction-stepI}$	$\Delta G^{\ddagger}_{stepII}$	$\Delta G_{reaction-stepII}$
NuS_8^-	6	8.3	16.4	-9.4
NuS_7^-	5	7.8	17.1	-9.8
NuS_6^-	4	7.0	18.2	-10.0
NuS_5^-	3	6.8	19.5	-6.0
NuS_4^-	2	6.2	20.0	-5.9
NuS_3^-	1	4.4	18.2	-3.8
NuS_2^-	0	2.4	21.8	-3.6

This process will continue until the complete degradation of polysulfide, which will lead to formation of 7 molecules of thiol with one monosulfide. The energy

obtained for all this cleavage has been summarized in Table 4.5 with each step independent calculation. The formation of the initial protonated poly-(octasulfide) (**4b'**) from poly-(octasulfide) (**4b**) required an energy input of 8.3 kcal/mol. The **4b'** then underwent conversion to the respective monosulfide thiol (**4b"**), releasing 1.1 kcal/mol of energy from **4b**. The conversion process involved an activation barrier of 16.4 kcal/mol. As a result of this transformation, **4b"** and shorter polysulfides were obtained. It has been observed from the calculation results that there is a correlation between the chain length of polysulfide and the reaction energy for sulfide protonation by **DEA**. As the polysulfide chain length decreases, the reaction energy decreases as well. Specifically, the NuS_2^- reaction only requires 2.4 kcal/mol of energy, whereas the NuS_8^- reaction necessitates 8.3 kcal/mol for the conversion of their respective thiol. This result is consistent with the pka value of polysulfide, as cited,[13] where long polysulfides are more acidic. The positive reaction energy for thiol formation from all respective sulfide anions shows that the thiolation procedure is always in thermodynamic equilibrium. Moreover, larger polysulfides exhibit lower pK_a values compared to smaller polysulfides, further supporting these findings.

The investigation of the bimolecular decomposition route (**Step - II**) reveals that shorter chain lengths of the thiol show higher activation and reaction energy compared to longer chains. For example, NuS_8H requires 16.4 (-9.4) kcal/mol of activation and reaction energy for bimolecular degradation, while NuS_2H requires an additional 5.4 (5.8) kcal/mol of activation and reaction energy compared to NuS_8H.

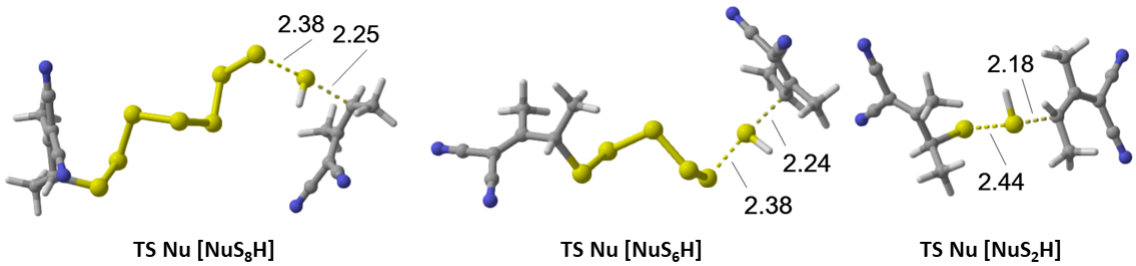

Figure 4.12 Representative TS structures for protonation-Induced intermolecular degradation of Polysulfides.

The phenomenon can be attributed to the nature of the leaving group that is linked to the thiol chain. In the case of longer polysulfide thiol, it cleaves to form longer polysulfides. Due to their weaker basicity, longer polysulfides function as good leaving groups. Nevertheless, in the case of smaller chain thiols, shorter polysulfides are generated, which possess a strong basic character and make their formation challenging. The transition state (TS) structures depicted in Figure 4.12 show minimal variation in bond breakage (S-SH) and formation (HS-Nu). This consistency is attributed to the nearly equal total barrier observed for systems of different chain lengths. For instance, the formation of $[NuS_7]^-$ + NuSH (TS) from $[NuS_8]^-$ requires a total energy of 24.7 kcal/mol, while the formation of $[NuS]^-$ + NuSH from $[NuS_2]^-$ requires 24.2 kcal/mol. This indicates that both steps are governed by acidity/basicity principles. Protonation of $[NuS_2]^-$ is relatively easier, but subsequent liberation of a monosulfide during the attack becomes more challenging due to its stronger basicity. The associated TS structure for all the entry for Table 4.5 has been shown in appendix (Figure 10).

We then considered the possibility of a different approach by **4a**, where instead of targeting the terminal SH group, an attack could be directed towards an adjacent sulfur atom using two distinct mechanisms (as depicted in Figure 4.13).

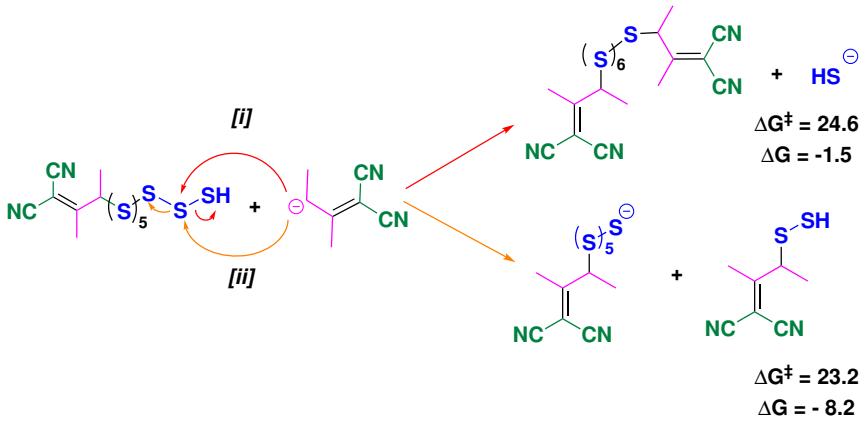

Figure 4.13 Example products from both possible bond cleavages upon nucleophilic attack on protonated polysulfide. Free energy in kcal/mol.

The attack via the first mechanism, denoted as **[i]**, resulted in the generation of a thiol anion $[HS]^-$ along with a disubstituted polysulfide $[NuS_6Nu]$, requiring 32.9 (8.3 + 24.6) kcal/mol of activation energy. On the other hand, in the second pathway, denoted as **[ii]**, the attack occurred at the same sulfur atom, but the cleavage of the S-S bond took place in the opposite direction compared to **[i]**. This led to the formation of a monosubstituted hexasulfide $[NuS_6]^-$ and a persulfide [NuSSH], necessitating 31.5 (8.3 + 23.2) kcal/mol of activation energy. For both the path, reaction energy shows negative value of -1.5 and -8.2 kcal/mol. Notably, both of these pathways exhibited an activation barrier 8.2 and 6.4 kcal/mol higher than that observed for the **4b** in entry 1 (Table 4.5).

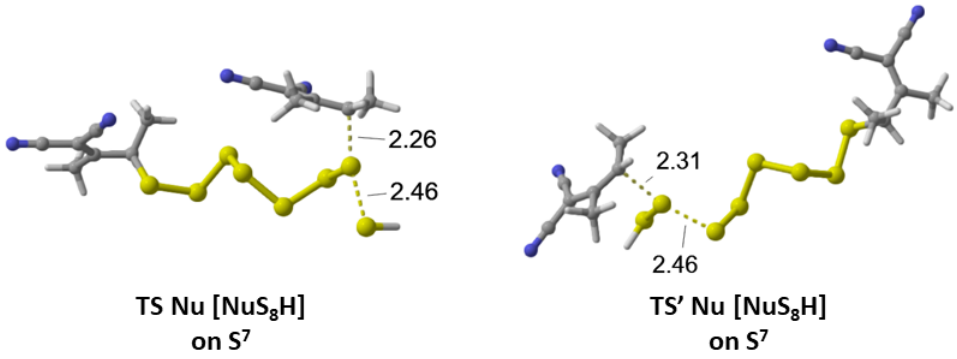

Figure 4.14 Associated TS structures for path (i) and path (ii).

Additional DFT calculations were performed for the second pathway involving attack on $\mathbf{S}^5$ (see appendix Figure 11). Nevertheless, due to the higher barrier, the possibility was discarded. Associated TS structures for path I and II has been shown in Figure 4.14.

4.3.9 Cyclization of monosulfide vs. disulfide.

From the above calculation, the initial degradation of poly-(octasulfide) via bi-molecular, unimolecular cyclization is competitive with protonation-induced inter-molecular degradation. Due to the positive value of reaction free energy or the

near-zero value of reaction energy, all these pathways are under thermodynamic equilibrium. Nevertheless, it is important to know how the formed disulfide and monosulfide, via unimolecular cyclization or proton-induced pathway, could further behave in the system. One of the most possible paths is cyclization. We calculated cyclization for both monosulfide and disulfide, that has been discussed below.

2-Aminothiophene formation from monosulfide The ultimate objective of this study is to investigate the mechanism through which 2-aminothiophene form via monosulfide. The reaction pathway has been shown in Figure 4.15.

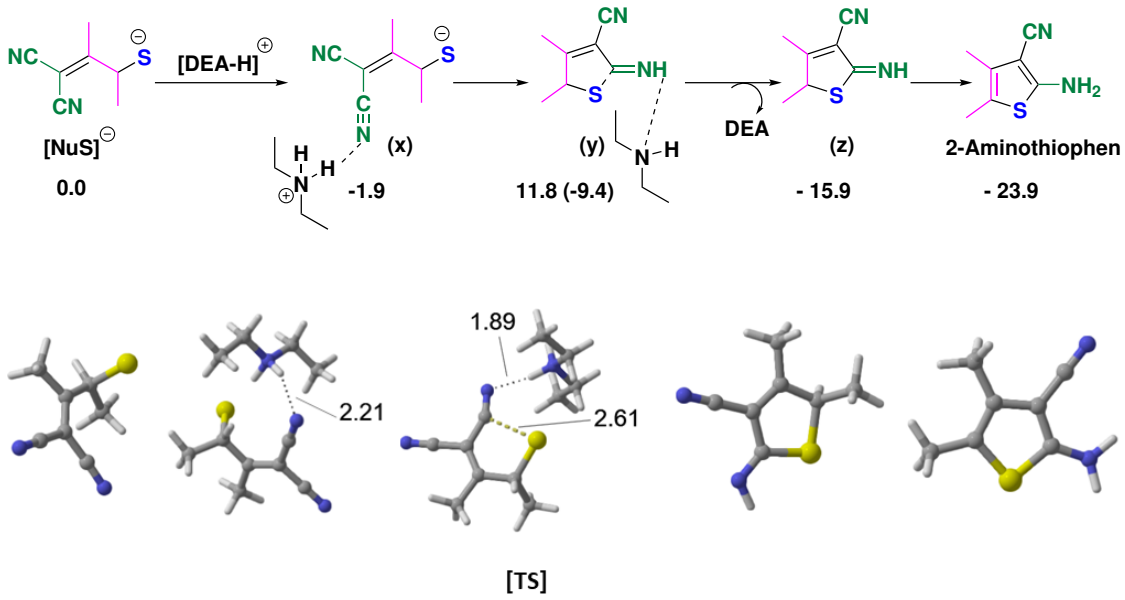

Figure 4.15 2-Aminothiophene formation from monosulfide. Free energy in kcal/mol.

The sulfide anion of $[NuS]^-$ first proceeds to attack the sp carbon of CN, initiating a cyclization. This step is promoted by the adduct formation between $[DEA\text{-}H]^+$ and the nitrogen attached to the sp carbon, resulting in the formation of species **y**. This pathway requires 11.8 kcal/mol of activation energy, while releasing 9.4 kcal/mol of energy during the process. Species **y** transforms by releasing 15.9

kcal/mol of energy through the removal of DEA. Finally, by releasing 23.9 kcal/mol, it tautomerizes to gain aromaticity and forms **2-aminothiophene**.

Cyclization of disulfide The disulfide, which is formed by unimolecular cyclization on S^3 or by protonation-induced intermolecular degradation of polysulfide from $[NuS_3]^-$, can cyclize to give the final product **z'** as shown in Figure 4.16. The first step of this cyclization is the attack of a sulfide anion of $[NuS_2]^-$ on its sp carbon atom, forming **x'**. It requires 14.2 kcal/mol of reaction energy, with activation barrier of 15.9 kcal/mol. The next step is DEA removal, which releases 2.7 kcal/mol of energy. Finally, by releasing 7.8 kcal/mol of energy, the cyclic product (Z') of the disulfide is formed.

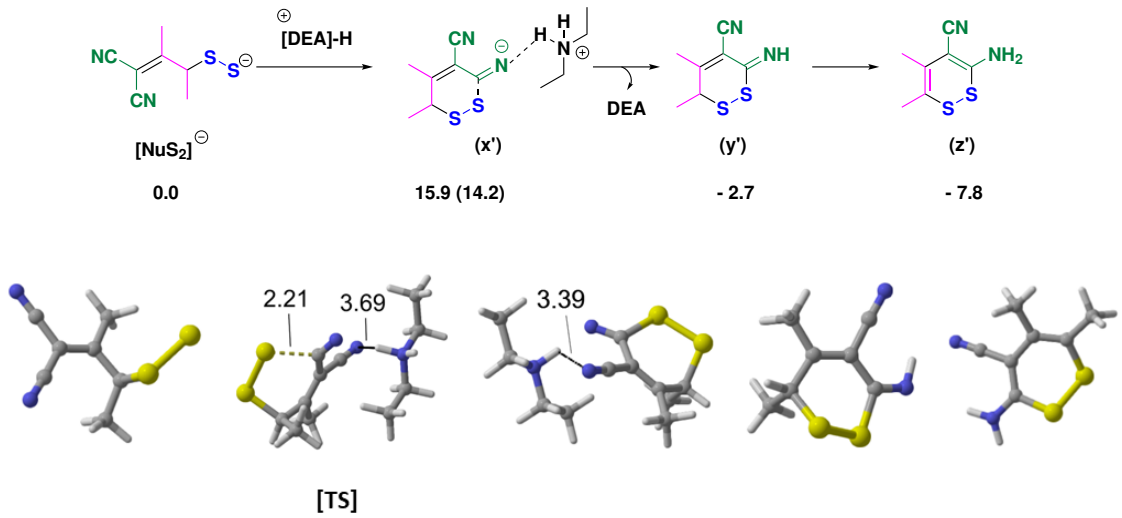

Figure 4.16 Cyclization of disulfide. Free energy in kcal/mol.

If we compare cyclization of $[\mathbf{NuS_2}]^-$ and $[\mathbf{NuS}]^-$, it is clear that the cyclization of disulfide is not as energetically favored as that of monosulfide. Disulfide requires energy for cyclization (14.2 kcal/mol), while monosulfide releases energy for cyclization (-9.4 kcal/mol). On the other hand, monosulfide eventually forms the aromatically stabilized product 2-aminothiophene, whereas the cyclized product of disulfide **(Z')** is not aromatically stabilized. This finding also clarifies that, despite

the higher activation energy associated with the unimolecular cyclization on S^2, our analysis reveals that this pathway remains competitive with unimolecular cyclization on S^3 and protonation-induced intermolecular degradation due to the direct formation of monosulfide, which subsequently leads to the production of 2-aminothiophene.

4.4 Full Reaction Pathway

The Figure 4.17 illustrates the complete pathways for the Gewald reaction mechanism. The initial step of the Gewald reaction involves the Knoevenagel-Cope condensation, where the deprotonated malononitrile anion and butanone react to form the Knoevenagel-Cope condensation product **3a**. This reaction serves as the starting point for the subsequent transformations. Subsequently, the active hydrogen present in compound 3a undergoes deprotonation by DEA (diethylamine) at the alpha hydrogen of the ethyl substituent, resulting in the formation of compound **4a**. Compound **4a** plays a crucial role in opening the elemental sulfur ring. The activation energy required for the opening of elemental sulfur through compound **4a** is 21.5 kcal/mol. This energy barrier is responsible for the stability exhibited by the octasulfur ring. Upon opening the elemental sulfur, compound **4a** leads to the formation of $[NuS_8]^-$ (**4b**).

At this point, the polysulfide $[NuS_8]^-$ presents itself with three potential alternatives for the chain sessions. Option (i) involves successive protonation-induced intermolecular degradation. This process leads to the formation of one molecule of monosulfide along with thiols. Notably, the first three steps of this path, compete with the other proposed pathways, namely option (ii), while path (iii) competes with the first step only. In the case of path (ii), the unimolecular cyclization at S^2 and S^3 both play a role in $[NuS_8]^-$ decomposition, which leads to the formation of S_7 and S_6 allotropes with $[NuS]^-$ and $[NuS_2]^-$. Both paths require activation barriers of 16.9 and 11.9 kcal/mol, respectively. Nevertheless, these two cyclizations require 1.3 and

0.5 kcal/mol of reaction energy, which brings this path to thermodynamic equilibrium. From here, S_7 leads to the formation of $[NuS_5]^-$ by releasing two molecules of $[NuS]^-$. The highest barrier for this transformation is 21.5 kcal/mol. On the other hand, S_6, which is formed via cyclization at S^3, opens up by 4a and forms $[NuS_5]^-$ by removing one molecule of $[NuS]^-$.

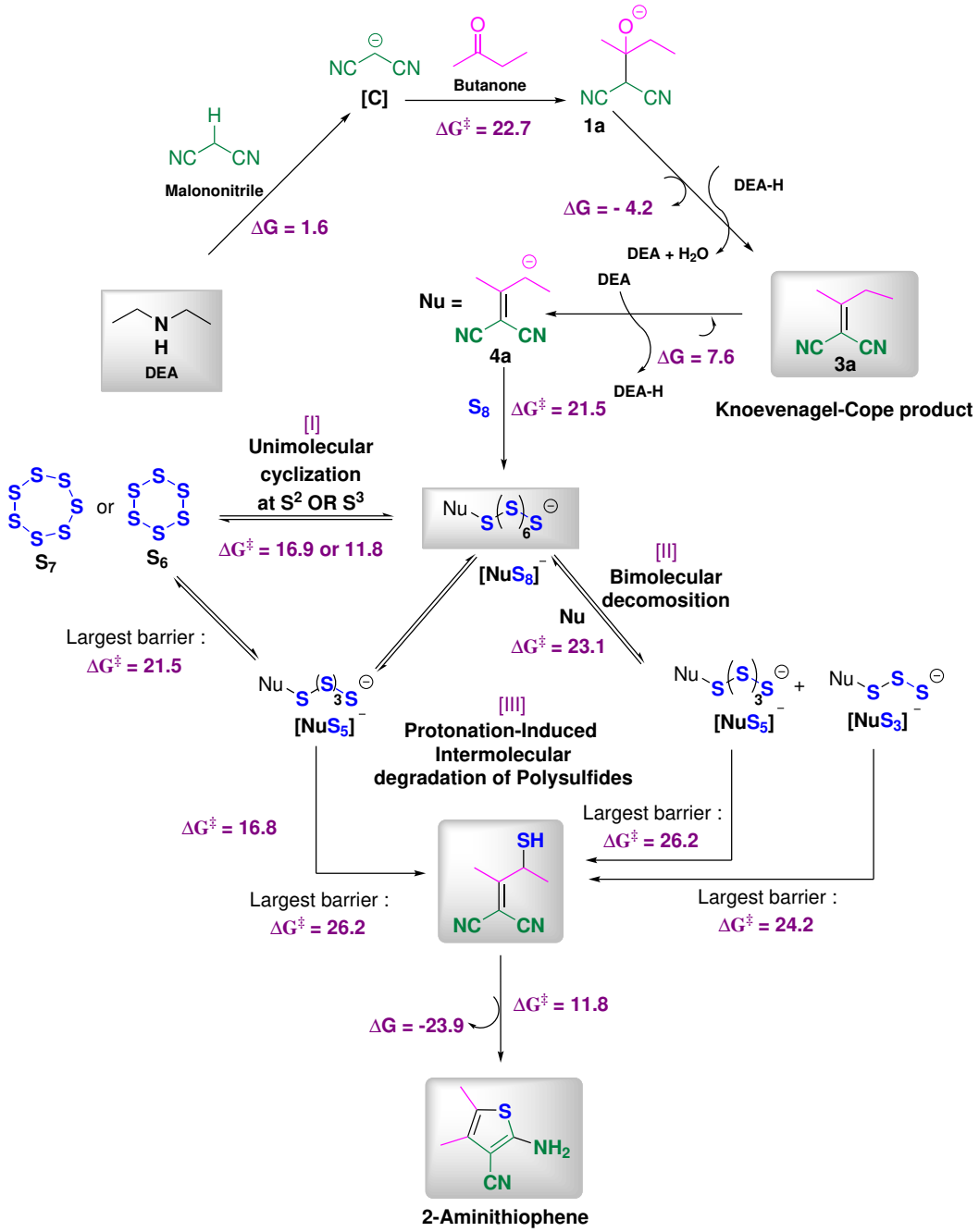

Figure 4.17 Plausible reaction pathway for Gewald reaction (version II)

The III path, which involves bimolecular degradation with 4a, can only compete for the first step of $[NuS_8]^-$ decomposition with the above two paths. The formation of monosulfide on S_4 is most favorable, leading to the formation of $[NuS_3]^-$ and $[NuS_5]^-$. Both polysulfides further decompose through protonation-induced intermolecular degradation. Regarding option **(i)**, the $[NuS_8]^-$ requires a total activation barrier of 24.7 kcal/mol and releases 0.9 kcal/mol of energy for the formation of $[NuS_7]^-$ and one corresponding thiol. The complete decomposition requires the highest activation barrier of 26.3 kcal/mol in total, resulting in the final products $[NuS]^-$ and HSNu, which finally form 2-aminothiophene as discussed in Subsection **4.3.9**. From the above discussion, it has become clear that until the formation of $[NuS_5]^-$, there is a thermodynamic equilibrium between all three paths. Nevertheless, after this point, only protonation-induced intermolecular degradation of polysulfides (option i) becomes the dominant path.

4.5 Conclusion and Future Work

Through an extensive Density Functional Theory (DFT) study, a comprehensive investigation of the Gewald reaction was carried out. Our initial findings indicate that the amine base does not play a role in the opening of the elemental sulfur ring at room temperature; rather, its role is primarily focused on the proton transfer step. Furthermore, our calculations have revealed that the enolate anion also does not contribute to the sulfur ring opening. As a result, we conclude that the Knoevenagel-Cope condensation serves as the first step in the Gewald reaction.

Following the condensation step, the opening of the sulfur ring occurs through the generated anion of the Knoevenagel-Cope condensation product via DEA, leading to the formation of poly-(octasulfide). To explore the degradation of poly-(octasulfide) and the subsequent formation of 2-aminothiophene, several potential pathways were investigated. This include a comparison of unimolecular cyclization,

bimolecular degradation, protonation-induced intermolecular degradation at various sulfur positions within the polysulfide structure.

Based on our analyses, it was concluded that the initial step of polysulfide degradation is a competitive process with all considered pathway (I, II, III) existing in thermodynamic equilibrium. Nevertheless, upon the formation of $[NuS_5]^-$ through these pathways, the dominant route is the protonation-induced intermolecular degradation, ultimately leading to the formation of the final product of the Gewald reaction, 2-aminothiophene. Moving forward, all calculations will be conducted utilizing a higher basis set while using the same DFT method. This approach aims to ensure the consistency of the DFT calculation results and enhance the accuracy and reliability of future investigations.

In summary, our thorough DFT (Density Functional Theory) study provides information about the complex processes involved in the Gewald reaction. This knowledge forms a strong basis for future research and advancements in this area.

CHAPTER 5

COMPUTATIONAL STUDY OF PERSULFIDE AND THIOL REACTIVITY

5.1 Introduction

Due to the presence of an empty 3d orbital, sulfur exhibits a diverse range of oxidation states,from -2 to +6. Among the many known compounds, hydrogen sulfide (H_2S) emerges as an exceptionally significant molecule. H_2S is similar to water (H_2O) and is a divalent hydride in the -2 oxidation state. Unlike water, hydrogen sulfide is a gas at room temperature. Until 1996 H_2S was believed to be poisonous gas,[191] nevertheless, subsequent studies conducted by Abe and Kimura revealed, H_2S has role in endogenous neuromodulator. Along with this, it acts as a source of metabolic energy. In green and sulfur bacteria, (H_2S) acts as an electron donor for the reduction of CO_2 during photosynthesis.[192] In mammalian systems, (H_2S) has various physiological and pathological effects on the cardiovascular, nervous, immune, and endocrine systems.[193–196] To explore the biological functions of H_2S, it is essential to understand H_2S activators and donors. Depending on the nature of the donor, various types of activators are known Figure 5.1. These include:

- Donors relying on thiols for the liberation of H_2S, such as Cys-S-SH and penicillamine perthiol-based donors.[197]
- Donors that generate H_2S through a reaction with bicarbonate, known as thioamino acids.[198]
- Donors that release H_2S via hydrolysis, with or without light, such as Lawesson's reagent and phosphorodithioate-based donors.[199, 200]
- Donors capable of releasing H_2S in the presence of carbonic anhydrase by liberating COS, such as thiocarbamates and N-thiocarboxyanhydrides.[201, 202]

An ideal H_2S donor is characterized by stability in aqueous solutions, long-term integrity and functionality. Furthermore, it should shows controlled release of H_2S.

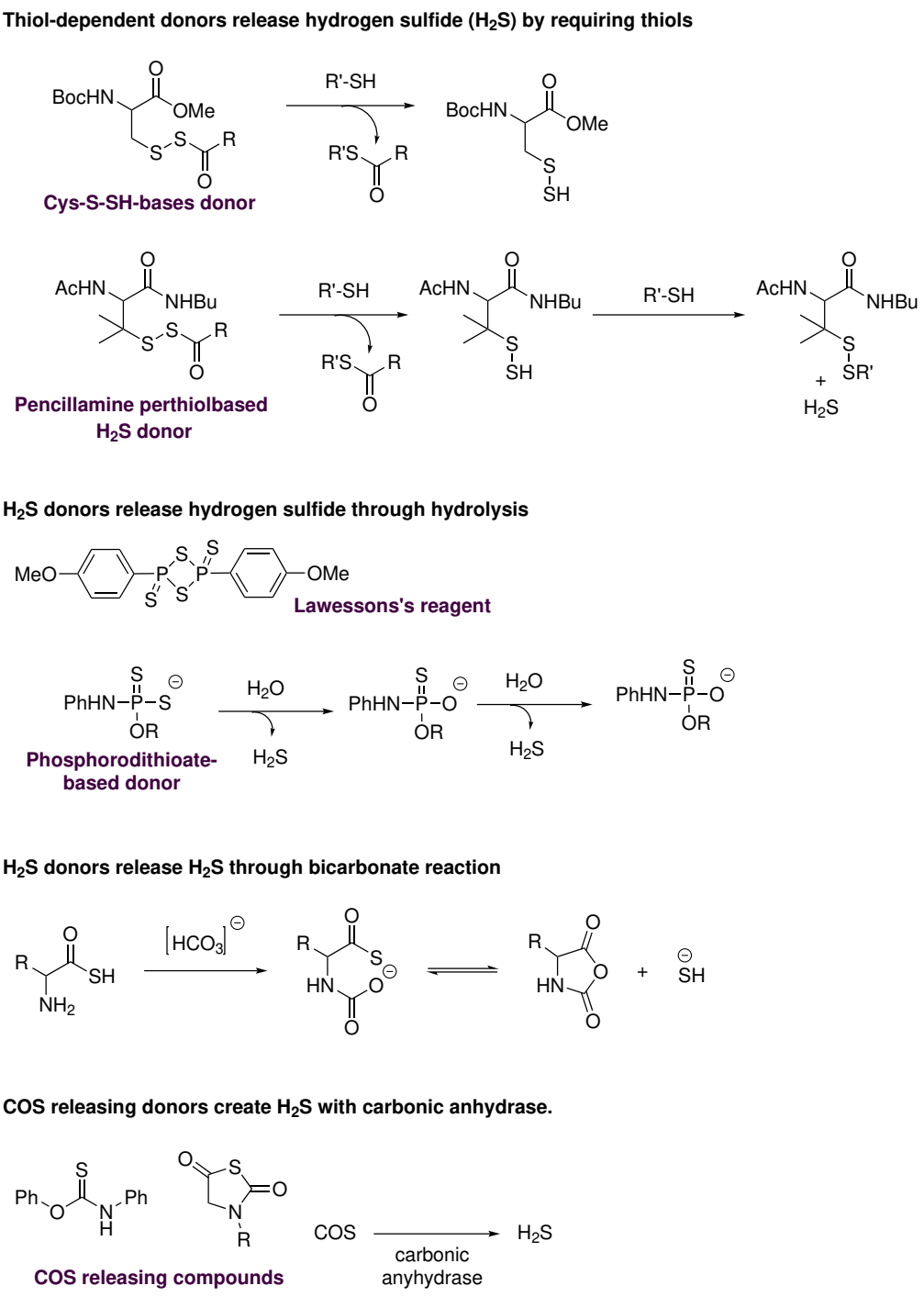

Figure 5.1 Various class of H_2S donor with their activator.

Additionally, H_2S donor should offer unique therapeutic benefits. In this study, the primary objective is to examine the H_2S release derived from thiol-based donors. These donors produce persulfides as intermediates while undergoing the process of H_2S generation. Furthermore, this intermediate is attacked by a thiol donor for the generation of H_2S through H_2S release (Path 1 - Figure 5.2) or transpersulfidation (Path 2 - Figure 5.2). Pathway 1 involves the thiol attacking the inner ($\mathbf{S^1}$) sulfur atom, resulting in the formation of a disulfide and subsequent release of H_2S. On the other hand, pathway 2 involves attacking the outer sulfur atom $\mathbf{(S^2)}$, leading to transpersulfidation.

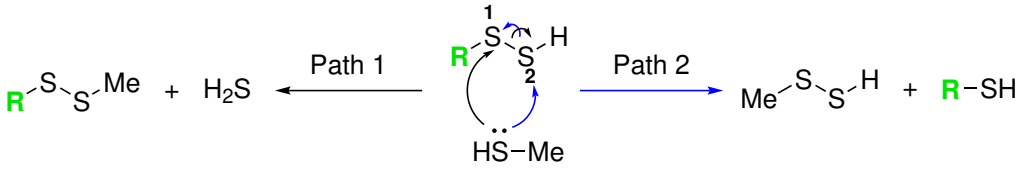

Figure 5.2 Dual pathways of Thiol reactivity with Persulfides.

To understand the relative rate of these two pathways and their dependence on the nature of the R group, this study used computational methods. In this study, our main goal is to use DFT to investigate the electronic and steric effects on H_2S release and transpersulfidation by varying the R group. Another aim is to investigate the reactivity of persulfides/thiols using Penicillamine-based persulfide donors.

5.2 Methodology and Computational Details

All Density Functional Theory (DFT) calculations were performed using Gaussian 16. The **ωB97X-D** [98] functional was selected as we have shown in our earlier work that it is one of the most accurate methods for the reaction of sulfur and sulfur containing compounds. For geometry optimizations and frequency calculations, the triple-zeta tight-d-augmented **aug-cc-pV(T + d)Z**,[81] basis set was used for investing electronic and steric effect on persulide, while for penicillamine-based persulfide donors, **aug-cc-pVDZ** basis set [187] was used due to involvement of large

number of atoms. Single-point energy refinements were then obtained with ω**B97X-D** and **M06-2X** methods and the **aug-cc-pV(T + d)Z**, necessary to obtain accurate energies.[186] At all stages, solvation effects were considered using the SMD solvation model for **water**.[143]

5.3 Results and Discussion

5.3.1 Variation in R group

To observe the influence of steric effects on both of the reaction pathway, DFT calculations were performed with various R groups. Figure 5.3 shows the relationship between the associated activation energy and reaction energy for the processes of H_2S release and transpersulfidation, considering various R groups. In the case of ethyl and methyl substituents, it was observed that the barrier for both H_2S release and transpersulfidation was similar due to their smaller size. The attack of thiol on both outer and inner sulfur atoms was comparable. Nevertheless, as the size of the R group increased, the activation barrier for both processes also increased. Among the different R groups tested, the t-butyl group exhibited the highest increase in activation energy. The barrier for H_2S release with the t-butyl group was measured at 25.2 kcal/mol, while for transpersulfidation, it was 17.5 kcal/mol. The increase in activation energy for H_2S release was more significant compared to transpersulfidation. This was because the thiol nucleophile faced greater steric hindrance from the t-butyl group when attacking the internal electrophilic sulfur for H_2S release, in contrast to the outer sulfur. In the case of the cystein group, which contained an electron-withdrawing group, the barriers for both H_2S release and persulfidation were minimized (13.3 and 12.4 kcal/mol, respectively) due to the enhanced electrophilicity of the persulfide sulfur atom. In terms of reaction energy, it has been observed that the energy for the H_2S release path is almost similar for all the substituent, ranging from 11.2 to 11.9 kcal/mol.

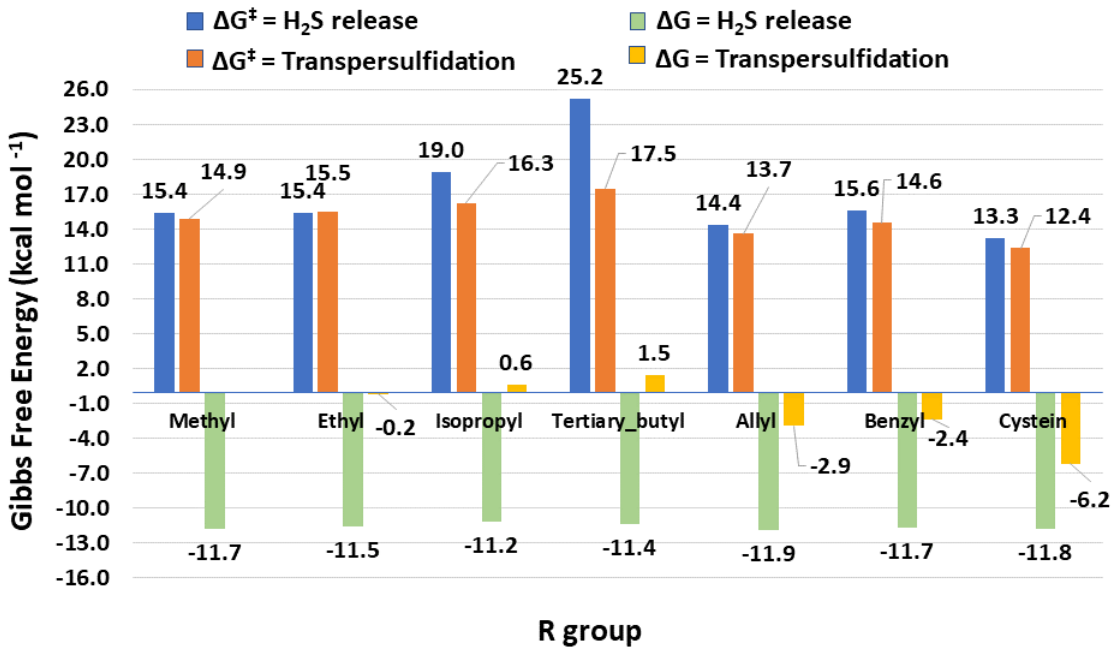

Figure 5.3 Activation and reaction energy for H_2S release and transpersulfidation for various 'R' group.

This observation suggests that the H_2S release path is governed by kinetics rather than thermodynamics. It is important to note that, the H_2S release process exhibits greater exergonicity in comparison to transpersulfidation. This is due to the formation of a stable disulfide, which contributes to the overall energy release. Furthermore, the generation of sulfide anions serves to enhance the reaction by capturing a proton from the system, ultimately facilitating the release of H_2S. This observation is further supported by the transition state (TS) structures (Figure 5.4) for H_2S release in various considered groups, which exhibit similar S-S bond breakage (2.30-2.39 Å) and formation (2.48-2.53 Å) distances.

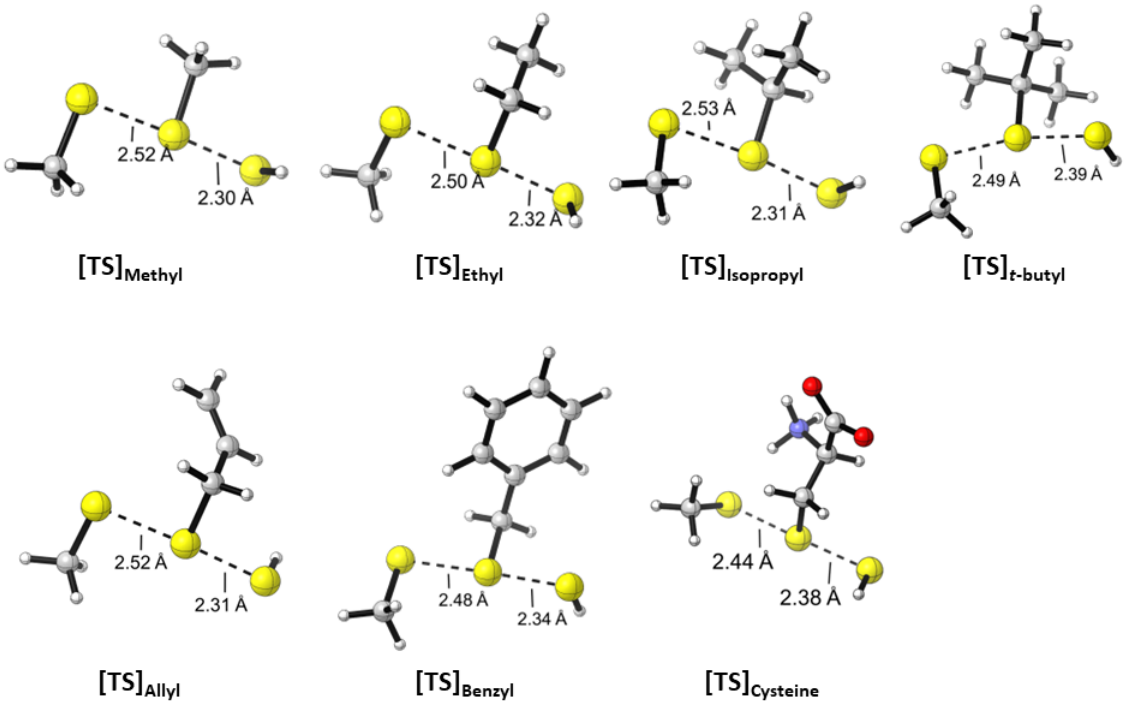

Figure 5.4 The TS structures associated with H_2S liberation for various considered R group.

On the other hand, the transpersulfidation process is not as favorable in terms of reaction energy due to the generation of unstable persulfide intermediates. Nevertheless, for the benzyl, allyl, and cystein groups, the reaction energy is lower compared to the other considered groups. This is due to resonance stabilization and presence of electron withdrawing group with cystein moiety. Once again, this observation is supported by the obtained TS structures. From methyl to t-butyl groups, the S-S bond formation (2.36-2.39 Å) and breakage distances (2.38-2.41 Å) are almost identical, whereas for allyl, benzyl, and cystein groups, the S-S bond breakage distance is shorter than the S-S bond formation distance, clearly satisfying the Hammond postulate (Figure 5.5).

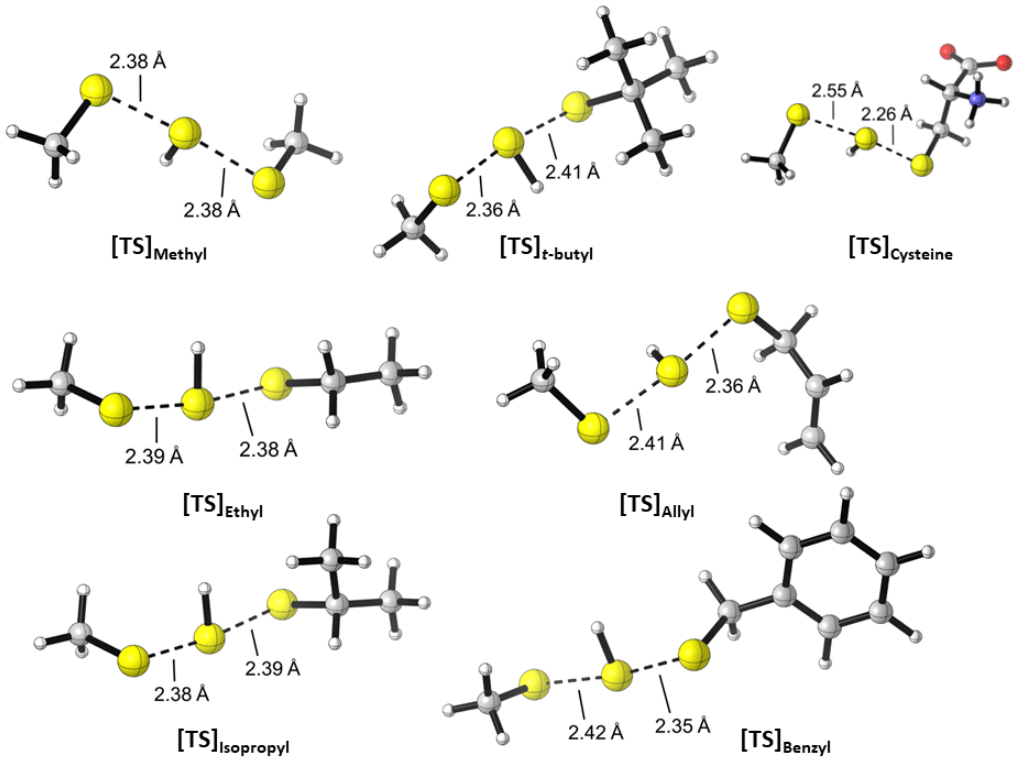

Figure 5.5 The TS structures associated with transpersulfidation for various considered R group.

5.3.2 Variation of para substitution

To investigate the electronic effect on H_2S release and transpersulfidation path, aryl persulfides with various substituents at the para position of the aryl group were examined (Figure 5.6). Both electron-donating and electron-withdrawing groups were placed at the para position of the aryl substituent in the persulfide.

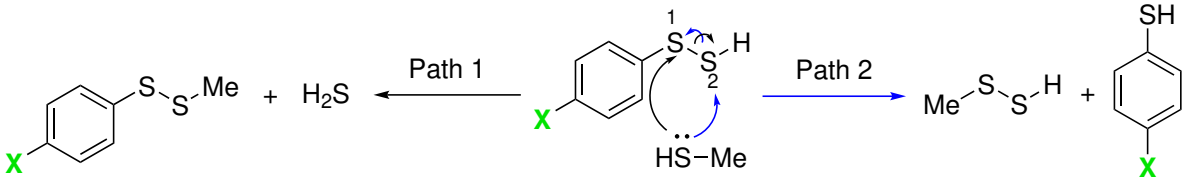

Figure 5.6 H_2S and transpersulfidation for different para substituent.

Based on the energy data, (Figure 5.7) it has been observed that H_2S release requires a higher activation energy compared to transpersulfidation due to thiol attack

on the inner sulfur. The electron-donating groups, such as H, CH_3, and OCH_3, at the para position enhance the activation energy for both the path, by diminishing the electrophilicity of both the inner and outer sulfur. Nevertheless, the inner sulfur has a greater effect compared to the outer sulfur because it is directly attached to the phenyl ring.

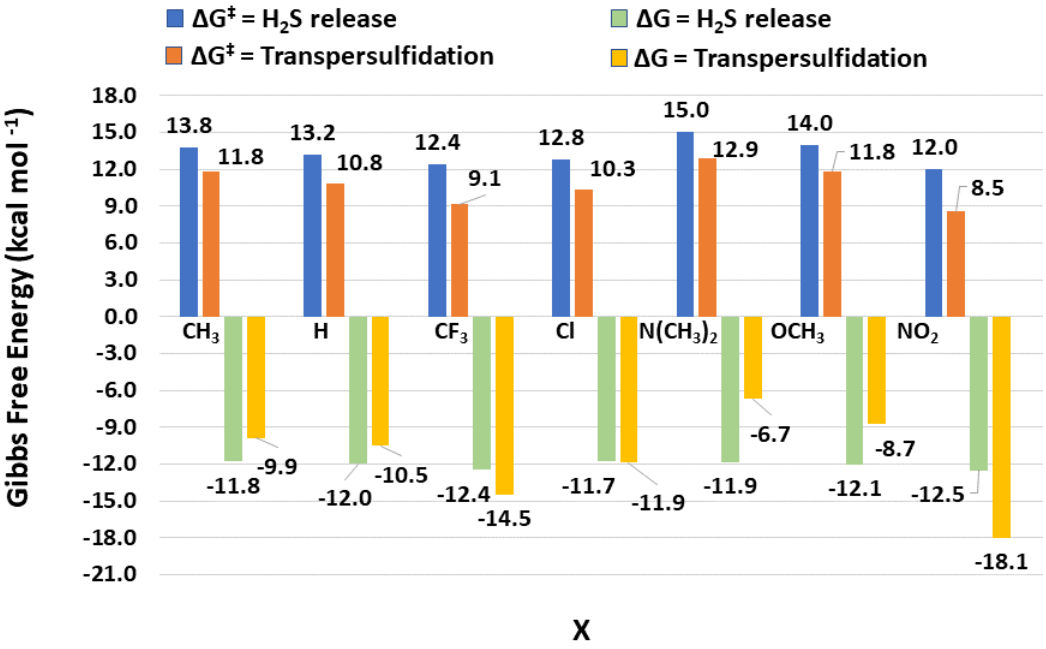

Figure 5.7 Activation and reaction energy for H_2S release and transpersulfidation for various 'X' group.

The largest increase in activation and reaction energy was associated with the dimethylamine substituent (15.0 and -11.9 kcal/mol) for H_2S release, (12.9 and -6.7 kcal/mol) for transpersulfidation due to its significant electron donation. On the other hand, electron-withdrawing substituents like Cl, CF_3, and NO_2 resulted in activation energy (reaction energy) of 12.8 (-11.7), 12.4(-12.4), and 12.0 (-12.5) kcal/mol, respectively, for H_2S release. For transpersulfidation, activation energy (reaction energy) of 10.3(-11.9), 9.1(-14.5), and 8.5 (-18.1) kcal/mol were observed for the same substituents.

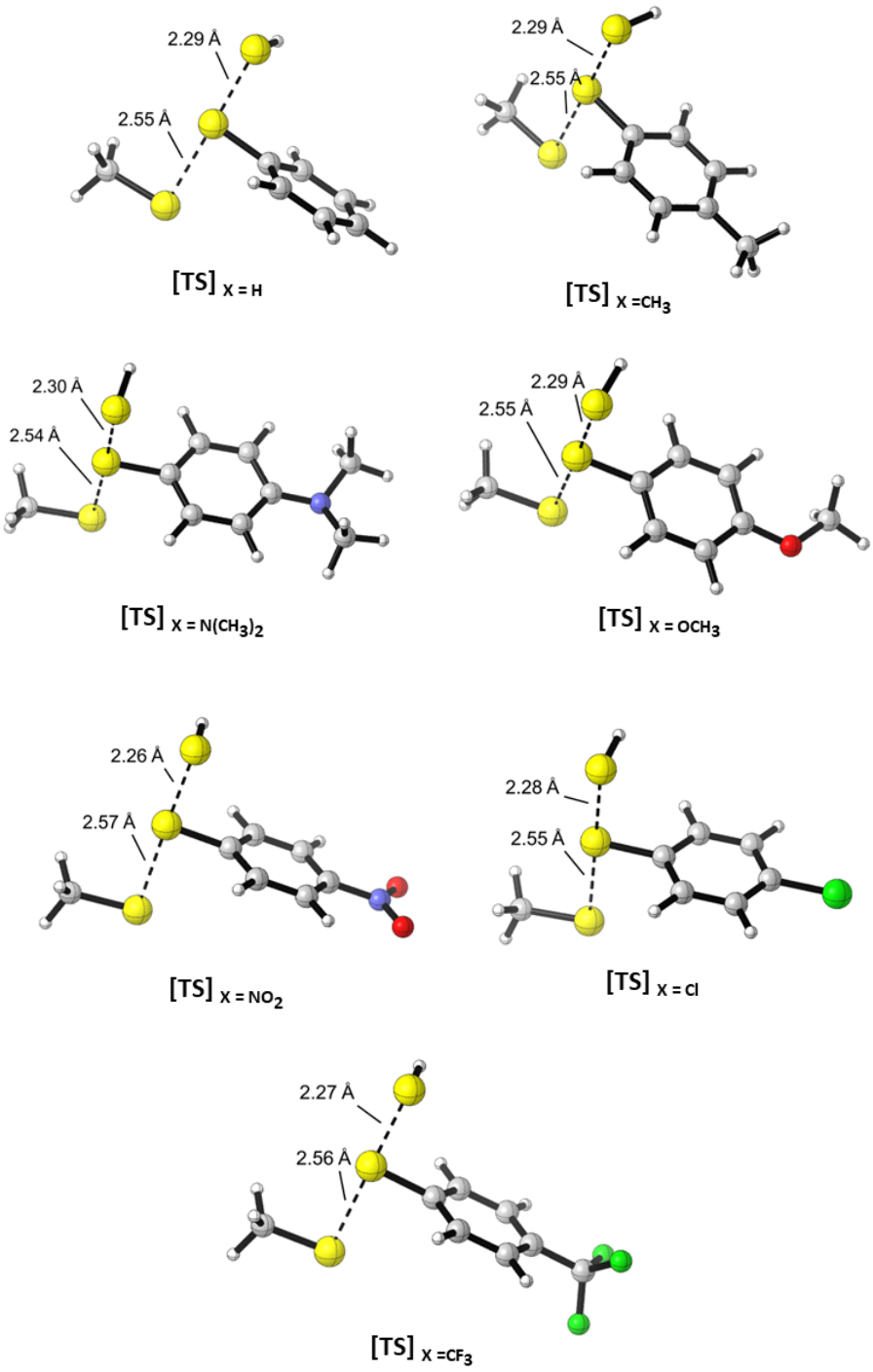

Figure 5.8 The TS structures associated with H_2S liberation for various considered 'X' group.

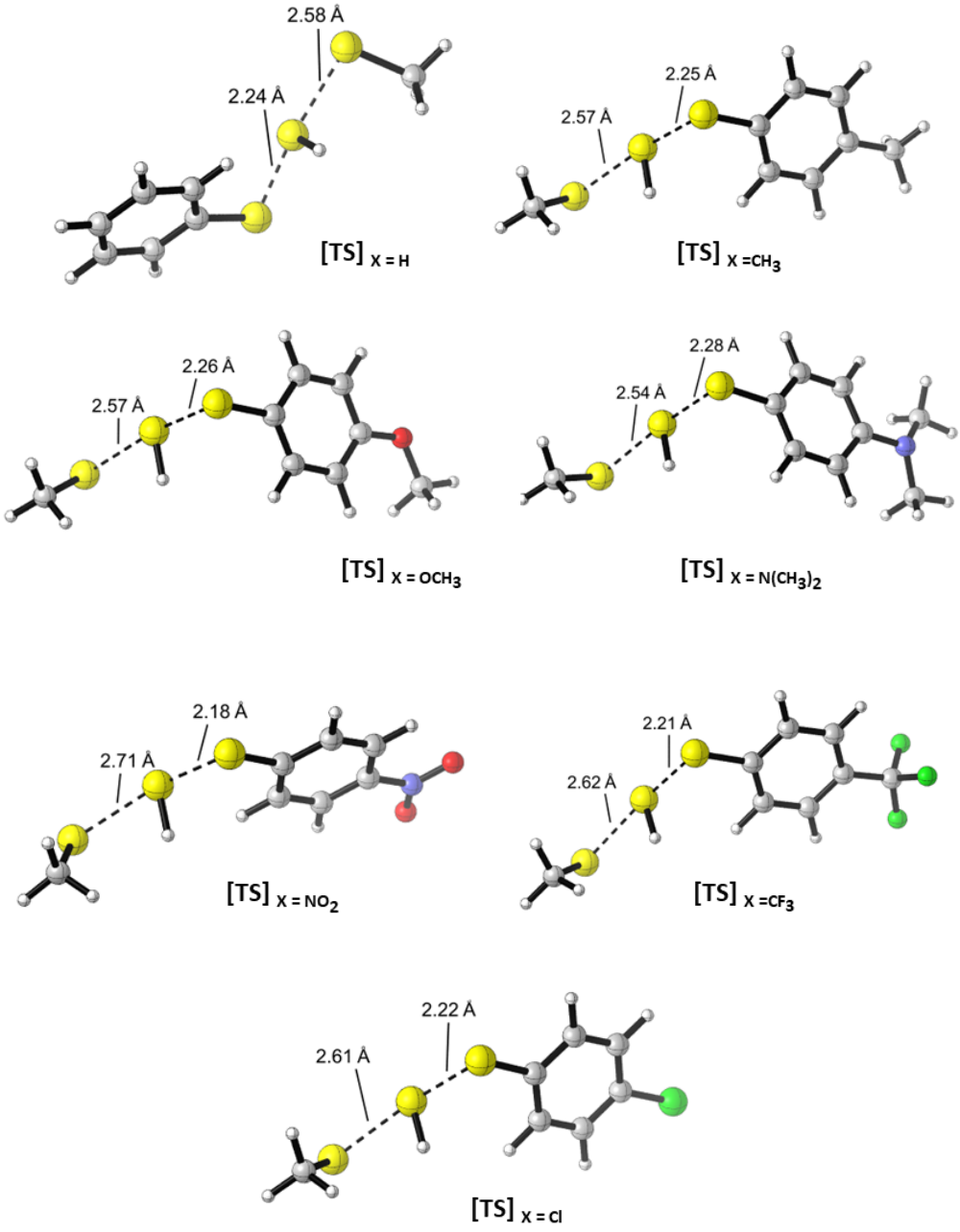

Figure 5.9 The TS structures associated with transpersulfidation liberation for various considered 'X' group.

Figure 5.8 shows the transition state (TS) structures associated with various para substituents for H_2S release. In all of the TS structures, the bond breakage (HS...S) and formation (S...SCH_3) are the same, indicating that path 1 is kinetically

governed rather than thermodynamically. While considering the TS structures associated with various para substituents for path 2 (Figure 5.9), there is an influence of thermodynamics. In the case of the most exergonic reaction (for the NO_2 substituent), the bond breakage occurs with the longest bond (2.71 Å), while the bond formation involves the shortest bond (2.18 Å). Conversely, for the least favorable substituent ($N(CH_3)_2$), the trend is opposite to that of NO_2.

5.4 Reactivity of Penicillamine-Based Persulfide

To understand the various biological functions of hydrogen sulfide (H_2S), scientists have used H_2S donor compounds, which can be found naturally or synthesized in the lab. These donors have also been used to observe the physiological effects on the endogenous system by releasing H_2S. There are various types of H_2S donors known that have been utilized for H_2S generation, such as: **sulfide salts**, including Na_2S, NaHS, and CaS, has been widely used in various applications and studies. These inorganic donors rapidly increase the concentration of H_2S. Within seconds, these salts can release H_2S to achieve its maximum concentration. Nevertheless, it is important to note that sudden increase of H_2S concentration, may lead to acute fluctuations in blood pressure.[203] In addition to inorganic sulfide salts, researchers also make use of **naturally occurring polysulfide compounds**, such as diallyl trisulfide (DATS), as H_2S donors. These polysulfide compounds have been used in vasodilation. Nevertheless, the release of H_2S is slow.[204] In addition to the utilization of inorganic salts and naturally occurring polysulfides, the introduction of **synthetic H_2S donors** has marked remarkable progress in scientific research. Within this class of donors, GYY4137, derivative of Lawesson's reagent, has shown biological activity by releasing H_2S through hydrolysis.[199, 205] In recent years, N-(benzoylthio)benzamide-based donors have been synthesized, which release H_2S in a controlled fashion. These donors generally release H_2S in the presence of thiol activators, such as cysteine or reduced

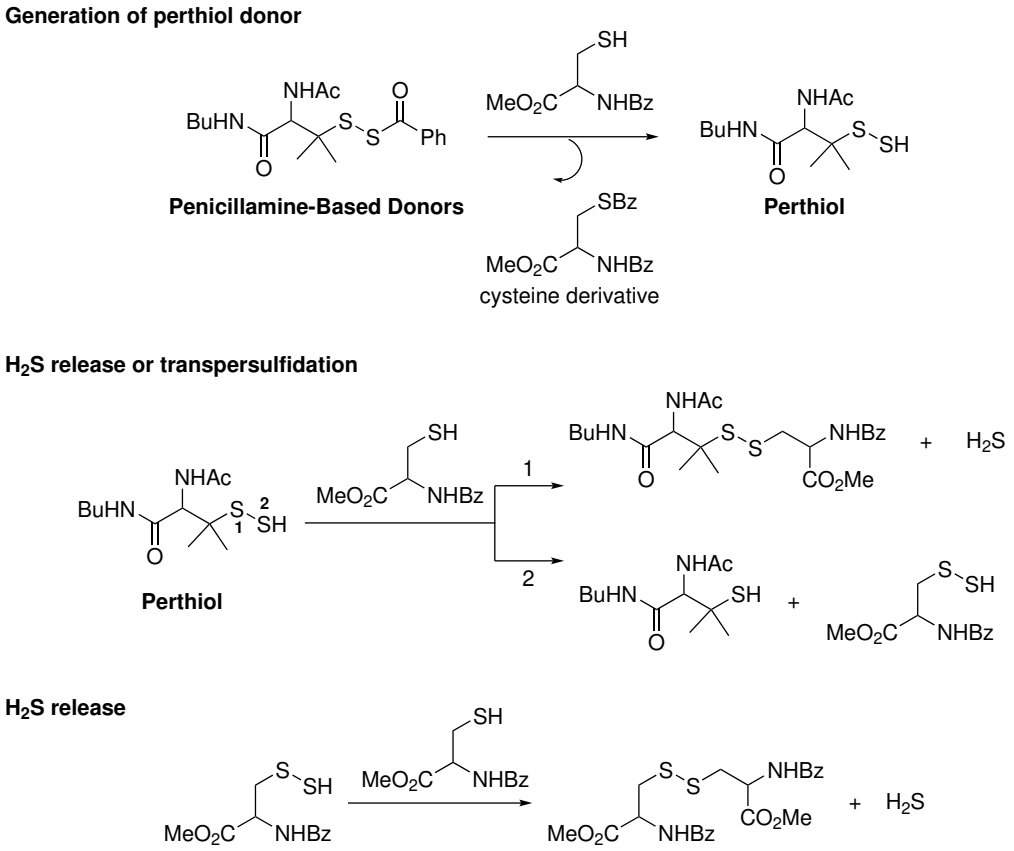

Figure 5.10 Plausible mechanism for H_2S generation from Penicillamine-based donors.

glutathione (GSH).[206] It has been also suggested that cysteine perthiol is a key intermediate in the H_2S release process. Penicillamine-based donors, derived from a penicillamine-benzothioazolyl disulfide by reaction with thioacids, have been used by Zhao et al. [197]. For H_2S generation from these penicillamine-based donors, cysteine or reduced glutathione (GSH) has been used as an activator. The plausible mechanism has been shown in Figure 5.10.

Nevertheless, the computational understanding of the mechanism behind H_2S release from these perthiol-based donors has not been properly investigated. To address this, a DFT study has been conducted to understand the mechanism of H_2S release and transpersulfidation from penicillamine-based persulfide donors in the presence of cysteine thiol (which remains in the zwitterion form in a buffer system).

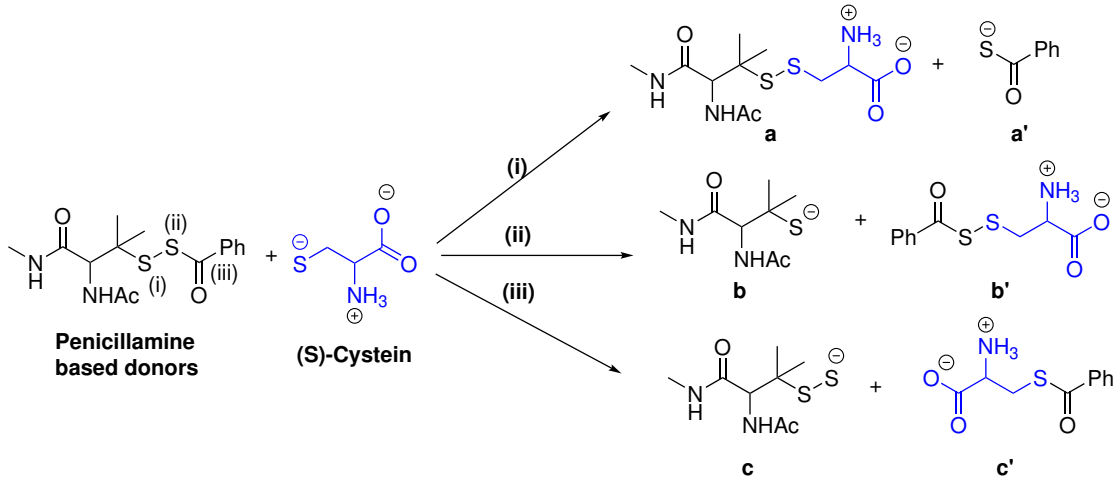

Figure 5.11 Cysteine sulfide attack on considered position.

5.5 Results and Discussion

In this study, penicillamine-based persulfide donors have been chosen instead of cysteine persulfide donors. This is because the penicillamine-based donors have steric crowding at the α-carbon of the disulfide bridge, which helps to prevent side reactions.[197]. Cysteine sulfide has been used as an activator. Three potential attack pathways of cysteine sulfide have been explored, as shown in Figure 5.11, to investigate the most favorable path.

5.5.1 Conformations search for penicillamine-based donors

A conformational analysis of the rotatable bond between the carbonyl carbon and phenyl carbon has been performed. Two predominant conformers, **TD1** and **TD2**, have been identified. The **TD1** conformer was observed to be 1.9 kcal/mol more thermodynamically stable than **TD2**, and this finding is consistent with other DFT method, such as M06-2X, which showed a stability difference of 2.7 kcal/mol in favor of **TD1** over **TD2**. The lower stability of **TD2** can be attributed to the presence of torsional strain between the phenyl group and the dimethyl group, along with the fact that the conformation of the thioester in **TD2** is not the s-trans conformation typically observed in esters (Figure 5.12).

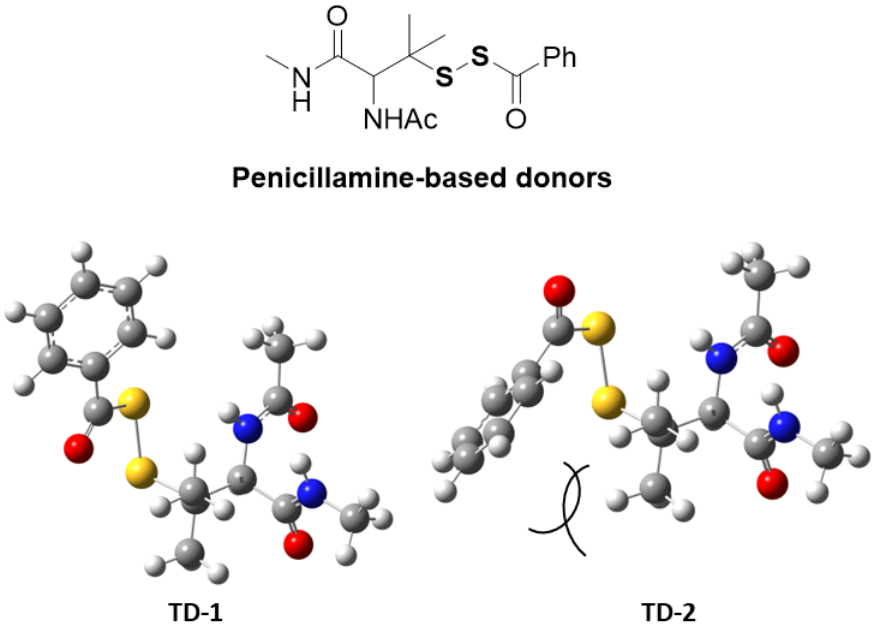

Figure 5.12 Conformers of penicillamine-based persulfide donors.

5.5.2 Cysteine sulfide attack on considered position

The sulfide attack of cysteine has been performed at all three possible positions. The corresponding energy results are presented in Figure 5.13. The black values correspond to ωB97X-D, while the blue values (in parenthesis) represent the results obtained using M06-2X for the single-point energy calculations. For all calculations, each potential energy surface (PES) begins from **TD1**. Upon analyzing the calculation results, it was observed that the activation barrier for attacking $\mathbf{S}^1$ in the **TD1** conformer is lower than that for attacking $\mathbf{S}^2$. The activation barrier for attacking on $\mathbf{S}^1$ is 19.6 kcal/mol, while the activation barrier for $\mathbf{S}^2$ is 2.7 kcal/mol higher. This difference in activation barriers can be attributed to the steric barriers created by the phenyl group. Notably, the trend was reversed for the **TD2** conformer, where attacking $\mathbf{S}^2$ became easier compared to attacking $\mathbf{S}^1$ for the sulfide anion of cysteine. This can be attributed to the presence of dimethyl steric crowding at $\mathbf{S}^1$. The activation barriers were computed at 24.1 kcal/mol for $\mathbf{S}^1$ and 22.2 kcal/mol for $\mathbf{S}^2$, respectively.

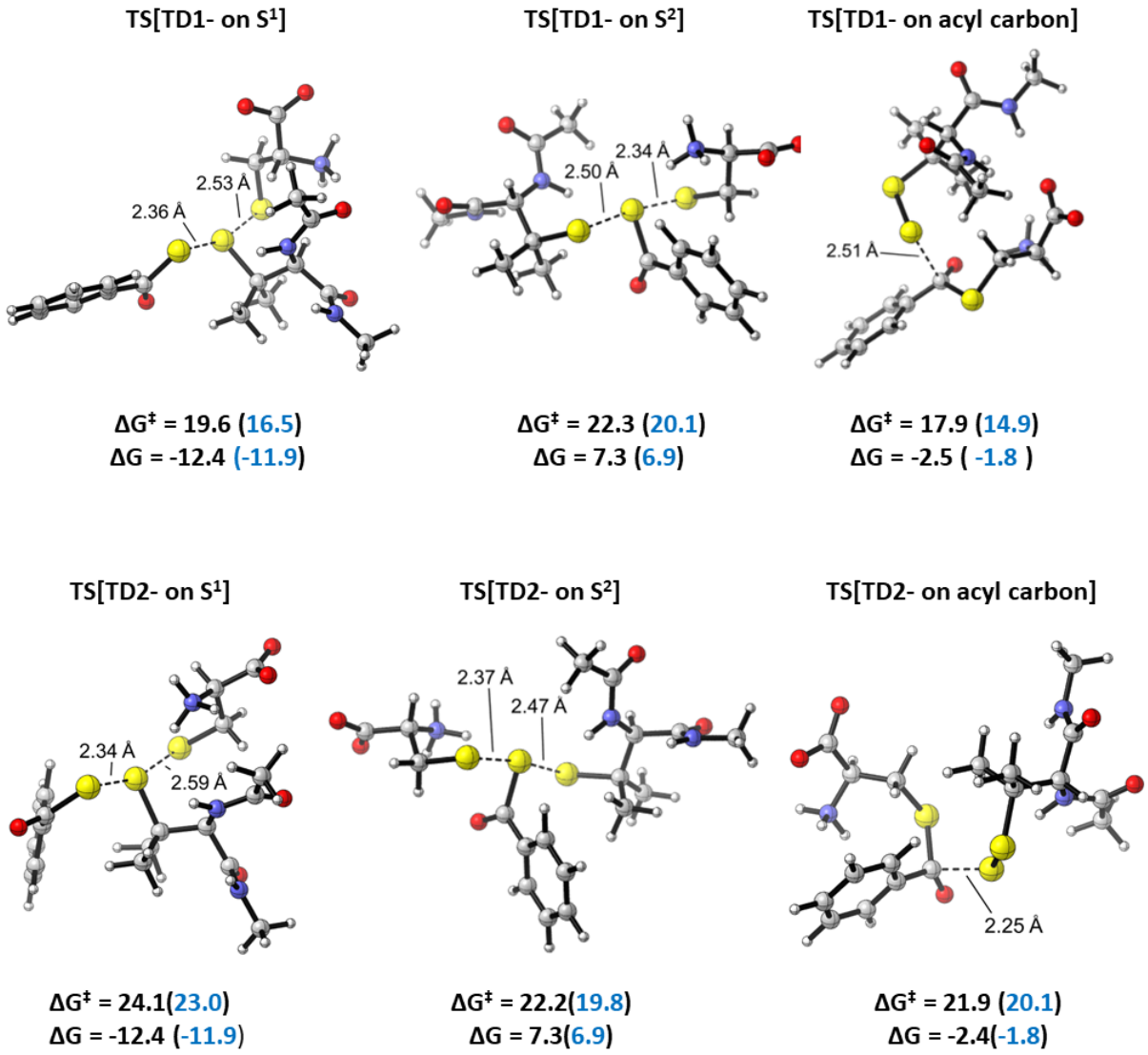

Figure 5.13 TS structures associated with possible attack on penicillamine-based persulfide donors. Free energy in kcal/mol.

For both **TD1** and **TD2**, the attack on $\mathbf{S}^1$ exhibits an exothermic nature, indicated by the negative values of the reaction energy -12.4 kcal/mol, primarily due to the formation of a resonance-stabilized sulfide anion (**a'**) and a disulfide compound (**a**). On the other hand, the attack on $\mathbf{S}^2$ is characterized as endothermic, and positive value of reaction energy 7.3 kcal/mol as it leads to the formation of an unstable sulfide ion (**b**).

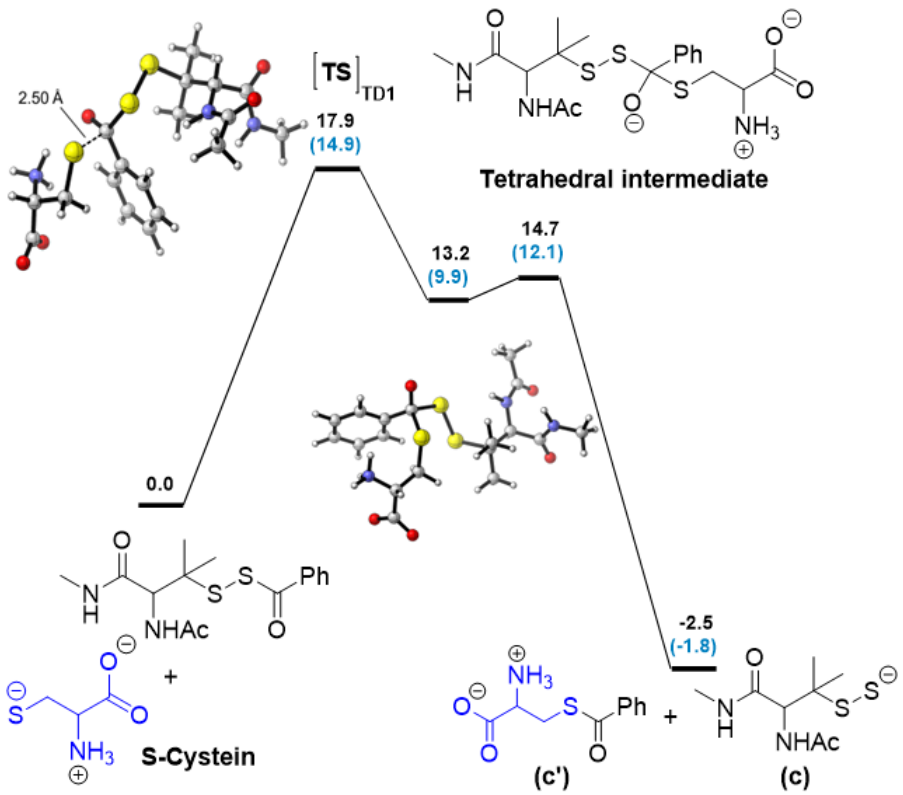

Figure 5.14 The potential energy surface associated with the formation of products by the attack of cysteine sulfide on the acyl carbon. Energy is in kcal/mol.

Interestingly, the activation barrier for attacking the acyl carbon (**iii**) and producing **c** and **c'** was found to be the lowest compared to the other two attack positions with both the considered DFT methods due to the high electrophilicity of the carbonyl carbon. When using the ωB97X-D method with **TD1**, an activation energy of 17.9 kcal/mol was obtained, whereas with the M06-2X method, it was 14.9 kcal/mol. Similarly, for **TD2**, the activation energies were 21.9 kcal/mol with ωB97X-D and 20.1 kcal/mol with M06-2X. Since **TD1** has a lower activation barrier compared to **TD2**, in the main text, a complete potential energy diagram for the generation of **c** and **c'** was discussed for **TD1** (Figure 5.14). The first step, which involves the formation of a tetrahedral intermediate, requires 17.9 kcal/mol of activation energy and 13.2 kcal/mol of reaction energy. Due to its unstable nature,

this tetrahedral intermediate further breaks into **c** and **c'**, which require 1.5 kcal/mol of activation energy and release -2.5 kcal/mol of reaction energy from the donor.

5.5.3 Generation of H_2S

In this DFT calculation, H_2S released path has been explored from the persulfide (**c**), generated from acyl carbon attack by cysteine sulfide. Due to unstable nature of persulfide, it further attacked by cysteine sulfide on two possible sulfur $\mathbf{S}^1$ and $\mathbf{S}^2$ as illustrated in Figure 5.15. An attack on $\mathbf{S}^1$ (inner sulfur) results in the formation of **a** and the release of H_2S. While, an attack on $\mathbf{S}^2$ (terminal sulfur) leads to the formation of persulfide **(d)** and thiol **(d')** through a process called transpersulfidation pathway. This persulfide again serves as a precursor for subsequent H_2S formation and led to formation of H_2S and disulfide **(e)**. DFT calculations were performed for all these potential paths (Figure 5.15). The calculation results indicate that an attack on $\mathbf{S}^2$ need 19.0(17.1) and 5.7(5.8) kcal/mol of activation and reaction energy, whereas an attack on $\mathbf{S}^1$ required a slightly more energy barrier of 2.8(1.6) kcal/mol due to steric crowding caused by the adjacent dimethyl group to $\mathbf{S}^1$ with -3.4 (-0.4) kcal/mol of reaction energy. The persulfide (**d**) formed requires 15.0(20.6) and -5.8(4.8) kcal/mol of activation and reaction energy for the conversion into disulfide (**e**) and H_2S formation. The associated TS structures for associated paths has been shown in Figure 5.16.

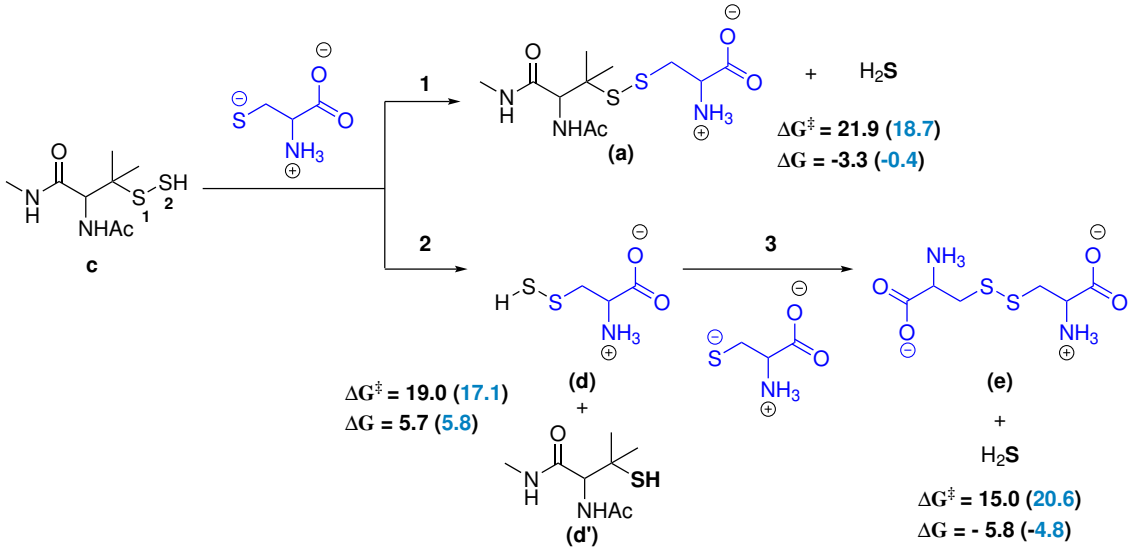

Figure 5.15 Proposed reaction pathway for H_2S generation. Free energy in kcal/mol.

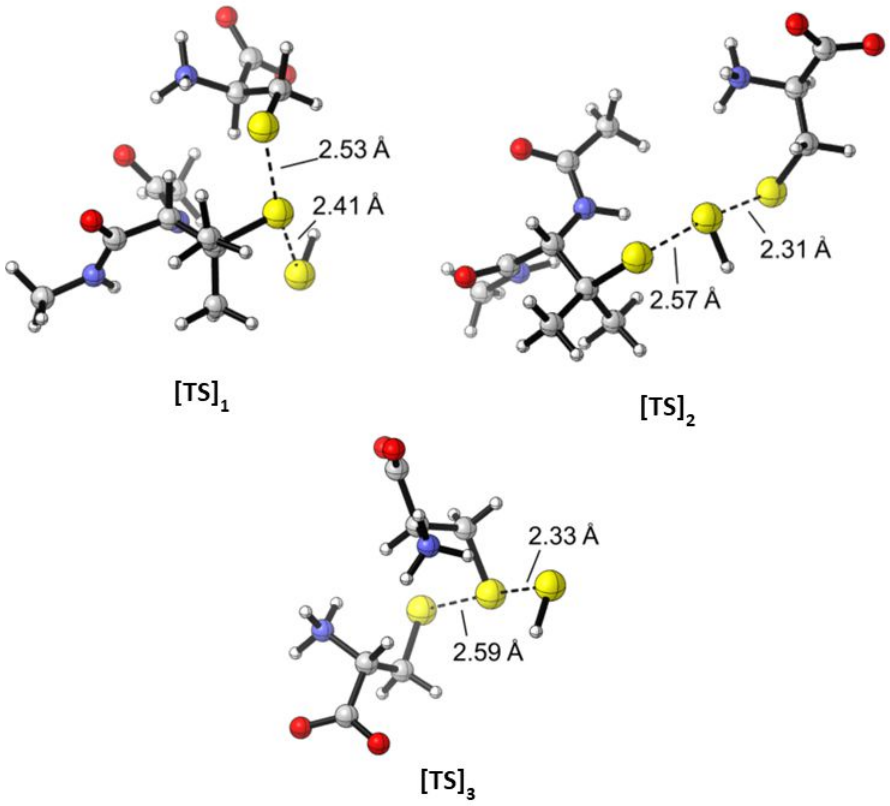

Figure 5.16 Associated TS structures for H_2S release and transpersulfidation.

5.6 Conclusion

A computational investigation of persulfide and thiol reactivity was performed. Our findings indicate that the inclusion of bulky substituents on persulfide molecules resulted in a decelerated release of H_2S and transpersulfidation reactions. When considering persulfides with an aryl group, the presence of electron-withdrawing groups on the phenyl moiety led to an accelerated generation of H_2S and transpersulfidation, while electron-donating groups caused a slower release in both processes. It is worth noting that the release of H_2S was more profoundly influenced by both electronic and steric effects compared to transpersulfidation. In the case of penicillamine-based donors, it was observed that the acyl carbon exhibited a higher susceptibility to attack by cysteine sulfide compared to the inner two sulfur atoms. This particular reaction gave rise to the formation of a persulfide compound, which subsequently facilitated the generation of H_2S through both H_2S release and transpersulfidation pathways. Overall, the findings presented in this study broaden our understanding of persulfide and thiol reactivity, offering promising avenues for future research and applications in the fields of chemistry, materials science, and medicine.

CHAPTER 6

SYNTHESIS OF SULFUR BASED ORGANIC COMPOUNDS

In this chapter, an attempt was made to synthesize sulfur-based organic compounds using elemental sulfur as a major source of sulfur or organic compounds with a sulfur source. Elemental sulfur was chosen for this study due to its non-hygroscopic, non-toxic, laboratory-friendly nature, and affordability. The first section of this chapter focuses on thiol preparation, utilizing boron source and 5-phenyl-1,3,4-oxathiazole-2-one. The second section covers the synthesis of 2-substituted benzothiazole using elemental sulfur along with imine or aryne source. The last part of the chapter involves the synthesis of sulfur-based fluorescent compounds with isoquinoline and aryne intermediates, along with elemental sulfur.

6.1 Synthesis of Thiols form Organoboranes

The synthesis of aryl, alkyl, and alicyclic thiols has been investigated using organoboron, boronoic acid or ester under different reaction conditions. 5-phenyl-1,3,4-oxathiazole-2-one has been used as a source of sulfur nucleophile with a good leaving group. Various high-boiling solvents have been explored.

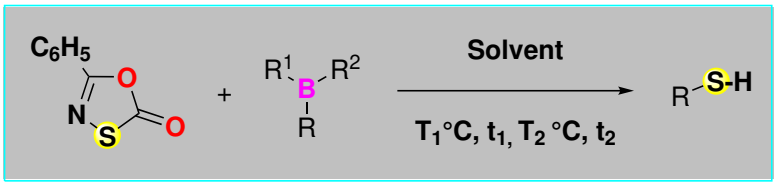

6.1.1 Introduction

Thiols (also known as mercaptans) are a class of organic compounds that contain a sulfur atom bonded to a hydrogen atom (-SH). They are widely used in many industrial and commercial applications because of their distinct odor and various

chemical properties. One of the most well-known uses of thiols is as odorants in the natural gas industry.[207] The pungent odor of thiols makes them useful for detecting leaks in gas pipelines, which can be hazardous if left undetected. In addition to this, thiols are also used as accelerators in the vulcanization of rubber,[208] which is the process of hardening rubber to make it more durable and resistant to wear. In biological systems, cysteine, an amino acid containing a thiol group, plays a significant role in biochemistry and is involved in many important biological processes.[202] Its nucleophilic character due to presence of thiol group, makes it particularly important in the formation of disulfide bonds, which play a crucial role in maintaining the structure of proteins. Along with cystein, glutathione also contain thiol, that are involved cellular redox reactions and play important roles in protecting cells from oxidative stress.[209]

Thiols are versatile intermediates in the synthesis of many natural and synthetic biologically active compounds. They can be synthesized from a variety of starting materials, including alcohols,[210] alkyl halides,[211] alkenes,[212] organometallic compounds,[213] and by the breakdown of sulfur-containing amino acids and lignin.[202] The ability to synthesize thiols from a wide range of starting materials makes them useful in a variety of applications, including as intermediates in the synthesis of other compounds and as precursors to other functional groups.

In parallel, the synthesis of organosulfur compound has been widely explored in past years using boron compounds like boranes[214], borinic or boronic acids or esters[215]. Boronic acids and esters are among the most extensively researched and practically useful organoboron compounds, primarily due to their air stability and moderate reactivity under various reaction conditions.[216] Boron compounds have played a significant role in several important chemical reactions, including the hydroboration and the Suzuki-Miyaura reaction. The Suzuki-Miyaura reaction, also known as the Suzuki coupling, is a widely used reaction for the synthesis of biaryls,

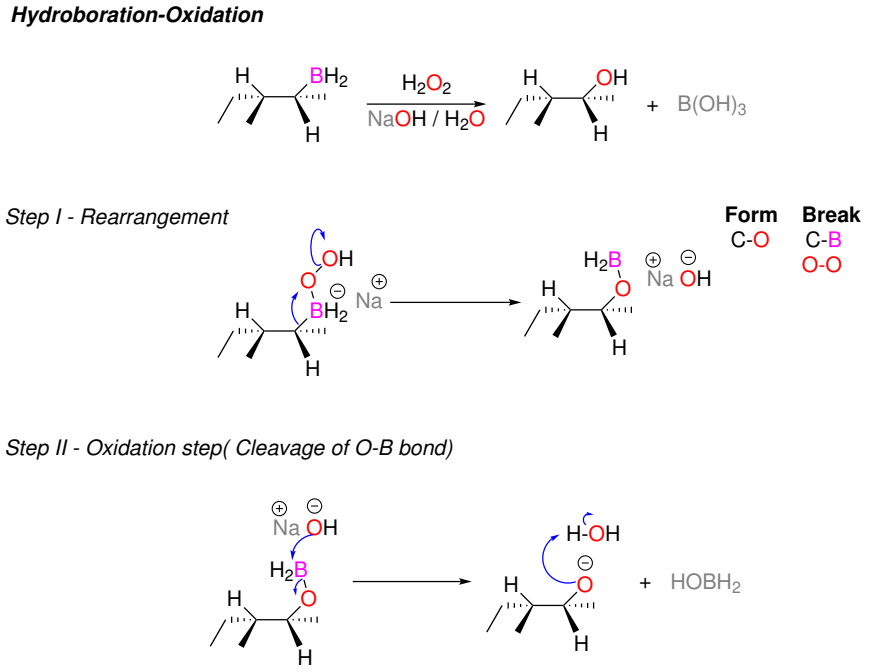

Figure 6.1 Hydroboration-oxidation reaction.

which are compounds that contain two aromatic rings. This reaction is based on the coupling of a boronic acid and an organic halide or triflate, and it is widely used in the synthesis of pharmaceuticals, agrochemicals, and materials.[217] Hydroboration is a reaction in which a boron atom is added to an unsaturated organic compound, such as an alkene or alkyne. This reaction allows for the introduction of a boron atom into the molecule, which can then be used as a starting material for further reactions.[218] One of major application is Hydroboration-Oxidation, where the boron atom is oxidized to generate a hydroxy group in the molecule.[219] Strong oxidizing agent, such as hydrogen peroxide (H_2O_2) or a peroxide compound can be use as oxidizing agent (Figure 6.1). The key step of this reaction is rearrangement, where C-O bond forms and C-B, O-O bond break. The essential component of this step is good leaving group (OH) attached to oxygen.

6.1.2 Problem statement

The immense importance of thiols still leaves scope for further investigations. Inspired with this procedure, we thought of making thiol using hydrogendisulfide (H_2S_2) instead of (H_2O_2). Nevertheless, (H_2S_2) is unstable species and decompose quickly to hydrogen sulfide and sulfur[220]. As it has been explained for doing above reaction sulfur or oxygen molecule should attached with good leaving group. Keeping this in mind, 5-phenyl-1,3,4-oxathiazole-2-one **(1)** (Figure 6.2) has been chosen to overcome the instability of hydrogendisulfide (H_2S_2) and produce a more controlled and stable reaction for the formation of thiols.

6.1.3 1-3, dipolor-sulfur source : 5-phenyl-1,3,4-oxathiazole-2-one

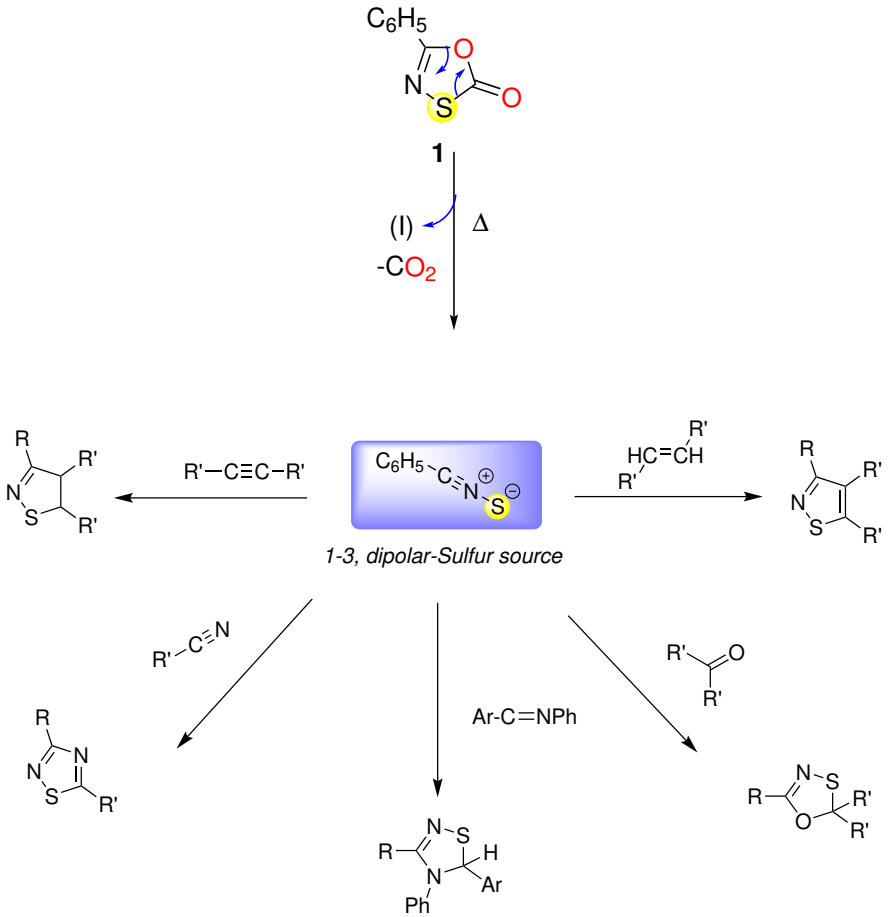

Figure 6.2 Aromatic nitrile sulfides (1-3 dipolor-sulfur source) addition reactions.

The 5-phenyl-1,3,4-oxathiazole-2-one **(1)** can indeed be used as a precursor to generate a 1,3-dipolar sulfur source (benzonitrile sulfide), through controlled heating.[221] The reaction of 5-phenyl-1,3,4-oxathiazole-2-one with the dipolarophile, leads to the formation of a 1,3-dipolar cycloaddition product, which is a common method for the synthesis of various heterocyclic compounds (Figure 6.2).[222] The rate of disappearance of oxathiazole in these reactions, is independent of the concentration of the dipolarophile, which is characteristic of a first-order reaction.[223] It is important to note that the reaction conditions, such as the temperature and the reaction time, need to be carefully controlled in order to achieve the desired product in high yield.

6.1.4 Proposed mechanism for thiol formation

The synthesis of thiols has been explored based on the Hydroboration-Oxidation concept, with organoboron **(3a)** serving as the source of boron that is attacked by benzonitrile sulfide **(2)**, a dipolar sulfur source, generated from 5-phenyl-1,3,4-oxathiazole-2-one **(1)**.

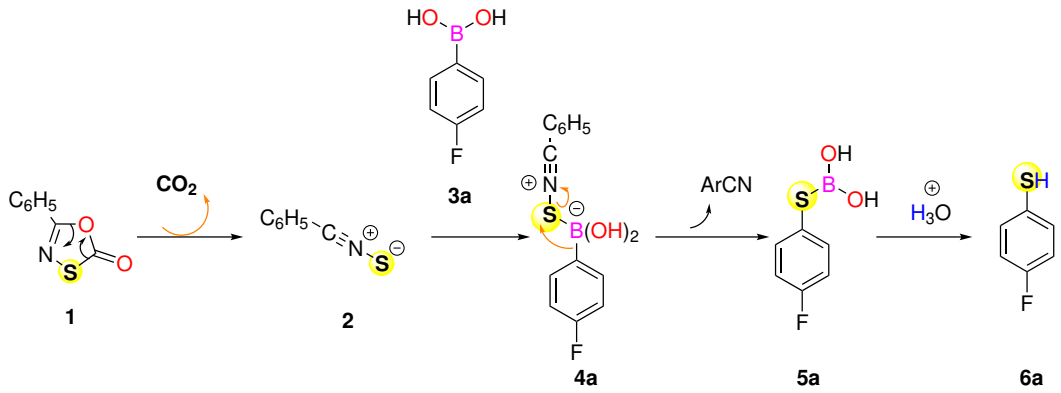

Figure 6.3 Proposed mechanism of aryl thiol formation from organoboron and 5-phenyl-1,3,4-oxathiazole-2-one.

The intermediate **(4a)** can undergo a rearrangement step, leading to the formation of **(5a)** through the breakage of the S-N and Ph-B bonds, resulting in the formation of an S-Ph bond. In this two-step reaction, acetonitrile leaves. Finally,

product **(6a)** is formed via hydrolysis of **(5a)**. The proposed mechanism has been shown in Figure 6.3.

6.1.5 Results and discussion

Optimization study To optimize the reaction, four boron sources **(3a, 3b, 3c, 3d)** were treated with 5-phenyl-1,3,4-oxathiazole-2-one **(1)** using three high-boiling solvents (DMF, HMPA, DMSO) in an argon atmosphere. The reaction proceeded in two steps with the goal of producing a nucleophile (benzonitrile sulfide) from **1** and then oxidizing it (Figure 6.1). For entry **1**, DMF and **1** were heated at 150 °C for 24 hours with the boron source, followed by stirring at room temperature. After performing the ^{19}F-NMR for entry **1**, we observed a peak around a chemical shift of 124 ppm (Figure 6.4), which was different from the starting boron source **3b** (^{19}F-NMR - 105 ppm). Nevertheless, the ^{1}H-NMR and TLC indicated the presence of benzonitrile and sulfur. To facilitate the reaction, a base was added (**entry 2**) or the second-step reaction temperature was increased (**entry 3**). Even though, same kind of spectra was observed. The presence of sulfur on TLC, suggesting the decomposition of benzonitrile sulfide. To overcome this issue, we lowered the T_1 reaction temperature and repeated the procedure as in entries **2** and **3**. But, the results did not change. So, we decided to change the solvents (HMPA and DMSO) and repeated everything (**entries 5-12)** with **3a** and **3b** in the same fashion. But we did not achieve any success and faced the same issue. In the end, to check if boron and sulfur were reacting with each other, the reaction was run without an oxathiazole source (**entry 13**). The same ^{19}F-NMR data was observed as we obtained with the oxathiazole source (Figure 6.4), (Figure 6.5).

Table 6.1 Optimization of the Reaction Conditions for Thiol Synthesis

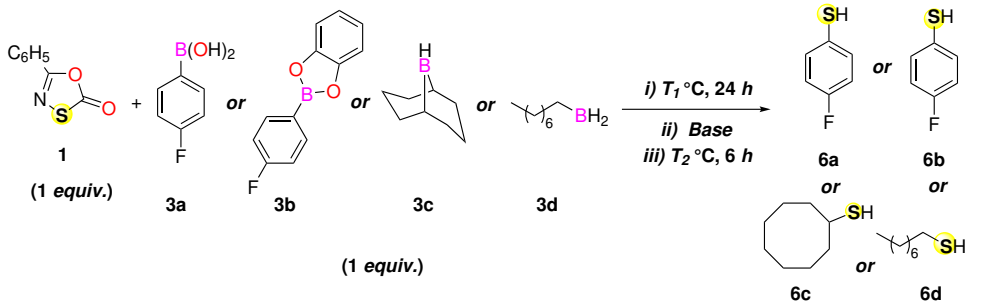

Entry	Solvent	Base	T_1 (°C)	T_2 (°C)	yield (%)
$1^{3a,3b,3c,3d}$	DMF	-	150	*r.t*	-
$2^{3a,3b,3c,3d}$	DMF	NaOH	150	*r.t*	-
$3^{3a,3b,3c,3d}$	DMF	NaOH	150	120	-
$4^{3a,3b,3c,3d}$	DMF	NaOH	120	120	-
$5^{3a,3b}$	HMPA	-	150	*r.t*	-
$6^{3a,3b}$	HMPA	NaOH	150	*r.t*	-
$7^{3a,3b}$	HMPA	NaOH	150	120	-
$8^{3a,3b}$	HMPA	NaOH	120	120	-
$9^{3a,3b}$	DMSO	-	150	*r.t*	-
$10^{3a,3b}$	DMSO	NaOH	150	*r.t*	-
$11^{3a,3b}$	DMSO	NaOH	150	120	-
$12^{3a,3b}$	DMSO	NaOH	120	120	-
13^{a*}	-	NaOH	*r.t*	-	-

a* reaction condition: only 3a and base was stirred together at room temperature for 3 hours.

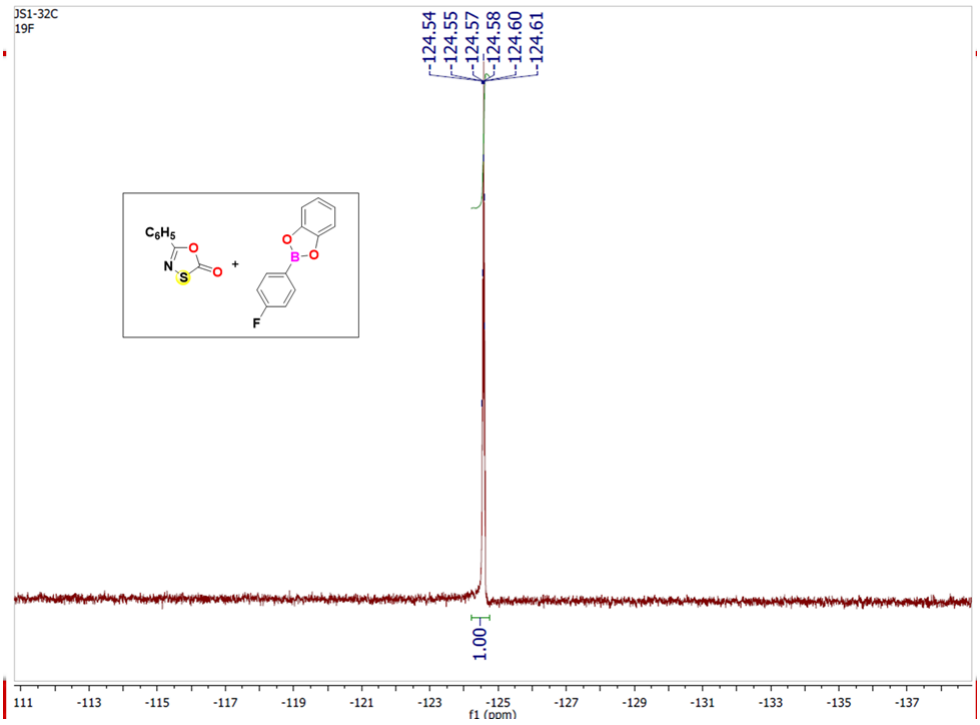

Figure 6.4 Representative ^{19}F–NMR spectra for entry **1** with **3b**.

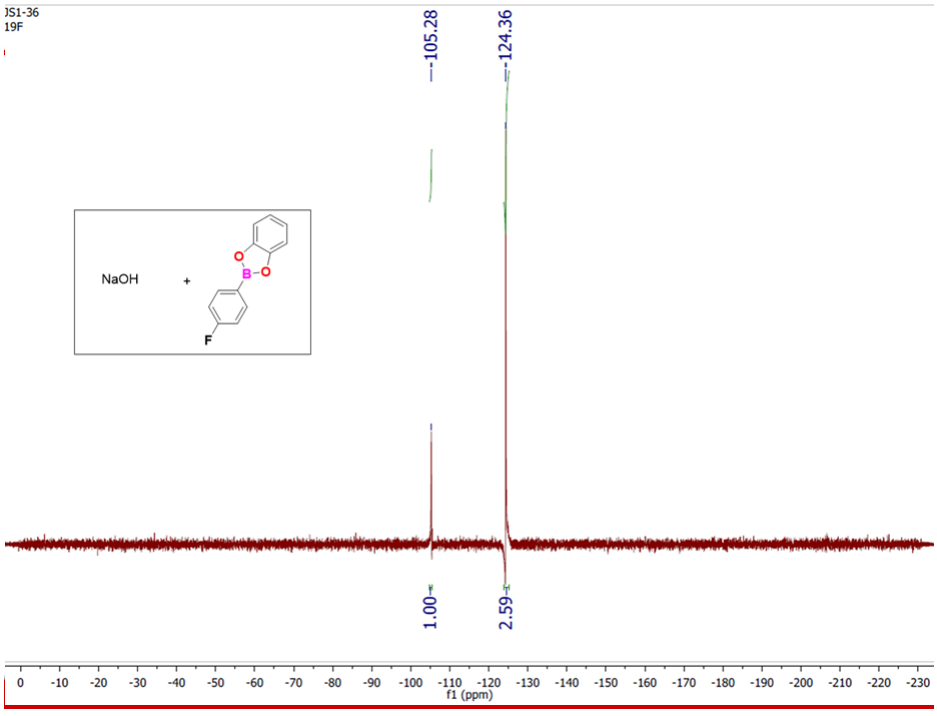

Figure 6.5 Representative ^{19}F–NMR spectra for entry **13** with **3b**.

6.1.6 Investigating the factors contributing to the lack of formation of the desired product

The goal of the reaction was to generate a nucleophile (benzonitrile sulfide), which can further react with boron source and produce thiol as a final product. Nevertheless, our the observation shows that **1** did not convert in to benzonitrile sulfide **(2)**, instead decomposed to form benzonitrile, sulfur, and CO_2 gas (Figure 6.6). To address this issue, the reaction was attempted by decreasing the reaction temperature but faced the same problem.

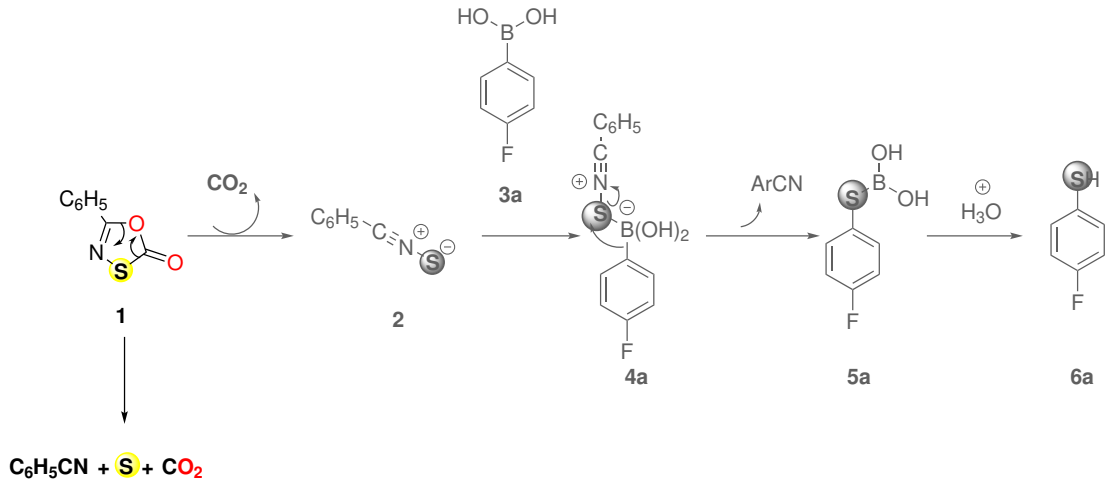

Figure 6.6 Decomposition of Benzonitrile Sulfide.

So, it was inferred that boron is not potent with sulfur atom due to its size difference. Boron is a small element with a radius of approximately 0.085 nm, while sulfur has a radius of approximately 0.180 nm. Due to the significant difference in size between the two elements, it is difficult for them to form stable bonds.

6.1.7 Conclusion

In conclusion, we attempted to synthesize the thiol using 5-phenyl-1,3,4-oxathiazole-2-one and various sources of boron under different reaction conditions. Our results indicate that the desired product was not formed due to the size difference between boron and sulfur. Further investigation and modifications to the reaction conditions

may be necessary to overcome these challenges and achieve the desired synthesis in future studies.

6.1.8 Experimental section

Procedure for the Preparation of 5-phenyl-1,3,4-oxathiazole-2-one(1) The precursor of benzonitrile sulfide was synthesized from benzamide and chlorocarbonyl sulfonylchloride.[224] To an oven–dried round bottom reaction flask, equipped with a magnetic stir bar was charged with benzamide (1.25 mmol, 1.25 equiv) as a limiting reactant (0.2 mmol), chlorocorbonyl sulfonylchloride (1.25 mmol, 1.25 equiv) and toluene solvent (10 mL, 0.1 M) under argon atmosphere. The reaction mixture was stirred at 100 °C for 2.5 h. After completion of the reaction, the reaction mixture was cooled to room temperature. Solid pure product was obtained that was further dried under vacuum pump.

6.1.9 Characterization data

5-phenyl-1,3,4-oxathiazole-2-one(1) Appearance - White crystalline solid; $\boldsymbol{R_f}$ = 0.90 (5% EtOAc/Hexane); ^{1}**H-NMR (500 MHz, CDCl$_3$)** δ 7.98 (dd-2H), 7.57(t, 1H,) ^{13}**C-NMR (500 MHz, CDCl$_3$)** δ 173.8, 157.4, 132.6, 129.0, 128.2, 127.4, 125.8, 124.1. 7.5(t, 2H); **Yield** = 62 %.

6.2 Synthesis of 2-Substituted Benzothiazole

The synthesis of 2-substituted benzothiazole has been investigated using ortho-metalated aryl imine with the ubiquitous S_8 as sulfur source.

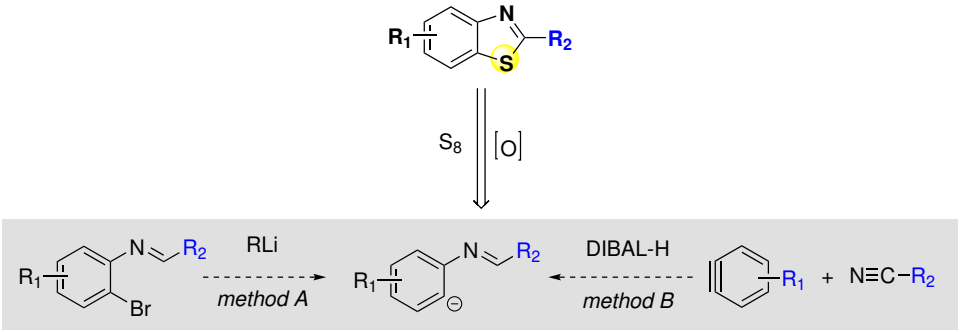

6.2.1 Introduction

2-Substituted benzothiazoles belong to a group of organic compounds that consist of a fused benzene and thiazole ring structure, with a substituent attached to the second carbon of the thiazole. 2-Substituted benzothiazoles are widely used in various fields such as pharmaceuticals, agrochemicals, dyes, and materials science due to their versatile biological activities[225]. Several 2-substituted benzothiazole derivatives have been identified as potential **drug** candidates[226, 227] with diverse biological activities, including antifungal, antibacterial, antitumor, and anti-inflammatory activities. For instance, riluzole and amitriptyline, 2-substituted benzothiazole derivatives, are used for treating neurological disorders. In **agrochemicals**, 2-substituted benzothiazole derivatives exhibit herbicidal, fungicidal, and insecticidal activities, and benzothiazole-2-thiol is utilized as a plant growth regulator.[228, 229] In **dyes**, 2-substituted benzothiazoles are utilized as intermediates for synthesizing dyes and pigments.[230, 231] For example, 2-methylbenzothiazole is a precursor for the synthesis of the dye disperse yellow 7. In **materials science**, 2-substituted benzothiazoles are utilized as building blocks for synthesizing materials with desired properties, including liquid crystals, polymers, and semiconductors.[232, 233] In the

past, consequently, substantial research efforts have been devoted to constructing these scaffolds. There are several methods for the synthesis of benzothiazole derivatives, but two main methods to access benzothiazole are the Hofmann condensation[234] of 2-aminothiophenols with aldehydes and the Jacobson oxidative cyclization of thioanilides (Figure 6.7.[235])

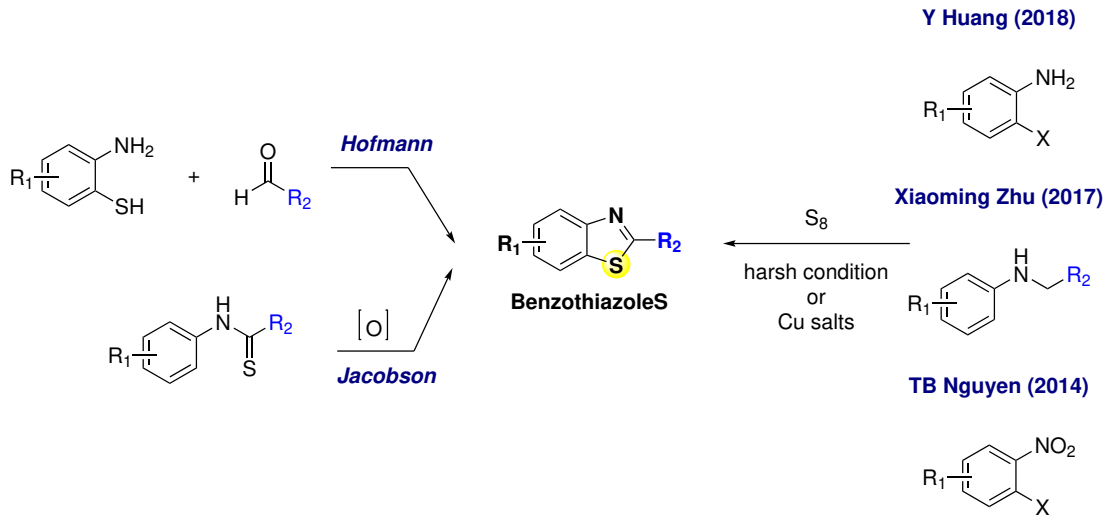

Figure 6.7 Common(left) and contemporary(right) methods for the synthesis of benzothiazoles.

Both the Hofmann condensation and the Jacobson oxidative cyclization methods have their advantages and limitations. The Hofmann condensation is a versatile method that can be used to synthesize a wide range of benzothiazole derivatives with different substituents. Nevertheless, the reaction conditions can be harsh, and the yield and selectivity of the reaction can be variable. The Jacobson oxidative cyclization, on the other hand, is a milder method that can be used to synthesize substituted benzothiazoles with good selectivity. Nevertheless, the starting materials for the reaction are limited to thioanilides, and the reaction conditions can be more complex than those of the Hofmann condensation. In recent years, a number of contemporary methods have been developed for the synthesis of benzothiazoles using elemental sulfur as a sulfur source for avoiding the limitations of these traditional methods (Figure 6.7 right).[236–238] Nevertheless, elemental sulfur is a relatively

inert and unreactive substance, and it is difficult to activate it for chemical reactions without the use of harsh conditions or reactive reagents.

6.2.2 Statement of the problem

The issue relate to the constraints and difficulties faced by conventional techniques in synthesizing benzothiazoles. Despite the availability of contemporary methods that used elemental sulfur, its activation for chemical reactions remains a challenge. Consequently, there is a requirement for novel, effective, and gentle approaches to producing benzothiazoles. Keeping the utility of elemental sulfur in mind, a transition-metal-free with mild condition synthesis of benzothiazole using ortho-metalated aryl imine has been explored.

6.2.3 Proposed reaction mechanism

Two methods have been proposed to create benzothiazoles by reacting S_8 with a bifunctional molecule that has both a nucleophilic site capable of attacking sulfur and an electrophilic site that facilitates the intermediate's cyclization (Figure 6.8). The hypothesis is that an ortho-metalated aryl imine (**16**) will open S_8 and cyclize in the presence of O_2, generating benzothiazoles through the oxidation of the intermediate benzothiazolines.[239] A proposed mechanism is shown in Figure 6.8. **Method A** involves reacting N-(2-bromoaryl) imines (**9a**) with an organolithium reagent in the presence of S_8. These imines will be synthesized using condensation procedures from functionalized aldehydes and 2-bromoanilines. Lithium-halogen exchange is the preferred reaction as it is faster than deprotonation for aryl bromides and iodides,[240] and quicker than adding the organolithium compound to an imine or acyliminium ion.[241, 242] As a result, we propose that by adding a single equivalent of n-BuLi to a mixture of **9a** along with 1/8 equivalents of S_8 at room temperature, the aryl lithium **16** will be produced as the only species in the solution.

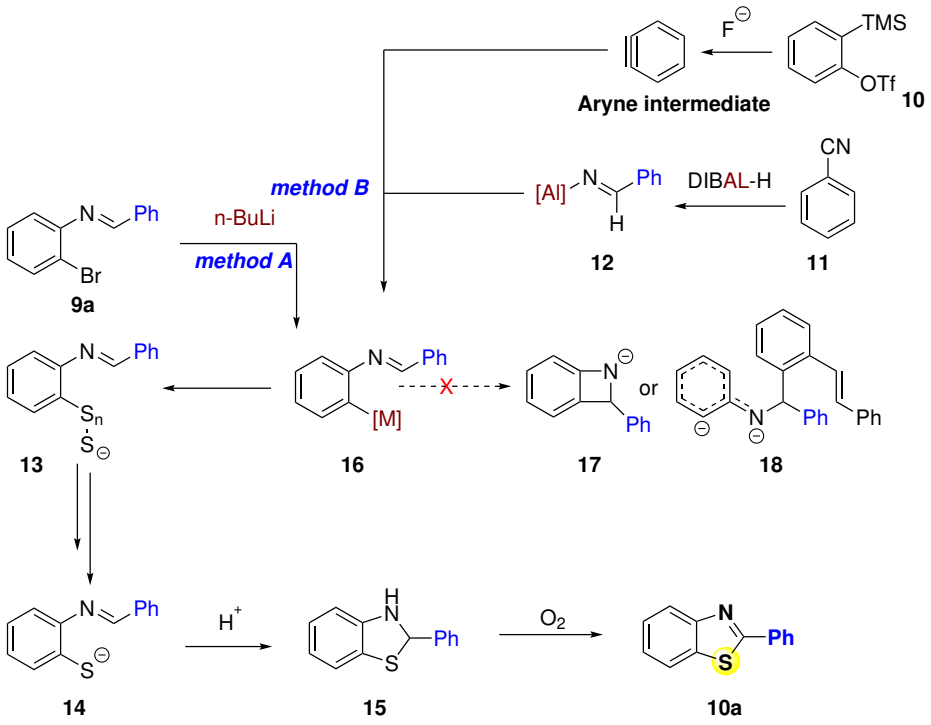

Figure 6.8 Proposed mechanisms for the synthesis of benzothiazoles from N-(o-bromoaryl) imines 9a (method A) or aryne intermediate and imine anions 12 (method B).

In accordance with Baldwin's rules, the 4 endo-trig cyclization to **17** is disfavored.[243] As an alternative, we propose that **16** will initiate an attack on sulfur, leading to the formation of a polysulfide **13**. Subsequently, this polysulfide will rearrange into the monosulfide **14**, which is a common reaction observed in aryl anions.[49, 118, 244, 245] We expect that the self-reaction of **16** is unlikely to occur due to the formation of the dianionic **19**. Furthermore, sulfide **14** can undergo the 5-endo-trig cyclization to benzothiazoline **15** under acidic conditions, followed by oxidation to produce the final benzothiazole product **10a**. Although Baldwin's rules do not favor 5-endo-trig cyclizations, they are frequently observed in organic chemistry. For instance, the addition of tethered alcohols to oxonium ions to form 5-membered acetals[141] is an example. Additionally, such cyclizations are known to be favorable with imines[246] or with third-row atoms such as sulfur.

A second approach (Method B, Figure 6.8) to produce metalated aryl imines **16** is visualized, as there are limited commercially available ortho-bromoanilines. In this method, nitriles are partially reduced to imine anions **12** using diisobutylaluminum hydride (**DIBAL-H)**.[247] We hypothesize that this anion, in the presence of arynes (generated from o-(trimethylsilyl)aryl triflates), would produce the aryl anion **16**. Since the reaction of imine with aryne precursor has already been studied extensively. **Method B** will use commercially-available nitriles, and 2-(trimethylsilyl)phenyl triflates **10** [248] will be synthesized from 2-bromophenols using a two-step procedure that has been established in previous studies.

6.2.4 Results and discussion

Optimization study - *method A* With a view to synthesize 2-substituted benzothiazole, the present study was initiated by treating the N-(2-bromoaryl) imines **9a** (synthesized from functionalized aldehydes and 2-bromoanilines) with one equivalent of n-BuLi in toluene followed by addition of elemental sulfur and air oxidation Table 6.2 **(entry 1)**. The expected product did not form, and the majority of imine remains unreacted with some decomposed product. In an attempt to get desired product, several condition was tried. In the **second trial**, reaction time was prolonged for the addition of **n-BuLi** while retaining all other conditions unchanged. In the **third** and **fourth** trials, reaction temperature was increased. For **entry 4** reaction time for n-BuLi addition was also extended. But the result remained the same. Despite these modifications, the expected product still did not form. To further investigate the reaction, entries **5 to 8** were conducted with THF instead of toluene, and all steps were repeated. Nevertheless, desired product was not observed, indicating that the modifications and alternative solvent did not enhance the reaction's efficacy. In summary, the attempts to synthesize 2-substituted benzothiazole were unsuccessful, despite various modifications to the

reaction conditions and solvent choice. Further investigation and alternative synthetic routes may be necessary to achieve the desired product.

Table 6.2 Optimization of the Reaction Conditions for Method A

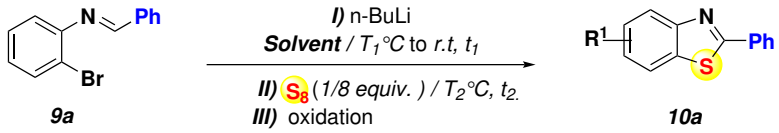

Entry	Solvent	n-BuLi	T_1 (°C)	t_1 (min)	T_2 (°C)	t_1 (h)
1	Toluene	1.0	-78	30	65	12
2	Toluene	1.0	-78	60	65	12
3	Toluene	1.0	0	60	65	24
4	Toluene	1.0	0	120	65	24
5	THF	1.0	-78	60	60	24
6	THF	1.0	0	60	60	24
7^a	THF	1.0	0	60	120	24
8^b	THF	1.0	0	60	*r.t*	24

Reaction conditions : a = Oxidation in $CHCl_3$ (open air),
b = Oxidation in 1M HCl in CH_3CN(Open air)

6.2.5 Investigating the factors contributing to the lack of formation of the desired product

The goal of reaction was to replace a bromine atom in a molecule with a lithium metal. The resulting compound will then undergo a ring-opening reaction with elemental

sulfur, followed by cyclization, which will lead to the final product. Nevertheless, there was also another nucleophile in the solution, namely butyl anion, which is the counterpart of Li metal. This butyl anion attacked the imine carbon (Figure 6.9), causing it to stop the reaction and prevent further progress towards the desired product.

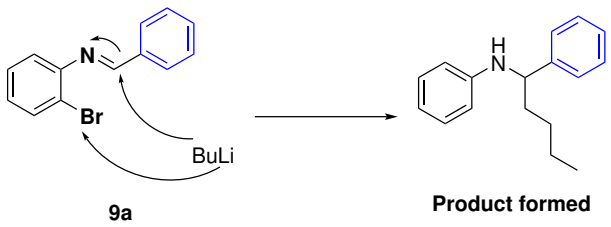

Figure 6.9 Attack of BuLi on imine carbon.

This observation was confirmed by proton ^{1}H-NMR (Figure 6.10) of the reaction between compound **9b** and n-BuLi.

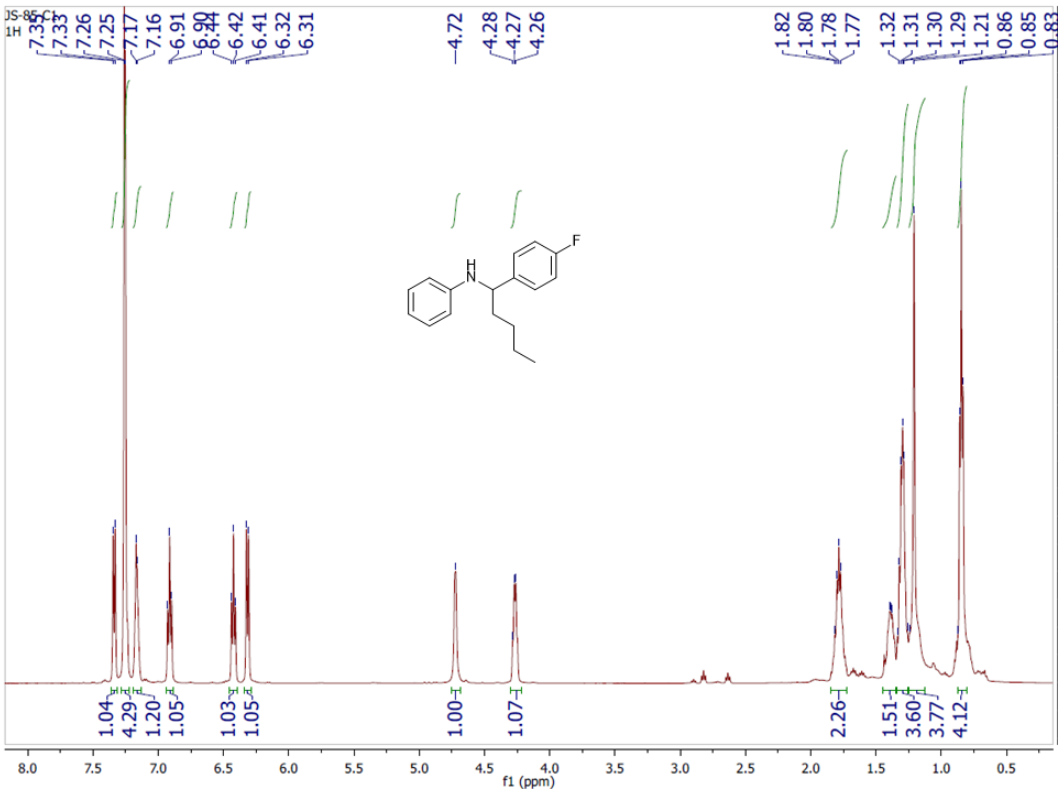

Figure 6.10 Representative ^{1}H–NMR spectra of reaction between **9b** and n-BuLi.

The chemical shift of the CH-NH proton at 4.27 ppm[249] with triplet splitting was observed, along with the butyl chain hydrogen ranging from 1.82 to 0.85 ppm. Another reaction was attempted with a different imine source (**9c**), that had a tertiary butyl group on the para position. The purpose of using this molecule was to lower the electrophilicity of the imine carbon, which means that it would be less attractive to nucleophiles and less likely to be attacked by them. Despite the use of this bulky group, which was expected to prevent the butyl anion from attaching to the imine carbon, the butyl anion still attached to the imine carbon.

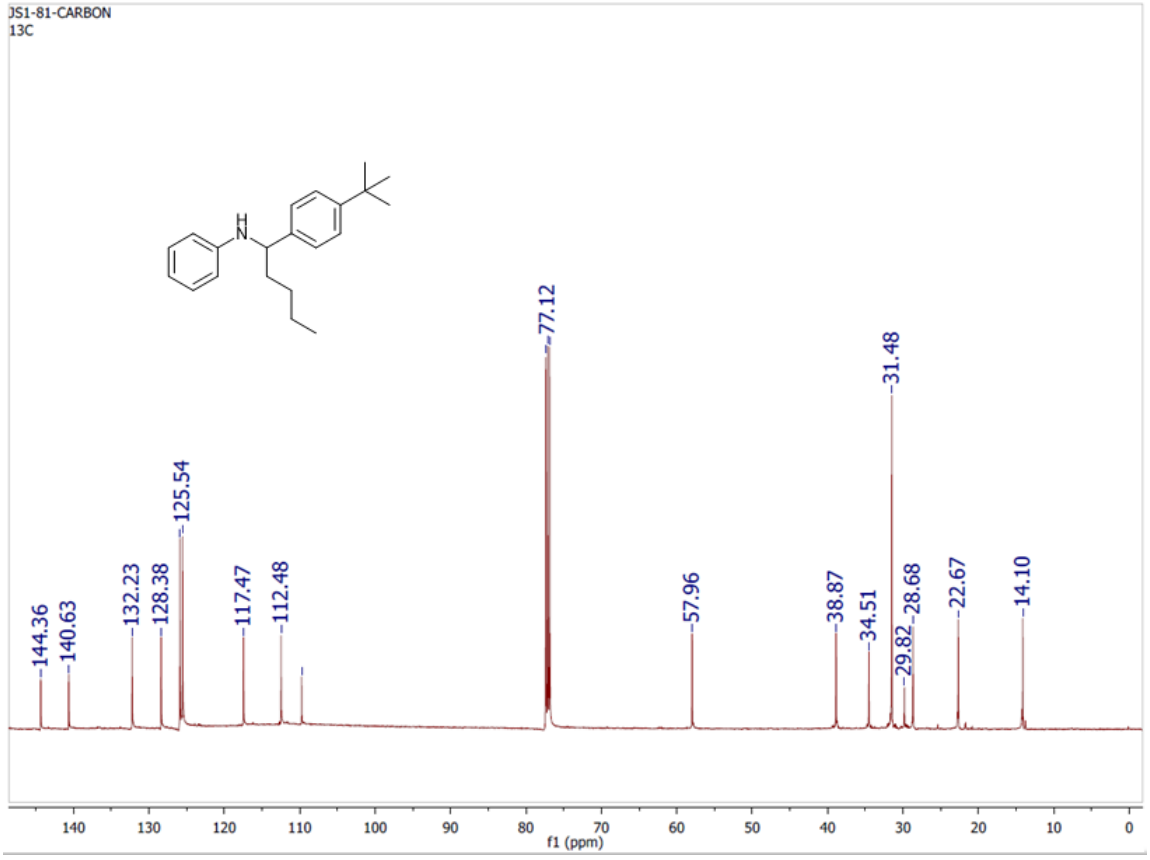

Figure 6.11 Representative ^{13}C–NMR spectra of reaction between **9c** and n-BuLi

The butyl anion's attachment to the imine carbon was confirmed by observing the carbon peak at 57.88 ppm in the ^{13}C-NMR (Figure 6.11). This observation confirms the presence of an NH-C linkage in the product. This result indicates that the electrophilicity of the imine carbon was still high enough to be attacked by the

external nucleophile.

6.2.6 Alternative reaction route

An alternative route was chosen for achieving the desired end product by using a different metal source. The reason for this is that the original metal source had an alkyl counterpart, which could potentially attack the imine carbon during the reaction. This unwanted reaction could lead to the formation of undesired products.

Table 6.3 Optimization of the Reaction Conditions for Alternative Reaction Route

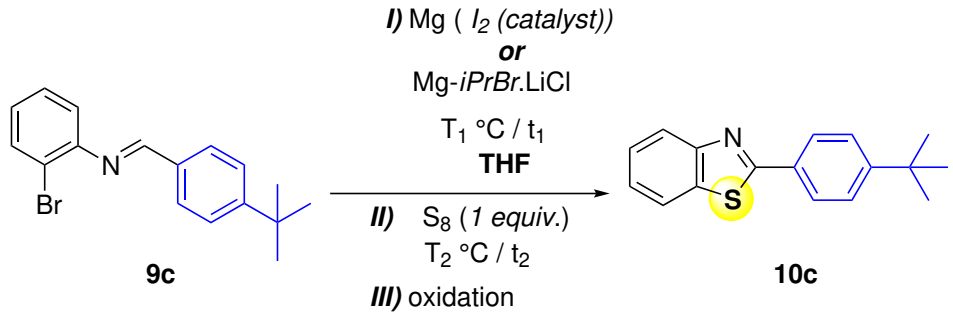

Entry	Metal source	T_1 (°C)	t_1 (min)	T_2 (°C)	yield
1^b	1.2	-10	90	*r.t*	-
$2^{b'}$	1.2	60	60	*r.t*	-
$3^{b'}$	2.0	40	12*60	*r.t*	-

Reaction conditions : b = $Mg(I_2)$,

b$'$ = Mg-*iPrBr*.LiCl

To avoid this problem, different metal source was selected that either does not have an alkyl counterpart or has a bulky group attached to it. A bulky group would not attached the imine carbon, thus enabling the reaction to proceed as planned.

6.2.7 Results and discussion

Optimization study The goal of the study was to synthesize 2-substituted benzothiazole. In the first experiment (Table 6.3 - entry 1), the imines were treated with magnesium metal that had been treated with iodine in THF, for synthesizing grignard reagent, followed by the addition of elemental sulfur and oxidation. Nevertheless, the 50 % of imines did not react and 50 % of decomposed product was obtained (Figure 6.12). In the subsequent experiments **(entry 2 and 3)**, Mg-iPrBr.LiCl, was taken instead of magnesium metal and carried out the reaction at high temperature. Despite these changes, same problem was faced, and the results were not successful.

6.2.8 Conclusion for method - A

Based on the attempted synthesis of 2-substituted benzothiazoles using N-(2-bromoaryl)imine, n-BuLi, and elemental sulfur, it can be concluded that the desired compound was not successfully obtained. The failure to achieve the synthesis can be attributed to the high electrophilicity of the imine sp^2 carbon, which made it susceptible to attack by the butyl anion of n-BuLi. This susceptibility hindered the crucial cyclization step of the reaction. Further investigation and modifications to the reaction conditions may be necessary to overcome these challenges and achieve the desired synthesis in future studies.

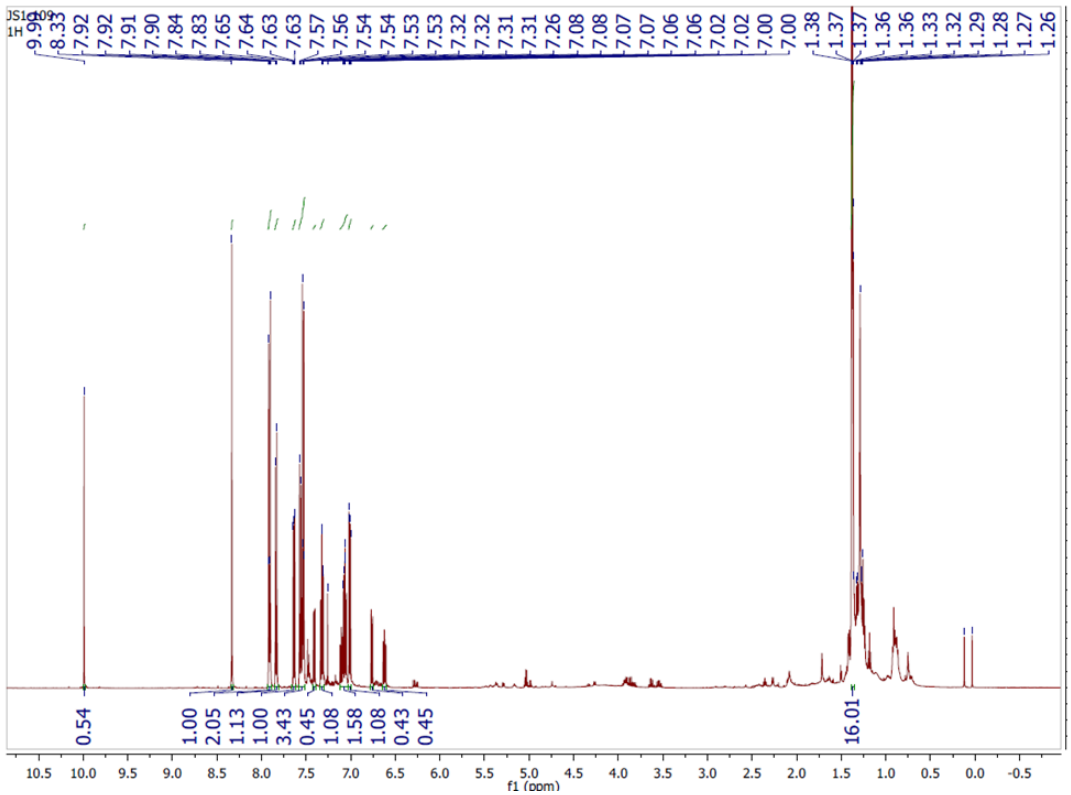

Figure 6.12 Representative ^{1}H–NMR spectra of reaction between **9c**, Mg(I_2) metal and S_8.

6.2.9 Experimental section

Preparation of N-(2-bromophenyl)-1-phenylmethanimine Under an argon atmosphere, oven dried round-bottomed flask was equipped with a magnetic stir bar.

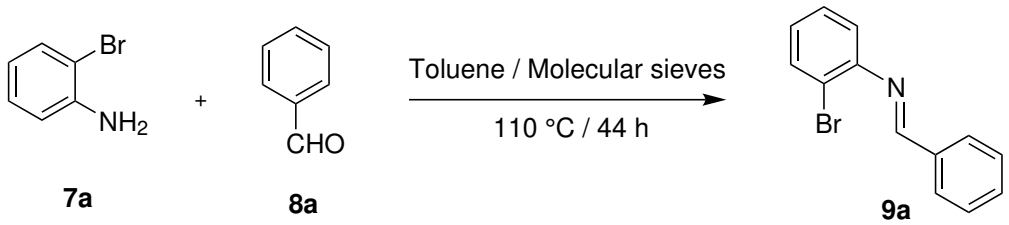

Figure 6.13 Synthesis of **9a**.

To the flask, 860 mg (5 mmol) of 2-bromoaniline **7a** and 540 mg (5 mmol) of benzaldehyde **8a** were added in 15 ml of toluene. The mixture was supplemented with approximately 1.7 g of molecular sieves and then refluxed for 44 hours. After cooling, the reaction mixture was subjected to vacuum drying for 5 hours at 80

°C to purify the resulting product (Figure 6.13). Brown oil of N-(2-bromophenyl)-1-phenylmethanimine **9a** was obtained (260.13 mg, 57% yield). Using the above procedure **9b, 9c, 9g** was synthesized.

Preparation of N-(2-bromophenyl)-1- (4-nitrophenyl)methanimine Under an argon atmosphere, a round-bottomed flask was dried in an oven and equipped with a magnetic stir bar.

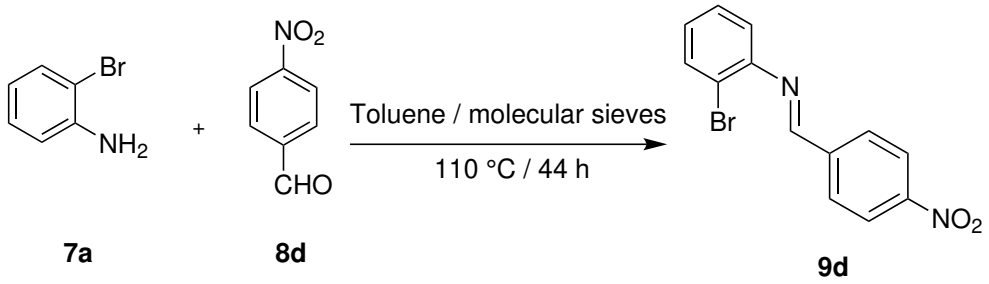

Figure 6.14 Synthesis of **9d**.

To the flask, 1204 mg (7 mmol) of 2-bromoaniline **7a** and 1511 mg (10 mmol) of benzaldehyde **8d** were added in 40 ml of toluene. The mixture was supplemented with approximately 3.0 g of molecular sieves and then refluxed for 44 hours (Figure 6.14). After cooling, the solvent was evaporated and the crude residue was recrystallized with ethanol. Yellow powder of N-(2-bromophenyl)-1-(4-nitrophenyl)methanimine **9d** was obtained (305.13 mg, 80% yield).

Preparation of N-(2-bromophenyl)-1,1-diphenylmethanimine Under an argon atmosphere, a round-bottomed flask was dried in an oven and equipped with a magnetic stir bar. To the flask, 172 mg (1 mmol) of 2-bromoaniline **7a** and 182 mg (1 mmol) of benzophenone **8e** with catalytic amount of p-Toluenesulfonic acid pentahydrate (PTSA- 19mg) were added in 10 ml of toluene.

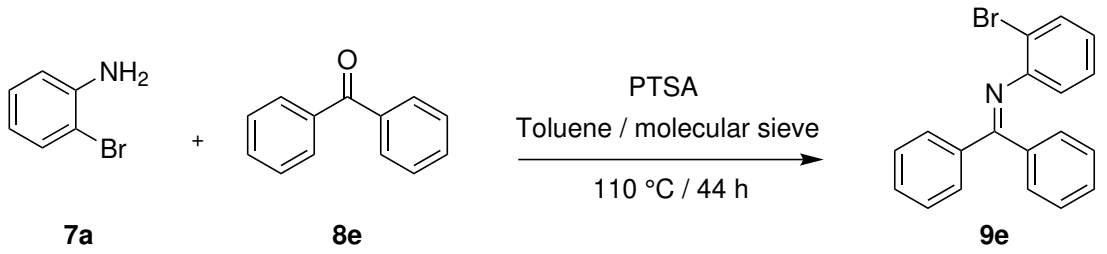

7a **8e** **9e**

Figure 6.15 Synthesis of **9e**.

The dean-stark apparatus was attached to the round bottom flask with molecular sieves and toluene. The mixture was refluxed for 24 hours (Figure 6.15). After cooling, the solvent was evaporated and the crude residue was purified on a silica gel using flash column chromatography using EtOAc /petroleum ether (95:5) as eluent to afford the desired product. Yellow crystals of N-(2-bromophenyl)-1,1-diphenylmethanimine **9e** was obtained (120.10 mg, 36% yield).

6.2.10 Characterization data

N-(2-bromophenyl)-1-phenylmethanimine (9a):

Appearance - brown oil; ^{1}**H NMR (500 MHz, CDCl$_3$)** δ 8.36(s, 1H), 7.95- 7.96 (d, 2H), 7.62-7.64 (d,1H),7.49-7.51(d, 3H),7.31-7.34(t, 1H).7.02-7.09(m. 2H), **Yield** = 57 %.

N-(2-bromophenyl)-1-(4-fluorophenyl) methanimine (9b):

Appearance - brown oil; ^{1}**H NMR (500 MHz, CDCl$_3$)** δ 8.39(s, 1H), 8.01- 8.03 (m, 2H), 7.69-7.71 (d,1H),7.38-7.40(t, 1H),7.23-7.24(d, 2H).7.07-7.16(m. 2H). ^{19}**F NMR (300 MHz, CDCl$_3$)** δ 111.75, **Yield** = 67 %.

N-(2-bromophenyl)-1-(4-(tert-butyl)phenyl)methanimine(9c):

Appearance - brown oil; ^{1}**H NMR (500 MHz, CDCl$_3$)** δ 8.32(s, 1H), 7.89 (d,

2H), 7.57 (d,3H),7.32(d, 1H),7.03(d, 2H),1.36(s, 9H), **Yield** = 35 %.

N-(2-bromophenyl)-1-(4-nitrophenyl)methanimine (9d):

Appearance - yellow powder; ^{1}**H NMR (500 MHz, CDCl$_3$)** δ 8.47(s, 1H), 8.35-8.36 (d,2H),8.13-8.15(d, 2H),7.66-7.68(d, 1H),7.35-7.38 (t,1H),7.13-7.16(t, 1H),7.05-7.06(d,1H), **Yield** = 80 %.

N-(2-bromophenyl)-1,1-diphenylmethanimine(9e):

Appearance - yellow crystals; ^{1}**H NMR (500 MHz, CDCl$_3$)** δ 7.81-7.82(d, 2H), 7.41-7.51(m-4H), 7.25-7.29 (m,3H) ,7.17-7.19(d, 2H),7.01-7.04(m, 1H),6.76-6.79(m,1H).6.52-6.54(dd,1H), **Yield** = 36 %.

N-(2-bromo-4-methylphenyl)-1-phenylmethanimine(9f): Appearance - brown oil; ^{1}**H NMR (500 MHz, CDCl$_3$)** δ 8.32(s, 1H), 7.91-7.93(dd-2H), 7.44-7.47 (m,4H) ,7.08-7.10(m, 1H),6.90-6.91(d, 1H),2.31(s,3H), **Yield** = 87 %.

6.2.11 Synthesis of benzothiazole from aryne precursor - *Method B*

Introduction Over a century ago, **aryne** were discovered as a extremely reactive intermediates. Chemists have used these transient intermediates to synthesize various compounds, including 1,2-disubstituted benzene derivatives, as well as benzo-fused carbocycles and heterocycles.[250–255] These compounds were previously challenging to create using conventional methods. Arynes can be produced through various means, but **Kobayashi's fluoride-induced aryne** generation is the most straightforward technique known.[248, 256] This method involves generating an aryne via fluoride-induced 1,2-elimination of 2-(trimethylsilyl)aryl triflates, which act as aryne precursors. Kobayashi's method can be conducted under mild, base-free

conditions. Kobayashi's aryne generation method is versatile and works well with many functional groups and reagents. Fluoride sources, such as KF (with 18-crown-6 as an additive) in THF, CsF in CH_3CN, TBAT in THF, and tetrabutyl ammonium fluoride (TBAF) in THF, are typically used for this method. Careful selection of the fluoride source and solvent combination can help control the rate of aryne generation in product formation. The mild and efficient procedure has encouraged chemists to revisit traditional aryne reactions to improve their scope and yield.

The bulk of aryne reactions involve the use of various nucleophilic initiators. The arynes' reactions stimulated by these nucleophiles are specifically classified as **arylation reaction**, **insertion reaction**, and **multicomponent coupling**.[257, 258] Multicomponent couplings (MCCs) with aryne, achieved significant success in recent years, that do not require transition-metal catalysts. The general reaction scheme has been shown in Figure 6.16. Multicomponent reactions have gained substantial interest and scrutiny in the field of aryne chemistry, particularly regarding the primary nucleophile addition to arynes, succeeded by the capture of the aryl anion intermediate with electrophiles. Valuable heterocycles have been synthesized using this versatile transition-metal-free approach, which has also found application in natural product synthesis. A plethora of nucleophiles can take part in MCCs, as elucidated below.

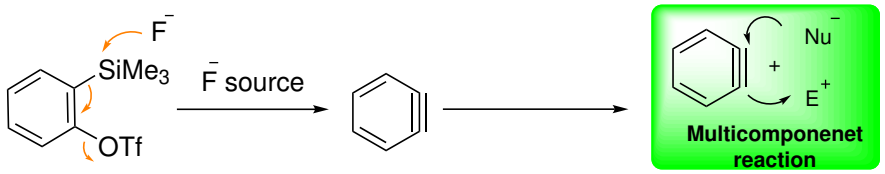

Figure 6.16 Multicomponent reaction of aryne.

6.2.12 Multicomponent reactions involving sulfur nucleophiles

Cyclic thioethers as a nuceophile Thietane, tetrahydrothiophene, and thiane, which are cyclic thioethers characterized by four- to six-membered rings, undergo facile zwitterion formation upon treatment with arynes.[259]

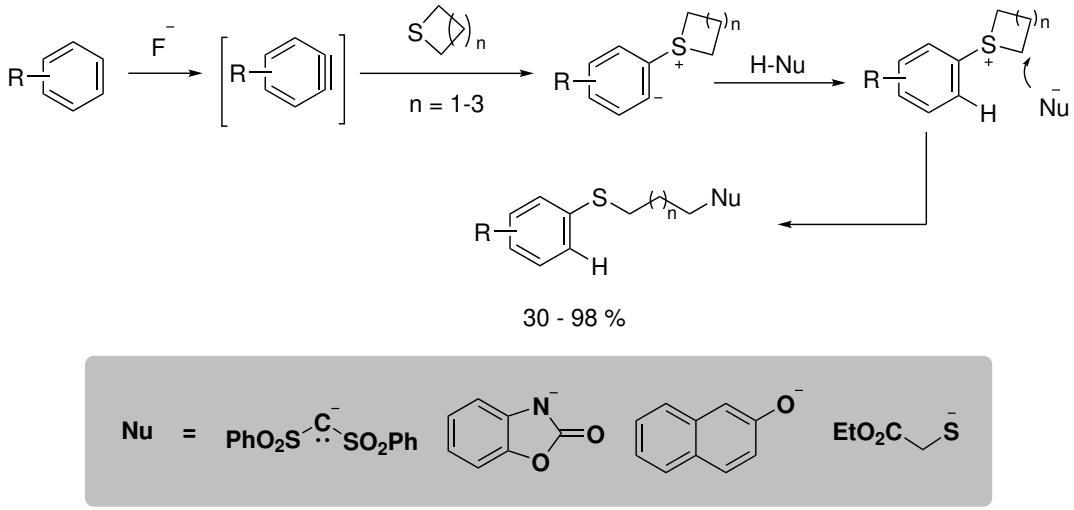

Figure 6.17 Multi-component reaction of arynes, cyclic thioethers, and pronucleophiles.

These zwitterions can then be transformed into valuable three-component products via ring-opening capture with pronucleophiles. Pronucleophiles possessing a pKa range of approximately 13-19, including carbon-, nitrogen-, oxygen-, and sulfur-centered ones, have demonstrated remarkable effectiveness in serving as a ring-opening agent.

Among the various pronucleophiles investigated, bis(phenylsulfonyl)methane, 2-benzoxazolinone, 2-naphthol, and ethyl 2-mercaptoacetate stand out as representative compounds yielding high product yields (Figure 6.17).

6.2.13 Multicomponent reactions involving carbon nucleophiles

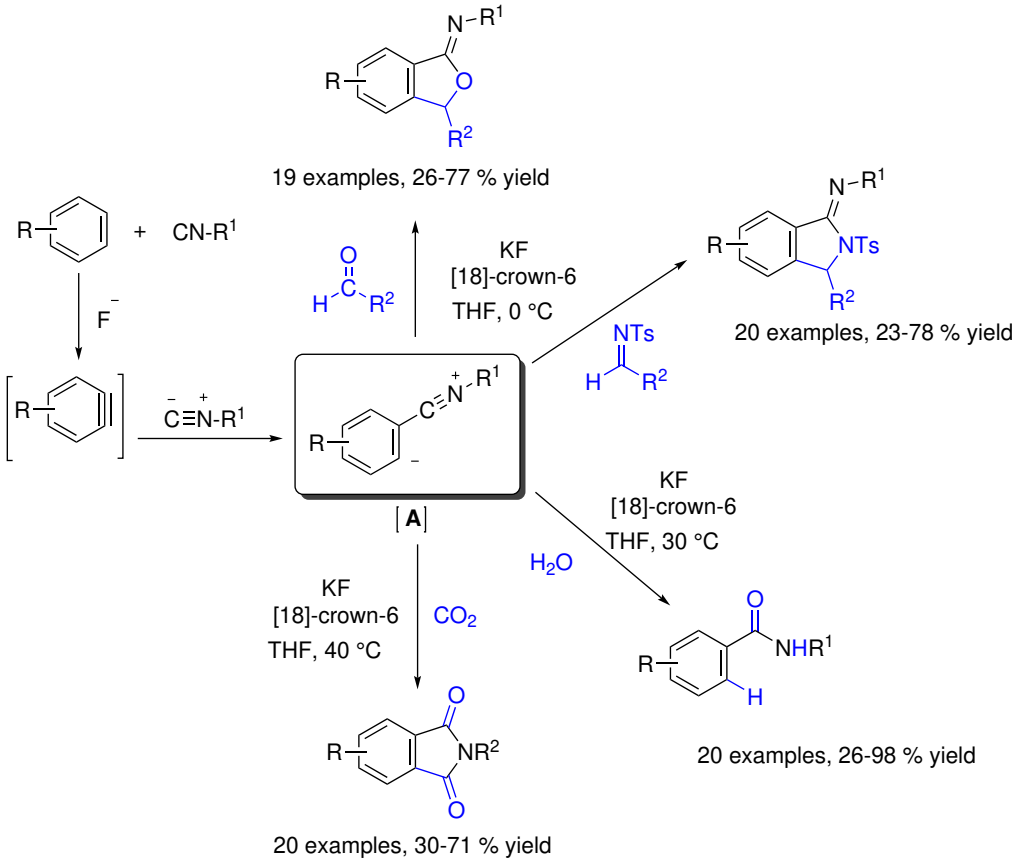

Figure 6.18 Multicomponent reaction involving isocyanides, aryne and electrophiles.

There are two main carbon based nucleophiles have been used with aryne precursor in multicomponent reaction, **isocyanide** and **active methylene** group. Yoshida was the first to develop a three-component reaction in 2004 that involved arynes, isocyanides, and aldehydes, leading to the production of benzannulated iminofurans with high yields.[260] The use of isocyanides as nucleophiles in multicomponent reactions involving arynes has proven practical and beneficial. The process involves a zwitterion **(A)** as a common intermediate. Further studies have demonstrated that the reaction is not limited to aldehydes as the electrophilic component. Instead, activated imines,[260] water,[261] and carbon dioxide[262] can also serve as suitable third components (Figure 6.18).

Active methylene compounds, such as aroylacetonitriles or diaroylmethanes, [263] are versatile intermediates that are widely used in organic synthesis. One of their significant applications is in the synthesis of naphthalene derivatives via a three-component route.

6.2.14 Multicomponent reactions involving nitrogen nucleophiles

Amine-based nitrogen nucleophiles, such as aziridines,[264] DABCO,[265] N,N-dialkylanilines,[266] N-methylindoline,[251] N-methyltetrahydroquinoline,[267] dialkylamines, alkylarylamines, and diarylamines, [268] have been extensively used in the synthesis of a diverse range of compounds (Figure 6.19). An alternative approach to executing a multicomponent reaction involves utilizing **imines** as nucleophiles.[262, 269–272] This technique involves the formation of a zwitterionic intermediate, which subsequently undergoes attack at the imine carbon by a pronucleophile, ultimately leading to the generation of a diverse range of products. **N-heteroarene**-based nitrogen nucleophiles, such as quinoline and isoquinolines, have been effectively utilized by Biju's research group to synthesize a broad spectrum of six-membered N,O-heterocyclic compounds.[273, 274] To achieve this, they have used a diverse array of electrophiles, including aldehydes and ketones (such as benzophenone, p-benzoquinone, and ethyl benzoylformate). In a similar manner to imines, chloroform has also been utilized as a pronucleophile with these two nucleophiles.[275] Moreover, Dai and He have recently revealed that dialkoxyphosphites can act as a pronucleophile in a three-component reaction with quinolines or isoquinolines, leading to the formation of dearomatized phosphonylated N-heterocycles in excellent yields.[276] This approach further demonstrates the versatile applications of N-heteroarene-based nitrogen nucleophiles in the synthesis of important organic compounds

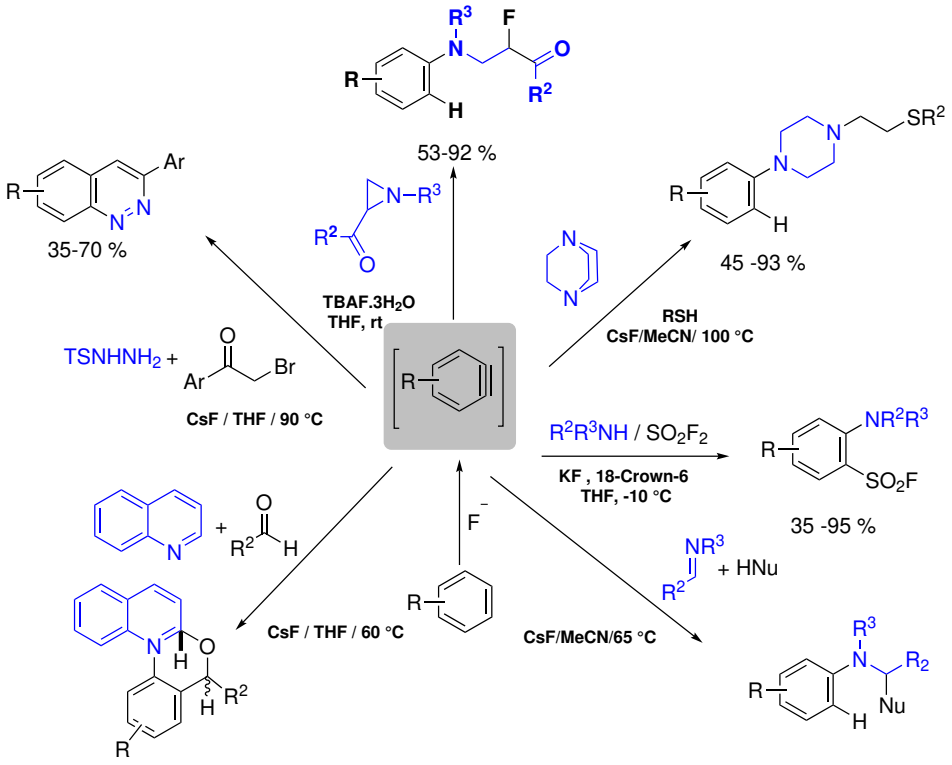

Figure 6.19 Multi-component reaction of arynes with nitrogen nucleophiles.

Diazene and Nitrite,[277, 278] nucleophiles such as tosylhydrazine and sodium nitrite, have been used in a medicinal reaction with an aryne precursor for the synthesis of cinnoline derivatives and nitrating aromatic rings. The reaction scheme for few selected nitrogen nucleophiles have been shown in Figure 6.19.

6.2.15 Results and discussion

Optimization study - *method B* With the objective of synthesizing 2-substituted benzothiazole, we started an initial effort to optimize the reaction for the synthesis of aryl imine (**19**) from Kobayashi aryne precursor (**10**) using a multicomponent reaction route in three distinct ways: two-pot, sequential, and one-pot reaction route. In the **two-pot reaction** method, the aryne precursor was combined with CsF in acetonitrile solvent in a round bottom flask and stirred at 0 °C for one hour, while benzonitrile was taken separately in another round bottom flask and stirred at 0 °C with DIBAL-H. After one hour, both reaction mixtures were combined and stirred at

room temperature for two hours (Table 6.4 - entry 1). But , the anticipated product failed to form, and the aryne precursor remained unreacted. In **entry 2**, the solvent and fluoride source were substituted with THF and KF (along with an additive) while maintaining the same reaction temperature and duration. Even though, the aryne precursor remained unreacted. In **entry 3**, reaction time for benzonitrile reduction had been increased from 1 hour to 2 hour, nevertheless result did not change. In **entry 4**, reaction temperature for benzolnitrile reduction had been lowered down from 0 to -78 °C, along with enhancement in stirring time for both mixture together. Still results came same. In **entry 5** and **6**, equivalence of KF was increased, and stirring temperature for both mixture together, result did not change. Entries **7** and **8** represent a sequential mode, where along with KF, TBAF was used as a fluoride source. In the sequential route, first benzonitrile was reduced with DIBAL-H at temperatures between -70 to -40 °C, followed by the addition of the aryne precursor at 0°C, and the reaction was stirred at 60°C for 24 hours, but no success was achieved, where along with KF, TBAF was used as fluoride source.

Table 6.4 Optimization of Reaction Conditions for Two Pot Reaction / Sequential Reaction.

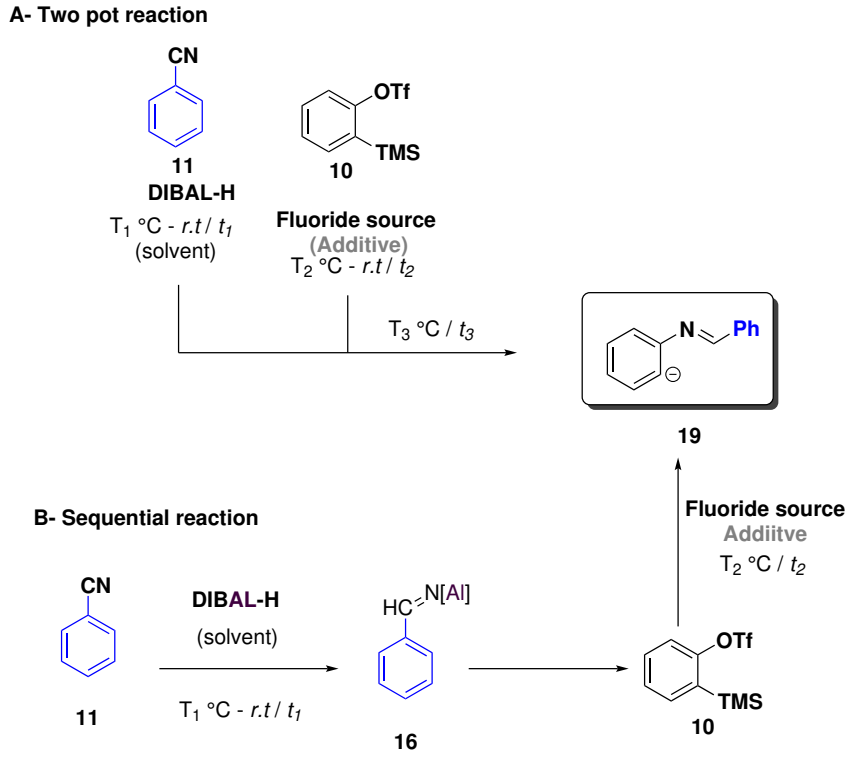

Entry	Solvent	T_1 (°C)	t_1 (min.)	Fluoride source	T_2 (°C)	t_1 (min)	T_3	t_3 (h)
1	CH_3CN	0	60	CsF (1)	0	60	*r.t.*	2
2	THF	0	60	KF (2)	0	60	*r.t.*	2
3	THF	0	120	KF (2)	0	60	*r.t.*	2
4	THF	-78	60	KF (2)	0	60	*r.t.*	12
5	THF	-78	120	KF (3)	0	60	65	12
6	THF	*r.t.*	60	KF (3)	0	120	65	12
7^x	THF	-70 to -40	120	KF (3)	0 - 60	24*60	-	-
$8^{x,y}$	THF	-70 to -40	120	TBAF (1.5)	0 - 60	24*60	-	-

Reaction conditions: KF is taken with the additive (18-crown-ether) x = Sequential reaction. Y= 1.5 equliv. of C has been used

Table 6.5 illustrates the optimization of a one-pot reaction, wherein all reactants were combined simultaneously. Each entry used a 1:1 ratio of benzonitrile (**11**) and

DIBAL-H. In **entry 1**, acetonitrile and CsF were used as the solvent and fluoride source, respectively. The reaction mixture was initially stirred at 0°C for two hours, followed by stirring at room temperature for 24 hours. Notably, the same outcome was achieved as in the preceding trial; the aryne remained unconsumed and expected product diphenyl imine (**19**) did not form. In **entries 2** and **3**, the solvent and fluoride source were substituted with THF and KF (with 18-crown-6). Additionally, the reaction temperature was increased. The use of KF as the fluoride source produced inferior outcomes. Substituting KF with tetrabutyl ammonium fluoride (TBAF), failed to yield any satisfactory results.

Table 6.5 Optimization of Reaction Conditions for One-pot Reaction

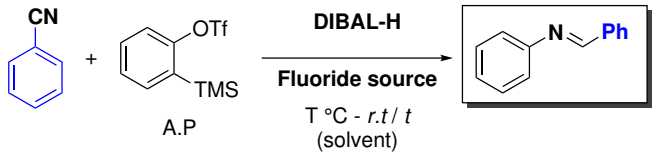

entry	A.P (10)	solvent	Fluoride source	T (°C)	t (h)
1	1	CH_3CN	CsF (2)	0 - *r.t.*	2 - 24
2	1	THF	KF (2)	*r.t.* - 65	2 - 12
3	1	THF	KF (3)	*r.t.* - 65	4 - 12
4	1.4	THF	TBAF (1.5)	*r.t.*	24
5	1.4	THF	TBAF (1.5)	*r.t.*- 65	24

Reaction conditions: KF is taken with the additive (18-crown-ether)

6.2.16 Investigating the factors contributing to the lack of formation of the desired product

In essence, the desired product was not obtained because the Kobayashi precursor failed to react with imine anion generated form reduction of benzonitrile form DIBAL-

H. After analyzing the crude ^{1}H NMR spectra, it was found that the initial reactants, namely the Kobayashi precursor and either benzonitrile or imine anion, were still present. Nevertheless, there is a possibility that a reaction occurred between the DIBAL-H and fluoride source, which stopped the generation of aryne intermediate.

6.2.17 Conclusion for method - B

Based on the attempted synthesis of 2-substituted benzothiazoles using benzonitrile, kobayashi aryne precursor, DIBAL-H, and elemental sulfur, it can be concluded that the desired compound was not successfully obtained. The failure to achieve the synthesis can be attributed to a reaction between the fluoride source and DIBAL-H, which stopped the generation of aryne intermediate. Further investigation and modifications to the reaction conditions may be necessary to overcome these challenges and achieve the desired synthesis in future studies.

6.3 Multicomponent Reactions Involving Arynes, Elemental sulfur, and Isoqunioline

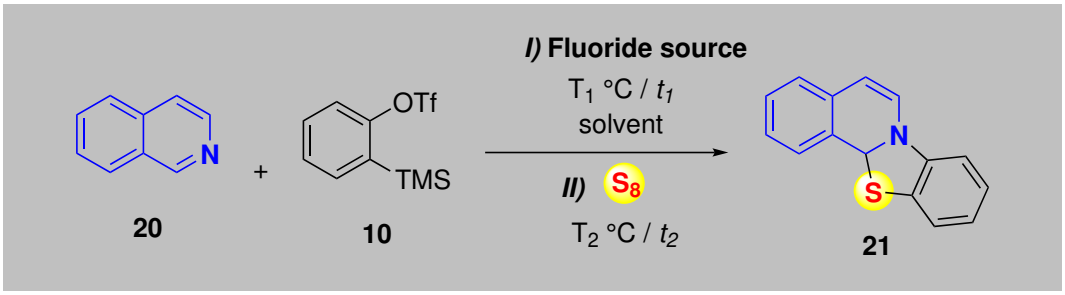

6.3.1 Introduction

The synthesis of sulfur derivative of isoqunioline has been investigated using aryne precursor with the S_8 as sulfur source. Isoquinoline derivatives are an important class of organic compounds that are widely used in pharmaceuticals, agrochemicals, and materials science.[279–281] One of the most important isoquinoline derivatives is the alkaloid morphine, which is widely used as an analgesic and pain reliever.[282] Other alkaloids such as codeine and noscapine are also important drugs derived from

isoquinoline.[283] Isoquinoline derivatives are also used as starting materials for the synthesis of other important compounds such as quinoline, and isoquinolone.[284, 285] These compounds have applications in various fields such as medicine, agriculture, and industry. In addition, isoquinoline derivatives have been found to exhibit fluorescent properties, making them useful in the development of fluorescent sensors and probes for bioimaging applications.[286] Overall, isoquinoline derivatives play an important role in various fields and continue to be an area of active research and development. The significance of isoquinoline derivatives in drug discovery and organic synthesis highlights the need for the developing easy and mild techniques to produce this compound.

6.3.2 Results and discussion

Optimization study The present study aimed to synthesize isoquinoline compounds with a sulfur atom incorporated into their structure. To study reaction optimization, the aryne precursor **10** was treated with isoquinoline **20**, followed by sulfur addition. From **entries 1-5** (Table 6.6), CH_3CN and CsF were taken as the solvent and fluoride source. For all these entries, **20** and **10** were stirred at T_1 temperature for 1-3 hours, followed by the addition of elemental sulfur with different molar ratios and stirring at T_2 temperature. From the ^1H and ^{13}C NMR of the crude product (Figure 6.21, Figure 6.22), it was found that the desired product **21** was not formed. Instead, product **22** (Figure 6.20) was obtained due to the presence of a proton source in the acetonitrile solvent. **The reaction mechanism behind the formation of 22 has been explained in our cited reference**. To get desired product, it was decided to switch to an aprotic solvent. In **entries 6-8** THF was used instead of CH_3CN, with KF as the fluoride source and 18-crown-6 as additive. Nevertheless, the desired product was not obtained; instead, we obtained an extremely unstable product that rapidly degraded, making its purification and characterization challenging.

Table 6.6 Optimization of Multi Component Reaction Conditions for Aryne, Sulfur and Isoqunioline

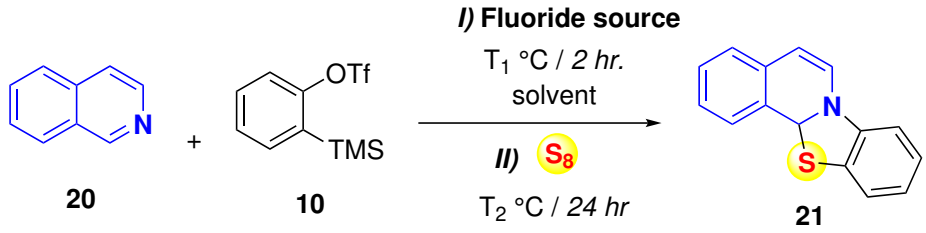

Entry	A.P (10)	Solvent	Fluoride source	T_1 (°C)	S_8	T_2 (°C)
1	1	CH_3CN	CsF(3)	30	2	30
2	1	CH_3CN	CsF(3)	60	2	60
3	1	CH_3CN	CsF(3)	30	1	30
4	1	CH_3CN	CsF(3)	60	1	60
5	1	CH_3CN	CsF(3)	60	3	60
6*	1	THF	KF(3)	30	2	60
7*	1	THF	KF(3)	30	3	60
8*	1	THF	KF(3)	60	3	60
9	1.5	PhCN	CsF(3)	30	3	60
10	1.5	PhCN	CsF(3)	60	3	60
11*	1.5	PhCN	KF(3)	30	3	60

Reaction conditions: * KF is taken with the additive (18-crown-ether).

We subsequently attempted to use benzonitrile as the solvent and increased the amount of aryne precursor from 1 to 1.5 equivalents in **entries 9-11**. Both CsF and KF were explored as fluoride sources. With CsF, the aryne precursor remained unreacted. But, using KF in **entry 11**, we were able to obtain a fluorescent product

(**23**), which was different from our desired product **21**. The complete characterization of compound**23** is discussed below.

6.3.3 Formation of 2-Phenyl-1,2-dihydro-1-isoquinolinyl methylcyanide- (22)

We have observed that alkyl nitriles containing an α hydrogen, which can act as both a proton donor and a nucleophile, react with pyridinebenzyne zwitterions (**10 b**) at both the aryne and pyridine groups. An important point to note is that CH_3CN acted as both a reagent and a solvent in the reaction. Figure 6.20 provides a mechanism that explains the formation of product **22**.

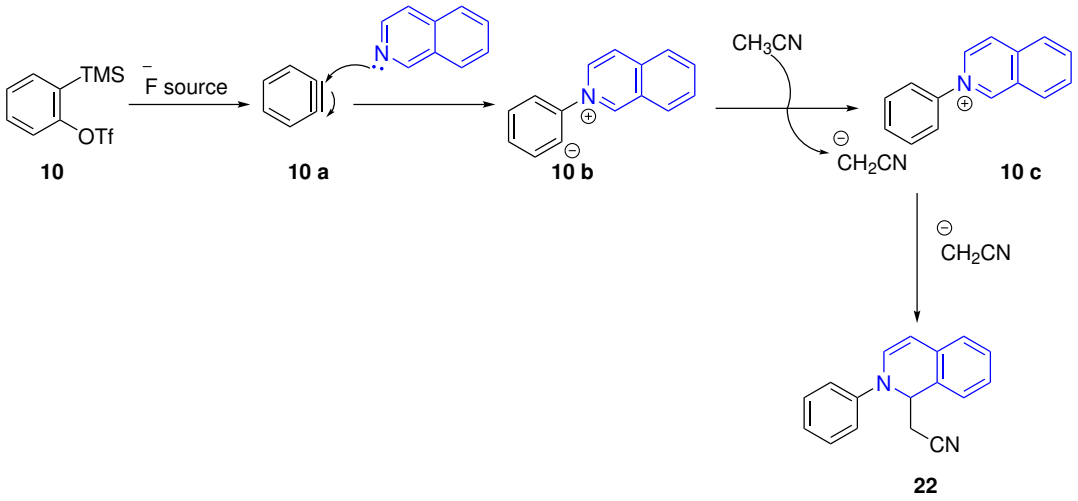

Figure 6.20 Reaction mechanism for formation of **22**.

The reaction involves the nucleophilic addition of isoquinoline to aryne **10 a**, resulting in the formation of zwitterionic species **10 b**. The negative charge on this species extracts a proton from CH_3CN, forming intermediate **10 c** and acetonitrile anion. The acetonitrile anion then undergoes nucleophilic addition to the C=N double bond of isoquinolinium cation **10 c**, ultimately leading to the formation of product (2-Phenyl-1,2-dihydro-1-isoquinolinyl)methyl cyanide (**22**).[287] The product 22 confirmation was confirmed by ^{1}H-NMR, showing two distinct doublet of doublet signals for the CH_2CN moiety at 2.81 and 2.71 of chemical shift (Figure 6.21). The

presence of alkyl chain also confirmed by ^{13}C- NMR, having chemical shift around 21.9 ppm (Figure 6.22).

Characterization data for (2-Phenyl-1,2-dihydro-1-isoquinolinyl)methyl-cyanide : **Appearance** Pale yellow viscous oil; ^{1}H-NMR (500 MHz, $CDCl_3$) δ 7.36 (t, 2H), 7.28 - 7.25 (m, 2H), 7.21(t, 2H). 7.12 (d, 1 H), 7.09(d. 2H), 7.02 (t, 1H), 6.58 (d, 1H), 5.99 (d, 1H), 5.42(t, 1 H), 2.83(dd, 1H), 2.75(dd, 1H). ^{13}C- NMR (500 MHz,$CDCl_3$) δ 144.3, 130.98, 129.7, 128.6, 127.8, 127.6, 126.5, 126.4, 124.0, 122.3, 118.8, 116.5, 105.9, 57.2, 21.9 (Figure 6.21, Figure 6.22).

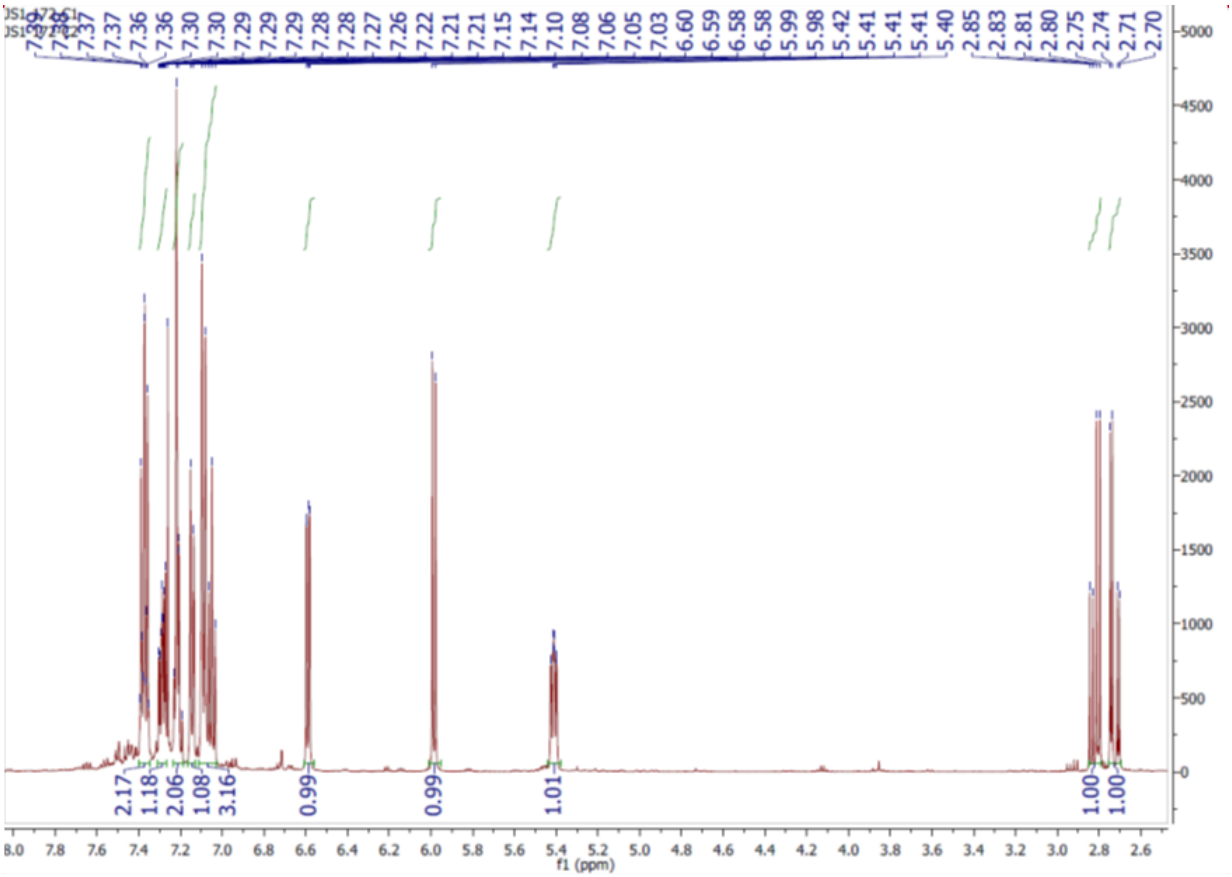

Figure 6.21 Representative ^{1}H–NMR spectra of **22**.

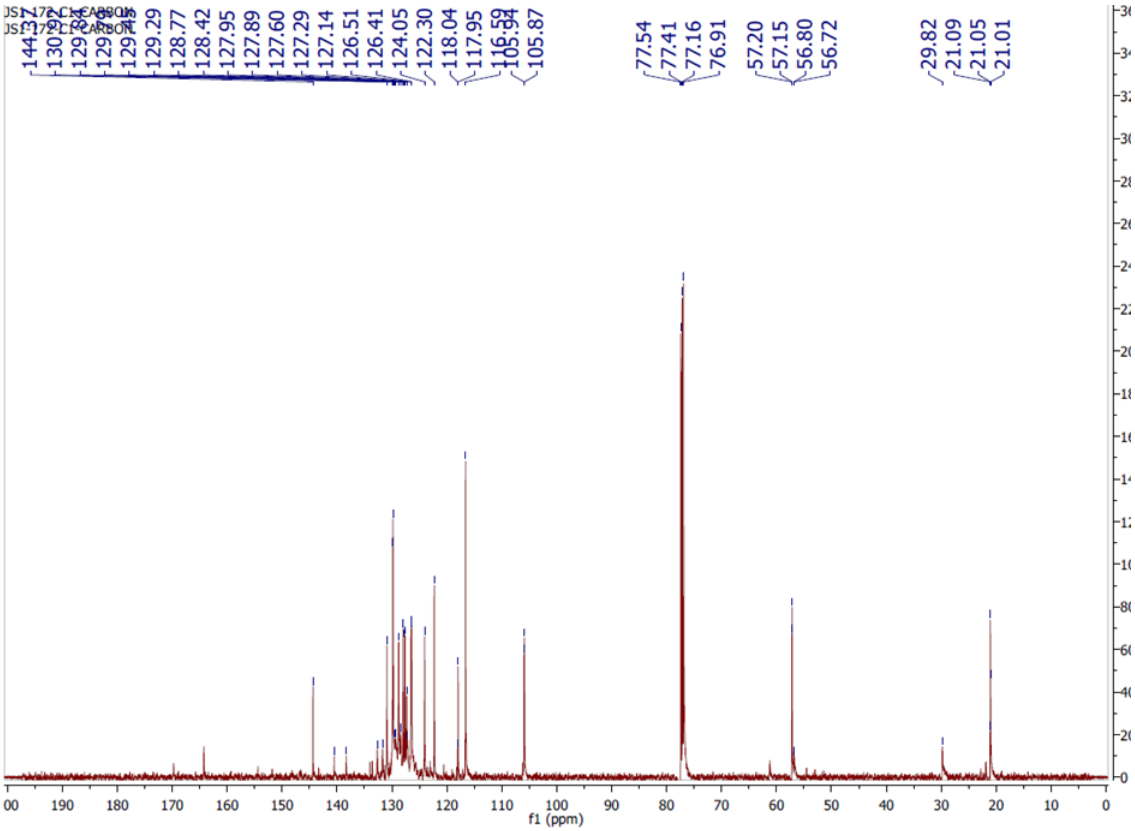

Figure 6.22 Representative ^{13}C–NMR spectra of **22**.

6.3.4 Formation of 23

The desired product **21** has a mass of 237.06 g/mol. Nevertheless, upon conducting mass spectroscopy, we discovered that the molecular ion has a mass of 303.12 (Figure 6.25). In addition, due to its fluorescence nature, we conducted UV analysis which resulted in emission spectra at approximately 400 nm wavelength (Figure 6.26). After conducting an extensive study of previously published papers on isoquinoline derivatives emission spectra, we concluded that one more phenyl ring must be attached to the product skeleton. Based on these observations, we proposed an alternative mechanism (Figure 6.23). The transformation of **21** to **10 f** is difficult part, but similar type of conversion has been reported by Biju group.[274] To confirm the accuracy of our proposed structure, we compared it with proton NMR and found that the number of protons almost matched with the expected product.

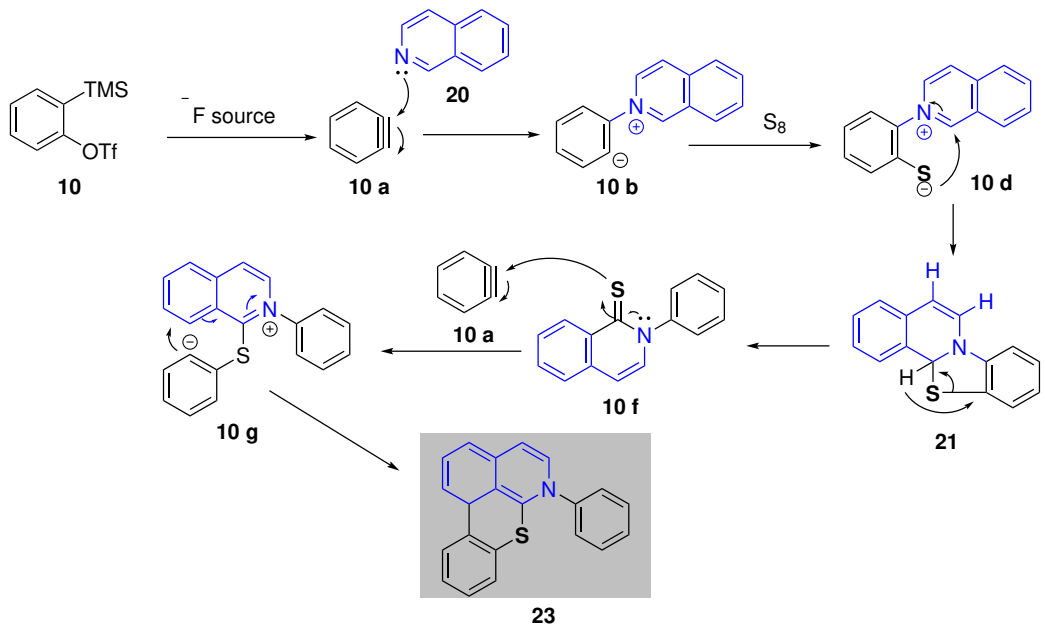

Figure 6.23 Proposed reaction mechanism for formation of **23**.

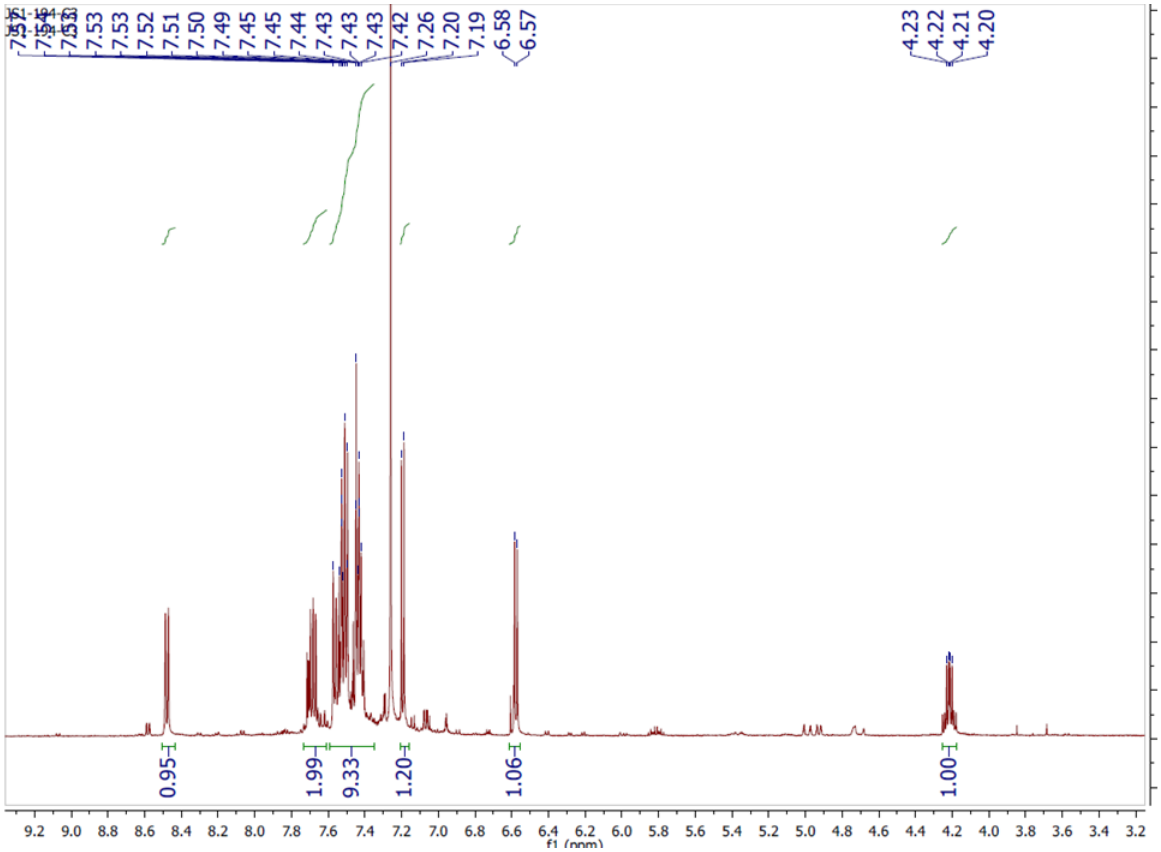

Figure 6.24 Representative ^{1}H–NMR spectra of **23**.

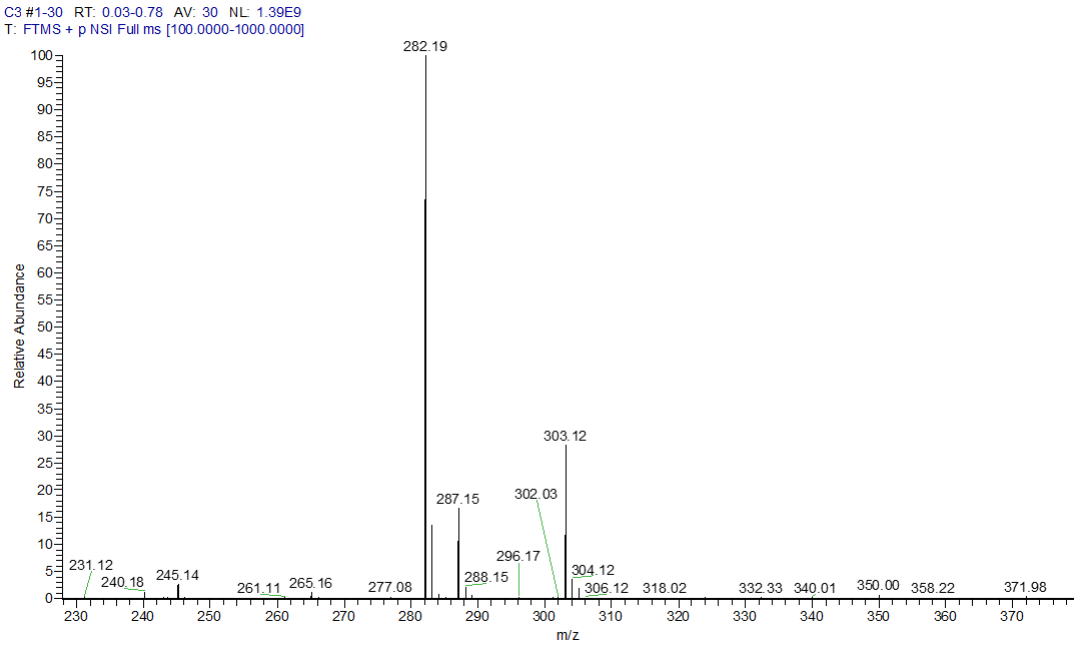

Figure 6.25 Representative mass spectra of **23**.

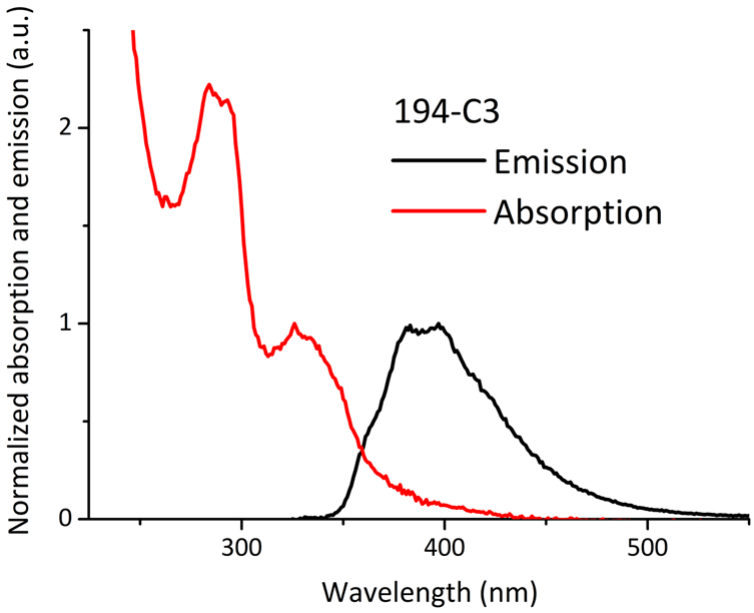

Figure 6.26 Absorption and emission spectra of **23**.

The doublet peak at around 8.47 and 7.20 ppm represents two CH protons associated with a carbon double bond near a nitrogen atom. The multiplate peak at 4.2 ppm represent the hydrogen of sp^3 carbon (Figure 6.24). Nevertheless, the mass

analysis did not exactly match the molar mass of the molecular ion. The calculated molecular weight is 313.09 g/mol, but the mass spectra show a mass of 303.12 g/mol (Figure 6.25). This discrepancy in results indicates a need for further exploration.

6.3.5 Conclusion

In conclusion, we attempted the reaction of isoquinoline, aryne precursor, and elemental sulfur to synthesize an isoquinoline derivative with broad applications in dye chemistry. Our results indicated that using a protonated solvent is not a suitable choice as it interferes with the reaction. Instead, our findings demonstrated that benzonitrile as a solvent and KF with 18-crown-ether are the optimal choices for this synthesis. Additionally, we observed that compound **21** is unstable and cannot be synthesized. Nevertheless, a slightly higher equivalent of aryne precursor compared to isoquinoline can form a fluorescent compound like 23. Further investigation is required because the calculated mass and the mass obtained from mass spectroscopy do not match.

CHAPTER 7

CONCLUSION AND FUTURE WORK

7.1 Conclusions for Computational Study

The mechanism of elemental sulfur and polysulfide with a nucleophile in organic reactions was unknown. To address this issue, a computational approach (DFT) was used. A benchmarking study was conducted to identify the best DFT method, comparing various DFT methods with the gold standard method, DLPNO-CCSD(T). The calculation results revealed that most functionals yielded accurate geometries, except for B97D3. MN15-L and M06-2X performed exceptionally well for transition states. All functionals accurately reproduced energy values. **M06-2X**, **B3LYP-D3(BJ)**, ω**B97X-D**, and **MN15** were recommended for further mechanistic investigations. Using best performing DFT methods, the decomposition pathways of elemental sulfur and polysulfides using cyanide $[\mathbf{NC}]^-$ and triphenyl phosphine $\mathbf{PMe_3}$ nucleophiles was investigated. The calculation result show that the dominance of the **Foss-Bartlett** mechanism over the **Schmidt** mechanism for bimolecular nucleophilic decomposition. We also identified, barrierless intramolecular cyclization for long polysulfides and a mixture of unimolecular and nucleophilic decompositions for shorter ones. Scrambling reactions and the influence of polysulfide substituent were observed. In the **second application** of this benchmarking DFT result, we aimed to explain the reaction mechanism of the Gewald reaction for the formation of 2-aminothiophen. Based on the calculation results, it was concluded that the amine base primarily facilitates deprotonation rather than sulfur ring opening. The Knoevenagel-Cope condensation was identified as the crucial first step, leading to polysulfide formation through the generated anion. We explored various pathways for polysulfide degradation and 2-aminothiophen formation. The dominant

route for $[\mathbf{NuS}_5]^-$ degradation was found to be protonation-induced intermolecular degradation, while polysulfide longer than $[\mathbf{NuS}_5]^-$ decomposition competed with bimolecular decomposition, unimolecular cyclization, and protonation-induced intermolecular degradation. The results also revealed that all the steps involved in the degradation of polysulfide to the formation of monosulfide are in thermal equilibrium. The results also revealed that all the steps involved in the degradation of polysulfide to the formation of monosulfide are in thermal equilibrium. Despite this, the driving force for the formation of 2-aminothiophen from monosulfide is the release of a large amount of reaction energy.

7.2 Conclusion for Experimental Study

The **first objective** of the experimental part was the synthesis of **thiol** from an organoboron precursor using 5-phenyl-1,3,4-oxathiazole-2-one as a source of benzonitrile sulfide, which serves as a nucleophile. Nevertheless, the experimental results from all attempted optimization steps using different boron sources, solvents, and temperature ranges did not yield the desired product. Therefore, we concluded that boron is not effective in bonding with sulfur atoms due to the significant size difference between the two elements. This size difference makes it challenging for them to form stable bonds. The **second objective** was the synthesis of 2-substituted benzothiazole using an imine (method 1) or aryne (method 2) precursor and elemental sulfur as the source of sulfur. For the imine precursor, n-BuLi was utilized to generate ortho-metalated aryl imine, which would serve as a nucleophile for opening the elemental sulfur. But, the experimental results revealed that the butyl chain of n-BuLi attacked the imine N-C carbon, blocking the cyclization pathway for the formation of the desired product. In an attempt to address the issue, the replacement of n-BuLi with different metal sources having bulky alkyl chains or without any alkyl chain, such as Mg-iPrBr.LiCl or Mg (I_2 catalyst), was explored. Even with these

modifications, the desired product was not formed, and the starting reactant remained unconsumed. In **method 2**, Kobayashi's aryne was used with benzonitrile and DIBAL-H. Optimization results under various conditions revealed that ,the desired product was not obtained as the Kobayashi aryne precursor failed to react effectively with the imine anion generated from DIBAL-H. Analysis indicated the presence of the aryne precursor, which may be due to the capture of a fluoride anion by DIBAL, resulting in the inhibition of aryne intermediate generation. In the **last part** of the experimental section, the reaction of Kobayashi aryne precursor, isoquinoline, and elemental sulfur was explored using different fluoride sources and various solvent options. Based on the experimental results, we concluded that protic solvents are not suitable as generated nucelophile in aryne skeleton, capture this proton and being unable to open the elemental sulfur. When using other solvent like KF, the formed product was highly unstable, making its analysis challenging. But, with larger molar ratio of the aryne precursor, a fluorescent product was formed, as confirmed by its emission spectra. Nonetheless, there was a partial mismatch between the mass and ^{1}H-NMR of the desired product, indicating the need for further exploration to determine the exact formed compound.

7.3 Future Study for Computational Work

Until then, elemental sulfur had been explored with carbon and phosphorous nucleophiles. Consequently, there are still a few more nucleophiles, such as **oxygen**, **nitrogen**, and **sulfur**, that need to be investigated. Additionally, the thermal or photolytic decomposition of elemental sulfur, leading to the formation of **sulfur radical** via homolytic cleavage, requires further exploration. The oxygen nucleophile is known to produce the trisulfur radical anion ($S_3^{-\cdot}$), resulting in a blue-colored solution. Understanding why this radical formation is consistently observed with the oxygen nucleophile is crucial. The behavior of the nitrogen nucleophile differs from

other nucleophiles. Nitrogen nucleophiles can include ammonia, primary amines, secondary amines, or tertiary amines. With primary amines, S_3^- generation has been reported, while with secondary and tertiary amines, S_8^{n-} was observed. It is computationally important to understand why different species are observed with different amine sources.

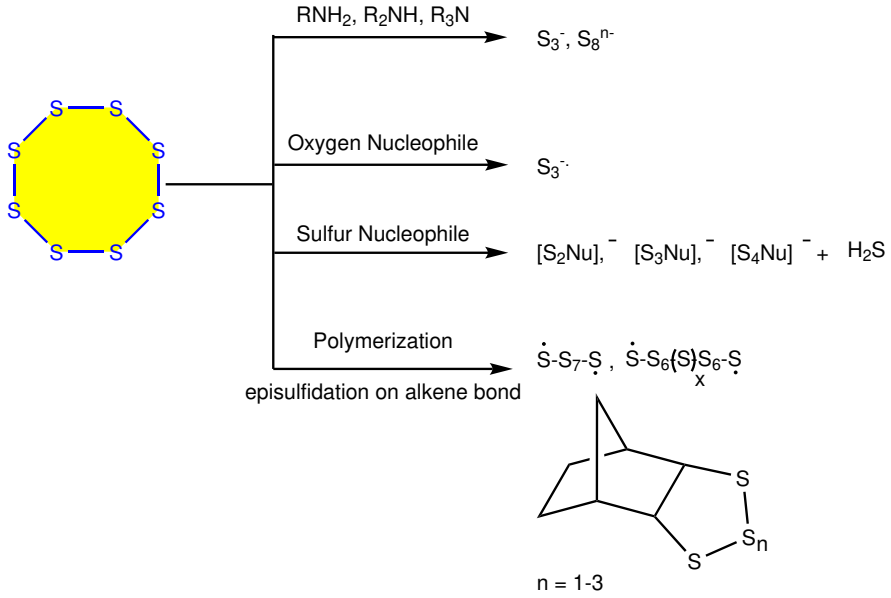

Figure 7.1 Future study for computational work.

The last nucleophile of interest is sulfur. Considering thiols as nucleophiles, it has been reported that disulfide, trisulfide, and tetrasulfide are formed along with H_2S. The dominant generation of disulfides occurs with secondary and primary thiols, while tetrasulfides are favored by tertiary thiols under moderate conditions. Nevertheless, the generation of disulfides was observed with all types of thiols. It is crucial to computationally investigate the formation of these species with different sulfur sources. Along with these nucleophiles, understanding the homolytic cleavage of elemental sulfur is necessary. Through this pathway, polymers containing sulfur have been extensively explored. In addition to large molecules, small molecules like episulfides have been synthesized, which contain a varying number of sulfur atoms in

the skeleton. Determining the factors that favor the formation of these radicals is an interesting question that can be addressed using DFT methods Figure 7.1.

7.4 Future Study for Experimental Work

The reaction of aryne with a nitrogen nucleophile has been well explored. In this study, elemental sulfur has been used as an electrophile partner, and we attempted to open elemental sulfur by generating anion on the aryne skeleton. But, it is still a question whether this anion can open elemental sulfur. Since the reaction of elemental sulfur with a nitrogen nucleophile has been well stabilized. Based on all the experimental results, it would be a nice idea to first open elemental sulfur using a nitrogen nucleophile (imine as the nitrogen source), which will generate a sulfide anion. This sulfide will act as a source of nucleophile and attack the aryne precursor, generating an anion on the aryne precursor that will subsequently attack the imine carbon, followed by ring cyclization (Figure 7.2).

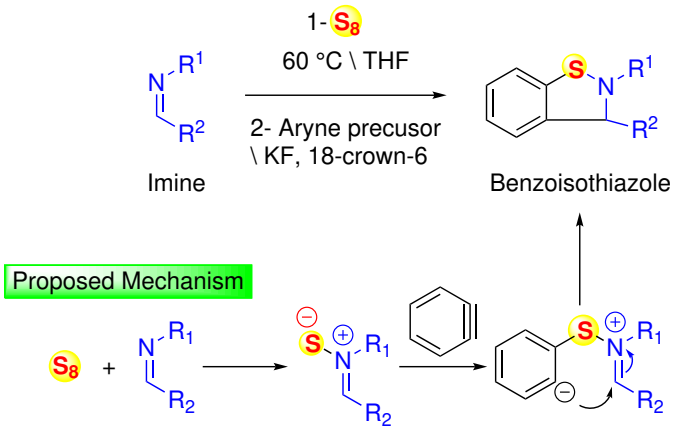

Figure 7.2 Future study for experimental work.

APPENDIX

COMPUTATIONAL INVESTIGATIONS ON THE MECHANISM OF THE GEWALD REACTION

In the appendix section, full computation details, and associated TS and GS structures with their corresponding energy have been shown.

A.1 Full Computational details

Density functional theory calculations (DFT) were performed using Gaussian 16.[288] ωB97X-D method with the aug-cc-pVDZ basis set was utilized for geometry optimization calculations. Solvation effects were considered using the SMD implicit solvation model for ethanol. Gaussian 16 uses an ultrafine pruned (99,590) grid by default for numerical integrations of density in DFT, which effectively eliminates most orientation-specific issues.[289] Frequency calculations were performed during the optimization process to validate the nature of stationary points and obtain corrections for zero-point energy, enthalpy, and free energy. Goodvibes v2.0.3 was used to obtain these corrections,[290] applying Grimme's scheme for small frequencies. To visually represent the computed structures, CYLview was utilized for generating visualizations.[291]

A.2 Carbon Nucleophiles

To explore carbon nucleophiles for elemental sulfur rings opening, a variety of carbon-based nucleophiles have been chosen (Figure 1). The polysulfide decomposition of all nucleophiles was also investigated using DFT calculations, considering bimolecular decomposition by the nucleophile and unimolecular cyclization at $\mathbf{S}^2$. In Table 1, the opening of S_8 by all considered nucleophiles, along with the associated free energy, and their corresponding transition state (TS) structures, has been shown.

Based on the calculation results for sulfur opening, the reaction with $\mathbf{Nu}_2$ showed the least reaction energy. Although we were unable to locate the transition state (TS), the reaction energy results indicate that it should have the lowest activation energy. This observation aligns with the trends in deprotonation energy, as the reaction with Nu_2 exhibited the highest deprotonation energy, indicating a higher pKa value, that makes it strongest nuceophile. Nevertheless, this observation deviates from the common trend observed for other nucleophiles, which can be attributed to other factors, such as the nature of the group attached to the carbon anion center. The obtained octa-polysulfide for all the nucleophile has been shown in Figure 2. Bimolecular decomposition and unimolecular cyclization on $\mathbf{S}^2$ are shown in **Table 2** and **3**, respectively. For bimolecular decomposition, the least activation barrier (14.4 kcal/mol) was observed for $\mathbf{Nu}_2$ due to its strong nucleophilic nature. In contrast, for unimolecular cyclization, the least barrier was observed for $\mathbf{Nu}_7$ (9.3 kcal/mol). It is important to perform NBO analysis to understand the complete calculation investigation associated with the bimolecular and unimolecular paths.

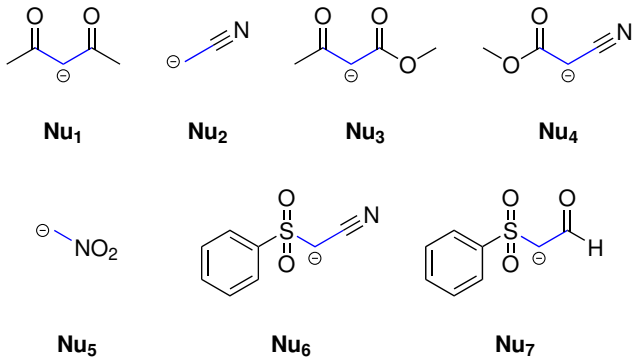

Figure 1 Various considered carbon nucleophiles.

Table 1 Cyclo Octasulfur (S_8) Opening by Considered Nucleophiles with Transition State Structures. Free Energy in kcal/mol

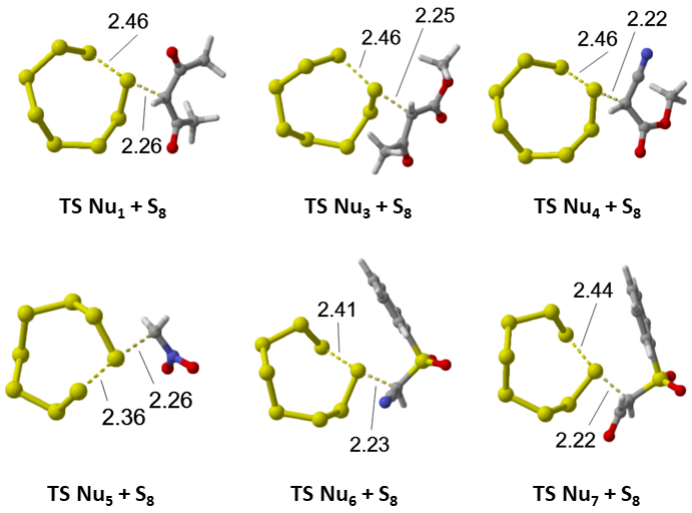

Nucleophile	Deprotonation energy	$\Delta G^{\ddagger}$	ΔG_{rex}
Nu_1	13.5	21.1	5.9
Nu_2	31.1	n.l.	-17.8
Nu_3	11.9	22.2	4.7
Nu_4	10.7	21.6	11.4
Nu_5	19.0	18.7	3.3
Nu_6	9.2	19.0	10.2
Nu_7	12.1	24.4	12.3

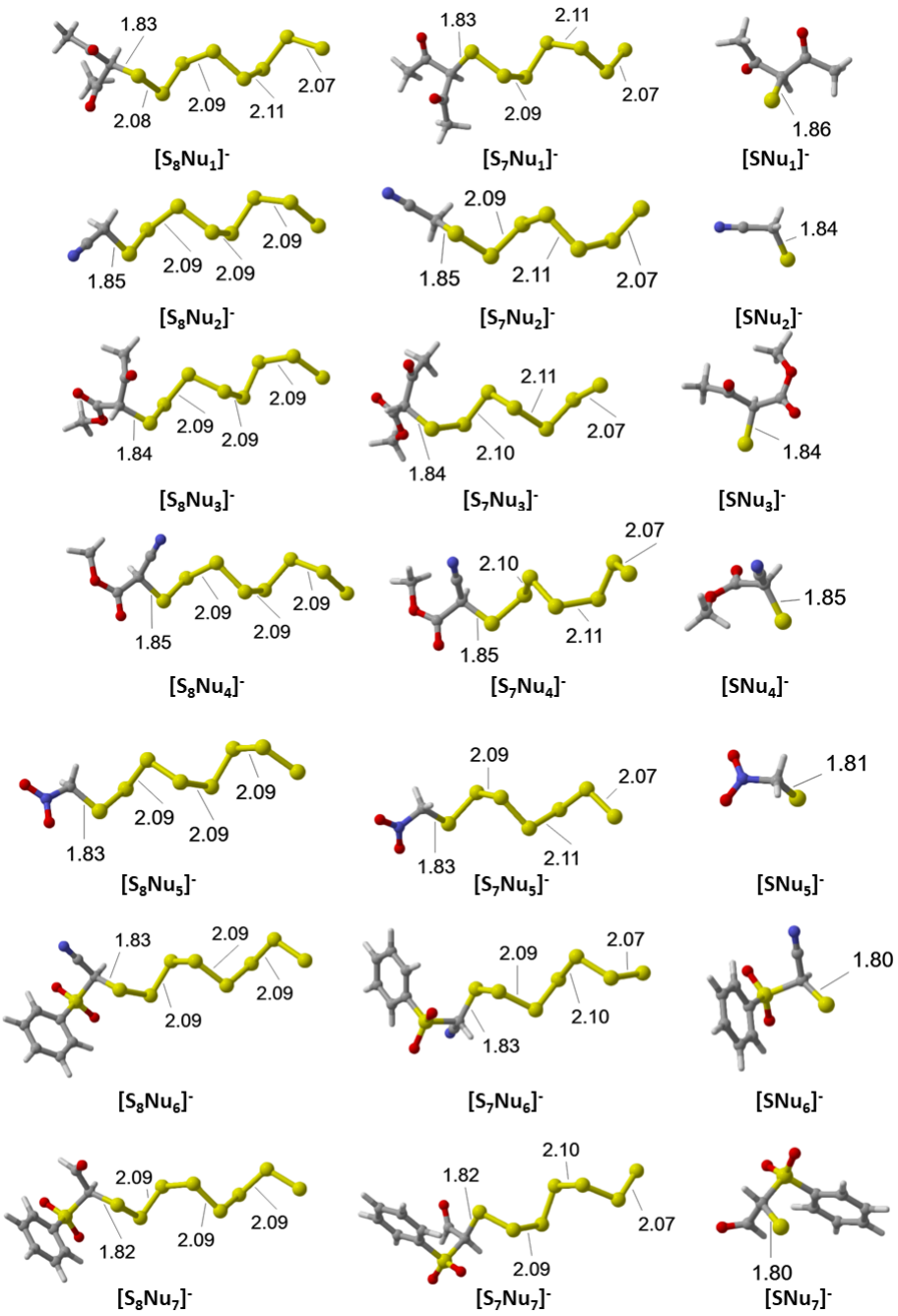

Figure 2 All structures of computed polysulfides with consider nucleophiles.

Table 2 The Bimolecular Decomposition of Poly(octasulfide) by Considered Nucleophile on S^2 with Transition State Structures. Free Energy in kcal/mol

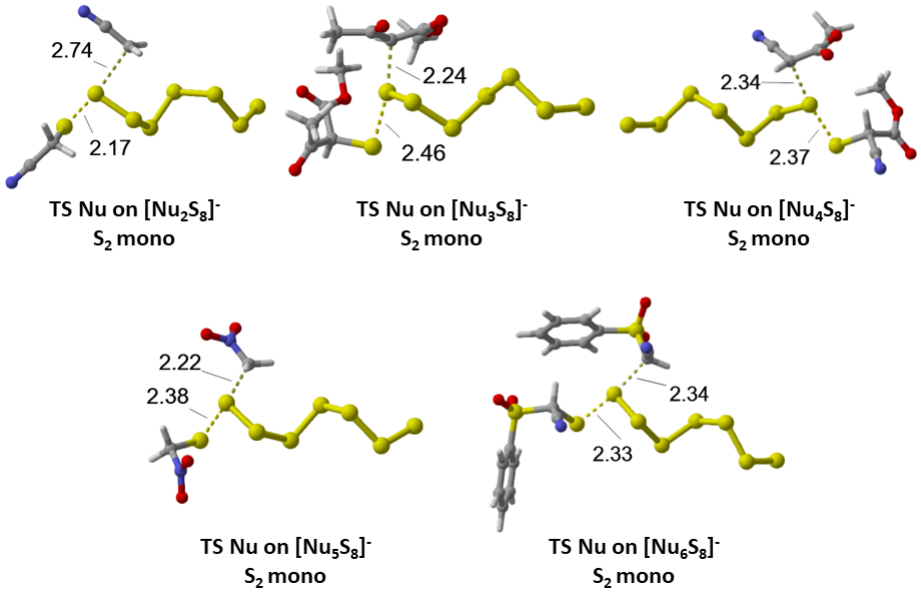

Octa-(polysulfide)	$\Delta G^{\ddagger}$	ΔG_{rex}
$Nu_1S_8^-$	n.l.	-0.4
$Nu_2S_8^-$	12.3	-22.8
$Nu_3S_8^-$	26.7	1.5
$Nu_4S_8^-$	20.4	-0.7
$Nu_5S_8^-$	19.5	-6.8
$Nu_6S_8^-$	16.5	-7.8
$Nu_7S_8^-$	n.l.	-3.7

Table 3 The Unimolecular Cyclization of Poly(octasulfide) on S^2 with Transition State Structures. Free Energy in kcal/mol

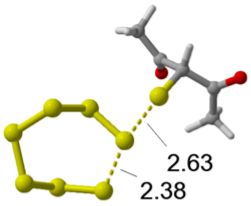

TS Unimolecular
$[Nu_1S_8]^-$

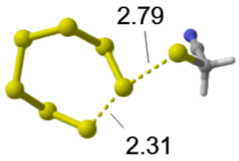

TS Unimolecular
$[Nu_2S_8]^-$

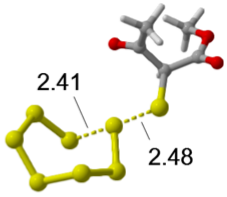

TS Unimolecular
$[Nu_3S_8]^-$

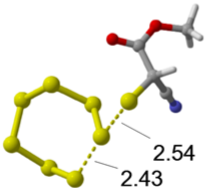

TS Unimolecular
$[Nu_4S_8]^-$

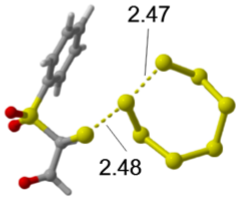

TS Unimolecular
$[Nu_7S_8]^-$

Octa-(polysulfide)	$\Delta G^{\ddagger}$	ΔG_{rex}
$Nu_1S_8^-$	13.9	1.1
$Nu_2S_8^-$	13.3	2.0
$Nu_3S_8^-$	18.0	4.1
$Nu_4S_8^-$	12.0	-4.8
$Nu_5S_8^-$	n.l.	-3.1
$Nu_6S_8^-$	n.l.	-11.0
$Nu_7S_8^-$	6.4	-9.2

A.3 Associated Polysulfide Structures with 4a.

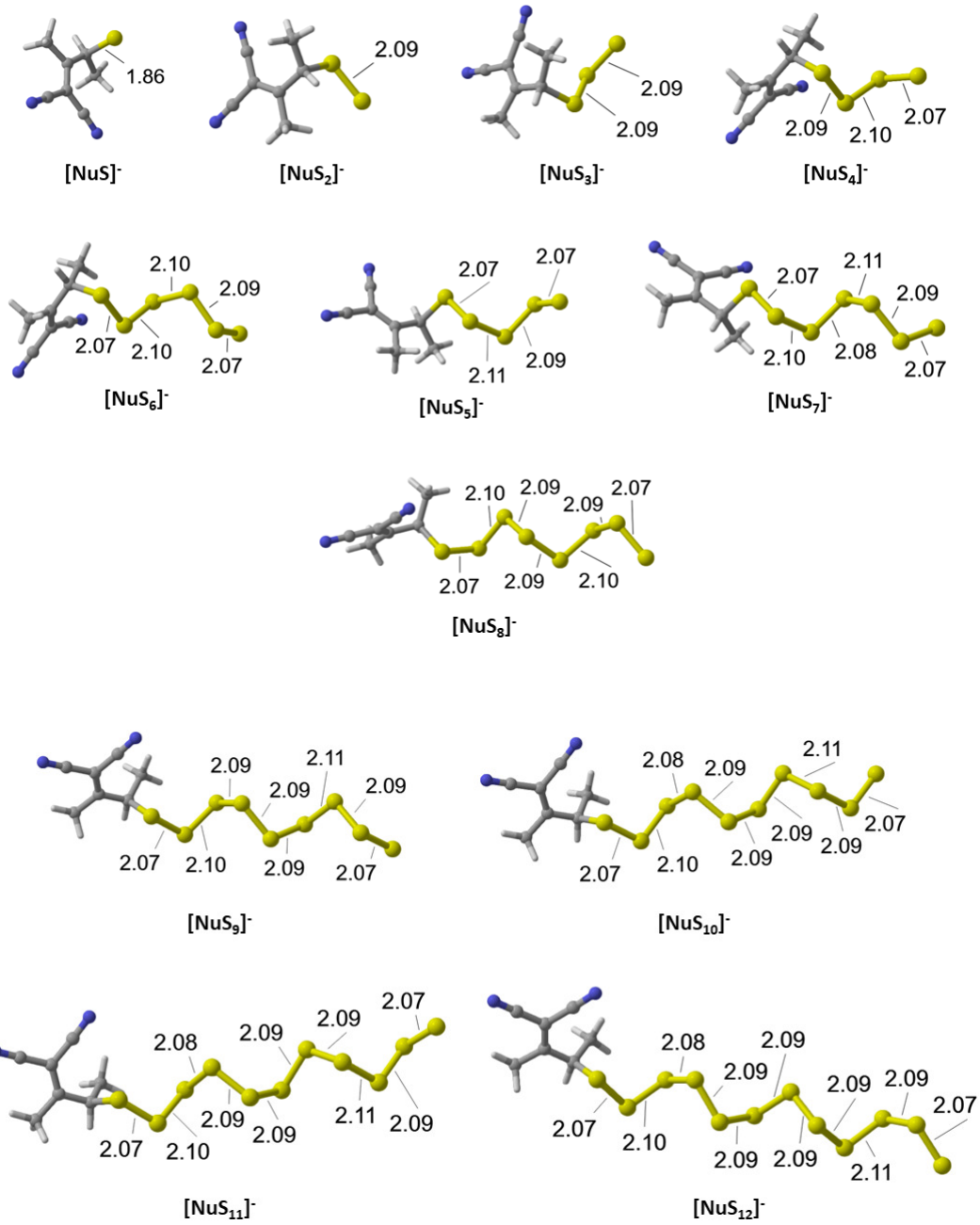

Figure 3 All structures of computed polysulfides.

Table 4 NBO energies and coefficients on FMOs of NuS_n^-

Polysulfide	Orbital	Energy (hartrees)	Coefficients
$[NuS_8]^-$	HOMO (nS_8)	-0.13103	
	LUMO (σ^*_{S3-S4})	0.14466	47.92% S3
			52.08% S4
	LUMO-2 (σ^*_{S2-S3})	0.16158	49.27% S2
			50.73% S3
$[NuS_7]^-$	HOMO (nS_7)	-0.19537	
	LUMO (σ^*_{S3-S4})	0.15813	47.34% S3
			52.66% S4
$[NuS_6]^-$	HOMO (nS_6)	-0.12896	
	LUMO (σ^*_{S2-S3})	0.17737	46.48% S2
			53.52% S3
$[NuS_5]^-$	HOMO (nS_5)	-0.13436	
	LUMO (σ^*_{S2-S3})	0.17519	45.75% S2
			54.25% S3
$[NuS_4]^-$	HOMO (nS_4)	-0.12702	
	LUMO (σ^*_{S1-S2})	0.20581	46.79% S1
			53.21% S2
$[NuS_3]^-$	HOMO (nS_3)	-0.12751	
	LUMO (σ^*_{S1-S2})	0.22983	45.62% S1
			54.38% S2
$[NuS_2]^-$	HOMO (nS_2)	-0.12955	
	LUMO (σ^*_{S1-S2})	0.28516	42.24% S1
			57.76% S2

A.4 HS_nNu Analogue Structures

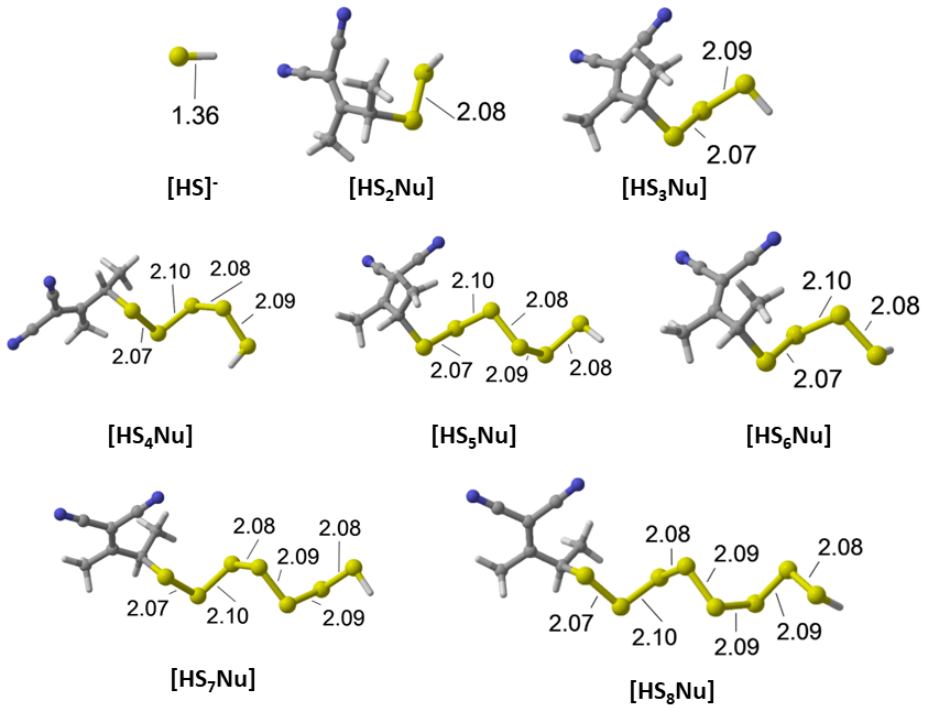

Figure 4 All structures of computed HS_nNu analogues.

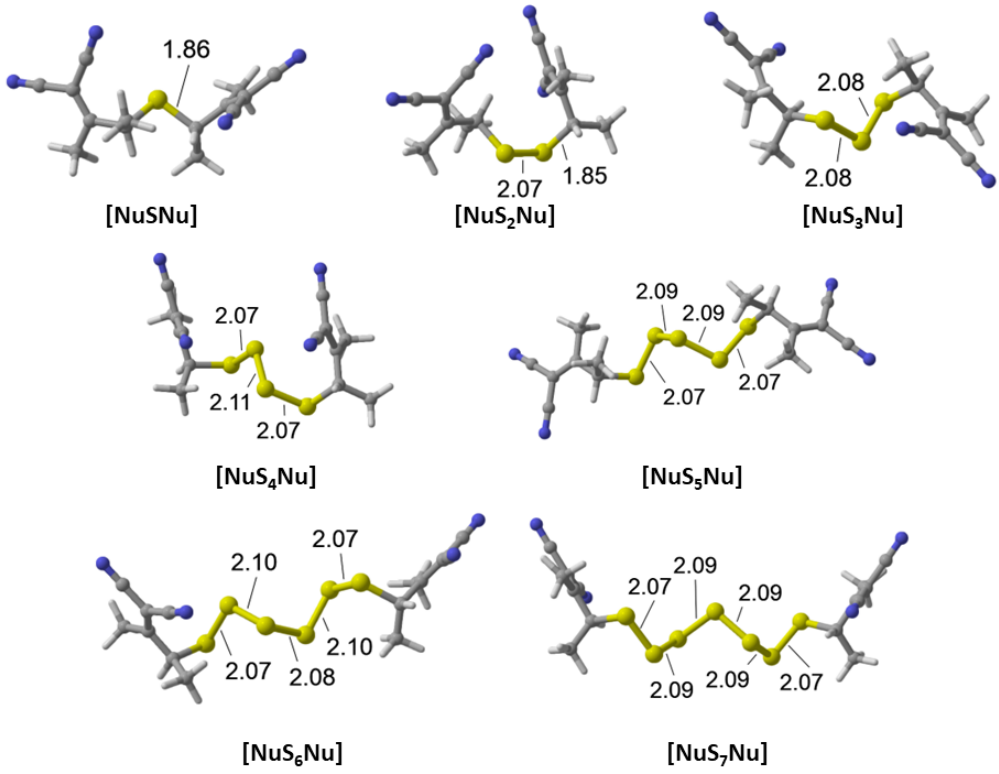

Figure 5 All computed structures of disubstituted polysulfides.

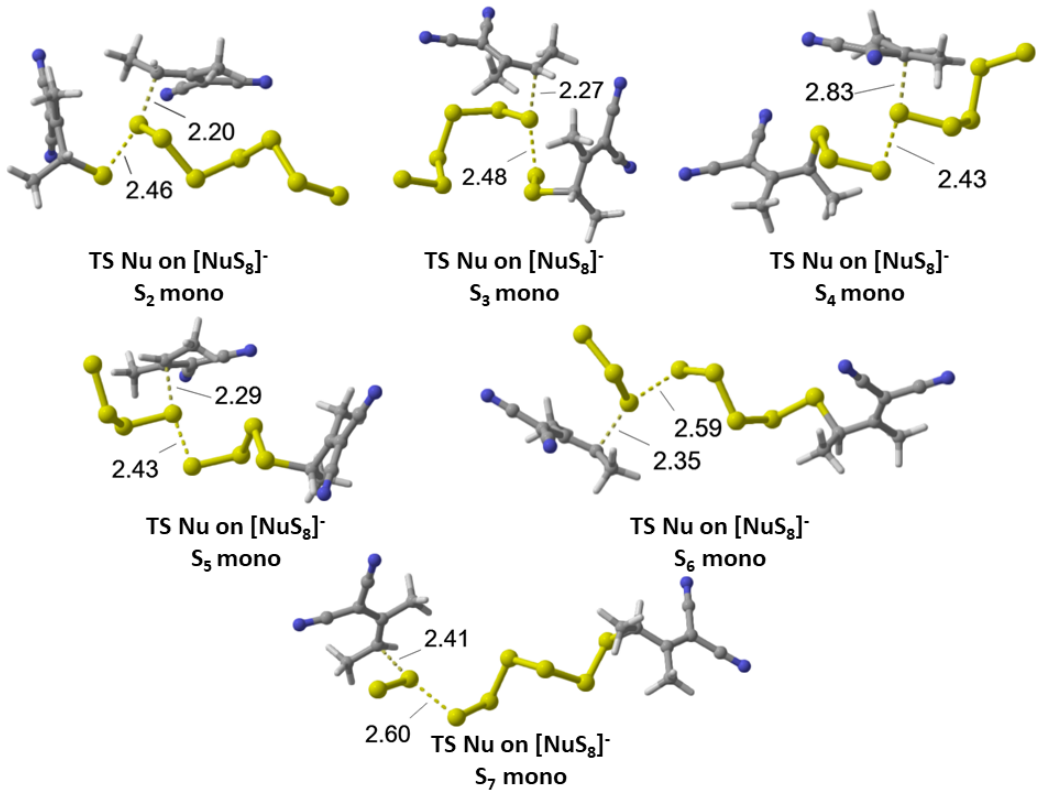

Figure 6 TSs for the monosubstituted pathways for Nucleophile**(4a)**.

A.5 Intermolecular Decomposition on S^2 by 4a

Table 5 The Intermolecular Decomposition of Poly(octasulfide) on S^2. Free Energy in kcal/mol

Polysulfide	$\Delta G^{\ddagger}$	ΔG_{rex}
NuS_8^-	29.1	-2.2
NuS_7^-	29.0	-3.1
NuS_6^-	32.2	-4.1
NuS_5^-	31.5	-0.3
NuS_4^-	31.1	-0.8
NuS_3^-	35.6	-0.5
NuS_2^-	35.8	-2.3

The intermolecular decomposition on S^2 by **4a** has not been discussed in the main text due to the high activation barrier associated with all the steps (see Table 5).

Based on the calculation results, it has been observed that as the chain length of polysulfide decreases, the activation barrier increases (e.g., for $[NuS_2]^-$ = 35.8 kcal/mol). This increase in activation barrier can be attributed to the dominance of steric and repulsive forces as the chain length becomes shorter.

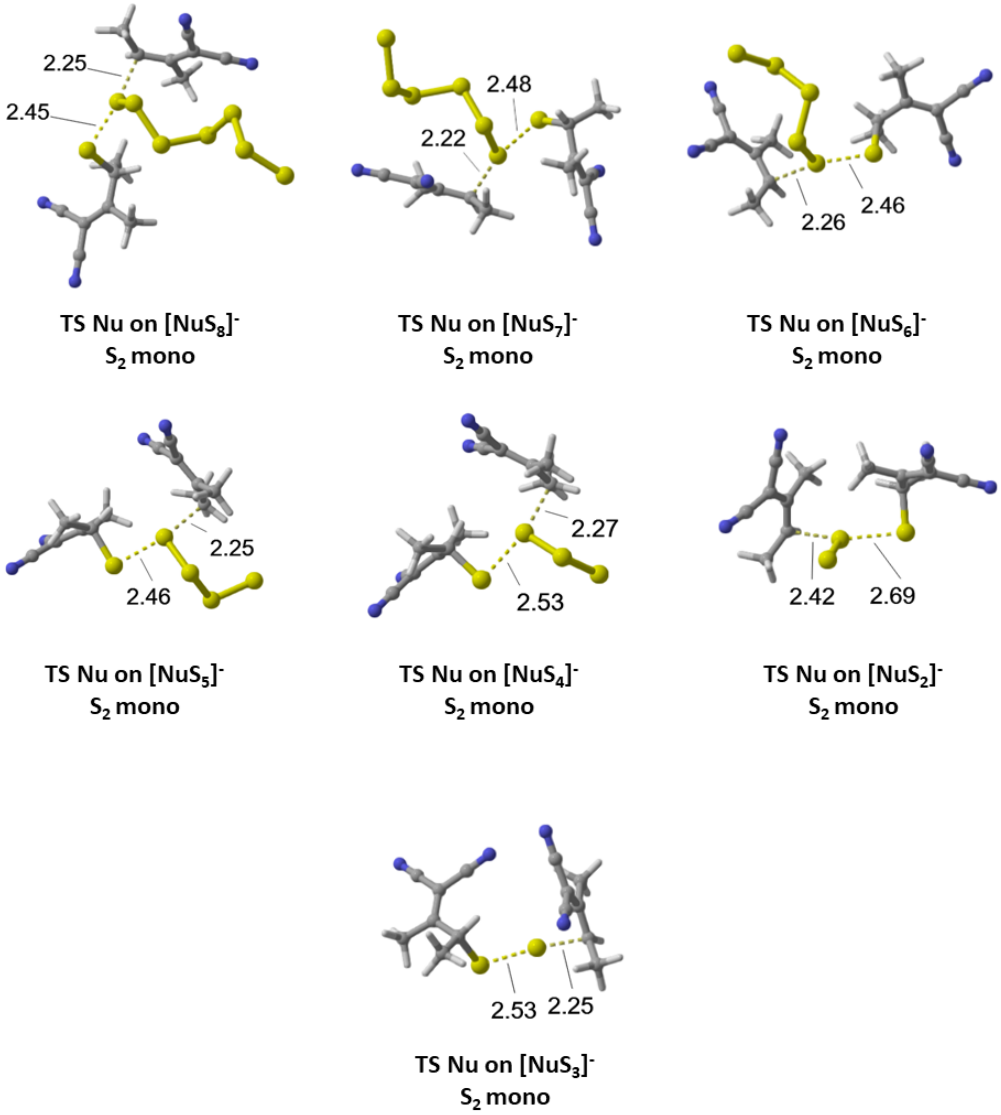

Figure 7 Transition state structures of intermolecular decomposition of polysulfide.

A.6 Ring Opening by 4a

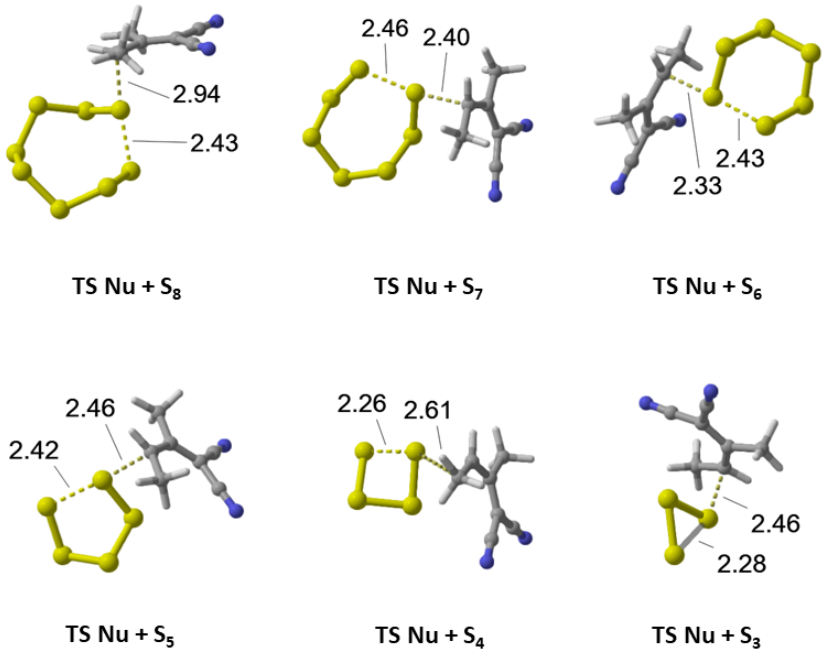

Figure 8 Transition state structures of cyclic allotropes ring opening by nucleophile **(4a)**.

A.7 Dianion and substituted Polysulfide formation by 4a

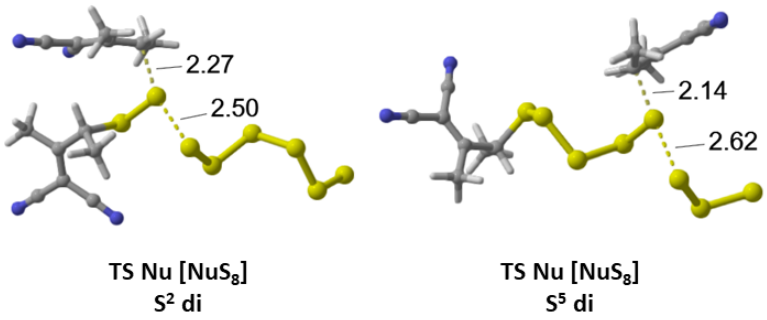

Figure 9 TSs for the disubstituted pathways for nucleophile **(4a)**.

A.8 Protonation-induced Intermolecular Degradation of Polysulfides

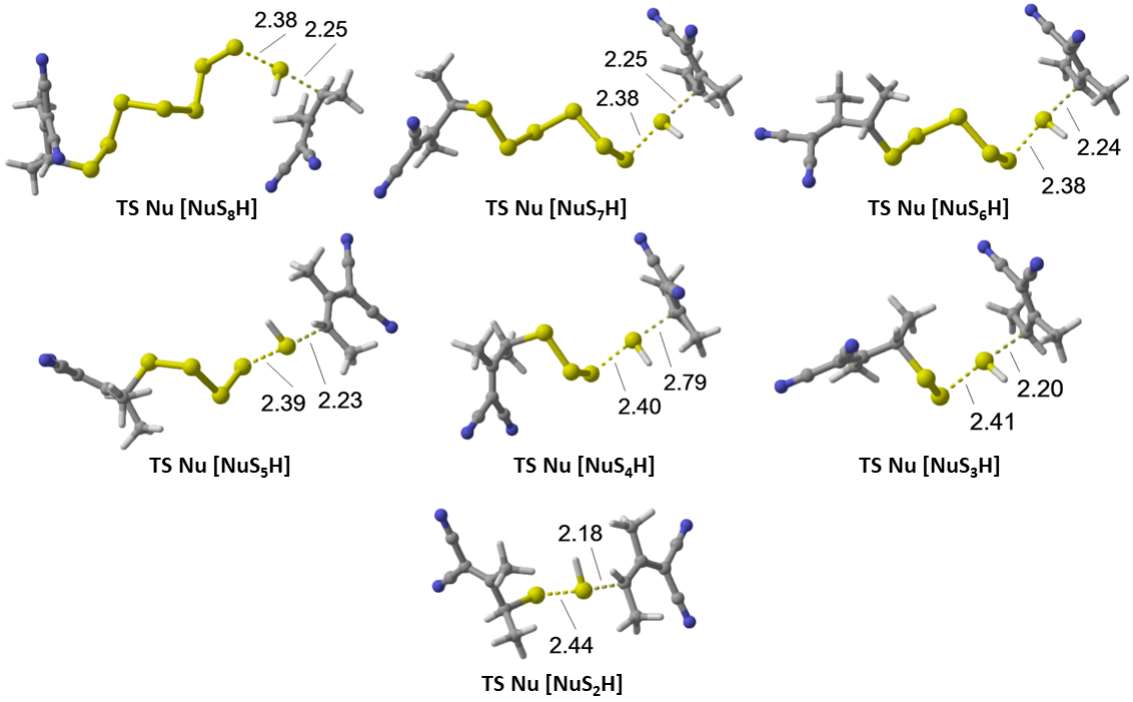

Figure 10 Transition state structures of Protonation-Induced Intermolecular degradation of Polysulfides on S^7 by nucleophile **(4a)**.

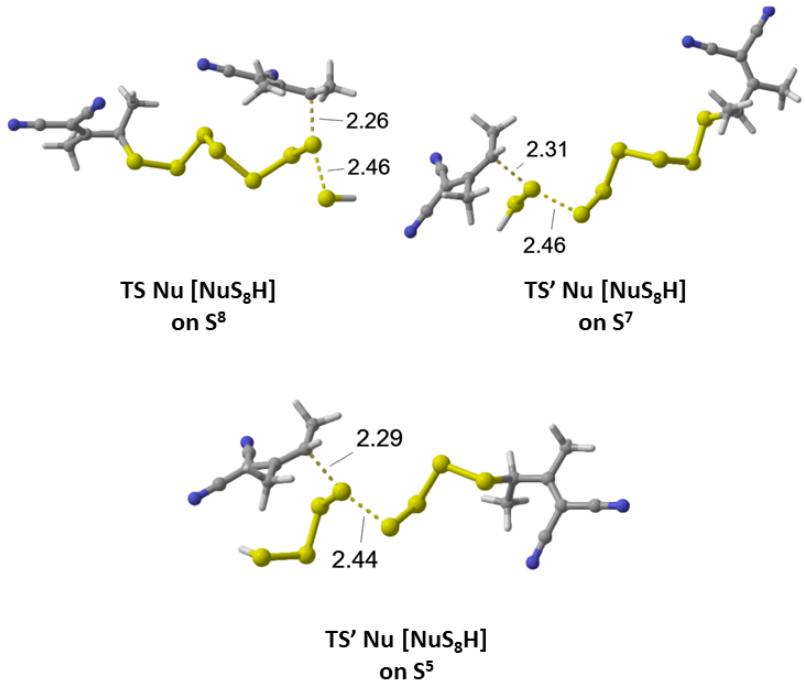

Figure 11 Transition state structures of Protonation-Induced Intermolecular degradation of Polysulfides on S^7, S^5 by nucleophile **(4a)**.

REFERENCES

[1] Max Schmidt. "Elemental sulfur—A challenge to theory and practice". In: *Angewandte Chemie International Edition in English* 12.6 (1973), pp. 445–455.

[2] Ralf Steudel. "Liquid sulfur". In: *Elemental sulfur and sulfur-rich compounds I* (2003), pp. 81–116.

[3] Ralf Steudel. "Properties of sulfur-sulfur bonds". In: *Angewandte Chemie International Edition in English* 14.10 (1975), pp. 655–664.

[4] Ralf Steudel and Bodo Eckert. "Solid sulfur allotropes". In: *Elemental sulfur and sulfur-rich compounds I* (2003), pp. 1–80.

[5] Beat Meyer. "Preparation and properties of sulfur allotropes". In: *Elemental Sulfur* (1965), pp. 71–94.

[6] WL Bragg and JJ Thomson. "Mr Bragg, Diffraction of short electromagnetic waves, etc. 43". In: *Proceedings of the Cambridge Philosophical Society: Mathematical and physical sciences*. Vol. 17. Cambridge Philosophical Society. 1914, p. 43.

[7] BE Warren and JT Burwell. "The structure of rhombic sulphur". In: *The Journal of Chemical Physics* 3.1 (1935), pp. 6–8.

[8] Sidney Cyril Abrahams. "The crystal and molecular structure of orthorhombic sulfur". In: *Acta Crystallographica* 8.11 (1955), pp. 661–671.

[9] Steven J. Rettig and James Trotter. "Refinement of the structure of orthorhombic sulfur, α-S8". In: *Acta Crystallographica Section C: Crystal Structure Communications* 43.12 (1987), pp. 2260–2262.

[10] Richard E Powell and Henry Eyring. "The properties of liquid sulfur". In: *Journal of the American Chemical Society* 65.4 (1943), pp. 648–654.

[11] Sidney Cyril Abrahams. "The crystal structure of barium tetrasulfide monohydrate". In: *Acta Crystallographica* 7.5 (1954), pp. 423–429.

[12] Kenneth Y Chen and J Carrell Morris. "Kinetics of oxidation of aqueous sulfide by oxygen". In: *Environmental Science and Technology* 6.6 (1972), pp. 529–537.

[13] Michael R Hoffmann. "Kinetics and mechanism of oxidation of hydrogen sulfide by hydrogen peroxide in acidic solution". In: *Environmental Science and Technology* 11.1 (1977), pp. 61–66.

[14] MA Vairavmurthy and Weiqing Zhou. *Characterization of a transient+ 2 sulfur oxidation state intermediate from the oxidation of aqueous sulfide*. Tech. rep. Brookhaven National Lab.(BNL), Upton, NY (United States), 1995.

[15] George W Luther III. "Pyrite synthesis via polysulfide compounds". In: *Geochimica et Cosmochimica Acta* 55.10 (1991), pp. 2839–2849.

[16] MEL Kohnen, JS Sinninghe Damsté, HL Ten Haven, and JW De Leeuw. "Early incorporation of polysulphides in sedimentary organic matter". In: *Nature* 341.6243 (1989), pp. 640–641.

[17] A Vairavamurthy, B Manowitz, GW Luther Iii, and Y Jeon. "Oxidation state of sulfur in thiosulfate and implications for anaerobic energy metabolism". In: *Geochimica et Cosmochimica Acta* 57.7 (1993), pp. 1619–1623.

[18] Janet W Terry. "The Alberta sulphur industry". In: *Journal of Canadian Petroleum Technology* 23.05 (1984).

[19] JE Halfyard and K Hawboldt. "Separation of elemental sulfur from hydrometallurgical residue: A review". In: *Hydrometallurgy* 109.1-2 (2011), pp. 80–89.

[20] Quan Shi and Jianxun Wu. "Review on sulfur compounds in petroleum and its products: state-of-the-art and perspectives". In: *Energy and Fuels* 35.18 (2021), pp. 14445–14461.

[21] John S Eow. "Recovery of sulfur from sour acid gas: A review of the technology". In: *Environmental Progress* 21.3 (2002), pp. 143–162.

[22] USGS Mineral Commodity Summaries and USGS Unnumbered Series. *US geological survey: Reston, VA, USA, 2019*. 2019.

[23] Francesco Crescenzi, Antonella Crisari, Edoardo D'Angel, and Alessandro Nardella. "Control of acidity development on solid sulfur due to bacterial action". In: *Environmental Science and Technology* 40.21 (2006), pp. 6782–6786.

[24] JL Havlin, JD Beaton, SL Tisdale, and WL Nelson. "An introduction to nutrient management". In: *Soil Fertility and Fertilizers, 6th ed.; Prentice Hall: Upper Saddle River, NJ, USA* (1999), p. 499.

[25] Kevin A Scott and Jon T Njardarson. "Analysis of US FDA-approved drugs containing sulfur atoms". In: *Sulfur Chemistry* (2019), pp. 1–34.

[26] Elizabeth A Ilardi, Edon Vitaku, and Jon T Njardarson. "Data-mining for sulfur and fluorine: An evaluation of pharmaceuticals to reveal opportunities for drug design and discovery: Miniperspective". In: *Journal of Medicinal Chemistry* 57.7 (2014), pp. 2832–2842.

[27] Leonard Gianessi and Nathan Reigner. "Pesticide use in US crop production: 2002". In: *Crop Protection Research Institute: Washington, DC, USA* (2006).

[28] Wei Guo and Yongzhu Fu. "A perspective on energy densities of rechargeable Li-S batteries and alternative sulfur-based cathode materials". In: *Energy and Environmental Materials* 1.1 (2018), pp. 20–27.

[29] Chen-Xi Bi, Li-Peng Hou, Zheng Li, Meng Zhao, Xue-Qiang Zhang, Bo-Quan Li, Qiang Zhang, and Jia-Qi Huang. "Protecting lithium metal anodes in lithium–sulfur batteries: A review". In: *Energy Material Advances* 4 (2023), p. 0010.

[30] James Sudworth and AR Tiley. *Sodium sulphur battery*. Springer Science and Business Media, 1985.

[31] Thanh Binh Nguyen. "Recent advances in organic reactions involving elemental sulfur". In: *Advanced Synthesis and Catalysis* 359.7 (2017), pp. 1066–1130.

[32] Thanh Binh Nguyen. "Recent advances in the synthesis of heterocycles via reactions involving elemental sulfur". In: *Advanced Synthesis and Catalysis* 362.17 (2020), pp. 3448–3484.

[33] Viacheslav Petrov, Rebecca J Dooley, Alexander A Marchione, Elizabeth L Diaz, and Brittany S Clem. "Simple protocol for preparation of Diels-Alder adducts of perfluorinated thioketones". In: *Journal of Fluorine Chemistry* 225 (2019), pp. 1–10.

[34] Norio Sakai, Shuhei Horikawa, and Yohei Ogiwara. "Indium-catalyzed direct conversion of lactones into thiolactones and selenolactones in the presence of elemental sulfur and selenium". In: *Synthesis* 50.03 (2018), pp. 565–574.

[35] Lidiya G Fedenok, Kirill Yu Fedotov, Elena A Pritchina, and Nikolaj E Polyakov. "In situ generated reagent from sulfur for alkynylanthraquinone cyclization. The simple synthesis of angular thienoanthraquinones". In: *Tetrahedron Letters* 57.11 (2016), pp. 1273–1276.

[36] Saiwen Liu, Guo-Jun Deng, and Huawen Huang. "Recent advances in sulfur-containing heterocycle formation via direct C–H sulfuration with elemental Sulfur". In: *Synlett* 32.02 (2021), pp. 142–158.

[37] Joseph C Bear, William J Peveler, Paul D McNaughter, Ivan P Parkin, Paul O'Brien, and Charles W Dunnill. "Nanoparticle–sulphur "inverse vulcanisation" polymer composites". In: *Chemical Communications* 51.52 (2015), pp. 10467–10470.

[38] Sergej Diez, Alexander Hoefling, Patrick Theato, and Werner Pauer. "Mechanical and electrical properties of sulfur-containing polymeric materials prepared via inverse vulcanization". In: *Polymers* 9.2 (2017), p. 59.

[39] Jinhong Jia, Jingjiang Liu, Zhi-Qiang Wang, Tao Liu, Peiyao Yan, Xue-Qing Gong, Chengxi Zhao, Linjiang Chen, Congcong Miao, Wei Zhao, et al. "Photoinduced inverse vulcanization". In: *Nature Chemistry* (2022), pp. 1–9.

[40] Michael P Crockett, Austin M Evans, Max JH Worthington, Inês S Albuquerque, Ashley D Slattery, Christopher T Gibson, Jonathan A Campbell, David A Lewis, Gonçalo JL Bernardes, and Justin M Chalker. "Sulfur-limonene polysulfide: A material synthesized entirely from industrial by-products and its use in removing toxic metals from water and soil". In: *Angewandte Chemie International Edition* 55.5 (2016), pp. 1714–1718.

[41] Takayoshi Hashimoto, Yasuhiro Ohki, and Kazuyuki Tatsumi. "Synthesis of coordinatively unsaturated mesityliron thiolate complexes and their reactions with elemental sulfur". In: *Inorganic Chemistry* 49.13 (2010), pp. 6102–6109.

[42] Thanh Binh Nguyen, Julie Le Bescont, Ludmila Ermolenko, and Ali Al-Mourabit. "Cobalt-and iron-catalyzed redox condensation of o-substituted nitrobenzenes with alkylamines: a step-and redox-economical synthesis of diazaheterocycles". In: *Organic Letters* 15.24 (2013), pp. 6218–6221.

[43] Fumitoshi Shibahara, Rie Sugiura, Eiji Yamaguchi, Asumi Kitagawa, and Toshiaki Murai. "Synthesis of fluorescent 1, 3-diarylated imidazo [1, 5-a] pyridines: oxidative condensation- cyclization of aryl-2-pyridylmethylamines and aldehydes with elemental sulfur as an oxidant". In: *The Journal of Organic Chemistry* 74.9 (2009), pp. 3566–3568.

[44] Thanh Binh Nguyen, Ludmila Ermolenko, William A Dean, and Ali Al-Mourabit. "Benzazoles from aliphatic amines and o-amino/mercaptan/hydroxyanilines: elemental sulfur as a highly efficient and traceless oxidizing agent". In: *Organic Letters* 14.23 (2012), pp. 5948–5951.

[45] Rajeshwer Vanjari, Tirumaleswararao Guntreddi, Saurabh Kumar, and Krishna Nand Singh. "Sulphur promoted C (sp 3)–C (sp 2) cross dehydrogenative cyclisation of acetophenone hydrazones with aldehydes: efficient synthesis of 3, 4, 5-trisubstituted 1 H-pyrazoles". In: *Chemical Communications* 51.2 (2015), pp. 366–369.

[46] IZ Kondyukov, Yu V Karpychev, PG Belyaev, and G Kh. "Khisamutdinov, SI Valeshnii, SP Smirnov, VP Il'in". In: *Russian Journal of Organic Chemistry* 43 (2007), p. 635.

[47] Zitao Wang, Weizhi Geng, Hanliu Wang, Shaoguang Zhang, Wen-Xiong Zhang, and Zhenfeng Xi. "Synthesis of benzothiophene derivatives from dilithio reagents, sulfur, and electrophiles via electrophilic cyclization". In: *Tetrahedron Letters* 52.51 (2011), pp. 6997–6999.

[48] Karl Gewald. "Methods for the synthesis of 2-aminothiophenes and their reactions". In: *Chemistry of Heterocyclic Compounds* 12.10 (1976), pp. 1077–1090.

[49] Eric Block, Venkatachalam Eswarakrishnan, Michael Gernon, Gabriel Ofori-Okai, Chantu Saha, Kaluo Tang, and Jon Zubieta. "o-Lithiothiophenol equivalents. Generation, reactions and applications in synthesis of hindered thiolate ligands". In: *Journal of the American Chemical Society* 111.2 (1989), pp. 658–665.

[50] Peiqi Zhou, Yubing Huang, Wanqing Wu, Jiaming Zhou, Wentao Yu, and Huanfeng Jiang. "Access to 2-aroylthienothiazoles via C–H/N–O bond functionalization of oximes". In: *Organic Letters* 21.24 (2019), pp. 9976–9980.

[51] Paul D Bartlett and Robert Earl Davis. "Reactions of elemental sulfur. II. The reaction of alkali cyanides with sulfur, and some single-sulfur transfer reactions1". In: *Journal of the American Chemical Society* 80.10 (1958), pp. 2513–2516.

[52] Paul D Bartlett and Garbis Meguerian. "Reactions of elemental sulfur. I. The uncatalyzed reaction of sulfur with triarylphosphines1". In: *Journal of the American Chemical Society* 78.15 (1956), pp. 3710–3715.

[53] Masashi Hojo and Donald T Sawyer. "Hydroxide-induced reduction of elemental sulfur (S8) to trisulfur anion radical (S3. bul.-)". In: *Inorganic Chemistry* 28.6 (1989), pp. 1201–1202.

[54] Guoting Zhang, Hong Yi, Hong Chen, Changliang Bian, Chao Liu, and Aiwen Lei. "Trisulfur radical anion as the key intermediate for the synthesis of thiophene via the interaction between elemental sulfur and NaO t Bu". In: *Organic Letters* 16.23 (2014), pp. 6156–6159.

[55] Shengnan Jin, Shi-Jun Li, Xingxing Ma, Jianke Su, Haohua Chen, Yu Lan, and Qiuling Song. "Elemental-sulfur-Enabled divergent synthesis of disulfides, diselenides, and polythiophenes from β-CF3-1, 3-enynes". In: *Angewandte Chemie International Edition* 60.2 (2021), pp. 881–888.

[56] Pingshun Zhang, Linjie Yang, Wanzhi Chen, Miaochang Liu, and Huayue Wu. "Synthesis of [1, 4] thiazino [4, 3-a] indol-10-one derivatives through radical anti aza-Michael addition of 2-aminochalcones". In: *Organic Letters* 23.15 (2021), pp. 6094–6098.

[57] Ming Wang, Qiaoling Fan, and Xuefeng Jiang. "Transition-metal-free diarylannulated sulfide and selenide construction via radical/anion-mediated sulfur–iodine and selenium–iodine exchange". In: *Organic Letters* 18.21 (2016), pp. 5756–5759.

[58] Jun Ying, Hai Wang, Xinxin Qi, Jin-Bao Peng, and Xiao-Feng Wu. "Base-promoted sulfur-mediated carbonylative cyclization of propargylic amines". In: *European Journal of Organic Chemistry* 2018.5 (2018), pp. 688–692.

[59] Robert Earl Davis and Hisham F Nakshbendi. "Sulfur in amine solvents". In: *Journal of the American Chemical Society* 84.11 (1962), pp. 2085–2090.

[60] Francis P Daly and Chris W Brown. "Raman spectra of sulfur dissolved in primary amines". In: *The Journal of Physical Chemistry* 77.15 (1973), pp. 1859–1861.

[61] Francis P Daly and Chris W Brown. "Raman spectra of rhombic sulfur dissolved in secondary amines". In: *The Journal of Physical Chemistry* 80.5 (1976), pp. 480–482.

[62] Maria Koyioni, Maria Manoli, and Panayiotis A Koutentis. "Synthesis of fused 1, 2, 4-dithiazines and 1, 2, 3, 5-trithiazepines". In: *The Journal of Organic Chemistry* 79.20 (2014), pp. 9717–9727.

[63] Thanh Binh Nguyen and Pascal Retailleau. "DIPEA-promoted reaction of 2-nitrochalcones with elemental sulfur: an unusual approach to 2-benzoyl-benzothiophenes". In: *Organic Letters* 19.18 (2017), pp. 4858–4860.

[64] Thanh Binh Nguyen and Pascal Retailleau. "Elemental sulfur-promoted oxidative rearranging coupling between o-aminophenols and ketones: A synthesis of 2-alkyl benzoxazoles under mild conditions". In: *Organic Letters* 19.14 (2017), pp. 3887–3890.

[65] Rong-Geng Fu, Yong Wang, Fei Xia, Hao-Lin Zhang, Yuan Sun, Duo-Wen Yang, Ye-Wei Wang, and Peng Yin. "Synthesis of 2-amino-5-acylthiazoles by a tertiary amine-promoted one-pot three-component cascade cyclization using elemental sulfur as a sulfur source". In: *The Journal of Organic Chemistry* 84.18 (2019), pp. 12237–12245.

[66] Sarah G Bolton, Matthew M Cerda, Annie K Gilbert, and Michael D Pluth. "Effects of sulfane sulfur content in benzyl polysulfides on thiol-triggered H2S release and cell proliferation". In: *Free Radical Biology and Medicine* 131 (2019), pp. 393–398.

[67] BD Vineyard. "Mercaptan—Sulfur reaction. Alkyl Trisulfides". In: *The Journal of Organic Chemistry* 31.2 (1966), pp. 601–602.

[68] Rui Xu, Jun Lu, and Khalil Amine. "Progress in mechanistic understanding and characterization techniques of Li-S batteries". In: *Advanced Energy Materials* 5.16 (2015), p. 1500408.

[69] Guiyin Xu, Bing Ding, Jin Pan, Ping Nie, Laifa Shen, and Xiaogang Zhang. "High performance lithium–sulfur batteries: advances and challenges". In: *Journal of Materials Chemistry A* 2.32 (2014), pp. 12662–12676.

[70] Wei Guo, Amruth Bhargav, Joseph D Ackerson, Yi Cui, Ying Ma, and Yongzhu Fu. "Mixture is better: enhanced electrochemical performance of phenyl selenosulfide in rechargeable lithium batteries". In: *Chemical Communications* 54.64 (2018), pp. 8873–8876.

[71] Kun Woo Park and Erin M Leitao. "The link to polysulfides and their applications". In: *Chemical Communications* 57.26 (2021), pp. 3190–3202.

[72] Beat Meyer. "Elemental sulfur". In: *Chemical Reviews* 76.3 (1976), pp. 367–388.

[73] Jenny Gun, Alexander D Modestov, Alexey Kamyshny, Dan Ryzkov, Vitaly Gitis, Anatoly Goifman, Ovadia Lev, Veit Hultsch, Thomas Grischek, and

Eckhard Worch. “Electrospray ionization mass spectrometric analysis of aqueous polysulfide solutions”. In: *Microchimica Acta* 146 (2004), pp. 229–237.

[74] Narbe Mardirossian and Martin Head-Gordon. “Thirty years of density functional theory in computational chemistry: an overview and extensive assessment of 200 density functionals”. In: *Molecular Physics* 115.19 (2017), pp. 2315–2372.

[75] Michael K Denk. *The Variable strength of the sulfur–sulfur bond: 78 to 41 kcal–G3, CBS-Q, and DFT bond energies of sulfur (S8) and disulfanes XSSX (X= H, F, Cl, CH3, CN, NH2, OH, SH)*. 2009.

[76] Qiu He, Xiaobin Liao, Lixue Xia, Zhaohuai Li, Huan Wang, Yan Zhao, and Donald G Truhlar. “Accurate binding energies for lithium polysulfides and assessment of density functionals for lithium–sulfur battery research”. In: *The Journal of Physical Chemistry C* 123.34 (2019), pp. 20737–20747.

[77] Wei-Hao Song and Ching-Han Hu. “Inorganic polysulfides: Quantum chemistry study and biological implications”. In: *Chemical Physics Letters* 761 (2020), p. 138069.

[78] T Urbański. “New colour reactions of elemental sulphur and carbon disulphide”. In: *Talanta* 9.9 (1962), pp. 799–800.

[79] Weibing Liu, Cui Chen, and Hailing Liu. “Synthesis of polysubstituted thiophenes via base-induced [2+ 2+ 1] cycloaddition reaction of alkynes and elemental sulfur”. In: *Advanced Synthesis and Catalysis* 357.18 (2015), pp. 4050–4054.

[80] Ray D Bell and Angela K Wilson. “SO3 revisited: Impact of tight d augmented correlation consistent basis sets on atomization energy and structure”. In: *Chemical Physics Letters* 394.1-3 (2004), pp. 105–109.

[81] Angela K Wilson and Thom H Dunning. “The HSO- SOH isomers revisited: The effect of tight d functions”. In: *The Journal of Physical Chemistry A* 108.15 (2004), pp. 3129–3133.

[82] Raphael F Ribeiro, Aleksandr V Marenich, Christopher J Cramer, and Donald G Truhlar. “Use of solution-phase vibrational frequencies in continuum models for the free energy of solvation”. In: *The Journal of Physical Chemistry B* 115.49 (2011), pp. 14556–14562.

[83] Christoph Riplinger and Frank Neese. "An efficient and near linear scaling pair natural orbital based local coupled cluster method". In: *The Journal of Chemical Physics* 138.3 (2013), p. 034106.

[84] Christoph Riplinger, Barbara Sandhoefer, Andreas Hansen, and Frank Neese. "Natural triple excitations in local coupled cluster calculations with pair natural orbitals". In: *The Journal of Chemical Physics* 139.13 (2013), p. 134101.

[85] Dimitrios G Liakos and Frank Neese. "Is it possible to obtain coupled cluster quality energies at near density functional theory cost? Domain-based local pair natural orbital coupled cluster vs modern density functional theory". In: *Journal of Chemical Theory and Computation* 11.9 (2015), pp. 4054–4063.

[86] Dimitrios G Liakos, Manuel Sparta, Manoj K Kesharwani, Jan ML Martin, and Frank Neese. "Exploring the accuracy limits of local pair natural orbital coupled-cluster theory". In: *Journal of Chemical Theory and Computation* 11.4 (2015), pp. 1525–1539.

[87] Haoyu S Yu, Xiao He, and Donald G Truhlar. "MN15-L: A new local exchange-correlation functional for Kohn–Sham density functional theory with broad accuracy for atoms, molecules, and solids". In: *Journal of Chemical Theory and Computation* 12.3 (2016), pp. 1280–1293.

[88] Yan Zhao and Donald G Truhlar. "A new local density functional for main-group thermochemistry, transition metal bonding, thermochemical kinetics, and noncovalent interactions". In: *The Journal of Chemical Physics* 125.19 (2006), p. 194101.

[89] Axel D Beeke. "Density-functional thermochemistry. III. The role of exact exchange". In: *Journal of Chemical Physics* 98.7 (1993), pp. 5648–6.

[90] Philip J Stephens, Frank J Devlin, Cary F Chabalowski, and Michael J Frisch. "Ab initio calculation of vibrational absorption and circular dichroism spectra using density functional force fields". In: *The Journal of Physical Chemistry* 98.45 (1994), pp. 11623–11627.

[91] Yan Zhao and Donald G Truhlar. "The M06 suite of density functionals for main group thermochemistry, thermochemical kinetics, noncovalent interactions, excited states, and transition elements: two new functionals and systematic testing of four M06-class functionals and 12 other functionals". In: *Theoretical Chemistry Accounts* 120 (2008), pp. 215–241.

[92] S Yu Haoyu, Xiao He, Shaohong L Li, and Donald G Truhlar. "MN15: A Kohn–Sham global-hybrid exchange–correlation density functional with broad

accuracy for multi-reference and single-reference systems and noncovalent interactions". In: *Chemical Science* 7.8 (2016), pp. 5032–5051.

[93] Carlo Adamo and Vincenzo Barone. "Toward reliable density functional methods without adjustable parameters: The PBE0 model". In: *The Journal of Chemical Physics* 110.13 (1999), pp. 6158–6170.

[94] Jianmin Tao, John P Perdew, Viktor N Staroverov, and Gustavo E Scuseria. "Climbing the density functional ladder: Nonempirical meta–generalized gradient approximation designed for molecules and solids". In: *Physical Review Letters* 91.14 (2003), p. 146401.

[95] Carlo Adamo and Vincenzo Barone. "Exchange functionals with improved long-range behavior and adiabatic connection methods without adjustable parameters: The m PW and m PW1PW models". In: *The Journal of Chemical Physics* 108.2 (1998), pp. 664–675.

[96] Lars Goerigk, Holger Kruse, and Stefan Grimme. "Benchmarking density functional methods against the S66 and S66x8 datasets for non-covalent interactions". In: *ChemPhysChem* 12.17 (2011), pp. 3421–3433.

[97] Narbe Mardirossian and Martin Head-Gordon. "ωB97X-V: A 10-parameter, range-separated hybrid, generalized gradient approximation density functional with nonlocal correlation, designed by a survival-of-the-fittest strategy". In: *Physical Chemistry Chemical Physics* 16.21 (2014), pp. 9904–9924.

[98] Jeng-Da Chai and Martin Head-Gordon. "Long-range corrected hybrid density functionals with damped atom–atom dispersion corrections". In: *Physical Chemistry Chemical Physics* 10.44 (2008), pp. 6615–6620.

[99] Eric Brémond and Carlo Adamo. "Seeking for parameter-free double-hybrid functionals: The PBE0-DH model". In: *The Journal of Chemical Physics* 135.2 (2011), p. 024106.

[100] Jerzy Cioslowski, Agnieszka Szarecka, and David Moncrieff. "Conformations and thermodynamic properties of sulfur homocycles. 1. The S5, S6, S7, and S8 molecules". In: *The Journal of Physical Chemistry A* 105.2 (2001), pp. 501–505.

[101] Ralf Steudel, Jürgen Steidel, Joachim Pickardt, Fritz Schuster, and Richard Reinhardt. "X-ray structural analyses of two allotropes of cycloheptasulfur (γ and δ-S7)[1]". In: *Zeitschrift für Naturforschung B* 35.11 (1980), pp. 1378–1383.

[102] Jerry Donohue, Aimery Caron, and Elihu Goldish. "The crystal and molecular structure of S6 (Sulfur-6)". In: *Journal of The American Chemical Society* 83.18 (1961), pp. 3748–3751.

[103] Xiaofeng Wu, Jessica A Smith, Samuel Petcher, Bowen Zhang, Douglas J Parker, John M Griffin, and Tom Hasell. "Catalytic inverse vulcanization". In: *Nature Communications* 10.1 (2019), p. 647.

[104] Ralf Steudel and Tristram Chivers. "The role of polysulfide dianions and radical anions in the chemical, physical and biological sciences, including sulfur-based batteries". In: *Chemical Society Reviews* 48.12 (2019), pp. 3279–3319.

[105] Meng Zhao, Bo-Quan Li, Xue-Qiang Zhang, Jia-Qi Huang, and Qiang Zhang. "A perspective toward practical lithium–sulfur batteries". In: *ACS Central Science* 6.7 (2020), pp. 1095–1104.

[106] Jon M Fukuto, Louis J Ignarro, Peter Nagy, David A Wink, Christopher G Kevil, Martin Feelisch, Miriam M Cortese-Krott, Christopher L Bianco, Yoshito Kumagai, Adrian J Hobbs, et al. "Biological hydropersulfides and related polysulfides–a new concept and perspective in redox biology". In: *FEBS Letters* 592.12 (2018), pp. 2140–2152.

[107] Antonio Francioso, Alessia Baseggio Conrado, Luciana Mosca, and Mario Fontana. "Chemistry and biochemistry of sulfur natural compounds: Key intermediates of metabolism and redox biology". In: *Oxidative Medicine and Cellular Longevity* 2020 (2020).

[108] Katsuhiko Ono, Takaaki Akaike, Tomohiro Sawa, Yoshito Kumagai, David A Wink, Dean J Tantillo, Adrian J Hobbs, Peter Nagy, Ming Xian, Joseph Lin, et al. "Redox chemistry and chemical biology of H2S, hydropersulfides, and derived species: implications of their possible biological activity and utility". In: *Free Radical Biology and Medicine* 77 (2014), pp. 82–94.

[109] Hideo Kimura. *Hydrogen sulfide and polysulfide signaling*. 2017.

[110] A Cahours and AW Hofmann. "Untersuchungen über die Phosphorbasen". In: *Justus Liebigs Annalen der Chemie* 104.1 (1857), pp. 1–39.

[111] Olav Foss. "The prevalence of unbranched sulphur chains in polysulphides and polythionic compounds". In: *Acta Chemica Scandinavica* 4 (1950), p. 404.

[112] DA Skoog and JK Bartlett. "Titration of elemental sulfur with solutions of sodium cyanide". In: *Analytical Chemistry* 27.3 (1955), pp. 369–371.

[113] Karl Gewald, Elfriede Schinke, and Horst Böttcher. "Heterocyclen aus CH-aciden nitrilen, VIII. 2-amino-thiophene aus methylenaktiven nitrilen, carbonylverbindungen und schwefel". In: *Chemische Berichte* 99.1 (1966), pp. 94–100.

[114] Zita Puterová, Alžbeta Krutošıková, and Daniel Végh. "Gewald reaction: synthesis, properties and applications of substituted 2-aminothiophenes". In: *Arkivoc* 1.209 (2010), pp. 209–46.

[115] Yijun Huang and Alexander Dömling. "The Gewald multicomponent reaction". In: *Molecular Diversity* 15 (2011), pp. 3–33.

[116] Daniel L Priebbenow and Carsten Bolm. "Recent advances in the Willgerodt–Kindler reaction". In: *Chemical Society Reviews* 42.19 (2013), pp. 7870–7880.

[117] Max Schmidt and Volker Potschka. "Über die Reaktion von Natriumphenylazetylid mit elementarem Schwefel". In: *Naturwissenschaften* 50.7 (1963), pp. 302–302.

[118] Zitao Wang, Yang Wang, Wen-Xiong Zhang, Zhaomin Hou, and Zhenfeng Xi. "Efficient one-pot synthesis of 2, 3-dihydropyrimidinthiones via multicomponent coupling of terminal alkynes, elemental sulfur, and carbodiimides". In: *Journal of the American Chemical Society* 131.42 (2009), pp. 15108–15109.

[119] Zilong Wang, Zhonghua Qu, Fuhong Xiao, Huawen Huang, and Guo-Jun Deng. "One-pot synthesis of 2, 3, 5-trisubstituted thiophenes through three-component assembly of arylacetaldehydes, elemental sulfur, and 1, 3-dicarbonyls". In: *Advanced Synthesis and Catalysis* 360.4 (2018), pp. 796–800.

[120] Jingjing Jiang, Huawen Huang, and Guo-Jun Deng. "Four-component thiazole formation from simple chemicals under metal-free conditions". In: *Green Chemistry* 21.5 (2019), pp. 986–990.

[121] Xingzong Che, Jingjing Jiang, Fuhong Xiao, Huawen Huang, and Guo-Jun Deng. "Assembly of 2-arylbenzothiazoles through three-component oxidative annulation under transition-metal-free conditions". In: *Organic Letters* 19.17 (2017), pp. 4576–4579.

[122] Jingjing Jiang, Xiaolong Tuo, Zhuquan Fu, Huawen Huang, and Guo-Jun Deng. "Three-component synthesis of 1, 4-benzothiazines via iodide-catalyzed aerobic C–H sulfuration with elemental sulfur". In: *Organic and Biomolecular Chemistry* 18.17 (2020), pp. 3234–3238.

[123] Stuart Licht and John Davis. "Disproportionation of aqueous sulfur and sulfide: kinetics of polysulfide decomposition". In: *The Journal of Physical Chemistry B* 101.14 (1997), pp. 2540–2545.

[124] FW Küster. "Beiträge zur Kenntnis der polysulfide. III. Die periodischen Vorgänge bei Elektrolyse der polysulfide". In: *Zeitschrift für anorganische Chemie* 46.1 (1905), pp. 113–143.

[125] Billy D Vineyard. "Versatility and the mechanism of the n-butyl-amine-catalyzed reaction of thiols with sulfur". In: *The Journal of Organic Chemistry* 32.12 (1967), pp. 3833–3836.

[126] Jonathan T Stoffel, Kimberly T Riordan, and Emily Y Tsui. "Accelerated reduction and solubilization of elemental sulfur by 1, 2-aminothiols". In: *Chemical Communications* 57.93 (2021), pp. 12488–12491.

[127] W Giggenbach. "Optical spectra and equilibrium distribution of polysulfide ions in aqueous solution at 20. deg." In: *Inorganic Chemistry* 11.6 (1972), pp. 1201–1207.

[128] Stuart Licht, Gary Hodes, and Joost Manassen. "Numerical analysis of aqueous polysulfide solutions and its application to cadmium chalcogenide/polysulfide photoelectrochemical solar cells". In: *Inorganic Chemistry* 25.15 (1986), pp. 2486–2489.

[129] Péter Nagy. "Mechanistic chemical perspective of hydrogen sulfide signaling". In: *Methods in Enzymology* 554 (2015), pp. 3–29.

[130] Nathanael Lau and Michael D Pluth. "Reactive sulfur species (RSS): persulfides, polysulfides, potential, and problems". In: *Current Opinion in Chemical Biology* 49 (2019), pp. 1–8.

[131] Virág Bogdándi, Tomoaki Ida, Thomas R Sutton, Christopher Bianco, Tamás Ditrói, Grielof Koster, Hillary A Henthorn, Magda Minnion, John P Toscano, Albert van der Vliet, et al. "Speciation of reactive sulfur species and their reactions with alkylating agents: do we have any clue about what is present inside the cell?" In: *British Journal of Pharmacology* 176.4 (2019), pp. 646–670.

[132] Danny Schilling, Uladzimir Barayeu, Raphael R Steimbach, Deepti Talwar, Aubry K Miller, and Tobias P Dick. "Commonly used alkylating agents limit persulfide detection by converting protein persulfides into thioethers". In: *Angewandte Chemie International Edition* 61.30 (2022), e202203684.

[133] Hideo Kimura. "Hydrogen sulfide and polysulfides as biological mediators". In: *Molecules* 19.10 (2014), pp. 16146–16157.

[134] W Cule Davies and WP Walters. "418. The constitution of some additive compounds of tertiary phosphines". In: *Journal of the Chemical Society (Resumed)* (1935), pp. 1786–1792.

[135] Alan J Parker and Norman Kharasch. "The scission of the sulfur-sulfur bond". In: *Chemical Reviews* 59.4 (1959), pp. 583–628.

[136] OLAV Foss. "Ionic scission of the sulfur-sulfur bond". In: *Organic Sulfur Compounds*. Elsevier, 1961, pp. 83–96.

[137] ROBERT EARL DAVIS. "Nucleophilic displacement reactions at the sulfur-sulfur bond". In: *Survey of Progress in Chemistry*. Vol. 2. Elsevier, 1964, pp. 189–238.

[138] Shigeru Oae and Joyce Doi. *Organic Sulfur Chemistry*. Vol. 2. CRC Press, 1991.

[139] Roland Mayer. "Elemental sulfur and its reactions". In: *Organic Chemistry of Sulfur* (1977), pp. 33–69.

[140] Jessica Zarenkiewicz, Vinayak S Khodade, and John P Toscano. "Reaction of nitroxyl (HNO) with hydrogen sulfide and hydropersulfides". In: *The Journal of Organic Chemistry* 86.1 (2020), pp. 868–877.

[141] T Spencer Bailey, Lev N Zakharov, and Michael D Pluth. "Understanding hydrogen sulfide storage: probing conditions for sulfide release from hydrodisulfides". In: *Journal of the American Chemical Society* 136.30 (2014), pp. 10573–10576.

[142] Jyoti Sharma and Pier Alexandre Champagne. "Benchmark of density functional theory methods for the study of organic polysulfides". In: *Journal of Computational Chemistry* 43.32 (2022), pp. 2131–2138.

[143] Aleksandr V Marenich, Christopher J Cramer, and Donald G Truhlar. "Universal solvation model based on solute electron density and on a continuum model of the solvent defined by the bulk dielectric constant and atomic surface tensions". In: *The Journal of Physical Chemistry B* 113.18 (2009), pp. 6378–6396.

[144] William P Jencks. “A primer for the Bema Hapothle. An empirical approach to the characterization of changing transition-state structures”. In: *Chemical Reviews* 85.6 (1985), pp. 511–527.

[145] Kirk A Peterson, James R Lyons, and Joseph S Francisco. “An ab initio study of the low-lying electronic states of S 3”. In: *The Journal of Chemical Physics* 125.8 (2006), p. 084314.

[146] Myrna H Matus, David A Dixon, Kirk A Peterson, John AW Harkless, and Joseph S Francisco. “Coupled-cluster study of the electronic structure and energetics of tetrasulfur, S 4”. In: *The Journal of Chemical Physics* 127.17 (2007), p. 174305.

[147] Adam J Jackson, Davide Tiana, and Aron Walsh. “A universal chemical potential for sulfur vapours”. In: *Chemical Science* 7.2 (2016), pp. 1082–1092.

[148] Heinz Gerischer. “Über die Auflösungsgeschwindigkeit von Schwefel in Sulfid- und Polysulfidlösungen”. In: *Zeitschrift für anorganische Chemie* 259.5-6 (1949), pp. 220–224.

[149] Ralf Steudel. “Inorganic polysulfides S n 2- and radical anions S n·-”. In: *Elemental sulfur und sulfur-Rich sompounds II* (2003), pp. 127–152.

[150] Phil Liebing, Marcel Kühling, Claudia Swanson, Martin Feneberg, Liane Hilfert, Rüdiger Goldhahn, Tristram Chivers, and Frank T Edelmann. “Catenated and spirocyclic polychalcogenides from potassium carbonate and elemental chalcogens”. In: *Chemical Communications* 55.99 (2019), pp. 14965–14967.

[151] Lennart Schotte and Göran Bergson. “A note on the structure and properties of thiokols”. In: *Journal of Polymer Science* 45.145 (1960), pp. 261–263.

[152] R Rahman, S Safe, and A Taylor. “The stereochemistry of polysulphides”. In: *Quarterly Reviews, Chemical Society* 24.2 (1970), pp. 208–237.

[153] Gerald W Kutney and Kenneth Turnbull. “Compounds containing the sulfur-sulfur double bond”. In: *Chemical Reviews* 82.4 (1982), pp. 333–357.

[154] Colin J Marsden, Heinz Oberhammer, Oliver Lösking, and Helge Willner. “The geometric structures of the disulphur difluoride isomers: an experimental and ab initio study”. In: *Journal of Molecular Structure* 193 (1989), pp. 233–245.

[155] Ralf Steudel, Yana Drozdova, Karol Miaskiewicz, Roland H Hertwig, and Wolfram Koch. "How unstable are thiosulfoxides? An ab initio MO study of various disulfanes RSSR (R= H, Me, Pr, all), their branched isomers R2SS, and the related transition states1, 2". In: *Journal of the American Chemical Society* 119.8 (1997), pp. 1990–1996.

[156] MD Chen, ML Liu, HB Luo, QE Zhang, and CT Au. "Geometric structures and structural stabilities of neutral sulfur clusters". In: *Journal of Molecular Structure: THEOCHEM* 548.1-3 (2001), pp. 133–141.

[157] Ming Wah Wong, Yana Steudel, and Ralf Steudel. "Novel species for the sulfur zoo: isomers of S8". In: *Chemical Physics Letters* 364.3-4 (2002), pp. 387–392.

[158] Ming Wah Wong, Yana Steudel, and Ralf Steudel. "Novel isomers of hexasulfur: Prediction of a stable prism isomer and implications for the thermal reactivity of elemental sulfur". In: *The Journal of Chemical Physics* 121.12 (2004), pp. 5899–5907.

[159] Ming Wah Wong, Yana Steudel, and Ralf Steudel. "Isomers of cyclo-heptasulfur and their coordination to Li+: an Ab initio molecular orbital study". In: *Inorganic Chemistry* 44.24 (2005), pp. 8908–8915.

[160] Brian P Prascher and Angela K Wilson. "A computational study of dihalogen-μ-dichalcogenides: XAAX (X= F, Cl, Br; A= S, Se)". In: *Journal of Molecular Structure: THEOCHEM* 814.1-3 (2007), pp. 1–10.

[161] Pascal Gerbaux, Jean-Yves Salpin, Guy Bouchoux, and Robert Flammang. "Thiosulfoxides (X_2S S) and disulfanes (XSSX):: first observation of organic thiosulfoxides". In: *International Journal of Mass Spectrometry* 195 (2000), pp. 239–249.

[162] Reijo J Suontamo, Risto S Laitinen, and Tapani A Pakkanen. "An Ab initio MO study of the pseudorotation in cyclohexasulfur, S6, and cycloheptasulfur, S7". In: *Acta Chemica Scandinavica* 45 (1991), p. 687.

[163] Fillmore Freeman, Jung H Hwang, Eun Hae Junge, Prem Dinesh Parmar, Zhongwei Renz, and James Trinh. "Conformational analysis of cycloheptane, oxacycloheptane, 1, 2-dioxacycloheptane, 1, 3-dioxacycloheptane, and 1, 4-dioxacycloheptane". In: *International Journal of Quantum Chemistry* 108.2 (2008), pp. 339–350.

[164] William A Pryor. *Mechanisms of sulfur reactions*. McGraw-Hill, 1962.

[165] Andreza Conception Véras of Aguiar, Ricardo Olımpio of Moura, Jaime Francisco Bezerra Mendonça Junior, Hugo Alexandre de Oliveira Rocha, Rafael Barros Gomes Câmara, and Manuela dos Santos Carvalho Schiavon. "Evaluation of the antiproliferative activity of 2-amino thiophene derivatives against human cancer cells lines". In: *Biomedicine and Pharmacotherapy* 84 (2016), pp. 403–414.

[166] Pankaj Mishra, Anil Middha, Vikas Saxena, and Abhishek Saxena. "Synthesis and evaluation of anti-inflammatory activity of some cinnoline derivatives-4 (-2-amino-thiophene) cinnoline-3-carboxamide". In: *Pharmaceutical and Biosciences Journal* (2016), pp. 64–68.

[167] Herbert Y Meltzer and H Christian Fibiger. "Olanzapine: a new atypical antipsychotic drug". In: *Neuropsychopharmacology* 14.2 (1996), pp. 83–85.

[168] Raghav Mishra, KK Jha, Sachin Kumar, and Isha Tomer. "Synthesis, properties and biological activity of thiophene: A review". In: *Der Pharma Chemica* 3.4 (2011), pp. 38–54.

[169] Dennis M Vriezema, Johan Hoogboom, Kelly Velonia, Ken Takazawa, Peter CM Christianen, Jan C Maan, Alan E Rowan, and Roeland JM Nolte. "Vesicles and polymerized vesicles from thiophene-containing rod–coil block copolymers". In: *Angewandte Chemie International Edition* 42.7 (2003), pp. 772–776.

[170] RW Sabnis and DW Rangnekar. "Synthesis of azo benzo [b] thiophene derivatives and their application as disperse dyes". In: *Dyes and Pigments* 10.4 (1989), pp. 295–302.

[171] D Binder, G Habison, and Ch R Noe. "Simple synthesis of 2-aminothiphenes". In: *Synthesis-stuttgart* 4 (1977), pp. 255–256.

[172] Ram W Sabnis. "The Gewald synthesis". In: *Sulfur Reports* 16.1 (1994), pp. 1–17.

[173] E Campaigne and Pearle A Monroe. "3-substituted thiophenes. VII. Derivatives of 3-aminothiophene". In: *Journal of the American Chemical Society* 76.9 (1954), pp. 2447–2450.

[174] Otto Meth-Cohn and Bramha Narine. "The preparation and formylation of 2-acetamidothiophenes". In: *Synthesis* 1980.02 (1980), pp. 133–135.

[175] M Augustin, W-D Rudorf, and U Schmidt. "Thiophene durch S-alkylierung". In: *Tetrahedron* 32.24 (1976), pp. 3055–3061.

[176] H Harlmann and R Mayer. "Aminothiophene aus N, N-disubstituierten Thioamiden". In: *Zeitschrift für Chemie* 6.1 (1966), pp. 28–28.

[177] Horst Hartmann. "Elektrophile Reaktionen am 2-Aminothiophensystem Darstellung und Eigenschaften von substituierten Thienyl-aryl-methinen". In: *Journal für Praktische Chemie* 36.1-2 (1967), pp. 50–72.

[178] Karl Gewald. "Heterocyclen aus CH-aciden Nitrilen, VII. 2-Amino-thiophene aus α-Oxo-mercaptanen und methylenaktiven Nitrilen". In: *Chemische Berichte* 98.11 (1965), pp. 3571–3577.

[179] VP Litvinov, Yu A Sharanin, and FS Babichev. "Cyclization of nitriles as synthetic route to 2-and 3-aminothiophenes". In: *Sulfur Reports* 6.2 (1986), pp. 97–128.

[180] Ram W Sabnis and Dinesh W Rangnekar. "Synthesis of 2-azo-3-cyano-5-carbethoxy thiophene derivatives and their application on polyester fibres". In: *Journal of Chemical Technology and Biotechnology* 47.1 (1990), pp. 39–46.

[181] Roland Mayer and Karl Gewald. "The action of carbon disulfide and sulfur on enamines, ketimines, and CH acids". In: *Angewandte Chemie International Edition in English* 6.4 (1967), pp. 294–306.

[182] Dao-Lin Wang, Jian-Ying Wu, and Qing-Tao Cui. "An efficient one-pot synthesis of thiophene-fused pyrido [3, 2-a] azulenes via Gewald reaction". In: *Chinese Chemical Letters* 25.12 (2014), pp. 1591–1594.

[183] Kotthireddy Kavitha, Devulapally Srikrishna, Pramod Kumar Dubey, and Pasula Aparna. "An efficient one-pot four-component Gewald reaction: Synthesis of substituted 2-aminothiophenes with coumarin–thiazole scaffolds under environmentally benign conditions". In: *Journal of Sulfur Chemistry* 40.2 (2019), pp. 195–208.

[184] Taoda Shi, Lynn Kaneko, Michael Sandino, Ryan Busse, Mae Zhang, Damian Mason, Jason Machulis, Andrew J Ambrose, Donna D Zhang, and Eli Chapman. "One-step synthesis of thieno [2, 3-d] pyrimidin-4 (3 H)-ones via a catalytic four-component reaction of ketones, ethyl cyanoacetate, S8, and formamide". In: *ACS sustainable chemistry and engineering* 7.1 (2018), pp. 1524–1528.

[185] Marta Feroci, Isabella Chiarotto, Leucio Rossi, and Achille Inesi. "Activation of elemental sulfur by electrogenerated cyanomethyl anion: synthesis of substituted 2-aminothiophenes by the Gewald reaction". In: *Advanced Synthesis and Catalysis* 350.17 (2008), pp. 2740–2746.

[186] Jyoti Sharma and Pier Alexandre Champagne. "Mechanisms of the reaction of elemental sulfur and polysulfides with cyanide and phosphines". In: *Chemistry–A European Journal* (2023), e202203906.

[187] Thom H Dunning, Kirk A Peterson, and Angela K Wilson. "Gaussian basis sets for use in correlated molecular calculations. X. The atoms aluminum through argon revisited". In: *The Journal of Chemical Physics* 114.21 (2001), pp. 9244–9253.

[188] Norton P Peet, Shyam Sunder, Robert J Barbuch, and Anna P Vinogradoff. "Mechanistic observations in the Gewald syntheses of 2-aminothiophenes". In: *Journal of Heterocyclic Chemistry* 23.1 (1986), pp. 129–134.

[189] Zita Puterová, Anita Andicsová, and Daniel Vegh. "Synthesis of π-conjugated thiophenes starting from substituted 3-oxopropanenitriles via Gewald reaction". In: *Tetrahedron* 64.49 (2008), pp. 11262–11269.

[190] Thanh Binh Nguyen, Dinh Hung Mac, and Pascal Retailleau. "Base-catalyzed three-component reaction of α-cyanoacetates with chalcones and elemental sulfur: access to 2-aminothiophenes unobtainable via the gewald reaction". In: *The Journal of Organic Chemistry* 86.14 (2021), pp. 9418–9427.

[191] Kazuho Abe and Hideo Kimura. "The possible role of hydrogen sulfide as an endogenous neuromodulator". In: *Journal of Neuroscience* 16.3 (1996), pp. 1066–1071.

[192] Douglas C Nelson, Bo Barker Jørgensen, and Niels Peter Revsbech. "Growth pattern and yield of a chemoautotrophic Beggiatoa sp. in oxygen-sulfide microgradients". In: *Applied and Environmental Microbiology* 52.2 (1986), pp. 225–233.

[193] Rui Wang. "Physiological implications of hydrogen sulfide: a whiff exploration that blossomed". In: *Physiological Reviews* 92.2 (2012), pp. 791–896.

[194] Qian Li and Jack R Lancaster Jr. "Chemical foundations of hydrogen sulfide biology". In: *Nitric Oxide* 35 (2013), pp. 21–34.

[195] Kenneth N Maclean and Jan P Kraus. "Hydrogen sulfide production and metabolism in mammalian tissues". In: *Signal Transduction and the Gasotransmitters: NO, CO, and H 2 S in Biology and Medicine* (2004), pp. 275–292.

[196] Hao-Jie Chen, Ebenezeri Erasto Ngowi, Lei Qian, Tao Li, Yang-Zhe Qin, Jing-Jing Zhou, Ke Li, Xin-Ying Ji, and Dong-Dong Wu. "Role of hydrogen sulfide in the endocrine system". In: *Frontiers in Endocrinology* (2021), p. 840.

[197] Yu Zhao, Shashi Bhushan, Chuntao Yang, Hiroyuki Otsuka, Jason D Stein, Armando Pacheco, Bo Peng, Nelmi O Devarie-Baez, Hector C Aguilar, David J Lefer, et al. "Controllable hydrogen sulfide donors and their activity against myocardial ischemia-reperfusion injury". In: *ACS Chemical Biology* 8.6 (2013), pp. 1283–1290.

[198] Zongmin Zhou, Margarete von Wantoch Rekowski, Ciro Coletta, Csaba Szabo, Mariarosaria Bucci, Giuseppe Cirino, Stavros Topouzis, Andreas Papapetropoulos, and Athanassios Giannis. "Thioglycine and L-thiovaline: biologically active H2S-donors". In: *Bioorganic and Medicinal Chemistry* 20.8 (2012), pp. 2675–2678.

[199] Ling Li, Matthew Whiteman, Yan Yi Guan, Kay Li Neo, Yvonne Cheng, Shiau Wei Lee, Yujun Zhao, Rajamanian Baskar, Choon-Hong Tan, and Philip K Moore. "Characterization of a novel, water-soluble hydrogen sulfide–releasing molecule (GYY4137) new insights into the biology of hydrogen sulfide". In: *Circulation* 117.18 (2008), pp. 2351–2360.

[200] Chung-Min Park, Yu Zhao, Zhaohui Zhu, Armando Pacheco, Bo Peng, Nelmi O Devarie-Baez, Powell Bagdon, Hui Zhang, and Ming Xian. "Synthesis and evaluation of phosphorodithioate-based hydrogen sulfide donors". In: *Molecular BioSystems* 9.10 (2013), pp. 2430–2434.

[201] Andrea K Steiger, Sibile Pardue, Christopher G Kevil, and Michael D Pluth. "Self-immolative thiocarbamates provide access to triggered H2S donors and analyte replacement fluorescent probes". In: *Journal of the American Chemical Society* 138.23 (2016), pp. 7256–7259.

[202] Leslie B Poole. "The basics of thiols and cysteines in redox biology and chemistry". In: *Free Radical Biology and Medicine* 80 (2015), pp. 148–157.

[203] Eric R DeLeon, Gilbrian F Stoy, and Kenneth R Olson. "Passive loss of hydrogen sulfide in biological experiments". In: *Analytical Biochemistry* 421.1 (2012), pp. 203–207.

[204] Gloria A Benavides, Giuseppe L Squadrito, Robert W Mills, Hetal D Patel, T Scott Isbell, Rakesh P Patel, Victor M Darley-Usmar, Jeannette E Doeller, and David W Kraus. "Hydrogen sulfide mediates the vasoactivity of garlic". In: *Proceedings of the National Academy of Sciences* 104.46 (2007), pp. 17977–17982.

[205] H Robinson and S Wray. "A new slow releasing". In: *H2S Generating* (2012).

[206] Yu Zhao, Hua Wang, and Ming Xian. "Cysteine-activated hydrogen sulfide (H2S) donors". In: *Journal of the American Chemical Society* 133.1 (2011), pp. 15–17.

[207] Sidney Hershberg Katz and EJ Talbert. *Intensities of odors and irritating effects of warning agents for inflammable and poisonous gases*. Vol. 480. US Government Printing Office, 1930.

[208] HW Engels, HJ Weidenhaupt, M Pieroth, W Hofmann, KH Menting, T Mergenhagen, R Schmoll, and S Uhrlandt. *Ullmann's encyclopedia of industrial chemistry*. 2004.

[209] Dean P Jones. "Redefining oxidative stress". In: *Antioxidants and redox signaling* 8.9-10 (2006), pp. 1865–1879.

[210] Takehiko Nishio. "Direct conversion of alcohols into thiols". In: *Journal of the Chemical Society, Perkin Transactions 1* 10 (1993), pp. 1113–1117.

[211] Robert J Ouellette and J David Rawn. *Organic chemistry study guide: Key concepts, problems, and solutions*. Elsevier, 2014.

[212] Walter A Schulze, JP Lyon, and GH Short. "Synthesis of tertiary alkyl mercaptans". In: *Industrial and Engineering Chemistry* 40.12 (1948), pp. 2308–2313.

[213] BC Cossar, Jane O Fournier, DL Fields, and DD Reynolds. "Preparation of thiols". In: *The Journal of Organic Chemistry* 27.1 (1962), pp. 93–95.

[214] José A Fernández-Salas, Simone Manzini, and Steven P Nolan. "Efficient ruthenium-catalysed S–S, S–Si and S–B bond forming reactions". In: *Chemical Communications* 49.52 (2013), pp. 5829–5831.

[215] Hua-Jian Xu, Yong-Qiang Zhao, Teng Feng, and Yi-Si Feng. "Chan–lam-type S-arylation of thiols with boronic acids at room temperature". In: *The Journal of Organic Chemistry* 77.6 (2012), pp. 2878–2884.

[216] Heather DeFrancesco, Joshua Dudley, and Adiel Coca. "Boron chemistry: an overview". In: *Boron Reagents in Synthesis* (2016), pp. 1–25.

[217] Irina P Beletskaya, Francisco Alonso, and Vladimir Tyurin. "The Suzuki-Miyaura reaction after the Nobel prize". In: *Coordination Chemistry Reviews* 385 (2019), pp. 137–173.

[218] Herbert C Brown and George Zweifel. "Hydroboration. VII. Directive effects in the hydroboration of olefins". In: *Journal of the American Chemical Society* 82.17 (1960), pp. 4708–4712.

[219] Clinton F Lane. "Organic synthesis using borane-methyl sulfide. Hydroboration-oxidation of alkenes". In: *The Journal of Organic Chemistry* 39.10 (1974), pp. 1437–1438.

[220] James H Walton and Llewellyn B Parsons. "The preparation and properties of the persulfides of hydrogen." In: *Journal of the American Chemical Society* 43.12 (1921), pp. 2539–2548.

[221] JE Franz and LL Black. "Thermolysis and photolysis of 1, 3, 4-oxathiazole-2-ones: I". In: *Tetrahedron Letters* 11.16 (1970), pp. 1381–1384.

[222] Curt Wentrup and Peter Kambouris. "N-sulfides. Dinitrogen sulfide, thiofulminic acid, and nitrile sulfides". In: *Chemical Reviews* 91.3 (1991), pp. 363–373.

[223] Robert K Howe, Terry A Gruner, Linda G Carter, Linda L Black, and John E Franz. "Cycloaddition reactions of nitrile sulfides with acetylenic esters. Synthesis of isothiazolecarboxylates". In: *The Journal of Organic Chemistry* 43.19 (1978), pp. 3736–3742.

[224] Anjaiah Aitha, Satyanarayana Yennam, Manoranjan Behera, and Jaya Shree Anireddy. "Design and synthesis of diaziridinyl quinone thiadiazole hybrids via nitrile sulfide cycloaddition reaction as a key step". In: *Tetrahedron Letters* 57.13 (2016), pp. 1507–1510.

[225] Rangappa S Keri, Mahadeo R Patil, Siddappa A Patil, and Srinivasa Budagumpi. "A comprehensive review in current developments of benzothiazole-based molecules in medicinal chemistry". In: *European Journal of Medicinal Chemistry* 89 (2015), pp. 207–251.

[226] Thomas Lonsdale Gilchrist. *Heterocyclic Chemistry*. Prentice Hall, 1997.

[227] Abdul Rouf and Cihangir Tanyeli. "Bioactive thiazole and benzothiazole derivatives". In: *European Journal of Medicinal Chemistry* 97 (2015), pp. 911–927.

[228] Agrochemical Handbook. *The Agrochemicals Handbook. 2nd Edn, Hartley D, Kidd H.* 1987.

[229] Thorsten Reemtsma, Oliver Fiehn, Guenter Kalnowski, and Martin Jekel. "Microbial transformations and biological effects of fungicide-derived benzothiazoles determined in industrial wastewater". In: *Environmental Science and Technology* 29.2 (1995), pp. 478–485.

[230] Seon-Yeong Gwon, Sue-Yeon Lee, Young-A Son, and Sung-Hoon Kim. "Benzothiazole and indole based dye sensor: Optical switching functions with pH stimuli". In: *Fibers and Polymers* 13 (2012), pp. 1101–1104.

[231] Okoh Adeyi Okoh, Roger H Bisby, Clare L Lawrence, Carole E Rolph, and Robert B Smith. "Promising near-infrared non-targeted probes: benzothiazole heptamethine cyanine dyes". In: *Journal of Sulfur Chemistry* 35.1 (2014), pp. 42–56.

[232] Hendrik Kokelenberg and CS Marvel. "Polymers containing anthraquinone units: Benzimidazole and benzothiazole polymers". In: *Journal of Polymer Science Part A-1: Polymer Chemistry* 8.11 (1970), pp. 3199–3209.

[233] Zhijuan Cao, Fengxian Qiu, Qing Wang, Guorong Cao, Lin Zhuang, Qiang Shen, Xiaolong Xu, Jie Wang, Qian Chen, and Dongya Yang. "Synthesis of azo benzothiazole polymer and its application of 1× 2 Y-branched and 2× 2 Mach–Zehnder interferometer switch". In: *Optik* 124.19 (2013), pp. 4036–4040.

[234] Herman P Lankelma and PX Sharnoff. "The condensation of aldehydes with ortho-aminothiophenols, benzothiazolines and benzothiazoles". In: *Journal of the American Chemical Society* 53.7 (1931), pp. 2654–2657.

[235] Dong-Fang Shi, Tracey D Bradshaw, Samantha Wrigley, Carol J McCall, Peter Lelieveld, Iduna Fichtner, and Malcolm FG Stevens. "Antitumor benzothiazoles. 3. Synthesis of 2-(4-aminophenyl) benzothiazoles and evaluation of their activities against breast cancer cell lines in vitro and in vivo". In: *Journal of Medicinal Chemistry* 39.17 (1996), pp. 3375–3384.

[236] Thanh Binh Nguyen, Ludmila Ermolenko, Pascal Retailleau, and Ali Al-Mourabit. "Elemental sulfur disproportionation in the redox condensation reaction between o-halonitrobenzenes and benzylamines". In: *Angewandte Chemie* 126.50 (2014), pp. 14028–14032.

[237] Xiaoming Zhu, Yuzhong Yang, Genhua Xiao, Jianxin Song, Yun Liang, and Guobo Deng. "Double C–S bond formation via C–H bond functionalization: Synthesis of benzothiazoles and naphtho [2, 1-d] thiazoles from N-substituted arylamines and elemental sulfur". In: *Chemical Communications* 53.87 (2017), pp. 11917–11920.

[238] Yubing Huang, Peiqi Zhou, Wanqing Wu, and Huanfeng Jiang. "Selective construction of 2-substituted benzothiazoles from o-iodoaniline derivatives S8 and N-tosylhydrazones". In: *The Journal of Organic Chemistry* 83.4 (2018), pp. 2460–2466.

[239] Matthew A Lynn, Lauren J Carlson, Hyeon Hwangbo, Joseph M Tanski, and Laurie A Tyler. "Structural influences on the oxidation of a series of 2-benzothiazoline analogs". In: *Journal of Molecular Structure* 1011 (2012), pp. 81–93.

[240] Nurani S Narasimhan, Nurani M Sunder, Radhakrishna Ammanamanchi, and Bhagavat D Bonde. "Evidence in favor of lithium-halogen exchange being faster than lithium-acidic hydrogen (deuterium) exchange". In: *Journal of the American Chemical Society* 112.11 (1990), pp. 4431–4435.

[241] James B Campbell, Robert F Dedinas, and Sally A Trumbower-Walsh. "Addition of transiently-generated methyl o-lithiobenzoate to imines. An isoindolone annulation". In: *The Journal of Organic Chemistry* 61.18 (1996), pp. 6205–6211.

[242] James B Campbell, Robert F Dedinas, and Sally Trumbower-Walsh. "Preparation of isoindolones by a lithium-iodide exchange-induced intramolecular Wurtz-Fittig reaction of o-iodobenzoyl chloride/imine adducts". In: *Synlett* 2010.20 (2010), pp. 3008–3010.

[243] Jack E Baldwin. "Rules for ring closure". In: *Journal of the Chemical Society, Chemical Communications* 18 (1976), pp. 734–736.

[244] SW Wright. "One-pot synthesis of novel sulfur and selenium heterocycles by directed ortho-lithiation". In: *Journal of Heterocyclic Chemistry* 38.3 (2001), pp. 723–726.

[245] Ryu Sato. "Heteroatom chemistry of cyclic benzopolychalcogenides: Synthesis and characterization". In: *Heteroatom Chemistry: An International Journal of Main Group Elements* 13.5 (2002), pp. 419–423.

[246] Mario E Alva Astudillo, Norris CJ Chokotho, Terence C Jarvis, C David Johnson, Colim C Lewis, and Peter D McDonnell. "Hydroxy Schiff base-oxazolidine tautomerism: apparent breakdown of Baldwin's rules". In: *Tetrahedron* 41.24 (1985), pp. 5919–5928.

[247] Francis A Carey and Richard J Sundberg. *Advanced organic chemistry: part b: reactions and synthesis*. Vol. 3. Springer, 2007.

[248] Yoshio Himeshima, Takaaki Sonoda, and Hiroshi Kobayashi. “Fluoride-induced 1, 2-elimination of o-trimethylsilylphenyl triflate to benzyne under mild conditions”. In: *Chemistry Letters* 12.8 (1983), pp. 1211–1214.

[249] Li-Ming Zhao, Shu-Qing Zhang, Hai-Shan Jin, Li-Jing Wan, and Fei Dou. “Zinc-mediated highly α-regioselective prenylation of imines with prenyl bromide”. In: *Organic Letters* 14.3 (2012), pp. 886–889.

[250] Hiroto Yoshida, Joji Ohshita, and Atsutaka Kunai. “Aryne, ortho-quinone methide, and ortho-quinodimethane: Synthesis of multisubstituted arenes using the aromatic reactive intermediates”. In: *Bulletin of the Chemical Society of Japan* 83.3 (2010), pp. 199–219.

[251] Kentaro Okuma. “Reaction of arynes with carbon-heteroatom double bonds”. In: *Heterocycles* 85.3 (2012), pp. 515–544.

[252] Anton V Dubrovskiy, Nataliya A Markina, and Richard C Larock. “Use of benzynes for the synthesis of heterocycles”. In: *Organic and Biomolecular Chemistry* 11.2 (2013), pp. 191–218.

[253] Adam E Goetz, Tejas K Shah, and Neil K Garg. “Pyridynes and indolynes as building blocks for functionalized heterocycles and natural products”. In: *Chemical Communications* 51.1 (2015), pp. 34–45.

[254] José-Antonio Garcıa-López and Michael F Greaney. “Synthesis of biaryls using aryne intermediates”. In: *Chemical Society Reviews* 45.24 (2016), pp. 6766–6798.

[255] Fahima IM Idiris and Christopher R Jones. “Recent advances in fluoride-free aryne generation from arene precursors”. In: *Organic and Biomolecular Chemistry* 15.43 (2017), pp. 9044–9056.

[256] Diego Peña, Agustın Cobas, Dolores Pérez, and Enrique Guitián. “An efficient procedure for the synthesis of ortho-trialkylsilylaryl triflates: Easy access to precursors of functionalized arynes”. In: *Synthesis* 2002.10 (2002), pp. 1454–1458.

[257] Tsubasa Matsuzawa, Suguru Yoshida, and Takamitsu Hosoya. “Recent advances in reactions between arynes and organosulfur compounds”. In: *Tetrahedron Letters* 59.48 (2018), pp. 4197–4208.

[258] Hemanta Hazarika and Pranjal Gogoi. “Access to diverse organosulfur compounds via arynes: a comprehensive review on Kobayashi’s aryne precursor”. In: *Organic and Biomolecular Chemistry* 19.39 (2021), pp. 8466–8481.

[259] Tianyu Zheng, Jiajing Tan, Rong Fan, Shuaisong Su, Binbin Liu, Chen Tan, and Kun Xu. "Diverse ring opening of thietanes and other cyclic sulfides: an electrophilic aryne activation approach". In: *Chemical Communications* 54.11 (2018), pp. 1303–1306.

[260] Hiroto Yoshida, Hiroyuki Fukushima, Joji Ohshita, and Atsutaka Kunai. "Arynes in a three-component coupling reaction: straightforward synthesis of benzoannulated iminofurans". In: *Angewandte Chemie* 116.30 (2004), pp. 4025–4028.

[261] Trinadh Kaicharla, Manikandan Thangaraj, and Akkattu T Biju. "Practical synthesis of phthalimides and benzamides by a multicomponent reaction involving arynes, isocyanides, and CO2/H2O". In: *Organic Letters* 16.6 (2014), pp. 1728–1731.

[262] Hiroto Yoshida, Hiroyuki Fukushima, Joji Ohshita, and Atsutaka Kunai. "CO2 incorporation reaction using arynes: Straightforward access to benzoxazinone". In: *Journal of the American Chemical Society* 128.34 (2006), pp. 11040–11041.

[263] Wen-Ming Shu, Shan Liu, Jian-Xin He, Shuai Wang, and An-Xin Wu. "Sequential σ-Bond insertion/benzannulation involving arynes: selective synthesis of polysubstituted naphthalenes". In: *The Journal of Organic Chemistry* 83.16 (2018), pp. 9156–9165.

[264] Chen-Yu Tang, Ge Wang, Xue-Yan Yang, Xin-Yan Wu, and Feng Sha. "One-pot synthesis of α-fluoro-β-amino acid and indole spiro-derivatives via CN bond cleavage/formation". In: *Tetrahedron Letters* 55.47 (2014), pp. 6447–6450.

[265] Gyoungwook Min, Jeongseob Seo, and Haye Min Ko. "Three-component reactions of arynes, amines, and nucleophiles via a one-Pot process". In: *The Journal of Organic Chemistry* 83.15 (2018), pp. 8417–8425.

[266] Sachin Suresh Bhojgude, Dnyaneshwar R Baviskar, Rajesh G Gonnade, and Akkattu T Biju. "Three-Component Coupling Involving Arynes, Aromatic Tertiary Amines, and Aldehydes via Aryl–Aryl Amino Group Migration". In: *Organic Letters* 17.24 (2015), pp. 6270–6273.

[267] Kentaro Okuma, Hiroaki Kinoshita, Noriyoshi Nagahora, and Kosei Shioji. *Tandem reaction of arynes with tertiary amines and Aadehydes: formation of 9-and 10-membered dibenzo [1, 5] oxaza heterocycles*. 2016.

[268] Jungmin Kwon and B Moon Kim. "Synthesis of arenesulfonyl fluorides via sulfuryl fluoride incorporation from arynes". In: *Organic Letters* 21.2 (2018), pp. 428–433.

[269] Jing-Kun Xu, Sheng-Jun Li, Hai-Yang Wang, Wen-Cong Xu, and Shi-Kai Tian. "Three-component carboarylation of unactivated imines with arynes and carbon nucleophiles". In: *Chemical Communications* 53.10 (2017), pp. 1708–1711.

[270] Xin Huang, Weizhao Zhao, De-Li Chen, Yaling Zhan, Tingting Zeng, Huiquan Jin, and Bo Peng. "Benzyne-mediated trichloromethylation of chiral oxazolines". In: *Chemical Communications* 55.14 (2019), pp. 2070–2073.

[271] Sheng-Jun Li, Yi Wang, Jing-Kun Xu, Dong Xie, Shi-Kai Tian, and Zhi-Xiang Yu. "Formal insertion of imines (or nitrogen heteroarenes) and arynes into the C–Cl bond of carbon tetrachloride". In: *Organic Letters* 20.15 (2018), pp. 4545–4548.

[272] Sharada P Swain, Yi-Chun Shih, Shwu-Chen Tsay, Joby Jacob, Chun-Cheng Lin, Kuo Chu Hwang, Jia-Cherng Horng, and Jih Ru Hwu. "Aryne-induced novel tandem 1, 2-addition/(3+ 2) cycloaddition to generate imidazolidines and pyrrolidines". In: *Angewandte Chemie* 127.34 (2015), pp. 10064–10068.

[273] Anup Bhunia, Digvijay Porwal, Rajesh G Gonnade, and Akkattu T Biju. "Multicomponent reactions involving arynes, quinolines, and aldehydes". In: *Organic Letters* 15.17 (2013), pp. 4620–4623.

[274] Anup Bhunia, Tony Roy, Pradip Pachfule, Pattuparambil R Rajamohanan, and Akkattu T Biju. "Transition-Metal-free multicomponent reactions involving arynes, N-heterocycles, and isatins". In: *Angewandte Chemie International Edition* 52.38 (2013), pp. 10040–10043.

[275] Jiajing Tan, Binbin Liu, and Shuaisong Su. "Aryne triggered dearomatization reaction of isoquinolines and quinolines with chloroform". In: *Organic Chemistry Frontiers* 5.21 (2018), pp. 3093–3097.

[276] Kai Liu, Li-Li Liu, Cheng-Zhi Gu, Bin Dai, and Lin He. "Aryne-induced dearomatized phosphonylation of electron-deficient azaarenes". In: *RSC advances* 6.40 (2016), pp. 33606–33610.

[277] Wen-Ming Shu, Jun-Rui Ma, Kai-Lu Zheng, and An-Xin Wu. "Multicomponent coupling cyclization access to cinnolines via in situ generated diazene with arynes, and α-bromo ketones". In: *Organic Letters* 18.2 (2016), pp. 196–199.

[278] Ranjeet A Dhokale and Santosh B Mhaske. "Nucleophilic nitration of arynes by sodium nitrite and its multicomponent reaction leading to double-functionalized arenes". In: *Organic Letters* 18.12 (2016), pp. 3010–3013.

[279] Dawid Maliszewski and Danuta Drozdowska. "Recent advances in the biological activity of s-triazine core compounds". In: *Pharmaceuticals* 15.2 (2022), p. 221.

[280] Ali Aldalbahi, Bander S AlOtaibi, Badr M Thamer, and Ayman El-Faham. "Synthesis of new S-triazine bishydrazino and bishydrazido-based polymers and their application in flame-Retardant polypropylene composites". In: *Polymers* 14.4 (2022), p. 784.

[281] Ayman M Atta, Mona A. Ahmed, Hamad A. Al-Lohedan, and Ayman El-Faham. "Multi-Functional cardanol triazine schiff base polyimine additives for self-healing and super-hydrophobic epoxy of steel coating". In: *Coatings* 10.4 (2020), p. 327.

[282] Prasanta Dey, Amit Kundu, Anoop Kumar, Meenakshi Gupta, Byung Mu Lee, Tejendra Bhakta, Suvakanta Dash, and Hyung Sik Kim. "Analysis of alkaloids (indole alkaloids, isoquinoline alkaloids, tropane alkaloids)". In: *Recent advances in natural products analysis*. Elsevier, 2020, pp. 505–567.

[283] John David Phillipson, Margaret F Roberts, and MH Zenk. *The chemistry and biology of isoquinoline alkaloids*. Springer Science and Business Media, 2012.

[284] A Marsili. "Conversion of indones to quinoline and isoquinoline derivatives—III: Schmidt reaction with 2, 3-diphenylindone and similar compounds". In: *Tetrahedron* 24.14 (1968), pp. 4981–4991.

[285] Ming Xu, Ty Wagerle, Jeffrey K Long, George P Lahm, James D Barry, and Rejane M Smith. "Insecticidal quinoline and isoquinoline isoxazolines". In: *Bioorganic and Medicinal Chemistry Letters* 24.16 (2014), pp. 4026–4030.

[286] Giovanny Carvalho Dos Santos, Roberta Oliveira Servilha, Eliézer Fernando de Oliveira, Francisco Carlos Lavarda, Valdecir Farias Ximenes, and Luiz Carlos da Silva-Filho. "Theoretical-experimental photophysical investigations of the solvent effect on the properties of green-and blue-light-emitting quinoline derivatives". In: *Journal of Fluorescence* 27 (2017), pp. 1709–1720.

[287] Masilamani Jeganmohan and Chien-Hong Cheng. "Reaction of arynes, N-heteroaromatics and nitriles". In: *Chemical Communications* 23 (2006), pp. 2454–2456.

[288] MJ Frisch, GW Trucks, HB Schlegel, GE Scuseria, MAn Robb, JR Cheeseman, G Scalmani, VPGA Barone, GA Petersson, HJRA Nakatsuji, et al. "Gaussian 16, revision A. 03,gaussian". In: *Inc., Wallingford CT* 3 (2016).

[289] Andrea N Bootsma and Steven Wheeler. “Popular integration grids can result in large errors in DFT-computed free energies”. In: (ChemRxiv 2019).

[290] I Funes-Ardoiz and RS Paton. *GoodVibes: GoodVibes 2.0. 3*. 2018.

[291] CY Legault. *CYLview, 1.0 b*. 2009.